The Digital Displacement Hydraulic Piston Pump

William Hugh Salvin Rampen

A Thesis Submitted for the
Degree of Doctor of Philosophy

The University of Edinburgh
December 1992

Declaration

I certify that the work presented in this thesis, except where explicitly credited to others, is of my own commission in both substance and composition.

_____ W.H.S. Rampen

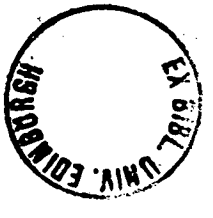

Abstract

The digital displacment hydraulic piston pump is a hybrid device which combines a microprocessor with an established form of high-pressure pump to create a highly integrated machine which can produce a variable high-power output directly from an electronic command. The actively controlled inlet poppet-valve in each cylinder can be held open against the discharging flow in order to disable it during a single cycle. Cylinders can be disabled in this manner, following a maximally smooth sequence, allowing a controlled output flow to be achieved. A compliant device located near the pump, such as an accumulator, provides time-averaging of the flow pulsations in order to minimise the effects of the quantisation error caused by cylinder disabling.

The advantages of this approach over the conventional variable-swash axial piston pump lie with both the response speed and the inherent energy efficiency of real-time cylinder selection. Disabling cylinders in this way restricts parasitic losses to very low levels since unused cylinders are not pressurised nor do they incur loads on their associated bearings. The response time of the pump is related to shaft speed, with the pump able to attain either full or zero output from any starting condition, in less than a single shaft revolution. At induction motor speeds this allows large-signal response times of the same order as those achieved by commercial proportional valves.

The thesis chronicles the development of the Digital Displacement pump. It begins with the formulation of a simulation model which is able to predict the behaviour of the machine in both flow and pressure control modes. The valve control possibilities are then explored and the

design of active valve latches using finite-element analysis described. The flow forces on the disabled poppet are evaluated through a large range of experiments and the results condensed into parametric equations useful for predicting the valve latching requirements of most machines. The mechanical and electronic hardware design, leading to the construction of the prototype, is then discussed.

The study concludes by comparing the performance of the actual pump against that of the predictive model developed at the beginning. The ability of the pump to recover following large disturbances in flow demand, both ramping and harmonic, is investigated.

Table of Contents

Appendices

A. Toggling Latch

B. Moving-Magnet Latch Analysis

C. Simple Numeric Modelling of Moving-Iron Latch Using TK!Solver

D. Derivation Equating Power to FFT Fundamental of Pressure Trace

E. Flow Rig Instrumentation Specification

F. Disabled Ellipsoidal Poppet Valve Flow Loss Calculated using a Minor Losses Approach

G. Disabled Ellipsoidal Poppet Experiment Data

H. Compressibility Testing of Liquids

I. Digital Displacement Pump Control Software Listing

List of Figures

1.0 Introduction

This thesis chronicles the development of a new type of hydraulic pump. It covers the very broad spectrum of activities required to carry a first concept to a working machine: from magnetic latch analysis to real-time software, from fluid forces on valves to computer simulation of pump response. As such, the work at hand deals with each obstacle, only to the extent that a suitable solution has been reached and progress has been made possible. In a work of this breadth there will necessarily be gaps left unfilled and many possibilities for further study and consequent improvements. These are left, in the event of commercial interest, to those who follow.

1.1 Background

In 1979 Stephen Salter, then working on electrical power generation from ocean waves, was asked to prepare a full scale design proposal [1] for the Department of Energy. The Salter Duck, shown in figure 1.1, moved in the water with a low frequency harmonic motion under the influence of ocean waves. The only feasible method to convert the immense torques and low velocities generated by the "Duck" into the high-speed input required by a synchronous generator appeared to be through the use of high-pressure oil hydraulics. In the absence of either suitable commercial units or in-house expertise, Salter recruited Robert Clerk, a retired design engineer, who had been developing high-efficiency, long-life axial-piston pumps. Together they developed a power transmission scheme which used Clerk's axial-piston machines for the high-speed work and an extremely large ring-cam pump for the low-speed high-torque side [2]. The ring-cam pump, of which the general arrangement

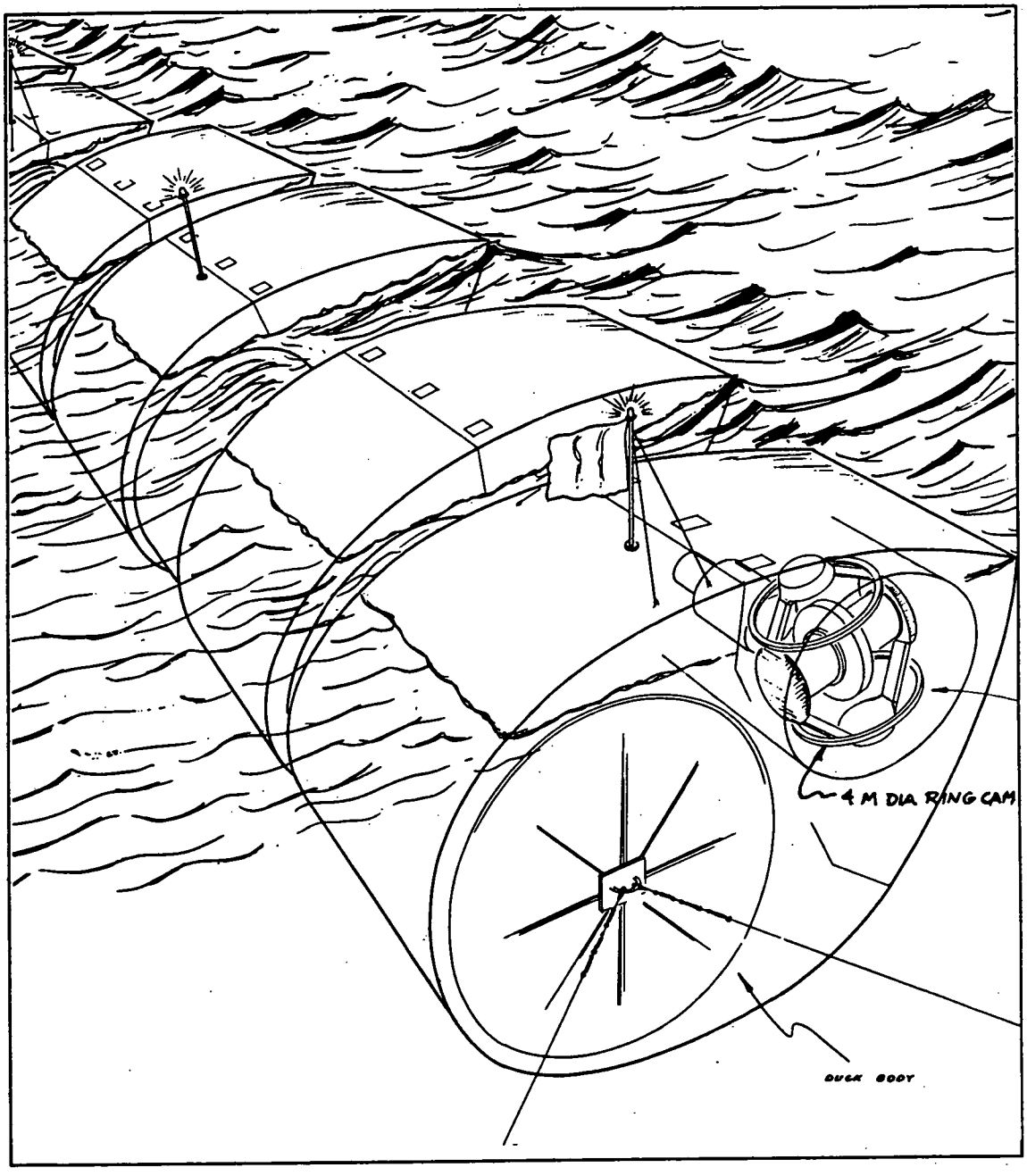

Figure 1.1: Artist's Impression of the Salter Duck circa 1980. From Edinburgh-Scopa-Laing 5th Year Report.

drawing of a single module is shown in figure 1.2, employed many interesting features including an evacuated sump, opposed cams on a conically profiled ring and stressed pressure mains rings which served to locate the many piston/cylinder units. Perhaps its most interesting

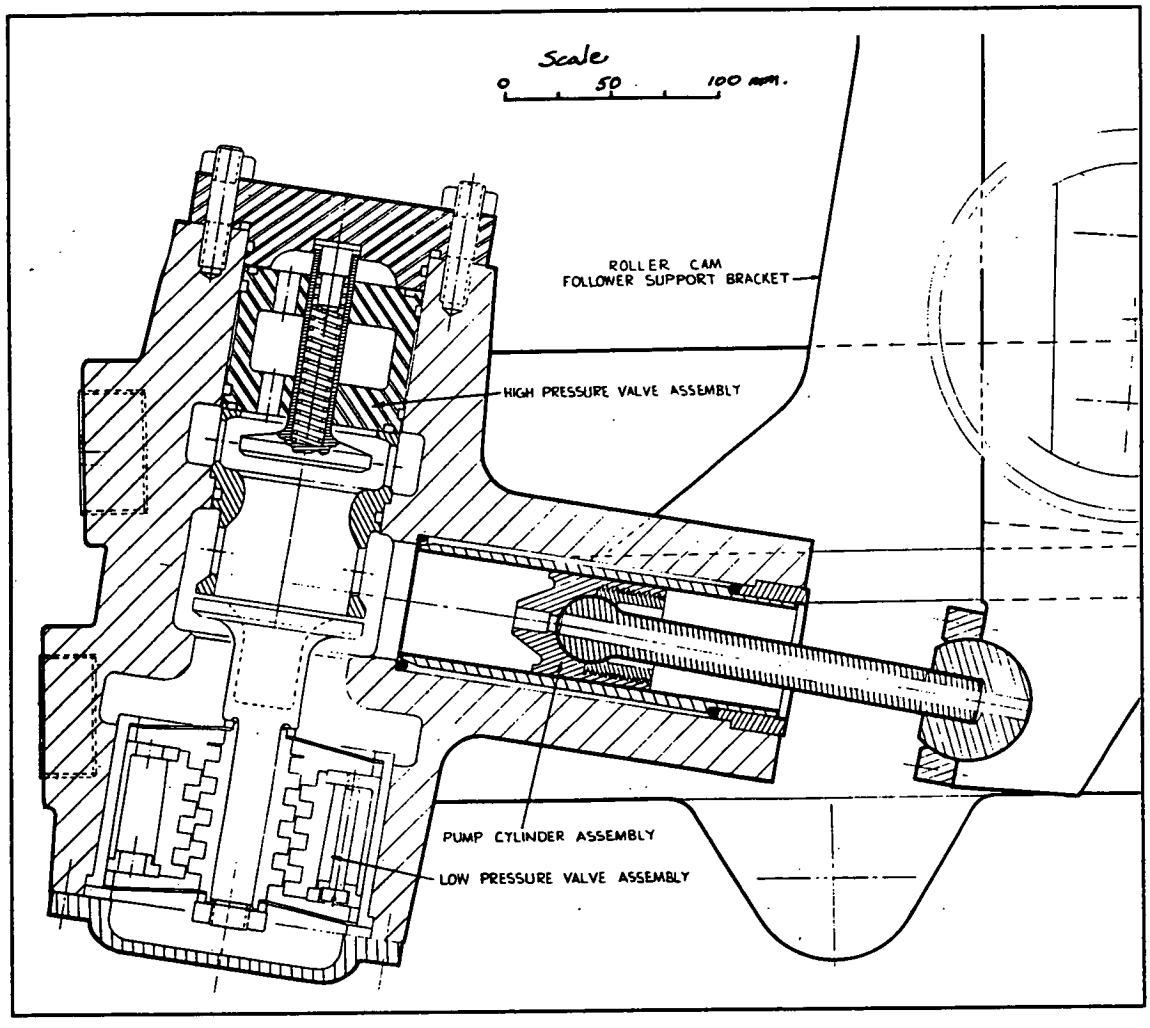

Figure 1.2: General Arrangement of Early Ring-Cam Pump Module. From Edinburgh-Scopa-Laing 5th Year Report.

characterictic was its ability to present a variable load to the duck through the disabling of some fraction of its cylinders such that the energy capture of the device was maximised. The enormity of the full scale design work prevented the pump development from proceeding beyond the initial hardware detailing stage. Very little thought was given to the process or technique of controlling the active intake poppet valves though it was assumed at the time that some form of computer would be used.

Although Department of Energy funding ended in 1982, Salter was able to continue his work on the "Duck" power transmission through SERC support. The objective of the second grant was to develop the active poppet valve of the ring-cam pump to the point where it could be sized for a range of machines and operating conditions (the first grant concerned Clerk's axial machine). This marked the beginning of the work for this thesis.

The word chronicle, as employed in the first sentence, is not strictly correct, as the text is organised in a substantially different sequence from the actual work. This is done only to improve comprehension for the reader and, if belatedly, to justify the SERC active valve work that it began with.

1.2 The Digital Displacement Pump Concept

The idea of using a fixed displacement pump and varying its output by disabling its cylinders is far from original. Several manufacturers have done this in the past, some by splitting the output manifold of a poppet-valve pump, others by holding inlet valves open mechanically. In both of these cases the objective was to achieve a crude staging of output rather than to achieve precise load-following.

If the system demand is evaluated on the basis of individual cylinder availability, that is each time a cylinder arrives at bottom-dead-centre and is ready to deliver, then the output of the pump can be continuously controlled to within a half of a single cylinder's displacement. The smoothness of the output will obviously vary enormously as the demand changes and the pattern of pumped cylinders grows closer or further apart.. The cylinder pulsing frequency, the product of

the number of cylinders in the pump and the shaft speed (or repetition rate for a multi-cam), will also influence the smoothness of response as well as the fundamental pulsation frequency.

Since there are physical limits to both cylinder numbers and shaft speeds, and, since the disabled cylinders will create sub-harmonics of the fundamental pulsation frequency, there will be pressure and flow pulsations throughout the frequency range where large mechanical systems are excited to resonance. From the beginning, therefore, it was understood that some form of compliant element would be needed close to the pump to serve both as a fluid store and to attenuate the low frequency pulsations caused by cylinder disabling.

The objective has now been described in broad terms;

To develop a poppet-valve pump and accumulator combination where the output can be varied by cylinder disabling to meet the system demand in real-time on a stroke-by-stroke basis.

1.3 Summary of Chapters

Before proceeding on a chapter by chapter summary, it should be pointed out that the usual literature survey chapter has been dispensed with. This has been done for two reasons:

1. the patent searches done during the work have not revealed any parallel results, so there is very little available material of relevance to the main objective, and,

2. since the references are about diverse subjects, they are more effectively presented in the context of the related chapter.

As such the literature survey has been subdivided and distributed into the relevant chapters.

Chapter two examines the concept of the digital displacement pump, develops the fundamental algorithms for flow and pressure control and then, concludes with the results of a computer simulation of the pump output under different loading conditions.

Having determined that there is some merit in the principle, and that it is worth proceeding, chapter three deals with ways of controlling active inlet valves. In this chapter the latch design evolves and its magnetic properties are analysed with the aid of a finite element model.

One of the main observations to emerge from chapter three is that the magnetic forces available to control the valve are small. Chapter four deals with the hydrodynamics of the poppet valve. Of interest in this case are ways of reducing the force required to hold the valve open against the flow as well as to keep flow losses low, since the off-loading technique involves pumping fluid back and forth through the open valve. The chapter describes the design and construction of a single cylinder flow testing rig. It concludes with the analysis of approximately 400 experiments, in which different valve shapes, sizes and openings were tested under varying operating conditions. These results are compressed into equations for holding force, power loss and minimum cylinder pressure which can be employed for

geometrically similar valves under a wide range of conditions.

Chapter five deals with the many practical problems which arose when the components were designed to modify an existing pump. In designing the hardware for actual service, many measurements and calculations were performed to ensure that stress levels, actuation times, damping factors etc. were within acceptable bounds. The chapter provides a summary of the final hydraulic hardware design.

Chapter six investigates the design of the electronic hardware and sets the specification for the micro-processor. It concludes by describing the operation of the real-time pump software.

In chapter seven the problems of developing the completed pump into a fully working device are examined. The results gleaned from a range of experiments are then compared to those from corresponding simulations. During these tests the pressure control algorithm is subjected to system demands ramping from one level to another and, later, tested with oscillatory demands of varying amplitude and frequency.

Chapter eight provides a summary of the digital displacement pump development. It ends with recommendations for further work.

2.0 Digital Pump Assessment

2.1 Introduction

It would seem sensible, before designing actual hardware for disabling cylinders in a pump, to try to model its expected behaviour so that the inherent pulsation problems can be quantified and weighed against the anticipated merits of the technique. This chapter describes this initial process. It then continues to compare the equivalent, servo-controlled, axial-piston pump with a similarly sized digital displacement one in terms of both response and other characteristics.

2.2 Literature Survey

The digital displacement pump is, as far as can be judged, novel. The patent searches which were carried out during the course of the work revealed quite a lot in the way of active valve hardware and also systems for mechanically off-loading pumping cylinders on a quasi-static basis [3,4,5]. Nothing which anticipated the ideas nor dealt with the problems associated with the digital displacement concept was revealed.

If the fluid pulsations associated with cylinder disabling are considered, then the area of fluid borne noise reduction comes into focus as being relevant. Several research groups worked in this area during the late 1970's and early 1980's. The UK Department of Trade and Industry sponsored an initiative in quieter hydraulic systems which resulted in work for quantifying and removing fluid-borne noise by Henderson and Whitson [6,7,8] at the NEL and Edge and Tilley at Bath University [9,10]. The problem with applying any of

the theory and solutions presented in these papers is that they all deal exclusively with resonant systems and, in the case of the NEL, the use of tuned resonators to damp pulsations over a range of frequencies. The cylinder selection (or digital displacement) machines will have a fundamental cylinder actuation frequency disrupted by the disabled cylinders which, when equipped with a tuned resonator, are likely to create a chaos of travelling pulses. Additionally, the enabling sequence of the cylinders will generate all sorts of lower frequency sub-harmonics which will be out of the effective range of a resonant chamber.

The word digital conjures up an association with electronics and electrical systems, which might also have led on to some analogous work which could be applied. However, there are deep and irreconcilable differences between hydraulic pumps and switch-mode power supplies. There is a fundamental difference between enabling a cylinder, which then goes on to produce a sinusoidally shaped flow pulse with respect to time, and turning on a power field effect transistor (FET), which raises the output to the supply level almost instantaneously and then turns it off at a similar rate [11].

2.3 Piston Pump Background

The poppet valves in a single cylinder pump rectify the fluid flow so that the flow rate function in both the intake and delivery manifolds could be described as half wave rectified sinusoids. Real poppet valves differ from the ideal since they are slightly delayed in their operation. This is due to the combination of inertia and damping as well as low actuation forces in the case of the inlet valve. Fluid compressibility also contributes to the opening delay of the delivery valve since the

contents of the cylinder must reach delivery pressure before the valve will open.

The behaviour of poppet-valves in piston pumps has been investigated by Edge et al. [12]. Their work shows that the non-ideal behaviour of poppet-valves can cause a substantial deviation from the expected sinusoidal cylinder output. The paper describes pressure waves, originating from the valve actuation, which travel up and down inside the cylinders and escape into the manifolds. It also demonstrates that correct valve lift and spring rate can make a noticeable improvement in volumetric and mechanical efficiencies. The digital displacement pump is identical to other fixed-displacement poppet-valve pumps in every way other than its actively controlled inlet valves. While the high frequency resonances, seen by Edge et al, will still be present to some extent, the ability to control the closing time of the inlet valves should allow the digital displacement pump to more closely approximate the ideal.

When digital displacement control is used, a decision is made as each cylinder approaches bottom-dead-centre. The controller considers the state of the system and takes a decision either to enable or disable the approaching cylinder. The result of an enabling decision is that an electrical pulse is sent to the solenoid coil of the inlet valve via a power semiconductor. The pulse closes the valve and causes the flow of a half sinusoid pulse of fluid to be pumped into the delivery manifold over the following 180 degrees of shaft revolution. A disabling decision leaves the inlet valve open so that the delivery manifold receives no fluid over the same period.

A pump with many cylinders will have the output of each one delayed in phase by the angle between the cylinders

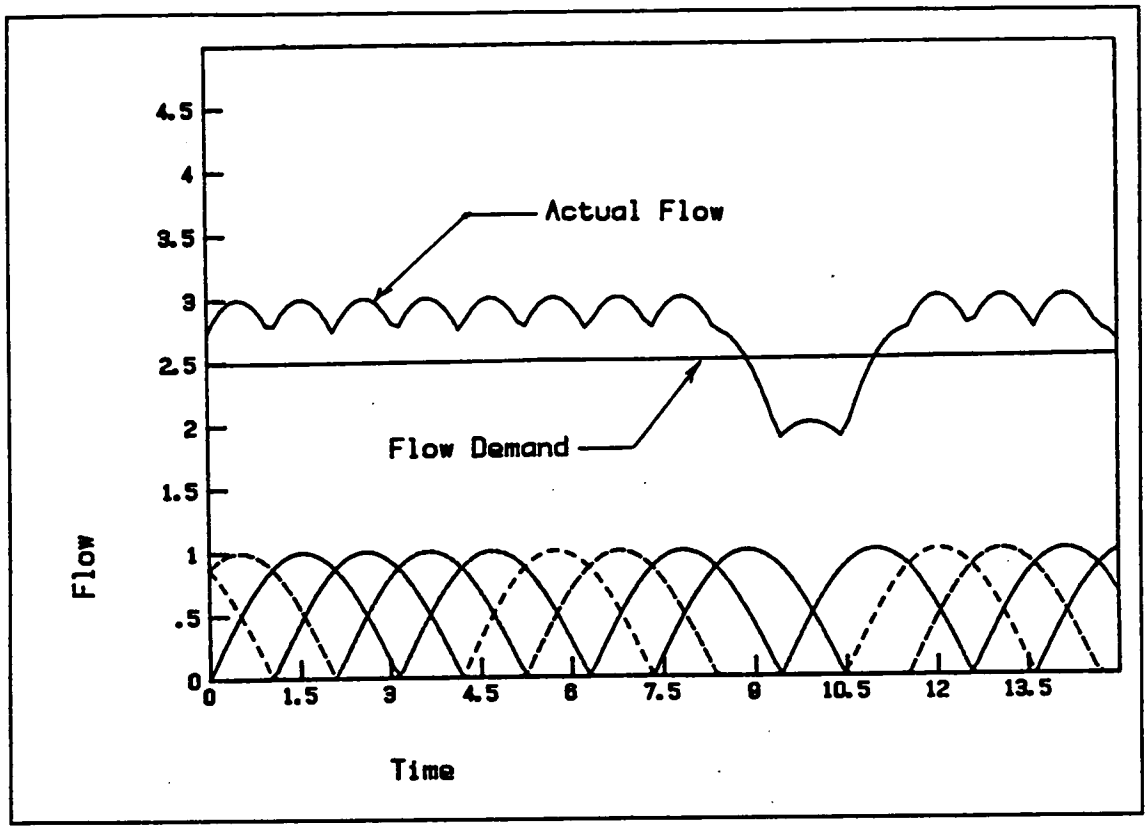

Figure 2.1: Flow Ripple Consequences of Cylinder Disabling in a Hard System.

so that the resulting flow function will be formed by the superposed rectified sine waves, much like a poly-phase electrical supply. Disabling one cylinder occasionally will cause a momentary droop in flow rate as one of the superposed components is skipped as shown in figure 2.1.

2.4 Cylinder Control characteristics

If a two cylinder pump is considered, so that the fully enabled output flow resembled a fully rectified sine wave (this combination is useful in that it has no dead time between cylinders and also no overlap). The controller will have to provide decisions twice per revolution in order to satisfy the system requirements. There are two control difficulties involved:

1. The first and most obvious is that the instantaneous flow demanded of the pump may only require part of the cylinder about which the current decision is being taken (henceforth called the decision cylinder). This leads to a quantisation error since the best that the controller can do is to provide either one or zero cylinders. This means that, for any constant demand, the system can have up to one half a cylinder of displacement error.

2. The second problem stems from the response delay. At the time that the decision is made the decision cylinder is contributing nothing, it is only ninety degrees of shaft rotation later that the cylinder will reach its maximum flow rate. The displacement from the cylinder is not complete until the shaft has finished one half of a revolution.

2.5 Quantisation error

There is at least one pump on the market which uses variable poppet-valve timing in order to achieve variable delivery [13]. Active inlet valves, which were electronically closed part way through the delivery stroke, could imitate their mechanically timed cousins in this respect. However, the various trials that have been made with active valve timing indicate that both shock and noise rise dramatically as the valve closure is delayed. This is due to the pressure rise in the cylinder and the venturi effect occuring in the region of the poppet valve seat, during the reversed flow, which pulls the valve onto its seat. The squeeze film effect of the approaching surfaces, which might damp the closure, is expected to be largely counteracted by the

low pressure region downstream of the seat which is caused by the inertia of the decelerating fluid column travelling away from the cylinder. The result of the sudden closure of the inlet valve is hydraulic hammer and shock waves travelling around the system [14]. A less violent solution is to position a very small accumulator near the delivery valves so that the quantisation error can be reduced to acceptable levels.

Unfortunately, the presence of an accumulator generates other difficulties:

1. The limited active pressure range restricts the acceptable range over which the system can work, and;

2. The stored energy increases the response time of the pump.

Neither of these problems are insurmountable since:

1. Many applications, where load following pumps are used, work at a constant pre-set line pressure, and also;

2. The energy stored in an accumulator designed to accept a fraction of a single cylinder will be very small.

2.6 Delay Error

One solution to the problem of delayed response is to set the decision making process in the future, at a point where the decision cylinder is making a substantial contribution to the pump's output. This is not really problematic from the standpoint of the control algorithm

so long as the system is not subject to either a major alteration in demand or an external disturbance between measuring the demand and delivering the cylinder's contents to the high-pressure manifold.

The difficulty comes in deciding just how far to look ahead. The reason for initially choosing a two cylinder pump as an example, is that there is no ambiguity in the choice. The decision look-ahead time in this case should be half a revolution since this allows the controller to incorporate the entire effect of the decision cylinder without having to forecast the contribution of future ones.

Problems arise when the cylinder number increases and the cylinder output's begin to overlap, since there are several ways in which the look-ahead rule could be extended from the two cylinder case. If the controller was always looking ahead one half of a revolution, then with a great many cylinders it would be taking a decision about a demand which might be largely met by future cylinders. The decision displacement then becomes too small a fraction of the unspecified displacement between the actual and the look-ahead time and the system becomes unstable. If the controller used the time to the next decision as the look-ahead period then, with a large number of cylinders, the contribution of the decision cylinder by the look-ahead time would only be a small part of its whole. Its greatest effect would be felt in the time following the next decision, when the corrective displacement produced by that cylinder would be insufficient to stop the system hunting.

A colleague [15], has suggested a third possible way of extending the two cylinder case. If it was accepted that, as with the two cylinder case, the algorithm should

look ahead to a point where there is one uncommitted cylinder's worth of displacement contributed to the output, then an appropriate look-ahead angle could be calculated for any number of cylinders. It is not clear how this hypothesis could be explicitly proven, however, it was found to work in the simulation which follows in this chapter.

2.7 Effect of Cylinder Pulse Rate

A high cylinder pulse rate is desirable in the digital displacement pump since it both simultaneously reduces the time between decisions and decreases the required cylinder volume, and therefore quantisation error, for a given flow-rate. There are two ways of increasing the cylinder rate, both with quite different effects. The first is simply to increase the shaft speed. This is only possible until the point is reached where the poppet valves become uncontrollable. The active inlet valves used in the digital displacement pump may prove to have a higher limit than do conventional valves with low-rate springs, but this still remains a limitation. The type of prime-mover being used will often dictate the shaft speed in any case.

Alternately, to increase the cylinder rate, one can increase the number of cylinders in the pump. This has the effect of increasing the overlap between cylinders and of decreasing the look-ahead time. This approach will also be limited, in practice, by the economics of machining and assembling large numbers of high precision parts.

2.8 System Configuration and Control Strategy

The first two types of control system that are required for digital displacement pump are:

1. An open loop flow-control system: where the pump is required to produce a flow proportional to some form of input signal irrespective of delivery pressure, and;

2. A closed loop pressure control system: where the controller monitors system pressure and attempts to hold it to a set point irrespective of flow demand.

The first system is very easy to model, since it is independent of other system components, whereas the second relies on a well defined system downstream of the pump delivery.

2.9 Flow Control

With a flow-control system there is no need to close a loop around the pump since the cylinder displacement is fixed and the certainty of actually enabling a cylinder from a command pulse very high. The algorithm attempts to minimise accumulated displacement error over the history of the pump and will thus manage to follow even small variations in load demand and maintain the positional accuracy of the load, subject to the inaccuracies created by the fluid compressibility.

The flow demand can be converted to displacement over the time period from the present to the look-ahead time. The previously committed cylinder's displacement over this time can be subtracted from this, as can the cumulative

quantisation error resulting from previous decisions. If the resulting displacement is greater than one half of the decision cylinder's displacement during the same period then the cylinder is enabled, otherwise not.

2.10 Pressure Control

The basic difficulty in maintaining a constant pressure at the pump discharge with a variable flow machine lies in converting the pressure error (which can be measured) into a change in demand flow (which cannot). A small accumulator incorporated into the discharge system provides a conversion tool since the gas in its bladder will be expanding and contracting adiabatically. The accumulator size can be chosen to allow one-half cylinder of error displacement either side of the zero-error volume without deviating more than a set percentage from the pressure set-point.

The second problem in achieving pressure control is that of determining the load flow out of the system. If the various known displacements from the previous time interval are summed, then the load flow during that interval can be inferred. The volume of fluid pumped, Sp, can be calculated for the interval preceding decision k:

$$S_p = \frac{V}{2} \sum_{i=1}^{ip(\frac{n}{2})+1} D_{k-i}(\cos((i-1)\phi) - \cos(i\phi)) \qquad (2.1)$$

where: V = *cylinder volume*
D = *decision value*
n = *number of cylinders*
$\phi = 2\frac{\pi}{n}$
(*ip* = *integer part*)

The displacement out of the accumulator, Sa, can be calculated from the pressure difference between the current and previous decisions.

$$S_a = C_1^{\frac{1}{\gamma}} \left(\frac{1}{p_k^{\frac{1}{\gamma}}} - \frac{1}{p_{k-1}^{\frac{1}{\gamma}}} \right) \qquad (2.2)$$

where: C_1 = *accumulator constant*
P = *System Pressure*
γ = *gas constant ratio*

The load flow, Qs, can be found by summing the two:

$$Q_s = \frac{S_p + S_a}{t} \qquad (2.3)$$

where: t = *interval time between decisions*

The algorithm can now change its time reference points and consider the time interval between the present and the look-ahead time. The displacement of the committed cylinders, Sc, is calculated in much the same way as Sp:

$$S_c = \frac{V}{2} \sum_{i=1}^{ip(\frac{n}{2})} D_{k-i}(\cos(i\phi) - \cos(i\phi + \psi)) \qquad (2.4)$$

where: ψ = *lookahead angle*

The accumulator displacement, S0, is then calculated so as to bring it back to the zero error position by the look-ahead point:

$$S_0 = C_1^{\frac{1}{\gamma}}\left(\frac{1}{P_{set}^{\frac{1}{\gamma}}} - \frac{1}{P_k^{\frac{1}{\gamma}}}\right) \qquad (2.5)$$

The displacement required by the load, Ss, is then calculated from the load flow:

$$S_s = Q_s\frac{\Psi}{\omega} \qquad (2.6)$$

where: ω = *rotational velocity*

Finally the decision, Dk, for the current cylinder is computed:

$$D_k = \frac{1}{V_d}(S_s - S_0 - S_c) \qquad (2.7)$$

$$\textit{where: } V_d = \frac{V}{2}(\cos(0) - \cos(\phi))$$

The quantisation problem occurs when Dk is either rounded up to 1 or down to 0. The error that this introduces is dealt with at the next decision.

One complication which needs to be considered is the practical requirement of end-stops on the accumulator. If the minimum size of accumulator is used then, when it is under-filled by half of a cylinder, the diaphragm will be against the retaining shell. Similarly, when the accumulator is over-filled by some amount a relief valve would normally open. Both of these situations create discontinuities in the system model which in turn generate faulty decisions. One solution to either of these is simply to determine at the outset if the system

pressure is beyond the normal bounds. An appropriate decision can then be made without further computation.

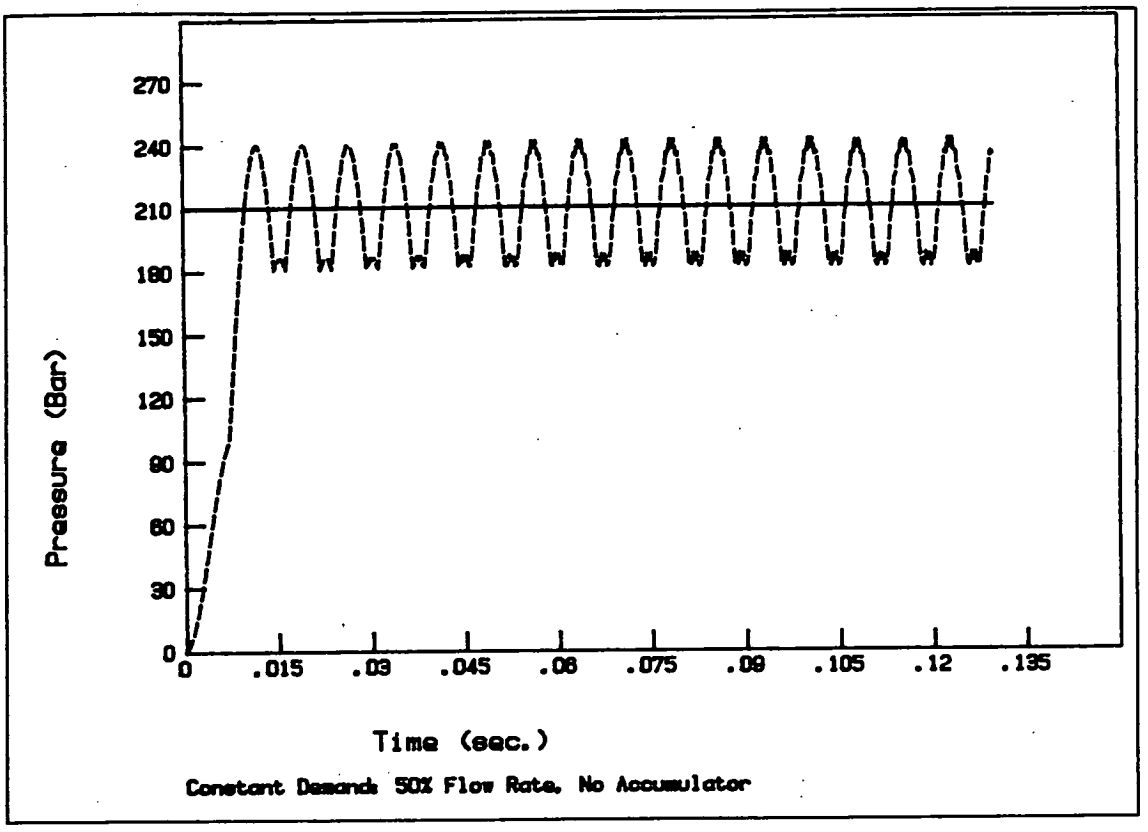

Figure 2.2: Pressure Ripple at 50% Output into a Hard System.

2.11 Pump Modelling

The flow control algorithm was implemented on a micro-computer using the Hewlett Packard Basic language. The model is very simplistic as it uses idealised harmonic flow and ignores the high frequency transients and volumetric inefficiencies found in a real pump. This simplification is justified, in the first instance, by the goal of this exercise; which is to determine the basic behaviour of the digital pump. The results of different flow demands are plotted as time traces such as that of figure 2.2. Alternate enabling and disabling of cylinders gives an average of 50 percent of the maximum

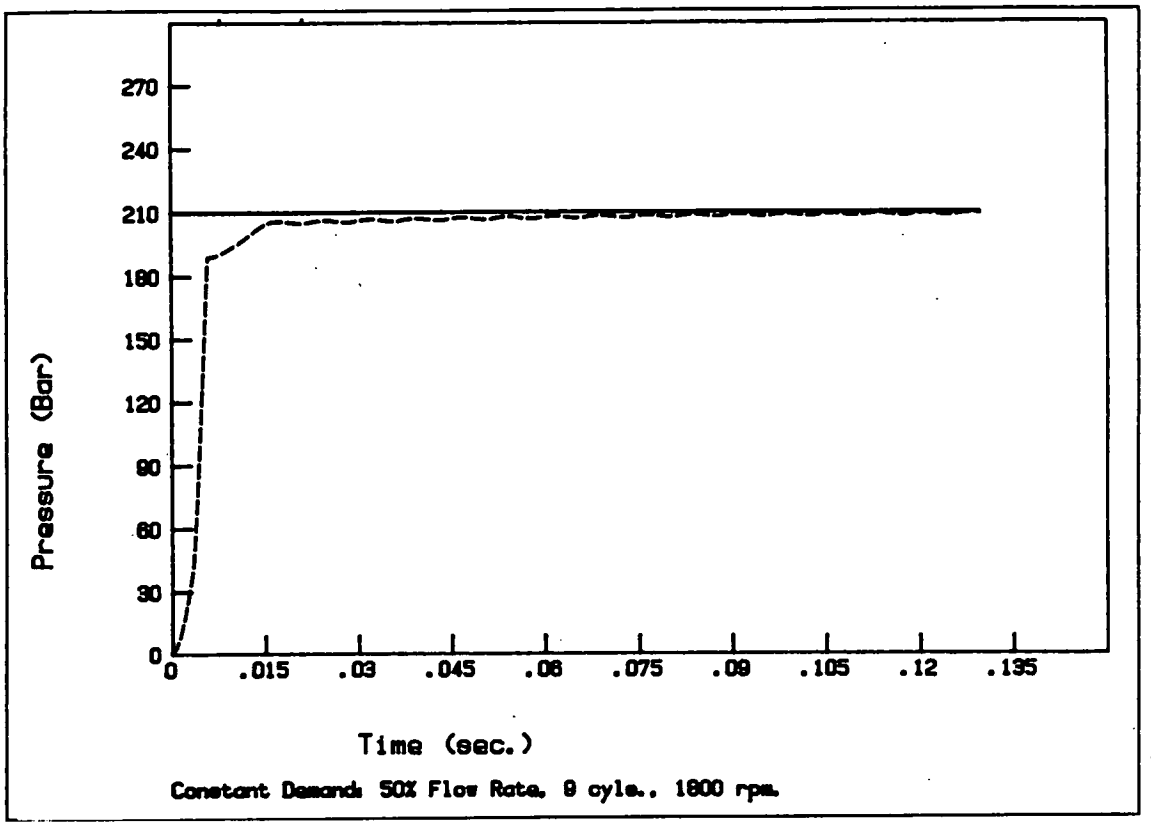

Figure 2.3: Pressure Ripple at 50% Pump Output with a Small Accumulator on the High-Pressure Side.

output, though with a pronounced flow ripple. If an accumulator, sized to permit a 10% deviation from mean pressure for a half cylinder error is located near the pump, then the ripple is very much reduced, as shown in figure 2.3, under the same output conditions. All flow levels produce a regular periodic ripple composed of cylinder pulsing frequency and other lower frequency components. The repetition period of the output pattern can become very long when the load flow is just off an even-fraction of total pump output. For example, at 51% output, two cylinders will be enabled in succession every hundred decisions. One aspect of this feature, from a human point of view, is that the machine may appear to be malfunctioning at anything other than a few operating points in its output range. The fluid-borne noise consequence of this will be that any low frequency

resonances in the hydraulic loading system will respond at some point in the output range of the pump. This may limit the application of the pump unless sufficient damping can be introduced at these frequencies. Equally, human acceptance of the varying acoustic output may prove more critical to the adoption of this technique than other, more measurable, operating characteristics.

To permit the modelling of a pressure controlled system the load characteristics must also be defined. In this case a variable orifice has been used since it is simple to model and can be effectively defined by a single

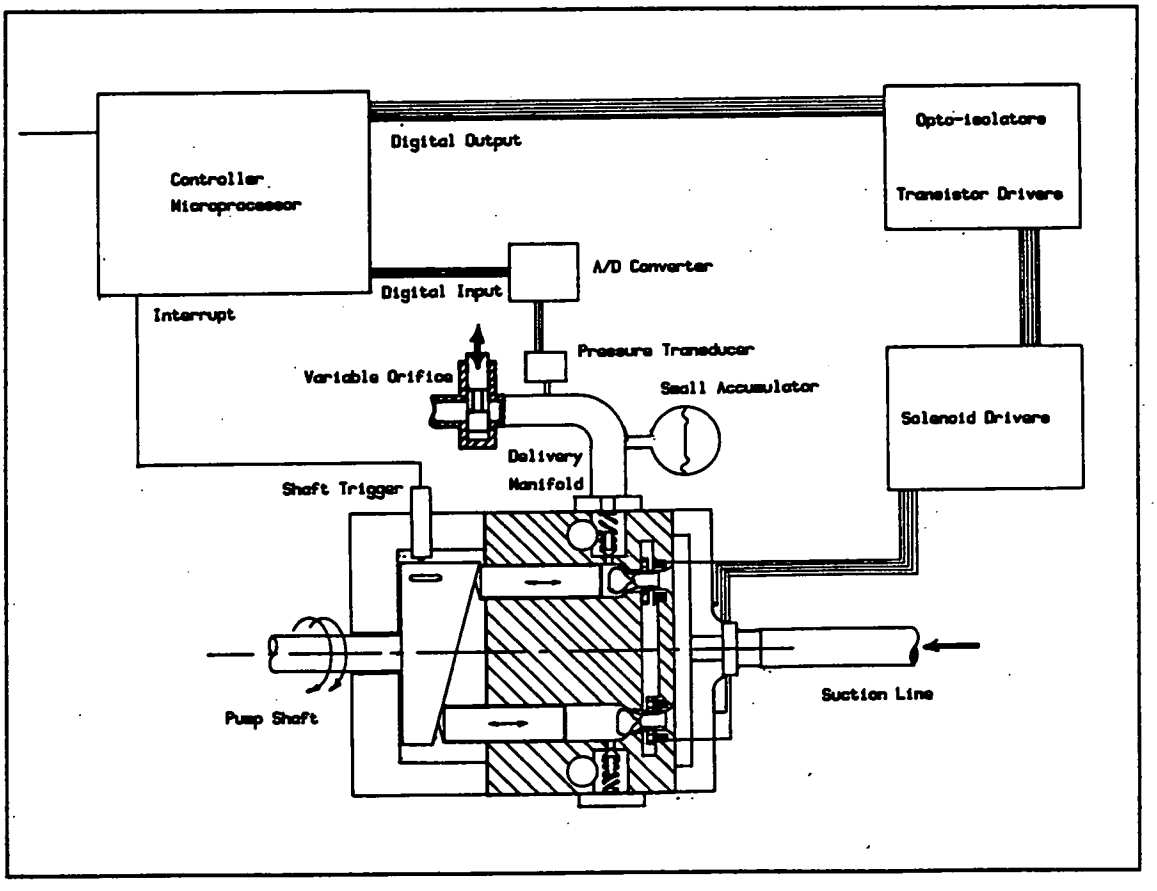

Figure 2.4: Schematic Arrangement of Digital Displacement Pump and Loading Orifice.

parameter. A schematic representation of the circuit is shown in figure 2.4.

The flow from an orifice, Qs, can be defined as:

$$Q_s = C_2 A P^{\frac{1}{2}} \qquad (2.8)$$

$$\text{where: } C_2 = \frac{\sqrt{2}\ C_D}{\rho^{\frac{1}{2}}}$$

A = *orifice area*

ρ = *fluid density*

C_D = *coefficient of discharge*

When combined with the load sensing algorithm described above, an equation for pressure can be written:

$$0 = S_a - \frac{C_2 A}{2}\left(P_k^{\frac{1}{2}} + P_{k-1}^{\frac{1}{2}}\right) + S_p \qquad (2.9)$$

where: P_k *is unknown*

Since pressure cannot be explicitly found, a Newton method solution was implemented in the simulation.

Two examples of modelling solutions are presented in figures 2.5 and 2.6. In the first, the pump has an initial set point of 10% maximum output flow which is abruptly increased to 90%. The beginning of the trace shows the first pumped cylinder bringing the pressure up to the operating point of the accumulator. Once this pressure is reached the change is less dramatic as fluid is supplied to both the load and the accumulator. After equilibrium has been established, the orifice is opened suddenly and the output flow increased accordingly. The pressure is initially maintained near the set-point as

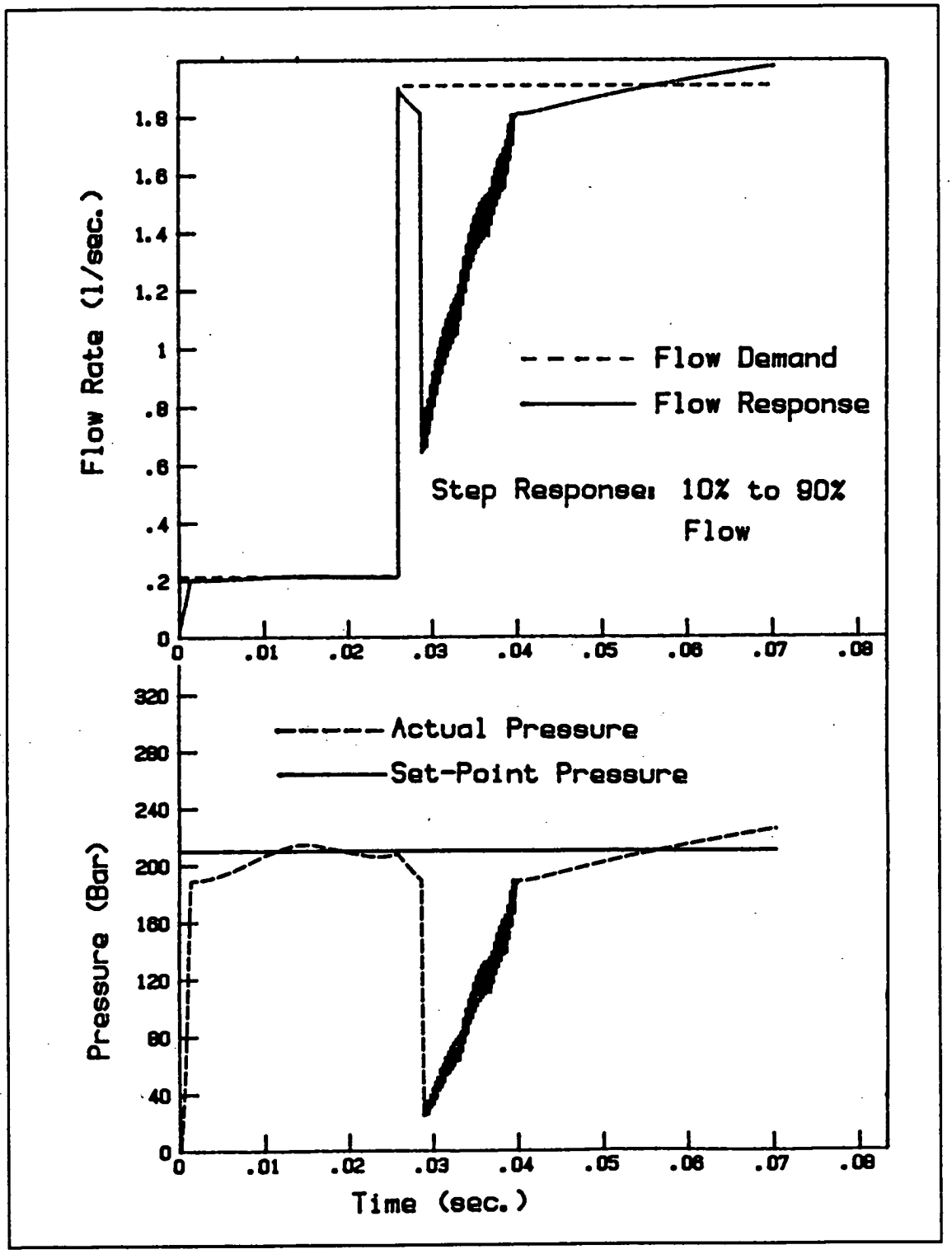

Figure 2.5: Simulation of Pressure and Flow Responses for Constant-Pressure Algorithm Following Sudden Orifice Opening.

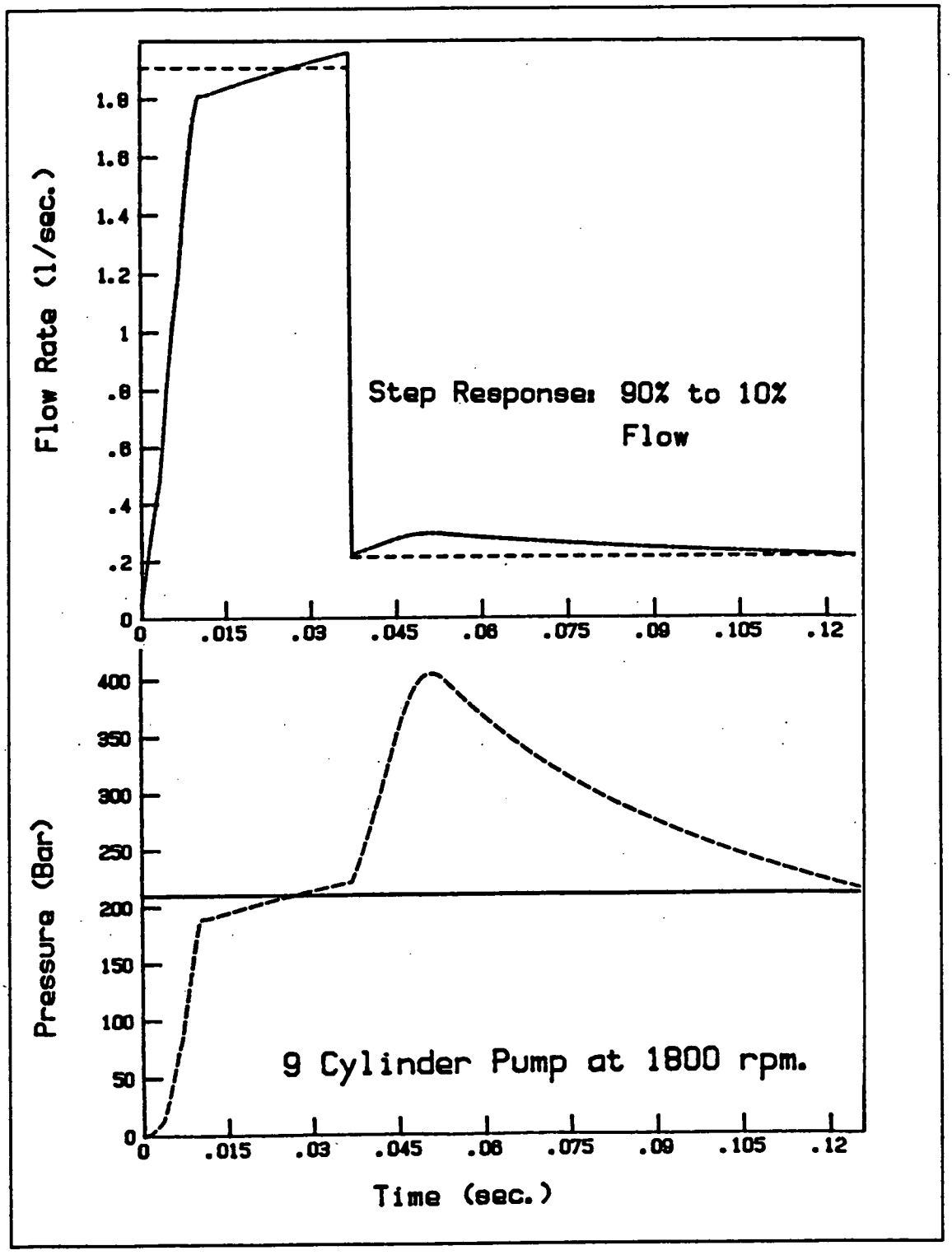

Figure 2.6: Simulation of Pressure and Flow Responses of the Constant-Pressure Algorithm Following a Sudden Orifice Contraction.

the accumulator empties to meet the demand of the orifice. Once this source is exhausted, the system is then entirely reliant on the instantaneous flow from the previously committed cylinders of the pump. Since the flow rate was initially low and enabling decisions ten cylinders apart, the instantaneous flow rate is very near zero and the pressure collapses. The decisions following detection of the change will cause the enabling of every available cylinder until the pressure recovers and the system establishes a new equilibrium. The model suggests that the pressure will rise rapidly (following the thick line in the graph) until it is once again within the design range of the accumulator, where the rise will be moderated by the compliance. The thick recovery line is the result of small oscillations in the modelling algorithm rather than the predicted behaviour.

Figure 2.6 shows the reverse step where the flow is suddenly decreased between the same limits. During the half revolution after the orifice closes, the committed cylinders are still delivering their unwanted displacement into the system. This pushes the pressure well above the error bounds of the set-point. The orifice eventually deals with this excess displacement by increasing the flow above the demand level. If the system were equipped with a relief valve for the occasional instantaneous over-pressure then a substantial amount of the unwanted displacement would pass through it instead of the orifice and the recovery would occur more rapidly.

The pump modelled in these examples is based on a nine cylinder MacTaggart-Scott radial piston pump of 25 mm bore and 16 mm stroke rotating at 1800 rpm. This was chosen for two reasons:

1. It was available for future testing, and;

2. Its displacement was exactly the same as the Sundstrand 22 variable-swash axial-pump, which permitted some comparison in terms of transient response.

Akers and Lin [16] present some curves describing the zero to full swash response of the Sundstrand pump when equipped with an appropriate servo-valve. When the servo-valve drive is saturated the response from the 10 to 90% flow rate swash positions is on the order of 300 milliseconds. The recovery from an instantaneous step response for a comparable digital displacement pump can be seen from figures 2.5 and 2.6 to be on the order of 10 milliseconds, or a factor of 30 faster. The abrupt change in flow rate possible for the pump may not, however, be acceptable to the rest of the system.

Figures 2.7 and 2.8 show the response of the pressure controlled digital pump ramping up from 10% flow and down from 90% at the maximum rate of change achievable with the Sundstrand unit. It can be noted that, while the response curves are not smooth they do remain quite close to the demand levels. The flow rate error is much higher at 90% output due to the square-law relationship between pressure drop and flow rate which applies to orifices.

2.12 Comparison between Variable-Swash pumps and Digital Displacement pumps

In attempting to establish the applications appropriate for the digital displacement pump one could begin by comparing it with its obvious and established rival. Poppet valve pumps have been on the market for a very

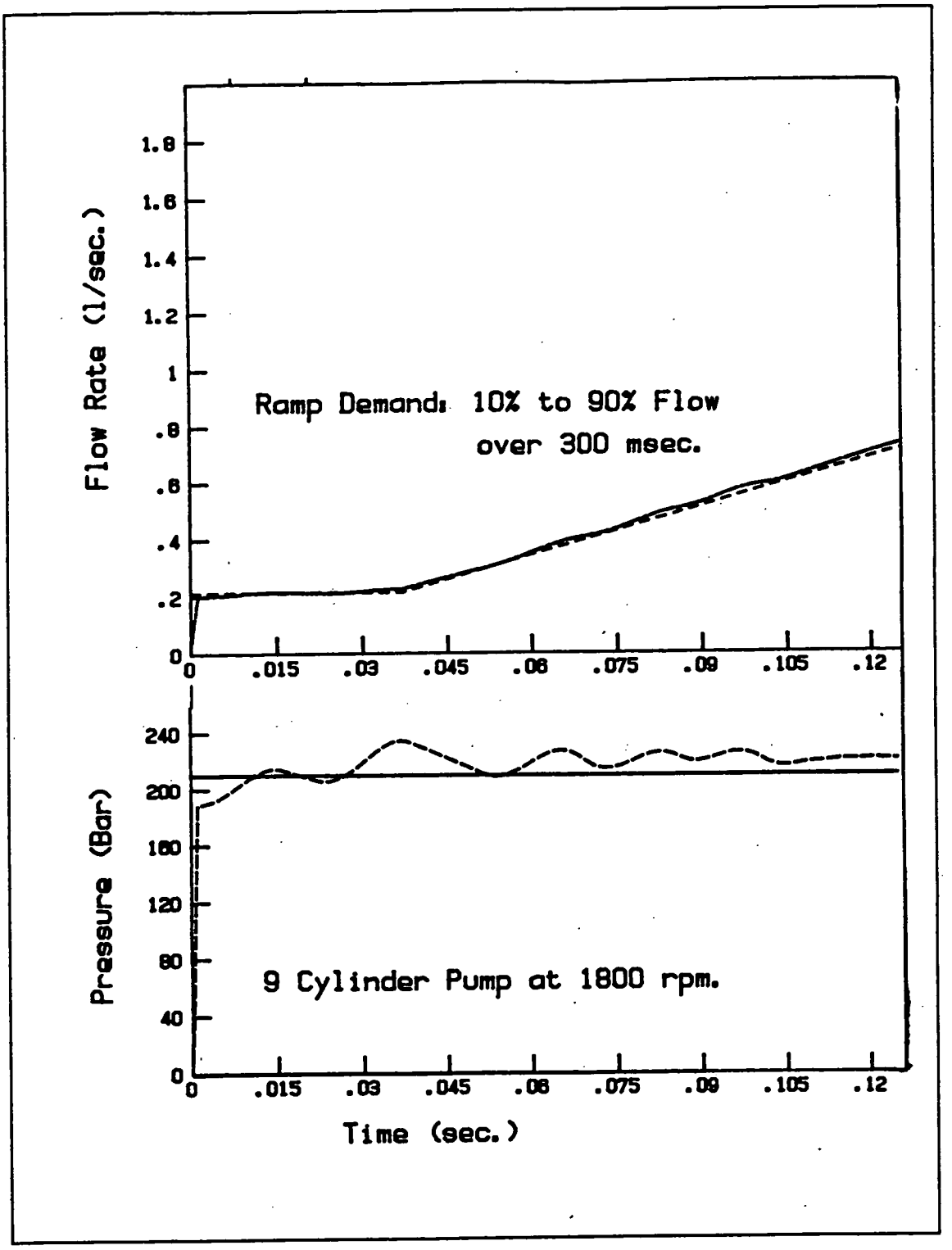

Figure 2.7: Simulation of Constant-Pressure Algorithm Following a Ramped Flow Increase at a Slope Representing the Maximum Rate of Change of the Sundstrand 22 Pump.

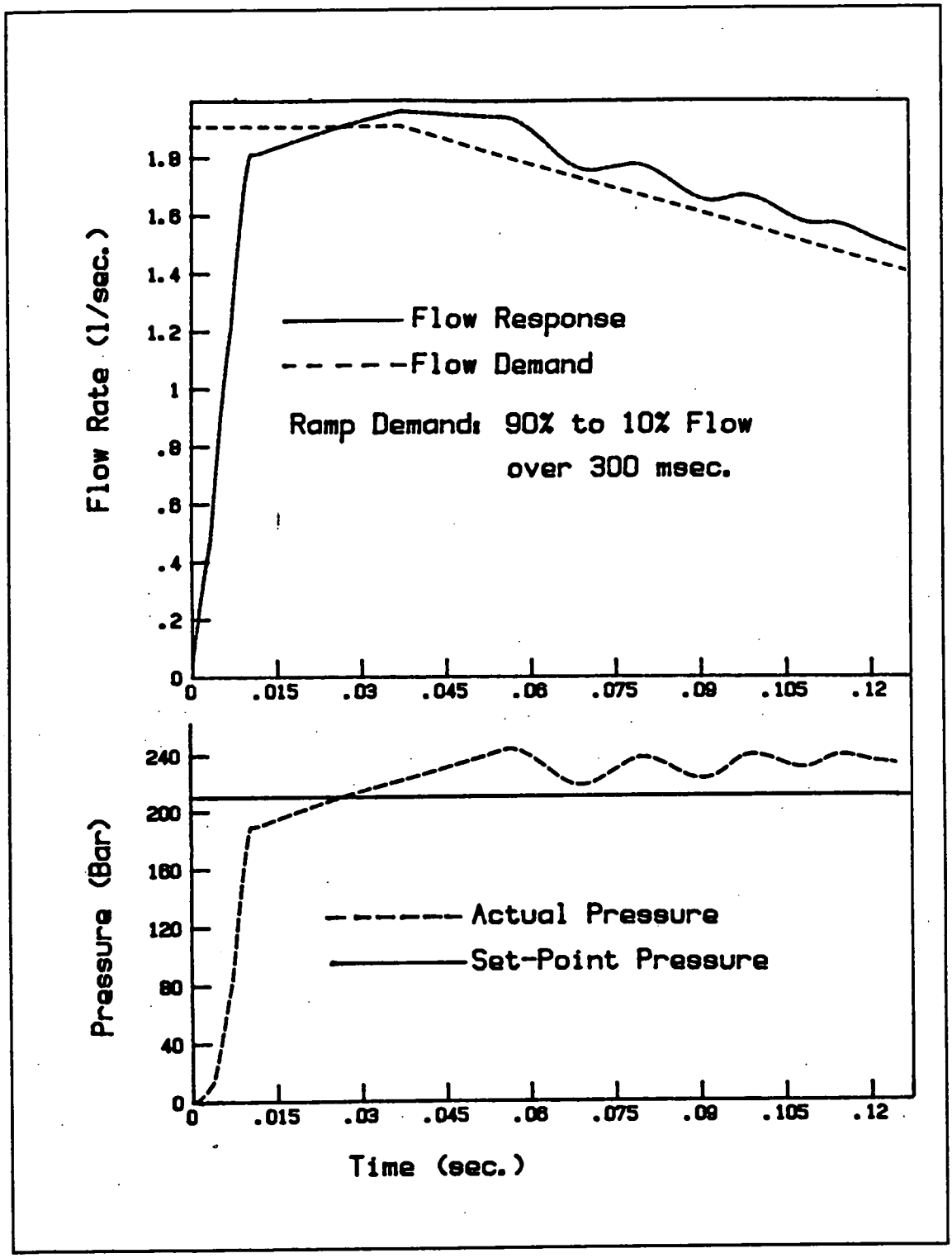

Figure 2.8: Simulation of Constant-Pressure Algorithm Following a Flow Demand Ramping Down at the Maximum Rate of the Sundstrand 22 Pump.

long time but have found use only in restricted markets. The two most obvious reasons for this are first; that they are limited to use as pumps and cannot be operated in reverse as motors, and second; that they are more expensive than their equivalents due to the increased number of components and small scale production. The applications where poppet valves have been exclusively used demonstrates their areas of superiority:

1. Pumping low lubricity fluids, such as water and emulsions:

   The seating of a poppet valve is unaffected by fluid lubricity whereas, on a port-face pump the rotating face must be properly lubricated while bearing heavy fluctuating loads.

2. Pumping poorly filtered fluids:

   The poppet valve seat is much less vulnerable to debris particles than is the fine clearance of the port-face.

3. Low noise applications:

   The inherently well timed poppet valve should open and close when the pressure across it is very low. Port-face pumps have fixed port timing which cannot accommodate changes to such variables as shaft speed and stroke. This timing deficiency results in an average efficiency drop of between one to two percent [17]. This energy is partially converted to shock and noise which is not desirable in applications which are, increasingly, governed by noise restrictions.

The poppet pump has a further advantage, which has carried little economic weight up to the present time, in that it is capable of higher mechanical efficiency than the port-face pump. The reason for this stems mainly from the leakage and shear losses across both the port-face and the swash-plate, though the greater surface area of immersed rotating parts contributes as well. The part-load efficiency of port-face machines is especially poor as the leakage losses past the pistons and the bearing losses remain constant irrespective of load. The digital displacement pump at part-load leaves disabled cylinders unpressurised and their associated bearings unloaded. This carries the secondary promise of extended life for machines running at less than full output.

The cost of producing a digital displacement pump does not look very different from that of a standard poppet valve one. The active inlet valves will be more expensive than their self-acting counterparts but this forms only a small part of the overall expenditure in manufacture. The economic advantages begin to appear when the entire chains of components, required in both types of system, are considered. To control a moving swash-plate electronically, one needs a controller, D/A converter and a servo-valve which, in turn, requires a high standard of filtration to function reliably. The digital displacement pump requires a small control computer, one power semiconductor per cylinder, a once-per-revolution shaft trigger and solenoid controlled inlet valves. The cost differential in these two chains of components should effectively equalise the overall system expense or, in the case of multiple units, reverse the advantage previously held by the swash-plate pump.

3.0 Active Valve Control

3.1 Literature Survey

While the patent search revealed a number of solenoid controlled poppet-valves [18,19,20], none of them displayed anything novel by way of electro-magnetic actuation. The principles of both permanent magnet and electro-magnetic holding devices and actuators are well established. As such there is a great deal of information available in the standard texts on the subject [21]. Perhaps the most accessible of these is a solenoid design text by Roters which, although dated, proved invaluable [22]. The universally accepted reference on permanent magnets is McCaig [23]. His book is also now showing its age, since it pre-dates the arrival of at least one new and important type of magnetic material, but is more than adequate in its coverage of the fundamentals. The one hybrid permanent/ electro-magnetic actuator principle which appeared useful was suggested by the French magnetics researcher Yonnet [24] and was later found described by Sauer in a relay design text [25]. The reference he cites for his hybrid design is his own patent.

Most texts start by developing the governing equations and then finish up by applying them to common examples of magnetic circuits [26]. This is not particularly helpful for solenoid design where it soon becomes evident from the literature that the quantities which are to be calculated are heavily influenced by rule-of-thumb factors introduced to cope with effects such as non-linear saturation of the iron and lost fringing flux [27]. As these constants vary substantially with geometry and, as the chosen valve latch configuration did not correspond closely with any of the examples, the

classical analysis approach was useful only as a guide to comparing magnetic pole configurations.

The equation solving software package, TK!solver [28], proved particularly helpful for investigating and optimising the latch parameters. This piece of software allows the governing equations of any situation to be solved for any of the variables irrespective of the order in which they are listed or expressed.

Once the fundamental configuration of the magnetic latch had been determined, the design process was continued with finite-element analysis packages [29,30] which could produce numerical solutions for almost any magnetic circuit geometry. These were employed, with some success, on the evolving series of valve latches.

3.2 Overview of Valve Control and Latching Requirements

The actuator of a conventional poppet valve is a low rate spring. There are two conflicting constraints on the selection of the spring rate:

1. During the intake stroke the spring should allow the poppet to open easily so as not to constrict the flow nor cause cavitation, and;

2. As the piston nears bottom-dead-centre and the flow stops, the spring should exert sufficient force to close the poppet prior to the start of the delivery stroke.

At bottom-dead-centre the fluid forces on the poppet are very small and the spring is essentially unaided in its attempt to pull the poppet closed [31,32]. The rate restriction on the spring generally means that valve closure does not occur until sometime later. After

bottom-dead-centre the rising piston starts pushing fluid backward through the intake valve and the flow forces belatedly come to the aid of the spring, though in a less than desirable way. The effects of rising cylinder pressure against the exposed poppet head, high flow velocity in the valve seat region and the inertia of the escaping fluid column sum to a massive closing force which accelerates the valve onto its seat. The squeeze film effect, expected with approaching surfaces in viscous fluids, is largely negated by the low pressure around the valve seat region. The net result is a very sudden valve closure and acoustic pressure waves which travel up the manifold and down the cylinder before propagating throughout the system. Valve springs of a higher rate can be used to improve closure, though, at the expense of requiring a positive boost pressure on the inlet side of the pump.

One of the advantages of an electro-magnetic actuator is its controllable force characteristic which can overcome the limitations of a self-acting valve. An actively controlled valve can be positively opened, in order to reduce the risk of cavitation, and positively closed at the correct instant to prevent slamming and attendant fluid-borne noise.

In designing such a device some thought must be given to the method of control. The following options for disabling valves have been considered:

1. Actively latch open and actively close the valve during every cycle.

2. Passively latch open and actively close the valve during each cycle.

3. Actively latch open and passively close the valve during each cycle.

4. Make a latch which is bi-stable, that either functions exactly like a sprung poppet or is held latched open, then actively toggle between states when the system demands a change.

The first option seemed more complex than was necessary as it involved an extra set of coils in each valve. It also had an undesirable fail-safe characteristic, since, if the electrical supply failed, the inlet valves would close belatedly during each revolution so that the pump would be running noisily at almost full output. The third option was discarded as it left the problem of closing the valve on time with a conventional spring. The second and fourth options were considered in some detail as both had advantages in different situations.

A substantial effort was put into the development of the fourth option, the toggling latch, the results of which are presented in Appendix A. At the outset, consideration was being given to a pump consisting of such large numbers of cylinder modules that, the idea of real-time enabling had not occurred. The large ring-cam required response times of such length that it was possible to think of the cylinders simply in terms of enabled versus disabled fractions. Output smoothness was of concern, though this was to be achieved by pre-determined patterns of enabled cylinders for different levels of flow. The toggling latch, in concept at least, allowed the controller to access a given inlet valve and set it into one state or other whenever the need arose for a change. There was also some thought given to the controller mapping failing modules and avoiding them in order to prolong pump life [33].

Three factors led to the discarding of the toggling latch:

1. The large multi-cylinder ring-cam machine development was reduced in priority due to the unfavourable politics of renewable energy research in the mid 1980s and so work concentrated on smaller units with fewer cylinders;

2. Inexpensive real-time controllers had become fast enough to control large numbers of cylinders on a stroke-by-stroke basis, and;

3. Work with the latch prototypes revealed that it was difficult to avoid unintentional toggling due to the kinetic energy stored in the moving poppet which, as the valve opened, pushed the latch past its over-centre point and caused it to latch permanently in the disabled position.

This last problem seemed particularly difficult to overcome as there was a limited amount that could be done to the geometry of magnetic poles to create the abrupt rise in rate needed to provide the magnetic end-stop which separated the two operating positions.

Of the four cylinder control options originally identified, only the passively-latched, actively-closed valve seemed worthy of further development. The operational cycle of a valve, working in this way, can be separated into the following events:

1. The intake stroke of the pump pulls the valve open positively aided by a spring.

2. When the moving pole contacts the end-stop, the valve is latched open and held in the disabled position.

3. During the intake stroke, the controller decides whether or not to enable the cylinder.

4a. In the event of a disabling decision, the controller does nothing and the valve remains latched in the open position throughout the delivery stroke.

4b. In the event of an enabling decision, the controller sends an appropriately timed pulse to the solenoid coil such that the valve closes at bottom-dead-centre prior to the start of the delivery stroke.

From a control standpoint, this principle of operation offered the great advantages of both leaving the valve in a known state midway through the intake stroke and also of requiring only one type of response to be sent.

3.3 The Passively Latched/Actively Closed Valve

The passive and active parts of the valve control latch can be considered, at least initially, as separate entities. The requirements for each function can be specified and these characteristics incorporated into a mechanism. The two magnetic configurations, which have been thus far identified for use in the latch, both have complex interactions between the passive and active functions. This makes their analysis somewhat more difficult than it would be for totally separate systems.

Perhaps the most important characteristic of a latch configuration is the orientation of the lines of flux

between the moving and stationary parts. While the flux needed to create a force in the direction of pole motion must obviously be present, it must also be returned from one body to the other in order to complete the circuit. The return path can be either radial or axial depending upon the desired characteristic of the solenoid. A radial path does not enhance the axial force, but does offer the advantage of restricting the demagnetising effect of the air gap between the poles to its minimum level. A circuit where both flux paths between poles occur in the axial direction offers the advantage of double the tractive pole area though at the cost of twice the air gap, and thus demagnetisation force, as compared to the previous case.

Roters describes an index, based on tractive force and actuation distance, which is useful for deciding which of the above arrangements should be used for optimal performance in a specific application [34]. Once the directions of flux in the circuit have been defined, the positions for the various components, such as permanent magnets and solenoids, can be decided.

In the case of the poppet-valve latch there seemed to be two possible component layouts:

1. One with a moving magnet and stationary solenoids, following the principle used by Sauer and suggested by Yonnet, which offered the possibility of force amplification due to the flux contribution of the permanent magnet, and;

2. A latch with both a stationary permanent magnet and solenoid which had a soft-iron moving pole.

Both types of latches were designed and tested in pumps during the course of this work. While the latter arrangement was found to be most useful for poppet valve actuation (and will be discussed in some detail in succeeding sections of the chapter), the moving-magnet work provided some useful insights which will be summarised in the following section. As this is included for the sake of completeness, the reader is advised that there are large leaps from theory to hardware description. The intervening design steps will be dealt with in greater detail for the second moving-iron configuration.

3.3.1 Moving-Magnet Latch Configuration

On the advice of J.P. Yonnet, the possibility of making a latch with a combined permanent-magnet and solenoid system, similar to that shown in figure 3.1 was investigated. At the outset this looked especially advantageous since the permanent magnet served to boost the flux levels, prior to the application of the solenoid, which greatly enhanced the forces on the moving pole. Several versions of this latch were designed, made and installed in pumps. A general arrangement drawing of a valve for a MacTaggart Scott RHP radial pump is shown in figure 3.2. These latches did function satisfactorily in short-term tests but were subject to several compromises which ultimately led to their rejection:

1. The moving-magnet latch configuration lends itself primarily to symmetrical applications, while the valve demanded an asymmetric characteristic. To achieve this asymmetry the valve end-stops were positioned so that the moving pole was able to approach the lower pole much more closely (when the valve was latched fully open) than the upper solenoid pole (when

COMBINED MAGNETIC SYSTEMS

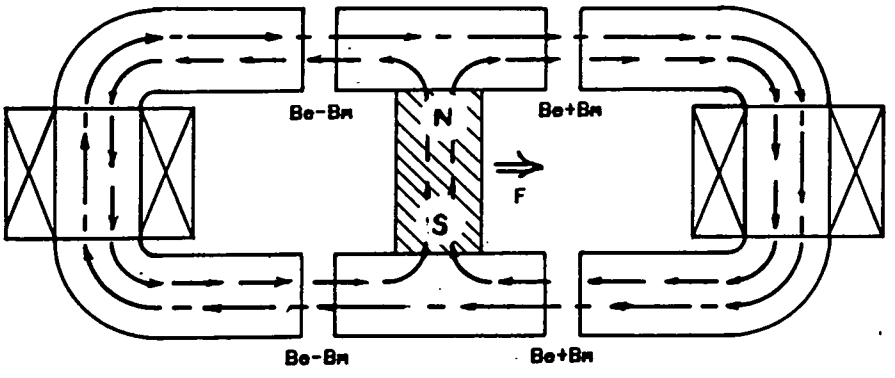

Where Bm= flux density of inner circuit created by permanent magnet.
Be= flux density generated by energised solenoid coils.
A = pole area
μ_o= permittivity, for air $\mu_o = 4\pi \times 10^{-7}$ in SI units

As long as Be $\geq$ Bm then

$$F = \Sigma \left[\frac{B^2 A}{2\mu_o} \right] = \frac{A}{2\mu_o} \left[2(B_m+B_e)^2 + 2(B_e-B_m)^2 \right]$$

$$F = \frac{A}{\mu_o} \left(2B_m^2 + 2B_e^2 + 2B_m.B_e - 2B_m.B_e \right)$$

$$F = \frac{2A}{\mu_o} \left(B_m^2 + B_e^2 \right)$$

now say Bm=0.5 Tesla and Be=0.5 Tesla

then $F = \frac{A}{\mu_o}$

if Bm=0 i.e. no permanent magnet in the circuit.

then $F = \frac{A}{2\mu_o}$ or 1/2 that of the permanent magnet circuit.

Figure 3.1: Principle of Combined Permanent/Electro-Magnetic Bi-Stable Latch.

the valve was closed). This had the effect of lengthening the air gap over which the solenoid had to operate, thus rendering it substantially

less efficient than it might have been in a symmetrical arrangement. It also meant that the valve was bi-stable and would stick in the closed position as well as the open one. The passive force from the permanent magnet, which held the valve closed, could be made small but only at the expense of a longer air gap.

2. There was the practical problem of magnetising the ring magnet with a radial field orientation. As the flux density levels required to magnetise the hard magnetic materials are considerably higher than the saturation limits of soft magnetic materials (such as iron), air cored coils must be used for this purpose. Since these coils are too large to insert into the centre of the magnet ring, the annulus needed to be made of small, mutually repulsive, segments. While these were easily magnetised, they proved difficult, in practice, to assemble.

3. The final problem was caused by the poor mechanical properties of most magnetic materials. Manufacturers are generally unwilling to quote these in order to discourage designers from using magnets as stressed components [35]. If magnets are mounted on a moving pole, which is subjected to large shocks during the closing and opening of the valve, then the fatigue properties of the material must either be known or found. They do not appear to be known. Finding them out for an indefinite life application is a long task, and one which would appear to be unnecessary given that an alternative configuration was available.

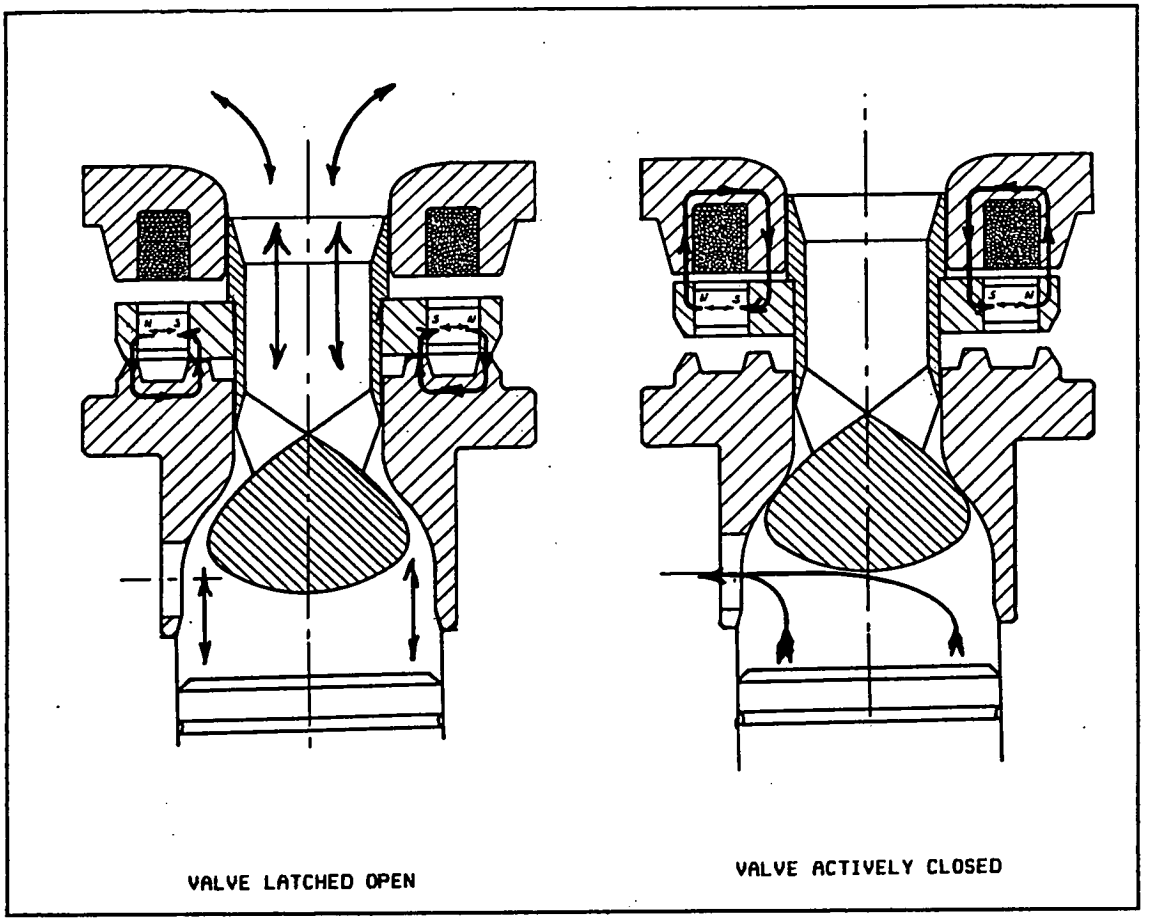

Figure 3.2: Moving Magnet Latch, as Employed in MacTaggart-Scott RHP Pump, in Both Limit Conditions.

The finite-element analyses and experimental work carried out on the moving magnet configuration has been summarised in Appendix B.

3.4 The Moving-Iron Latch Configuration

The moving-iron latch, as used to control poppets, can be reduced to its two separate mechanisms and their associated functions for the purposes of discussion and analysis. The first requirement of the latch is that it should attract and passively restrain the valve in the open position, while the second is that it should

actively close the valve upon receipt of an electrical pulse.

3.4.1 Passive Latches

To hold the poppet open against the return flow during a disabled delivery stroke, a passive force can be created either with the use of a mechanical spring or a permanent magnet latch.

Mechanical springs are not appropriate for two reasons:

1. They have a linear rate so that the holding force in the open position is bound to be lower than the force exerted by the spring on the poppet while it is in the closed position. The inverse effect would be desirable. This can be achieved with an over-centre configuration but not without the addition of pivots, which are unwelcome sources of both wear and side loading.

2. The actuator will have to survive more than a billion cycles over its lifetime so, with mechanical springs, fatigue becomes an important concern.

Permanent magnet holding circuits have a force to deflection relationship which follows an inverse-square function, a much more suitable characteristic for valve retention. Magnetic springs are also unaffected by fatigue and so are capable of indefinite life. The final property of such circuits, which made them appealing, if not easily analyzed, is that the magnetic flux can be turned off or redirected when a solenoid coil is incorporated into the magnetic circuit. The arguments for their use over wire springs seemed unassailable.

Roters suggests that the most suitable configuration for a holding circuit, to latch the open poppet, is that of the flat-faced armature [36], where the permanent magnet is located in one of the poles and drives flux through the circuit and across two small air gaps as shown in figure 3.3.

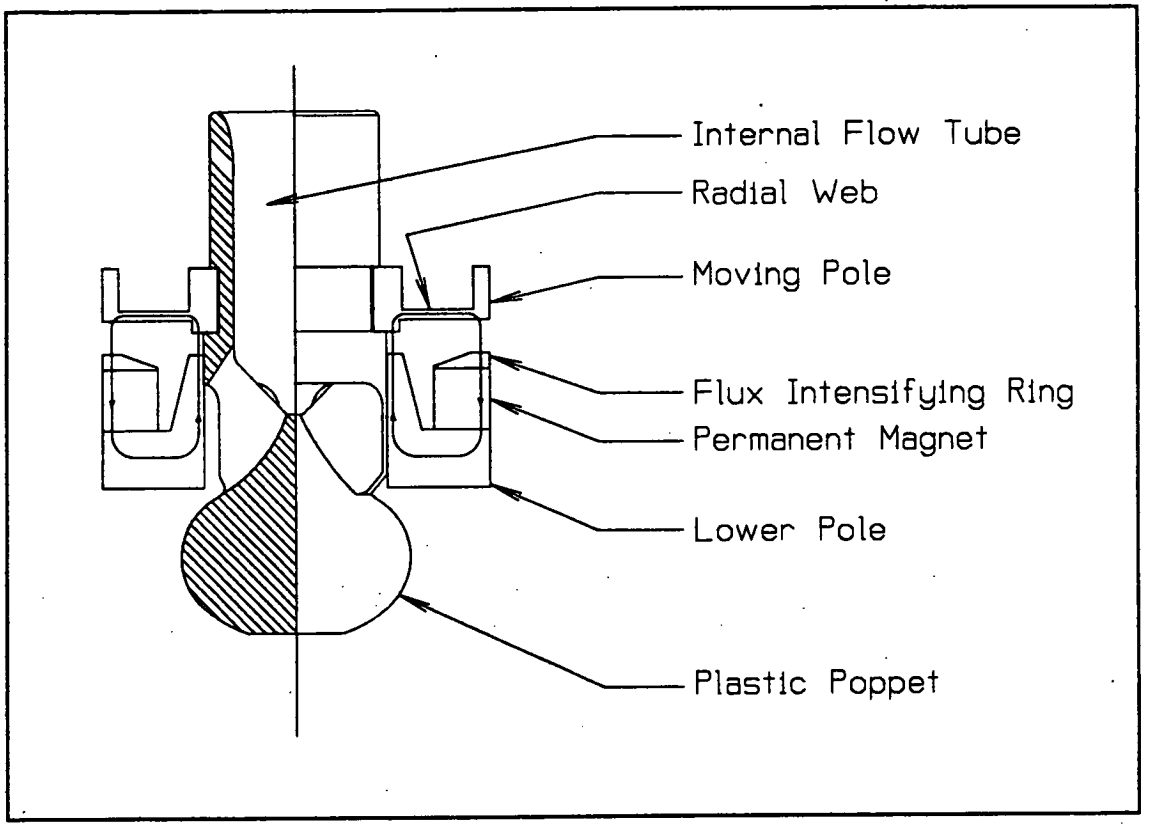

Figure 3.3: The Passive Component Layout and Flux Path of the Moving-Iron Latch.

Inspection of equation 3.1, which defines the attractive force between poles, should demonstrate the merit in concentrating the flux through intensifying pole-pieces made of magnetically soft iron, as in figure 3.3. Flux concentration becomes unprofitable when the level of saturation in the iron offers sufficient resistance to the permanent magnet such that the magnet is pushed down its operating line and the flux density reduced. The most effective latch can be designed only through

$$F = \frac{\beta^2 A}{2\mu_0} \qquad (3.1)$$

Where: F = *Force between poles (N)*
β = *Flux density (Tesla)*
A = *Pole area (m^2)*
μ_0 = *Permeability of free space*

optimisation of the various competing latch dimensions with respect to holding force.

3.4.2 Permanent Magnet Materials

There are four important classes of permanent magnet material [37,38]: iron alloy types (such as Alnico), ferrites, rare-earths (such as samarium-cobalt) and neodymium-iron-boron. The iron alloy types are not particularly suited to applications where the geometry varies since they are highly permeable and easily demagnetised. The other three types share the same type of linear flux/demagnetisation relationship and are difficult to demagnetise as a result. The ferrites have too low a flux density to be used in hydraulic machinery, where space is at a premium. Neodymium magnets have been severely limited in their application by operating temperature restrictions. Not only are there difficulties with large variations in magnetic properties over the operating temperature range of common hydraulic fluids but, in addition, these materials suffer irreversible magnetisation losses at the upper bounds of this range, i.e. 100 degrees Celsius. The extremely reactive nature of this type of material makes it unsuitable for immersion in corrosive fluids (like water), unless it has been protectively coated. As the coating increases the cost, the economic advantage of the Neodymium material over the Samarium-Cobalt type is effectively negated. The temperature restrictions make this material an unlikely choice for use in hydraulic applications at the time of writing.

Two forms of Samarium-Cobalt material are available: the first is a hard non-corroding sintered metal which has both a high flux density and a broad operating temperature range, while the second is a low-cost bonded material made by combining the discarded machining residue of the first type with a plastic resin. This bonded material has approximately twice the holding capability of the ferrites on a volumetric basis, is unaffected by common hydraulic fluids, has an adequate temperature range (stable to 100° C) and can be moulded or machined into rings. This would seem to be the material of choice, though it is quite conceivable that, in a very limited space, the sintered material would be used instead.

3.4.3 Active Valve Control

While it would be wrong to suggest that a solenoid coil is the only means of generating a mechanical force/motion from an electrical input, in this case, where the valve displacement was beyond the practical range of piezo-electric and magnetostrictive devices and not into that served by linear-motors and ball-screws, it seemed the only choice.

By calculating the index number described by Roters, based on the square root of force divided by displacement, the optimum solenoid configuration could be identified. When typical valve openings and holding forces (as determined in chapter 4) were used, the index fell firmly into the region occupied by the flat-faced plunger solenoid [39]. Other configurations were possible but this was certainly the most efficient in terms of space and operating power.

The one argument against this configuration was also convincing: A plunger type of solenoid will always have

magnetic flux transmitted radially across the sliding bearing surface between the plunger and the fixed pole. In the presence of hydraulic fluid, carrying minute debris, this field will attract the ferro-magnetic particles into the bearing. Since pumps are often required to process fluid prior to fine filtration (unlike control valves), the plunger configuration is effectively discounted in this application. It is possible to consider the use of debris excluding diaphragms but this is not a desirable solution for several reasons. The diaphragms would almost certainly add to assembly difficulties, they would be subjected to fatigue loading and their motion would displace fluid and so reduce the valve response.

While Roters predicts that the flat-faced armature solenoid is about 30% less volumetrically efficient at the same index number, it does solve the debris problem associated with the plunger configuration. The flux path through the moving pole is entirely axial and well away from the sliding bearing of the poppet. For this reason the flat-faced configuration was adopted over the plunger type.

When the solenoid is enabled it acts against the permanent magnet of the passive latch in two ways. While the solenoid creates an attractive flux path between itself and the moving pole, as might be expected, it also increases the flux density in the moving pole. The permanent magnet, in trying to drive a flux path requiring a higher demagnetising force, is pushed down its operating line and its flux density reduced. This interaction between circuits makes it impossible to analyze the effect of the solenoid on the moving pole in isolation.

3.4.4 Dynamic Latch Behaviour

The forces on the moving pole vary with respect to both position and time. The permanent magnet force drops rapidly as the pole moves away (and the operating point of the magnet drops to increasingly low flux densities) while the solenoid has progressively less air gap across which to push its flux. There are also dynamic effects. The moving pole is a conductor with a velocity in a magnetic field. It is also a single shorted turn in what amounts to a transformer. Both of these effects generate current in the moving pole and have the dual result of both absorbing power and resisting the closing motion. Radially slitting the moving pole substantially reduces these effects.

Once the valve is in motion, the closing forces acting on it increase progressively so that the valve will always close once it detaches. This important characteristic obviated the need to delve into the difficult area of transient solenoid response.

The possible benefit of creating a dynamic model of the valve lay in the forecasting of its actuation time. Such a model, if it were to be created, would have to combine the non-linear electro-magnetic effects of the latch with damping effects in the latch cavity, the inertial effects of the valve and its added hydrodynamic mass, and, finally, the flow forces of the non-steady flow created by the harmonic motion of the piston acting in a duct whose geometry varies with time as the valve closes. In practice, the determination of these closing times from experiments, with actual valve hardware, proved adequate for the immediate requirements of the pump control algorithms.

3.5 Initial Modelling of the Moving-Iron Latch

If the effect of pole fringing is incorporated into a constant, then the equations pertaining to both the attractive force between poles (equation 3.1) and the driving of flux across air gaps (equation 3.2) can be used to evaluate the holding force of a latch of known geometry.

$$NI_{gap} = \frac{l * \beta}{\mu_0} \qquad (3.2)$$

Where: NI_{gap} = *resistance of gap (Ampere-Turns)*
l = *length of gap (m)*

A third equation, that describing the permanent magnet flux density relative to the demagnetisation force of the magnet (commonly known as the B-H curve), must be incorporated to determine the operating point of the magnet. For a material such as Samarium-Cobalt, with a linear flux density/demagnetisation relationship, equation 3.3 can be applied:

$$\beta_m = \beta_r \left(1 - \frac{H_m}{H_{sc}}\right) \qquad (3.3)$$

where: β_m = *magnet operating flux density (Tesla)*
β_r = *remanent flux density*
H_m = *demagnetising force (A/m)*
H_{sc} = *coercive magnetising force*

The demagnetisation force of the soft iron in the circuit is small relative to that of the air gaps, as long as the flux densities remain below saturation levels, and so the bulk of the iron path is not included in the modelling equations. One particular location, the radial web in the moving pole, is designed to become saturated when the

solenoid is turned on and must, therefore, must be included in the model.

The program TK!solver can be employed to solve this set of simultaneous equations for moving-pole force. It also facilitates the variation of latch dimensions in order that the sensitivity of the force on the moving-pole to each of them can be evaluated. The non-linear BH curve of the steel can be incorporated into TK!solver as a user-defined function (a look-up table with linear interpolation). When the equations are solved, with a Newton-Raphson technique, the forces on the valve, both when latched and at the instant when the solenoid is turned on, can be calculated. The modelling equations, variables and a sample graph, showing optimisation of the web thickness, are presented in Appendix C.

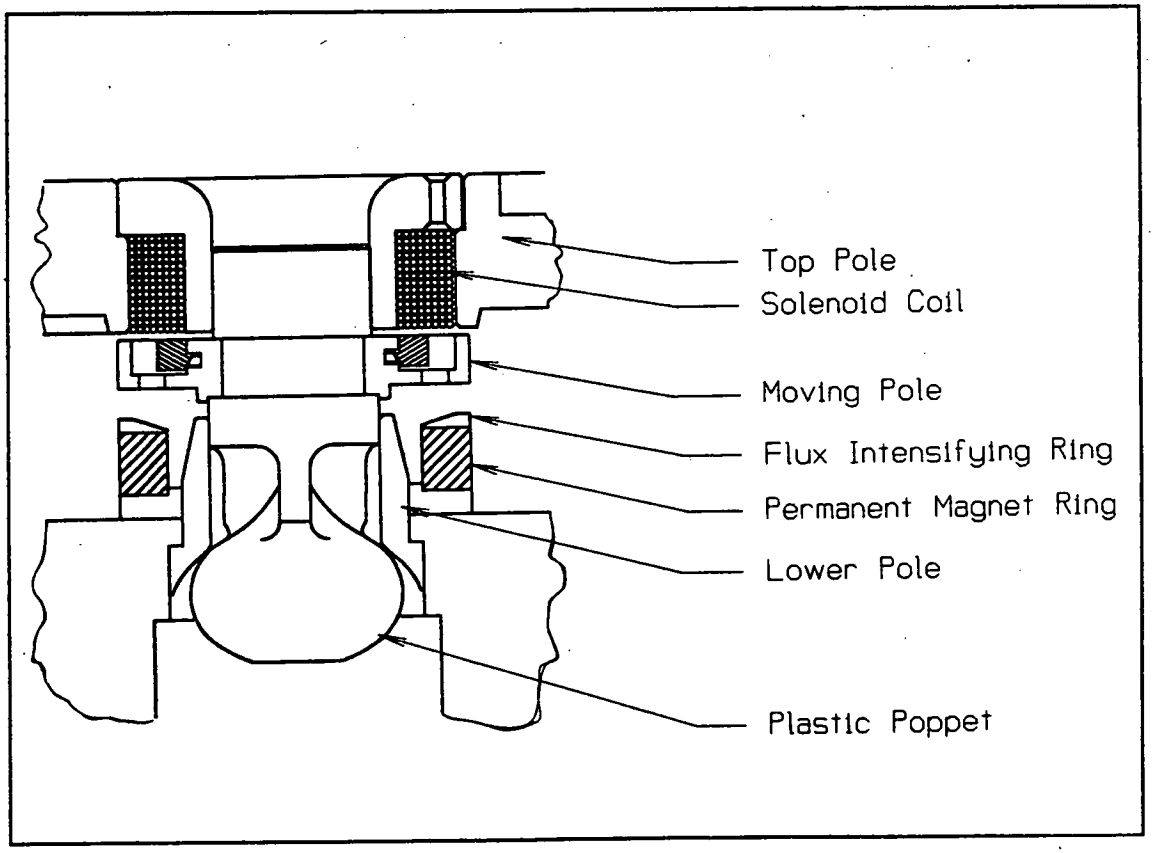

Figure 3.4: Component Layout of the Moving-Iron Latch.

The difficulty with using the forces calculated from these equations, for anything other than comparative purposes, is that they rely on a constant for flux leakage which can only be guessed within a factor of two [40]. As such the results have been used primarily as a way of proportioning a latch within a specified space. The end result of this exercise is a latch of the configuration and proportions shown in figure 3.4.

This analysis revealed some interesting effects:

1. By varying the web thickness an optimum could be established. The web cannot be so thin as to saturate with the permanent magnet alone, nor can it be thick enough to escape saturation when the solenoid is turned on.

2. If the solenoid current was applied in the reverse direction then the flux across the web would decrease to zero and the bulk of the flux would circulate around the periphery of the circuit in figure 3.4 such that the permanent magnet would be increasingly magnetised by the solenoid. This would push the magnet up the operating curve so that it pulled harder on the moving pole. The pole would move if sufficient current was applied, but only once the solenoid pushed enough flux through the web so as to create an unbalanced upward force on the moving pole. For this reason A.C. excitation of the latch will not work.

3.6 Finite Element Analysis of Magnetic Latch Circuits

3.6.1 Overview of Modelling Difficulties

Finite element modelling of the latch geometry can overcome both of the deficiencies of the previous crude model. It can deal with both the progressive iron saturation throughout the circuit and also the flow of flux along unseen and undesirable paths. There are difficulties with the technique as well, although these are caused more by the current limitations of computers and modelling packages than by the actual method:

1. Frequently, optimisation of the model geometry is necessary rather than simply an analysis of a given geometry. While there are optimisation routines designed for this purpose, they are not really flexible enough to be employed, since changes often disturb the element pattern to the extent of producing extreme element proportions. As a result, the process of magnetic circuit optimisation requires frequent manual adjustments to be made to the mesh as the geometry is varied. The relatively simple axisymmetric models employed here, of approximately 1500 elements, took twenty minutes in solution on a 386 micro-computer. While this may not seem long, it greatly lengthens the time required for a complex design to converge into a near optimal form.

2. For a finite-element solution to be accurate, forces must only be determined in a linear material such as air. This means that a moving pole must always be surrounded by an air boundary. This prevents a solution from being calculated at the actual point of interest,

i.e. when the valve is latched and the moving pole is in contact with the static one. While it should be possible to extrapolate back to this position, using several solutions at other points along the valve trajectory, in practice the force curve becomes almost asymptotic (in the case of the passive latch) and is difficult to accurately predict at the zero-crossing.

3. The small air gaps invariably required in the circuit, at or near the geometry of greatest interest, coupled with the radical changes in magnetic properties across material boundaries, dictate the use of meshes with a great range of element sizes in order to keep element aspect ratios within acceptable bounds. While adaptive algorithms may soon be available to achieve this, currently a model must be modified over a series of iterations to arrive at an acceptable mesh.

4. The calculation of forces with the finite element technique is prone to inaccuracy due to the summation of forces from the squares of flux density values which are, themselves, averaged across individual elements along a defined path. The success of this method is particularly reliant on the use of fine meshes in areas of high flux density. A second method, based on virtual work and the total energy of the system, is less sensitive to errors caused by slightly coarser meshes but involves double the computation since the moving pole must be perturbed slightly between solutions. The perturbation must be large enough to produce a distinct effect on the overall system energy, yet sufficiently subtle

to avoid destroying the geometrical relevance of the model. Since both methods are fallible in their own way, it has been suggested that they be used together in order to establish confidence in the model [41].

5. Finally there are the limitations of individual finite element packages. ANSYS 4.4 has a magnetics capability, but this is little more than a modified version of its thermal solver. Some of the commands must be used in ways not initially intended, which can result in errors and confusion. Other requirements, such as using nodes in the mesh as points along the path of integration for force calculation, create a major burden during the process of mesh generation since, in some cases, nodes must be strategically placed midway across very fine gaps. Vector Fields PE2D [42] is a specialised magnetics package, which is much easier to use for this type of analysis. It does not suffer from the node placement problem of ANSYS but it has very limited force calculation capabilities and no provision for creating sub-models.

3.6.2 Definition of the Geometry for the Finite Element Model

A finite-element model was created for a valve latch which was designed to fit into an existing Towler A-series axial piston pump unit. For this reason there was a restriction on the overall latch diameter, since the six valves had to fit around a small pitch circle. The second constraint on the radial pole dimensions was the requirement of equivalent areas for the inner and outer

pole to ensure that the flux densities were kept as uniform as possible within the steel.

The axial dimensions of the latch were kept as short as possible in order to retain as many of the pump's original pieces as possible. The magnet length was determined by the requirement of the valve self-opening. The gaps between the moving and static poles were determined by the valve opening and the need for pole stand-offs at each end-stop. This latter requirement was due to the squeeze film damping of the approaching surfaces and the desire to reduce the slope of the latching force curve at the point of pole contact. The axial length of the moving pole was largely determined by the fastening arrangement which secured it to the poppet. The solenoid coil was given an almost square section on the basis that it both reduced flux loss to a minimum and that, due to its pulsed operation, it could be operated at much higher current density levels than would be normally acceptable (due to heating). The axial length of the iron above the coil was determined both by the need to maintain an even flux density around the solenoid's iron path and by the flow requirement of a rounded entry to the poppet duct.

The required latching force was determined from the equation derived in chapter 4 for flow forces. The only variable which remained undefined in this equation, following the pump hardware selection, was that of valve opening. The determination of the valve opening involved trading off the increased flow losses and forces of small openings against the decreasing magnetic efficiency of the circuit at large ones. Both of these effects follow inverse square laws, though in the case of the magnetic latch this was only true if all of the pole dimensions were held constant despite the change in opening range. This would not represent an optimum design since

differing amounts of flux will be present in the latches at different starting points. Optimisation at any opening would involve altering such dimensions as moving-pole web thickness or the permanent magnet pole area.

In practice, other factors will determine the choice of valve opening. Perhaps the most important limitation on large openings is that, as holding forces drop, other effects, such as coulomb friction and squeeze-film damping, begin to dominate the closing force requirement of the valve. Since these effects are greatly influenced by such diverse things as wear, fluid viscosity (operating temperature), assembly tolerances and the ingress of debris, it seems that the closure of an enabled valve might become much less certain than would be desirable if the opening was large and the solenoid enfeebled.

The difference between the latching force of the permanent magnet and the net force generated by the solenoid must therefore be high enough to cope with the sum of these effects. This will effectively define the allowable opening, since the desire for low flow force and loss will tend to increase valve opening until another constraint is met. While the travel time of the valve in closing must also be considered, in practice it changes only slightly over the ranges in question (as discussed in 3.4.4). Such variations can easily be accommodated by the controller through adjustments in pulse timing.

Dimensions, such as moving pole web thickness, permanent magnet thickness and passive latch pole areas, were taken initially from the TK!solver model and then varied for different solution runs. Optimums were found for each dimension such that latching and take-off forces were

maximised. For the reasons noted in section 3.6.1, this was a very labour-intensive process.

3.6.3 Finite Element Model and Experimental Results

The magnetic circuit model was produced through a sequence of operations in different engineering software packages on a personal computer. The first stage involved the creation of the two dimensional axisymmetric latch geometry using CAD software (Fastcad). The resulting DXF file was then translated by a utility into a solid model (ANSYS) and completed through the conversion of lines and points into areas which could then be meshed into elements. Once the additional requirements of material property tables, boundary conditions, load steps, solenoid current densities and convergence criteria were specified, the model was submitted to the solver (which used a Newton-Raphson convergence algorithm).

An example of the meshed model is shown in figure 3.5. It should be evident that the mesh is particularly fine in the area of the narrow gap separating the moving pole from the lower pole piece. This was necessary to ensure that the air elements in the gap were not of extreme aspect ratio. The mesh density follows a gradient, such that it becomes more refined near the centre of revolution, as is required to achieve an accurate solution for an axisymmetric problem [43].

The models used multiple load steps, as is advised for solutions incorporating non-linear materials [44], and generally converged to a set limit after eleven iterations. The validity of the mesh and consequent solution can be gauged by examining the plots of flux densities, taken across radial trajectories in the air gaps below and above the moving pole, for conditions of

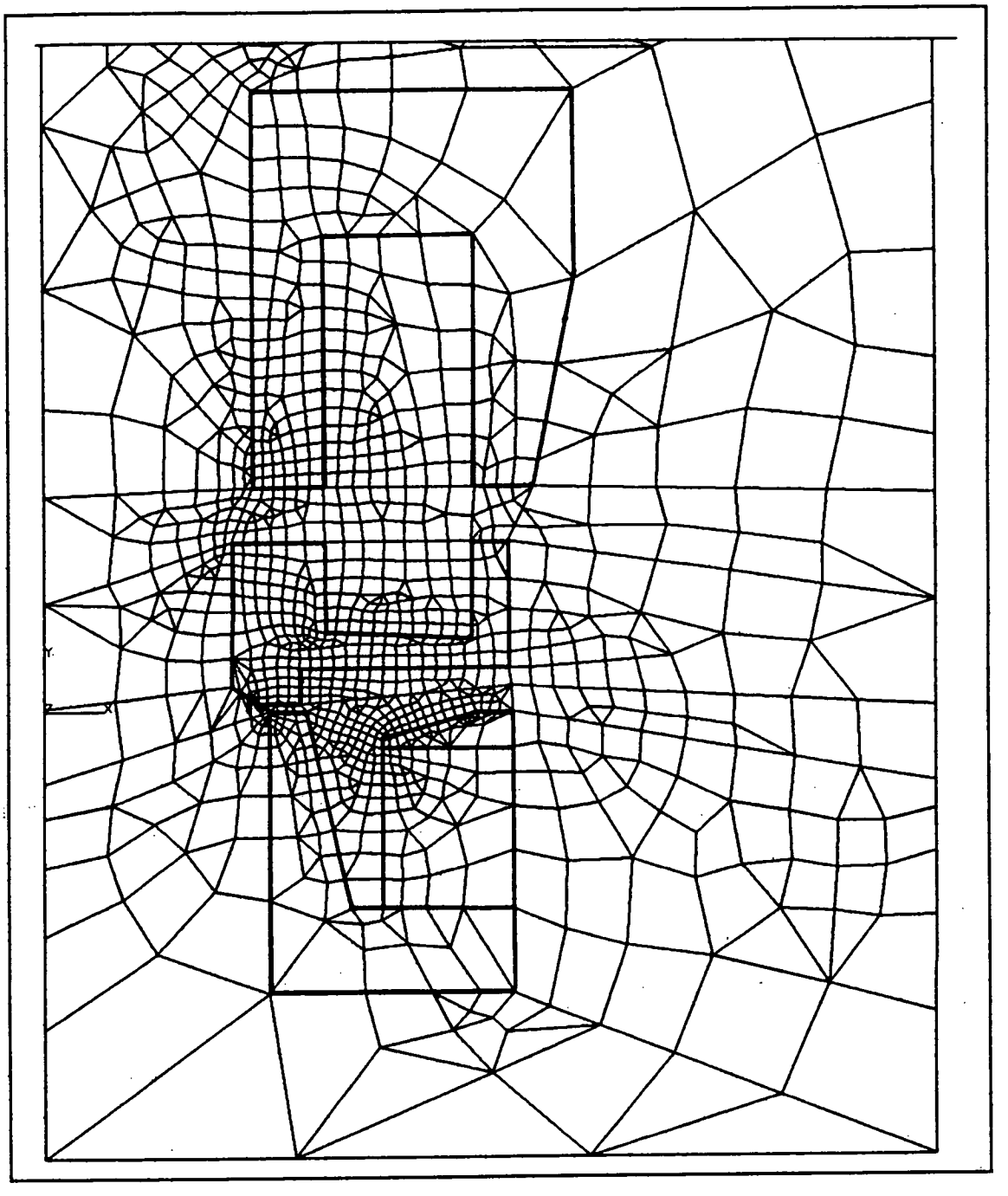

Figure 3.5: Element Plot of Axisymmetric Finite Element Model of Moving-Iron Latch.

both the solenoid enabled and then disabled. These, shown in figures 3.6 and 3.7 respectively for the solenoid active case and figure 3.8 for the lower pole in the disabled case, show reasonably smooth curves which confirm the choice of mesh density (the upper path is

effectively at zero flux density with the solenoid off and is, thus, of little interest).

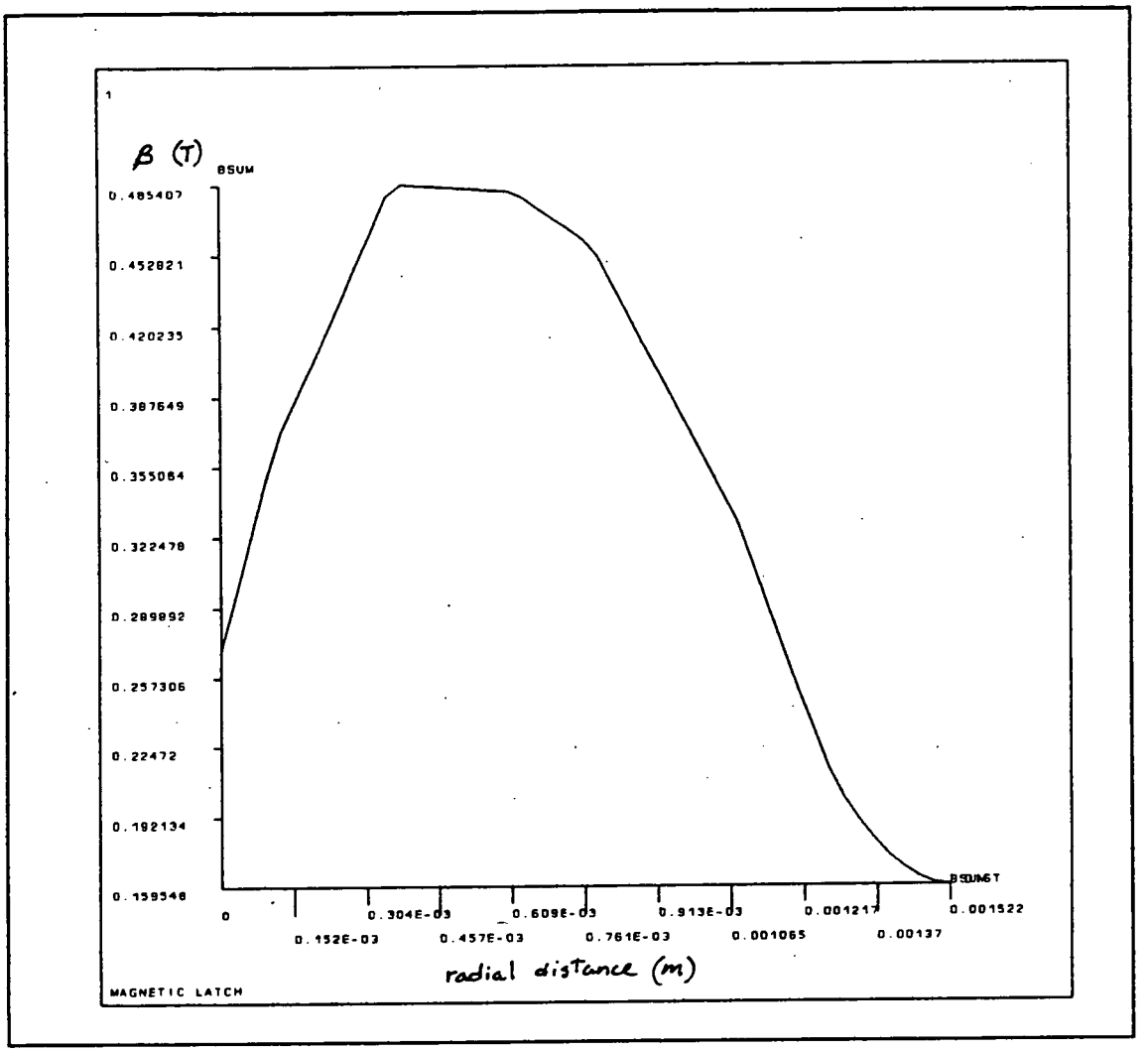

Figure 3.6: The Flux Density Along a Radial Path Between the Moving and Lower Poles with the Solenoid Enabled.

A second check on model validity was made by further refining the mesh. The Maxwell-tensor force calculation differed by one percent between the two solutions, indicating that the original mesh was adequate.

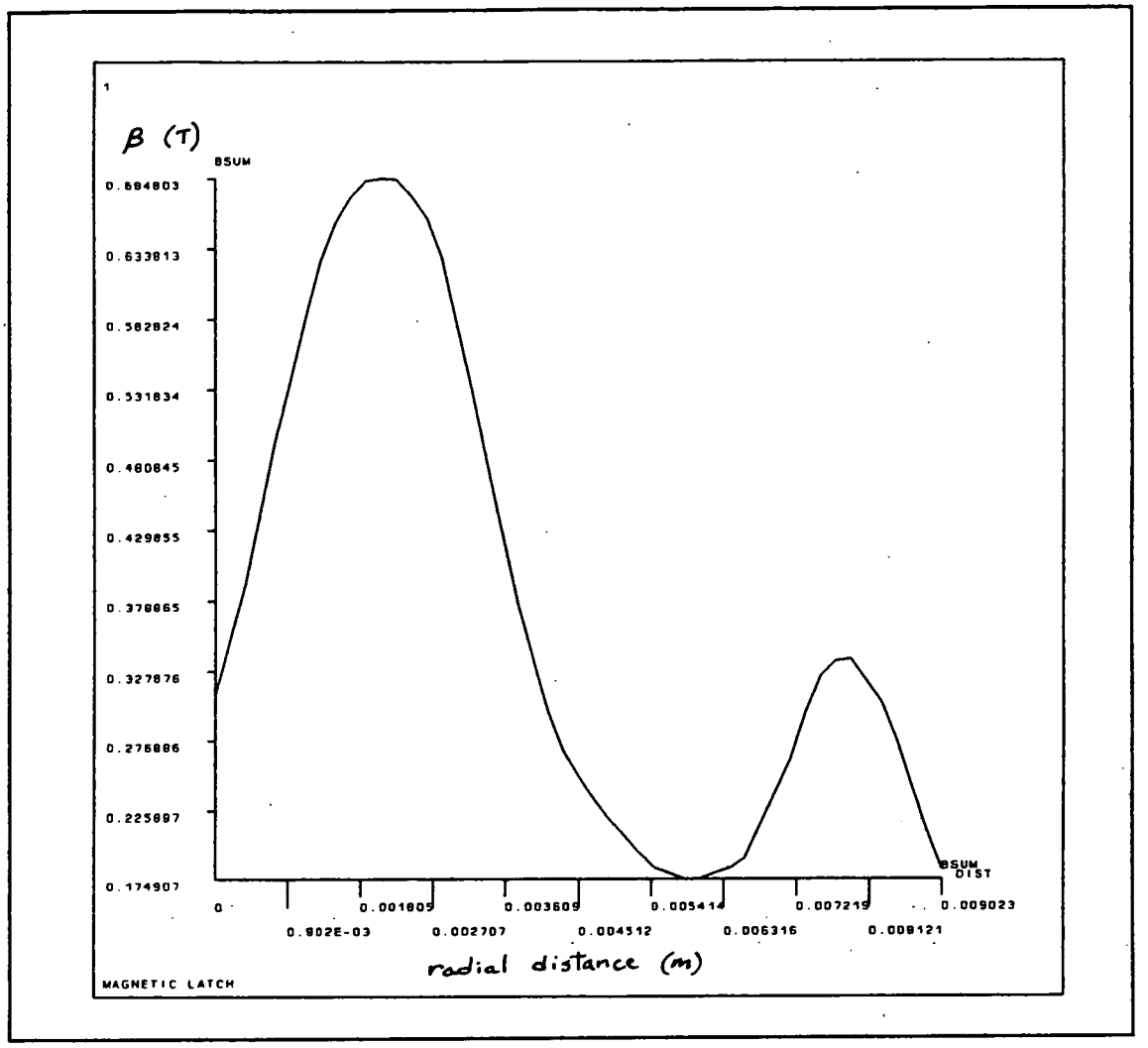

Figure 3.7: The Flux Density Along a Radial Path Between the Moving and Upper Poles with the Solenoid Enabled.

The resulting solution with the solenoid disabled is shown as a contour plot in figure 3.9 and, also, as a vector plot in figure 3.10. The vector plot is most useful in demonstrating the flow path of the magnetic flux while the contour plot gives a very helpful indicator of areas within the magnetic circuit which are more highly saturated than necessary.

Three methods of force measurement were used such that the results could be compared. These were:

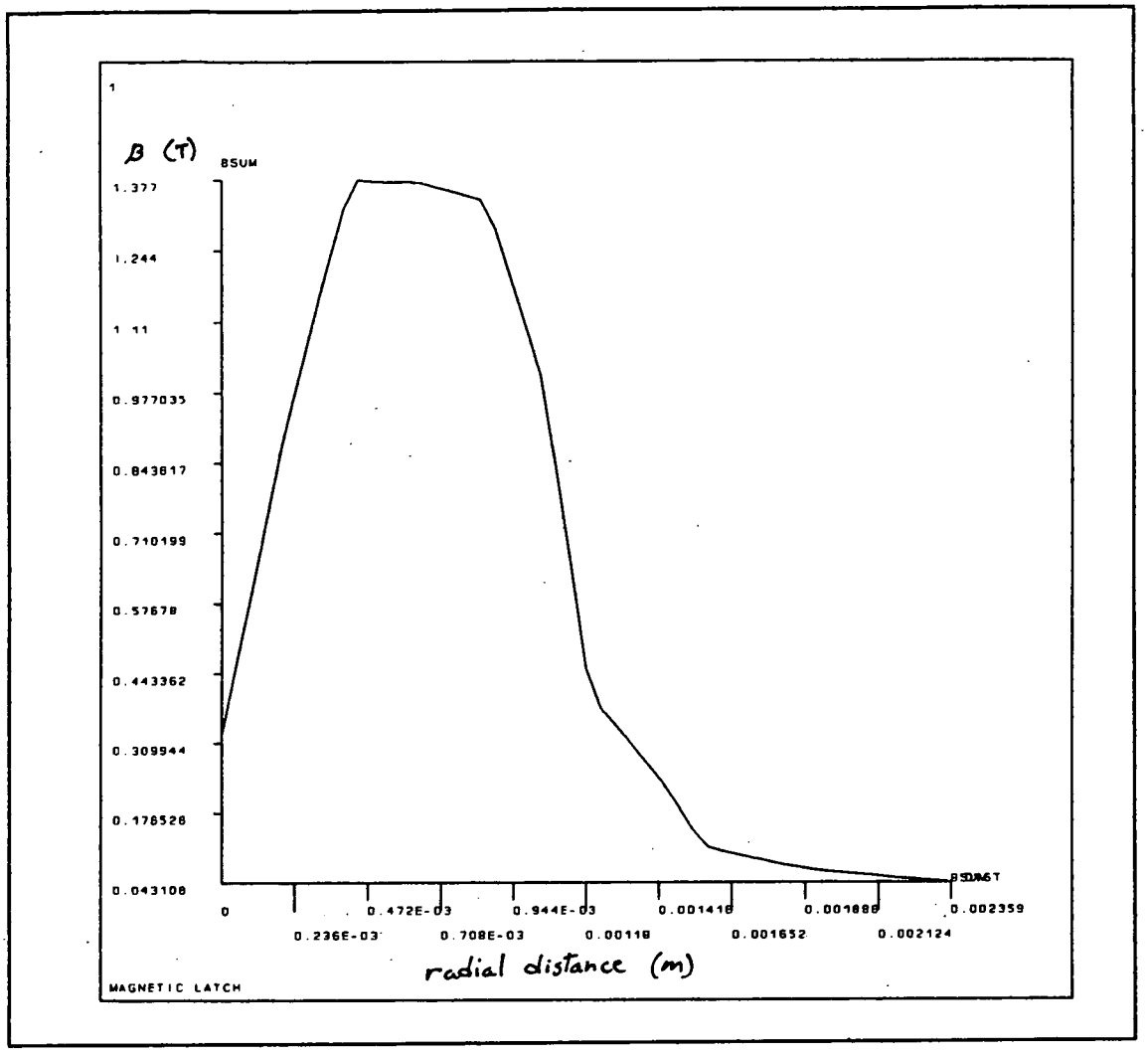

Figure 3.8: The Flux Density Along a Radial Path Between the Moving and Lower Poles with the Solenoid Off.

1. A Maxwell stress tensor method which calculated the sum of flux density squared along a path which was defined in terms of nodes in the mesh.

2. A Maxwell stress tensor method which summed the square of the averaged air element flux densities acting around the boundary of the moving pole.

3. A virtual work method in which the overall system energy for two model geometries is

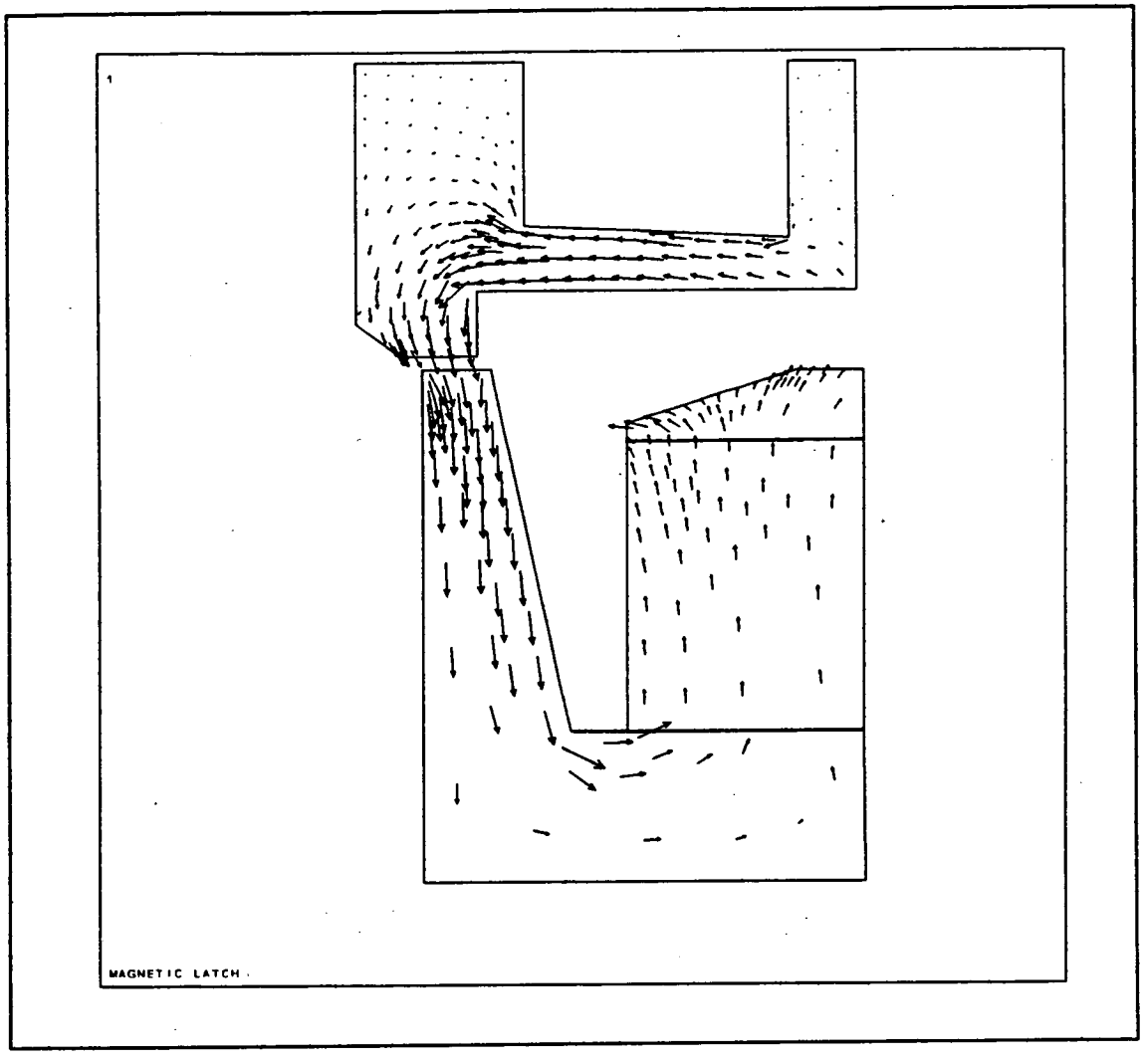

Figure 3.9: Vector Plot of Flux Density in the Passive Latch with the Solenoid Disabled.

calculated, with the second solution having the moving pole slightly displaced from its original position. The force is then calculated with the equation W=F*D.

For the passive latch solution, all three methods produced values within ten percent of one another at one particular pole position. The result of a series of solutions, ranging over the trajectory of the pole, is shown in the force/displacement curve of figure 3.11.

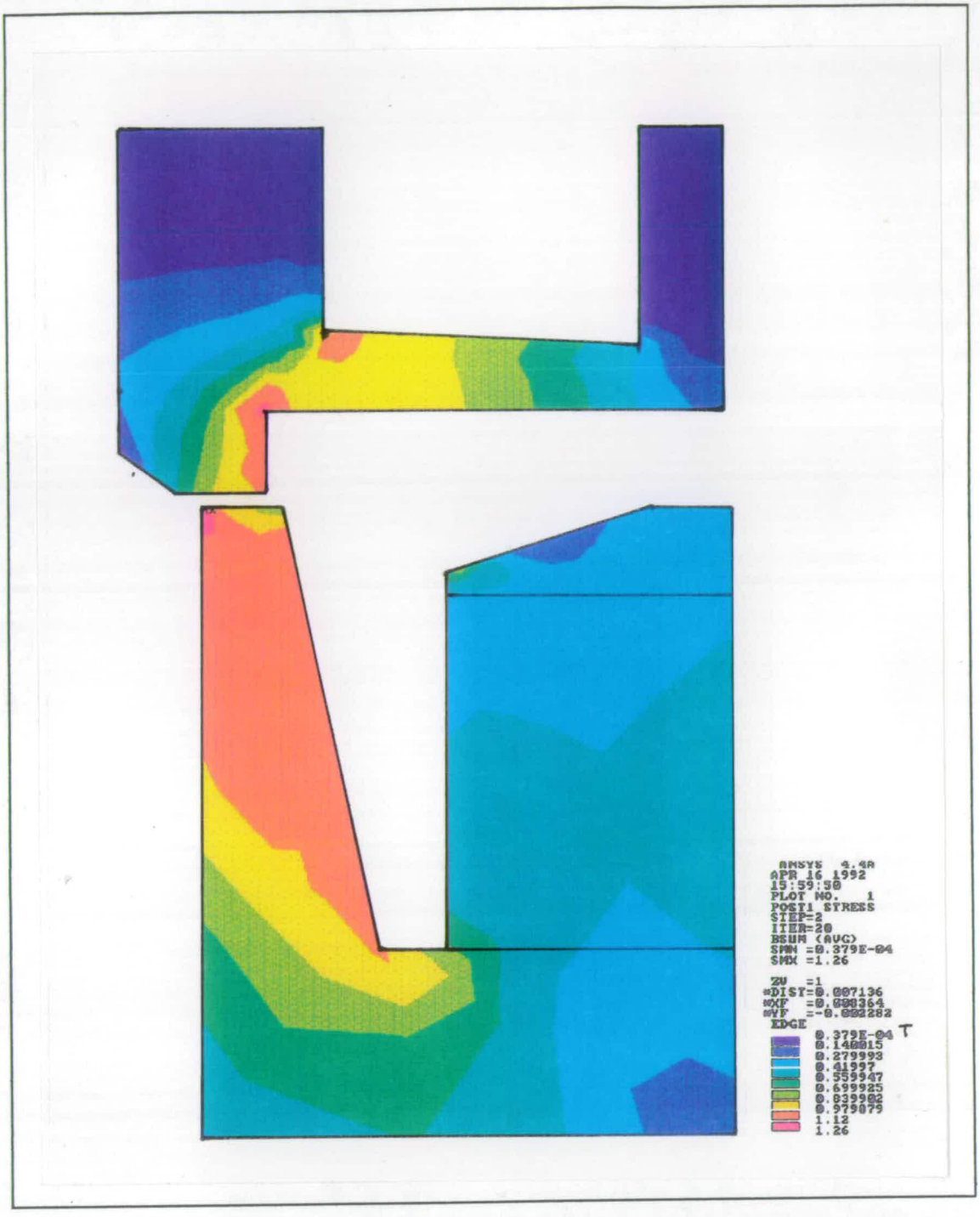

Figure 3.10: Contour Plot of the Flux Density in the Passive Latch with the Solenoid Disabled.

To test the accuracy of these predictions, a test latch of similar dimensions was constructed and a comparable set of measurements made and plotted. The piezo-resistive force transducer was calibrated by dead weight.

It was chosen for its high spring constant in order that there would be little interaction between it and the magnetic spring as the poles detached. The pole motion was measured directly with a dial indicator. Force repeatability was within five percent on consecutive runs. The tolerances of the latch parts were held to within 50 microns (or one percent on a radial basis).

The only variables not held under strict and observable control were the chemistry of the steel pole pieces and the magnetisation of the permanent magnet. Yet, despite the careful development of both the numerical and physical models, comparison between the finite element and experimental curves reveals a consistent, factor of two, disparity throughout the range of measurement as is clearly visible in figure 3.11.

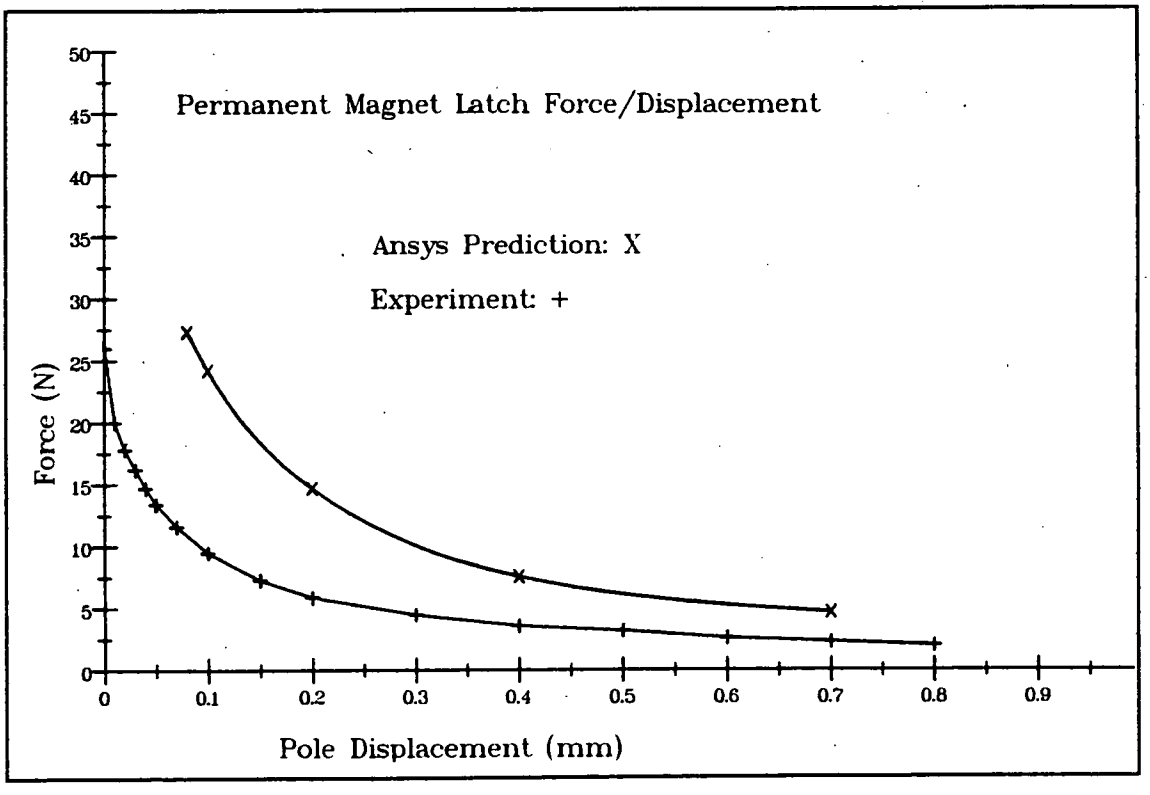

Figure 3.11: Experimental and F.E. Predicted Passive Latching Forces vs. Pole Displacement.

In an attempt to reconcile this large difference, adjustments were made to the model to see how sensitive the forces were to various dimensions. Varying the important dimensions by several times their expected manufacturing tolerances produced force changes on the order of ten percent. Substantial changes to the BH curve of the steel pole pieces (lowering the onset of saturation by 30 percent) made a similar difference. It would seem that the only remaining possibility for explaining the large difference lies in the magnetisation of the permanent magnet material. The manufacturers claim to hold the remanent flux density and coercivity to within four percent of the average values which does not provide an adequate explanation [45].

The magnet latch rig was disassembled and the magnet sent to the manufacturer to be tested. The remanent flux was found to be 17 percent below the stated figures after the magnet had been remagnetised. The original state of magnetisation was lost as a result of this process and no reliable conclusion can be reached regarding the discrepancy between the claimed and actual properties of the magnet. If after remagnetisation the flux levels were such that the magnet would produce only two thirds of the expected force, then it is very possible that the remaining error could be explained by it initially having an even lower level of magnetisation.

The force results from the model with the solenoid activated were much closer to those measured as can be seen in figure 3.12. This could be attributed to any one of several factors: The largest force is upward and acts across a larger gap with much less concentrated flux. Since the downward force, between the lower and moving poles, is very small when the pole detaches, any error

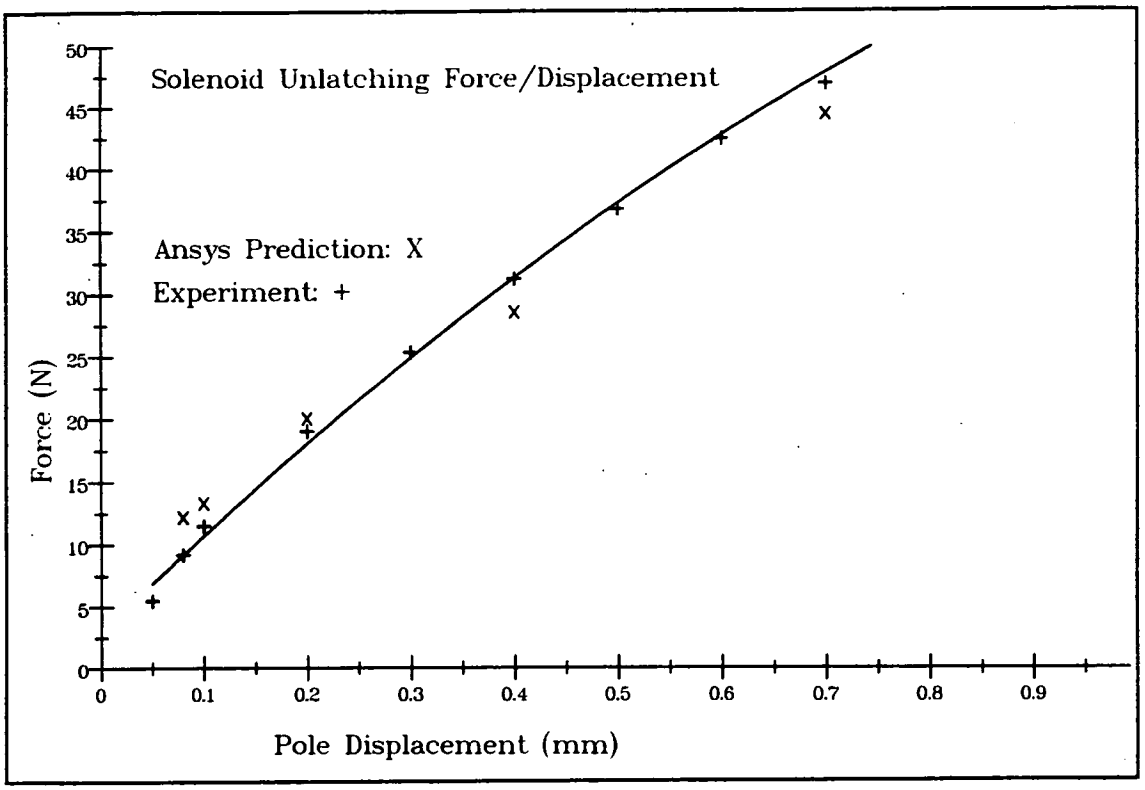

Figure 3.12: Experimental and F.E Predicted Unlatching Forces vs. Pole Displacement for the Entire Latch with the Solenoid Active.

resulting from its calculation is liable also to be small in relation to the upward force. One further observation about the nature of these curves is that, unlike those of the permanent magnet case, these seem to maintain a relatively constant slope at the point of zero-crossing which may make them useful in predicting take-off forces.

The vector and contour plots of the flux density, with the solenoid active, are presented in figures 3.13 and 3.14 respectively. The vector plot clearly illustrates the flux paths which cause the magnetic saturation in the web of the moving pole.

The contour plot shows an area of undesirably high magnetic flux within the innermost solenoid pole. An attempt was made to optimise the force by varying this radial dimension. Surprisingly, the net force was not

significantly altered across the range tested even though the level of saturation was substantially reduced with a minor thickening of the inner pole. The loss of an area of heavily magnetised steel, which increases the resistance to the passage of flux, is evidently counteracted in its effect through its replacement by an equal area of active solenoid.

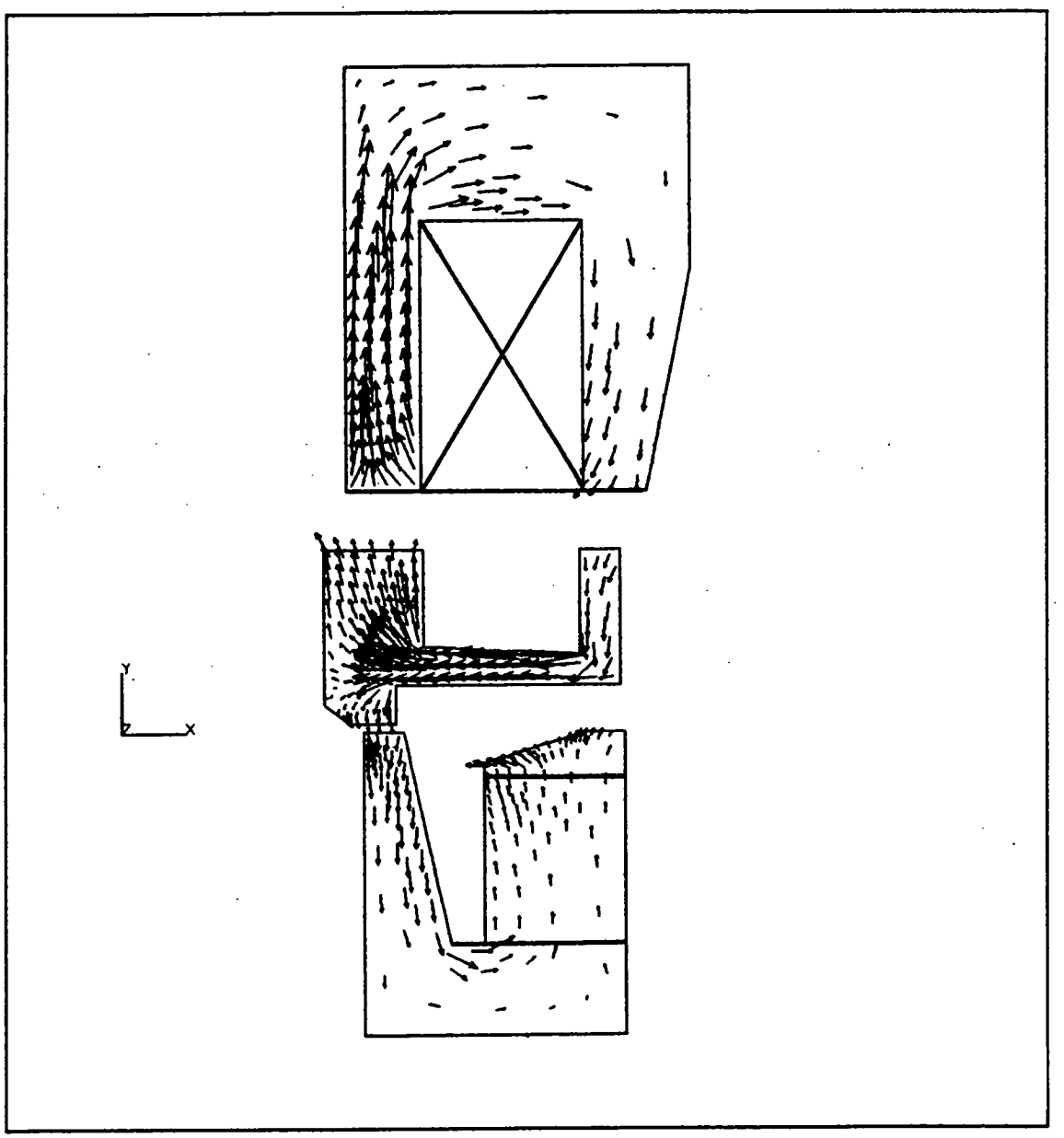

Figure 3.13: Vector Plot of Flux Density in the Moving-Iron Latch with the Solenoid Active.

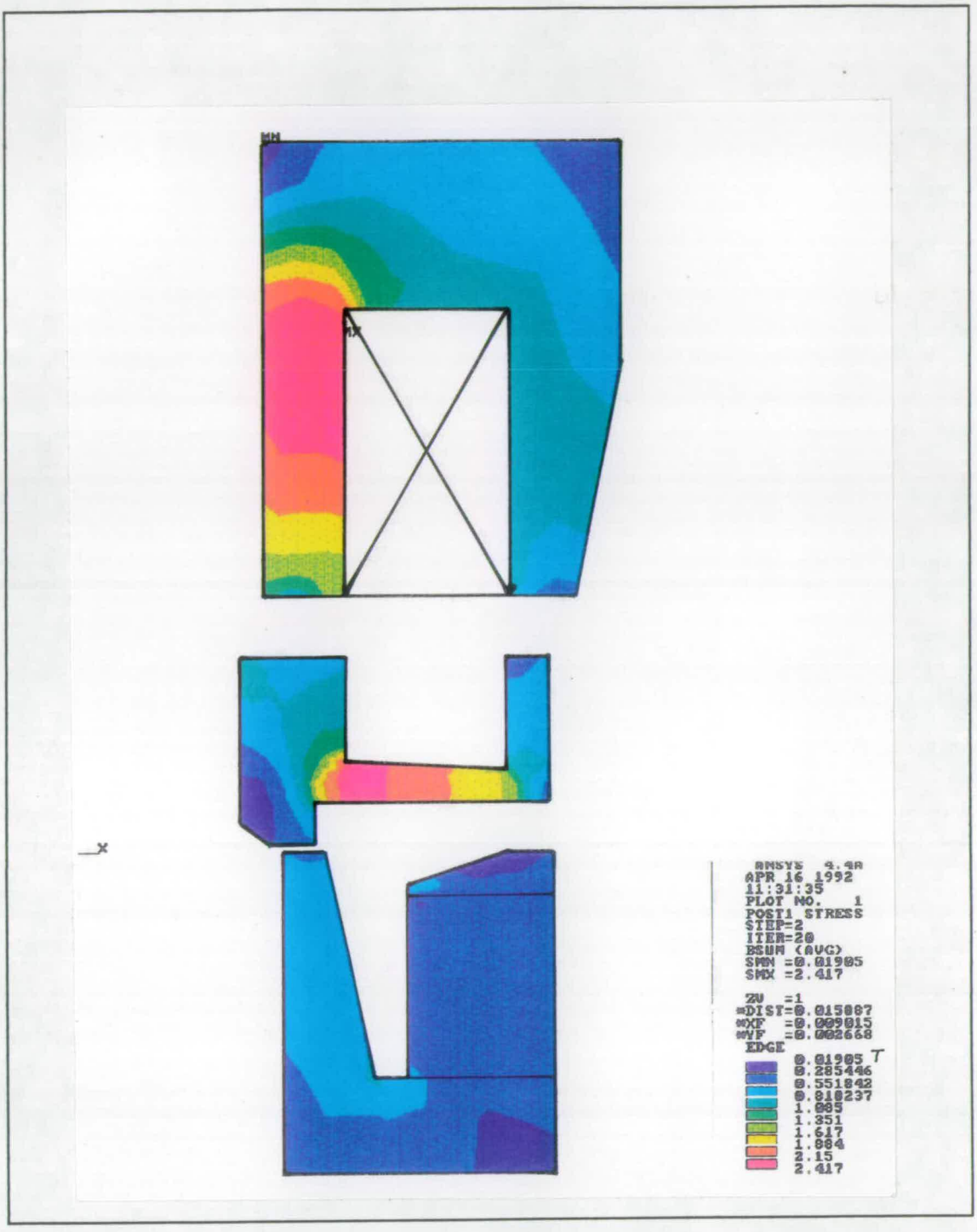

Figure 3.14: Contour Plot of Flux Density in Moving-Iron Latch with the Solenoid Active.

3.7 Closing Summary

The foregoing chapter can be reduced to a short list of design steps which might prove helpful for those contemplating further latch designs:

1. The active inlet valve is best designed to self-open, in order to reduce the risk of cavitation in an unboosted pump. It should latch open during the inlet stroke so that the controller has a known starting condition for the valve actuation and so that the pump fails safe to zero flow. The valve should be actively closed to ensure that the time of closure can be precisely controlled to coincide with the piston bottom-dead-centre position.

2. The valve controlling latch is best composed of a flat-faced armature permanent-magnet circuit for holding the valve open, with the magnet located in the fixed pole, and an opposing solenoid coil circuit for closing it. The solenoid will saturate the steel in the moving pole, which is common to both circuits, thereby defeating the permanent magnet and pulling the valve closed.

3. Simultaneous equation solving computer packages, such as TK!solver, are very useful for generating latch dimensions giving close to optimum magnetic performance. This technique is limited in accuracy since it relies on the use of constants to model the complex phenomena of steel saturation and flux leakage.

4. Finite element packages, such as ANSYS, allow more precise modelling of saturation and flux leakage. Unfortunately they are laborious to use while also suffering from several inherent shortcomings:

    1. The problems associated with correctly meshing a model with fine air gaps, and;

    2. The potential for inaccuracies in force calculation, and;

    3. The impossibility of calculating forces with the valve in a latched position since, for all methods of force calculation, the moving pole must be surrounded by air elements.

At this point in time, the use of finite element modelling is probably best limited to the checking and final optimisation of a latch that has been brought to a stage of completion by the use of the simultaneous equation solver. It is too slow and too delicate to be used as a preliminary design tool.

4.0 Fluid Flow Losses and Forces on Disabled Poppet-Valves

The design of the poppet-valve actuator, discussed in the previous chapter, is dependent on the magnitude of the fluid forces acting on the poppet-valve element. Thus the analysis of these forces becomes an essential component of the overall digital pump development. The other quantity of immediate interest, with regard to fluid flow, is the power loss caused by pumping fluid back and forth through the disabled inlet valve. As the part load efficiencies of the digital pump are highly dependent on this loss, it is imperative that it be kept as small as possible. There is also the allied constraint of keeping the cylinder suction pressure sufficiently high as to avoid cavitation and air release.

4.1 Literature Survey

There are a substantial number of references relating to poppet-valve performance. They are, without exception, aimed at either of two possible applications. The majority are concerned with poppets used as flow control devices [46,47,48]. In such instances the velocities and pressure drops are high, while the flow is both inviscid and steady. The second type of application is that of positive displacement pumps [49,50]. Here, the velocities and pressure drops are low, viscous effects may not be negligible and the flow is varying with time. There is one common element in these two diverse applications, however, in that the flow is always radially divergent if the poppets are performing as intended. As there has been no previous application for disabled poppets with convergent flow, they seem to have escaped the attention of researchers. The only reference to this possibility seems to be contained within the series of reports by Oshima and Ichikawa [51]. These

were experimental studies designed to determine the effects of geometry on the onset of cavitation and so are concerned with much higher pressure drops than might desirably occur in the inlet valve of a pump.

In so far as characterising the forces and losses on the disabled valve, where the flow is convergent, absolutely nothing has been found of direct applicability.

One consistent characteristic of all of the papers cited here is the limitation to conical and disk valve geometries. The general aim has been, understandably, to allow the geometries of the valve and seat to be incorporated into descriptive equations and thus allow the parameterisation of the basic poppet design, so that performance specifications such as pressure drop and force can be estimated. The problem with allowing the valve and seat to deviate from these rectilinear forms, and assume curved profiles, is that the geometrical possibilities become infinite. Equations equipped to handle so many geometric parameters would be impractical.

Several papers do suggest that hydrodynamically smooth valve ducts might be advantageous. Shrenk [52], in one of the earliest papers, described a smoothly profiled valve duct and then continued to show experimentally that the flow losses were much lower than the other conventional shapes. Stone [53], in a paper which considered only high velocity flow, suggested that mushroom-shaped poppets were effective in reducing flow forces, though it is not clear how he could justify this statement since there are no obviously mushroom shaped poppets described in his results.

In summarising the results of their experiments and simulations, Johnston et al. concluded that for pumps, where low flow losses and forces were required, chamfered

valve seats with an upstream fillet were most suitable for divergent flow.

The only way of proceeding toward the goal of lowest losses and forces was to design the valve duct as an expansion and contraction in series. Unfortunately the physical space restriction in the cylinder head prevents the duct from having the gentle divergence angle required to avoid flow separation. Ward-Smith [54] provides data for the losses generated by annular diffusers. This gives some guidance in determining the flow channel geometry of the valve and seat, though, the search for the optimum form is greatly constrained by the physical sealing requirements and stress limitations of the seat area.

Once a valve and duct are designed in this way, their characteristics must be analyzed in order to allow comparison with other shapes and, therefore, progress towards a practicable optimum. Numerical modelling, such as performed by Vaughan et al. [55], is becoming the most effective way of iterating a design towards an optimal solution but, at the time of the study, was greatly limited in terms of effectiveness by the computing power and the geometry restrictions of the analysis packages then commonly available.

Alternately, experimentation can be used to determine predictive equations for different duct geometries. The vast majority of poppet analyses have focused on the calculation or prediction of a non-dimensional coefficient of discharge dependent on the duct geometry and flow conditions. This approach ignores the non-negligible viscous effects in the low Reynolds number conditions in which poppet-valves might operate. Since the digital displacement pump must function with cold oil, having a viscosity perhaps ten times higher than

that seen at normal operating temperatures, the assumption of dominant inertial forces may not be justifiable.

Takenaka [56] provides a useful lead in solving this problem with his analysis of forces on disc valves. He considers the low Reynolds conditions and in doing so expresses the equations for force in terms of viscous, inertial and static pressure forces. McGinn [57], in an earlier paper describing radial flow between two fixed plates, derives a similar equation. Though, unlike the previously cited works, he considers both radially divergent and convergent flows. While the geometries described in these two papers are unlikely to resemble the optimum poppet, the groupings of non-geometric parameters can be usefully employed. McGinn's work is limited to the description of pressure drop, as his plates were fixed, but an approximation for the force on a disc valve could be made by integrating the product of pressure and area along the radial path of the valve seat.

The previously mentioned papers deal strictly with constant flow analysis. As the inlet valve flow is time-variant, there may well be non-negligible temporal effects on the poppet force and loss. Schlitting [58] describes the phenomenon of slug flow, neither laminar nor turbulent, which occurs during temporal acceleration of fluid in a pipe. The same effect will be occurring, to some extent, in the valve duct and across the valve seat.

4.2 Definition of an Optimum Valve Shape for Lowest Forces and Losses

The usual starting point in pump design is a knowledge of the required output, in terms of flow and pressure, as well as the input shaft speed of the prime-mover. The ratio of cylinder bore to stroke is effectively defined, where the piston is also functioning as a cantilever beam (in most axial and some radial pumps), by the allowable side forces on the piston. In such a case, the stroke is generally restricted to a fraction of the bore dimension [59].

The number of cylinders is determined by a trade-off which balances the desire to minimise pulsation against space considerations and the additional cost of extra pistons and valves [60]. With high-speed pumps the general solution to the above problem has been either seven or nine cylinders. The odd number provides a useful doubling of the fundamental pulsation frequency. Pumps of six and eight cylinders are more common in the poppet-valve configuration [61,62] since the manufacturing costs are slightly less and, since, the use of poppet-valves eliminates the cross-over problem which occurs in commutating port pumps (as cylinders are alternately disconnected and reconnected to manifolds at different pressures).

The valve design begins after the previous considerations have allowed the piston, cylinder and crankshaft (or cam) design to be completed. For the poppet-valve to function with the lowest possible losses in the latched open condition, it must present a hydrodynamically smooth profile to the flow in both directions. In the case of the radially converging flow, experienced during a disabled delivery stroke, there is not too much difficulty in creating such a duct since the contraction

around the valve head is able to function efficiently with relatively large angles of convergence. The expansion, following the valve seat region, can also be made sufficiently gradual without the need for an increase in duct length. The radially divergent flow of the inlet stroke is a different matter. While the gradual contraction upstream of the valve seat, dictated by the reversed flow, is compatible with the low loss aim, it is physically impossible to reconcile the expansion from the constricted valve seat region into the comparably vast cross-sectional area of the cylinder. For this reason, it is the disabled discharge stroke which effectively dictates the valve and duct shape.

The valve duct design approach can be condensed into a series of steps (based on optimising the disabled discharge flow):

1. The annular area surrounding the valve head, in the cylinder, must be smoothly blended into the seat area (defined by the valve seat diameter and valve opening) using a contraction angle not exceeding approximately 40 degrees [63]. The cylinder diameter, the contraction angle and the resulting cylinder to valve seat area ratio effectively defines the profile upstream of the seat. The general desire to limit the dead, or unswept, volume in the cylinder, because of the comparatively high compressibility of the fluid, will also tend to push the design toward compact forms and away from exaggerated, streamlined ones.

2. The valve seat width and angle will be determined by the hertzian stress limits of the valve and seat interface as well as by the debris tolerance required in the pump design.

The choice of a forty-five degree seat allows a relatively smooth duct to be incorporated into a limited space. Although smaller angles could be used for a smoother profile, there is an increasing danger of jamming and seat damage with trapped debris since the contact stress rises as the angle diminishes. Relatively large valve angles (i.e. disc) allow increased flow area for a given travel but are not desirable due to their higher flow losses.

3. The expansion downstream of the seat region will be determined by the desire to prevent flow separation. Design data can be found in Ward-Smith.

4.3 Determination of Flow Force and Loss Coefficients of the Disabled Poppet-valve

4.3.1 Power Measurement

Measuring the flow loss is not a trivial task. In the time-varying flow, consistent with harmonic piston motion, the pressure drop information must be precisely related to the piston velocity at its instant of capture. The phase information is of utmost importance to the accuracy of the resulting values. The average power loss during disabled operation can be obtained by sampling the pressure drop at discrete positions of the piston and then multiplying it by the instantaneous flow-rate, extracted from the derivative of piston position, and summing the product over several cycles before dividing by the elapsed cycle time. The same result can be found by taking an FFT (Fast Fourier Transform) of the pressure time signal and by using the imaginary component of the

fundamental multiplied by a maximum flow rate constant. The FFT method is able to provide accurate phase information so long as sampling has occurred over a number of integral cycles and has exactly 2^n samples. If the sampling of the pressure begins at a sensible point in the cycle, such as at top-dead-centre of the piston, then the real array of the FFT is in phase with acceleration and the imaginary one with flow velocity. A proof of the equivalence of the two flow loss calculations is presented in appendix D.

4.3.2 Force Measurement

There are four components which contribute to the phase and magnitude of the force on the poppet:

1. The skin friction force, in phase with and proportional to velocity, arises as a result of the fluid boundary layer shearing next to the poppet. The shear force rises with fluid viscosity which is of great concern since it is anticipated that the use of mineral oils, with a potential ten-fold increase of viscosity over the operating temperature range, will cause very large changes in the required latching force.

2. The force due to the velocity gradient around the poppet, which is also in phase with piston velocity and proportional to its square. The increased velocity in the region of the valve seat results in a localized zone of low pressure and, consequently, a rectified force which tends to close the valve irrespective of the flow direction.

3. The pressure differential across the poppet, acting on the head of the poppet, which is due to the viscous and turbulent flow losses through the valve duct.

4. The temporal acceleration force, 90 degrees out of phase with the flow but with a magnitude proportional to the square of pump speed, arising from the fluid being accelerated in and out of the cylinder. The magnitude of this pressure drop is increased by the flow area reduction in and around the valve seat region.

The force signal, measured at discrete angles of flywheel position, can have an FFT applied to it in order to extract the component of force in phase with acceleration at the fundamental frequency. This component of poppet force can be graphically estimated by drawing a streamline through the sectioned drawing of the duct and by then calculating a sum of area ratios to find the equivalent length. If the pressure drop, at the instant of maximum acceleration, is found along the length of the valve by this means, then the local pressures can be applied to the developed areas of the poppet in order to calculate the overall force due to temporal acceleration.

The same type of verification cannot be applied to the component of force in phase with piston velocity since it contains both inertial and viscous components which are not analytically separable. While it might be argued that the viscous forces are likely to be similar in both directions of flow, the inertial ones are not since the duct is assymetric in terms of fluid flow direction.

4.4 Design of an Experimental Rig for Poppet Testing

In order to measure the flow forces and losses of poppet-valves a single-cylinder pump rig, with the provision for parameter alteration and instrumentation, was required. Every aspect of the pump needed to be variable: speed, stroke, cylinder bore, valve and duct geometry, valve opening and working fluid. For each of these variables, practical ranges were specified for the rig. At the start of the project the target wind turbine pump had the following characteristics: cylinder bore 80 mm, stroke 80 mm, oil SAE 30 at 60 deg. C, and an operational speed of 10 Hz. As an 80 mm bore was extremely large in terms of commercial hydraulic machinery, this was set as the upper limit for the rig. The collaborating firm, in designing conventional solid-piston pumps, generally employed stroke/bore ratios below 1/1.5 in order to avoid unacceptable piston wear. The maximum stroke was put at 80 mm as well since it was enough to meet the requirements of the initial application and was beyond those of our collaborators. The selected oil was retained but, as there was concern about the effects of viscosity and cold starting, a range of oils which would give different viscosities at room temperature was used. Shell Tellus R10 at 20 degrees C was used to simulate the SAE 30 oil at the specified working temperature of 60 degrees C. Century PWLA (SAE 33) was used to provide a higher viscosity oil and Shell Tellus R5 a lower one. In order that tests could be conducted up to induction motor speeds, the maximum speed of the pump was set at 24 Hz.

Care was taken in the design of the pump mechanism to ensure that unwanted signals were suppressed:

1. Lost motion in bearings, which can create anomalies in time traces, was minimised through

the use of ball races with minimal play in relation to the piston stroke;

2. The imperfect simple harmonic motion of the crankshaft/con-rod mechanism was reduced through the use of a con-rod which was long relative to piston stroke, and;

3. Attention was paid to the mechanical rigidity of the pump structure in order to avoid resonances in the frequency band of interest.

The various components of the duct and valve were made so that small parts of the geometry could be easily removed and altered. The duct and cylinder head was made of perspex so that flow visualisation could be used to improve the geometry. The poppet was suspended from a tower which located it in all but the axial direction. The guide bearings were made of glass-fibre filled PTFE and machined to a close running fit in order to prevent radial oscillation of the valve and yet allow the axial forces to be passed on to the load cell without significant corruption.

The general arrangement drawing of the test pump rig is shown in figure 4.1. The photo in figure 4.2 shows the completed rig without its perspex reservoir. The poppet in its duct is shown, in the photograph of figure 4.3, with the duct filled with a darker oil to illustrate the annular flow path.

Overleaf:

Figure 4.1: General Arrangement of Poppet Flow Force Rig

Figure 4.2: Assembled Poppet Flow Force Rig

Figure 4.3: Poppet Flow Force Rig: Detail of Poppet Duct

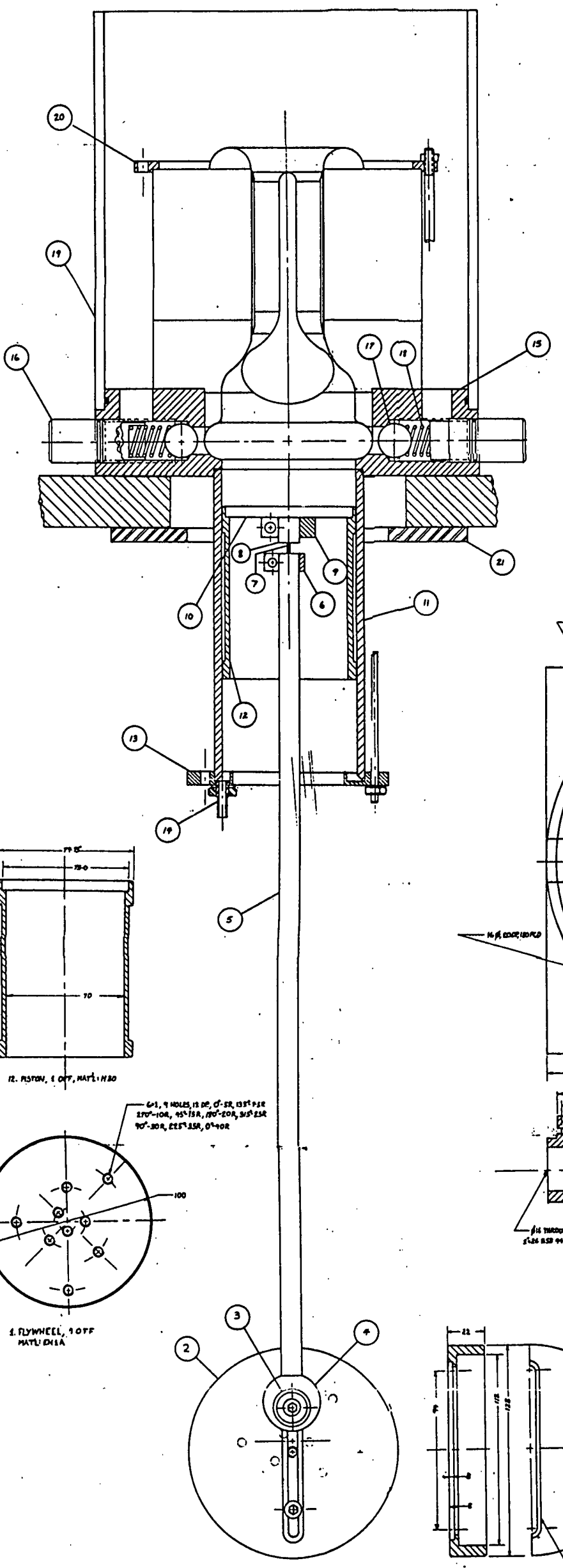

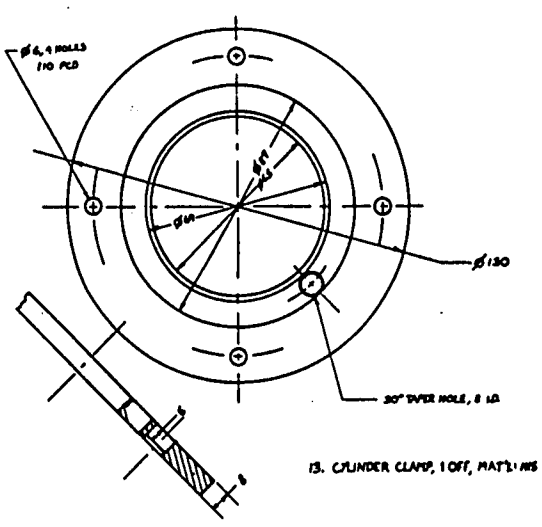

13. CYLINDER CLAMP, 1 OFF, MAT'L: MS

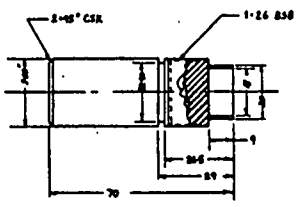

16. ADJUSTMENT KNOB, 2 OFF, MAT'L: BRASS

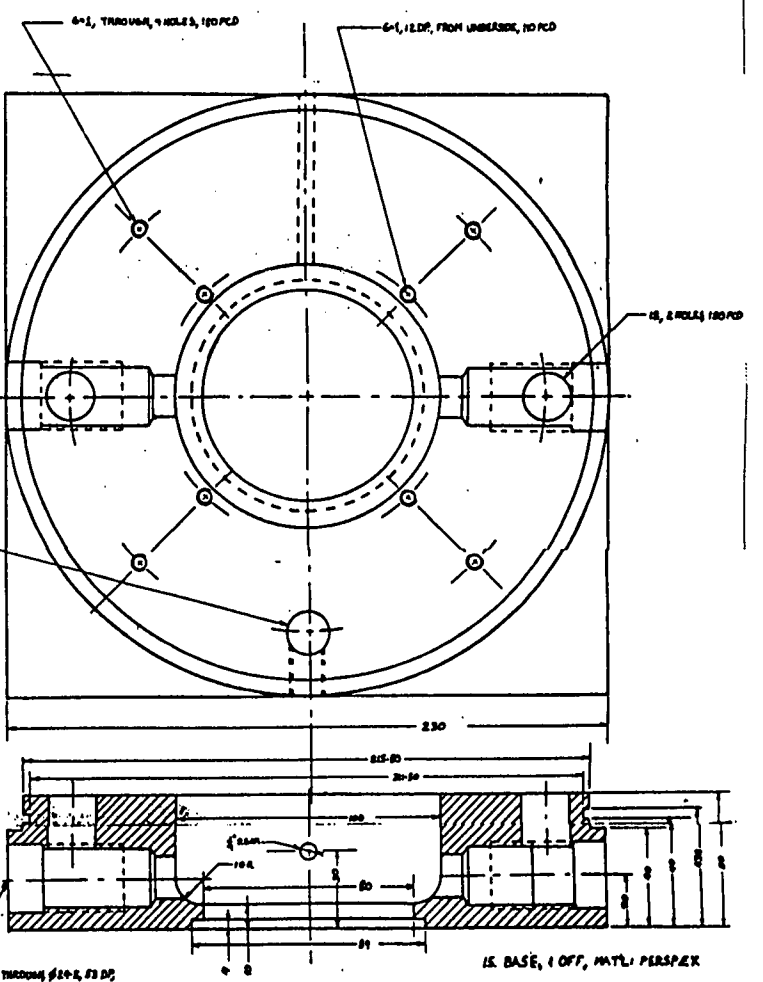

15. BASE, 1 OFF, MAT'L: PERSPEX

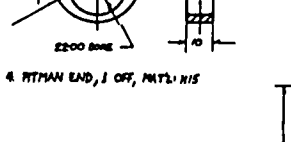

4. PITMAN END, 1 OFF, MAT'L: HS

12. PISTON, 1 OFF, MAT'L: HSO

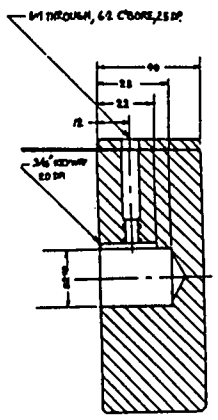

1. FLYWHEEL, 1 OFF
MAT'L: EN1A

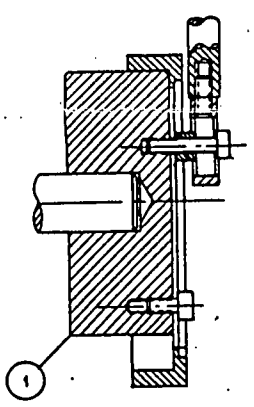

2. BALANCE DISC, 1 OFF
MAT'L: HS

6mm WIDE SLOT WITH 12mm C'BORE

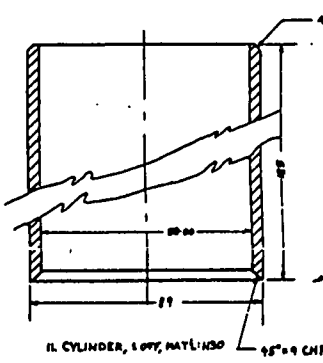

11. CYLINDER, 1 OFF, MAT'L: HSO

University of Edinburgh				
			Mr. Rogers	POPPET-VALVE FLOW TEST RIG
			JAN 22/97	Drawing Number A-FIG 1
			FULL	

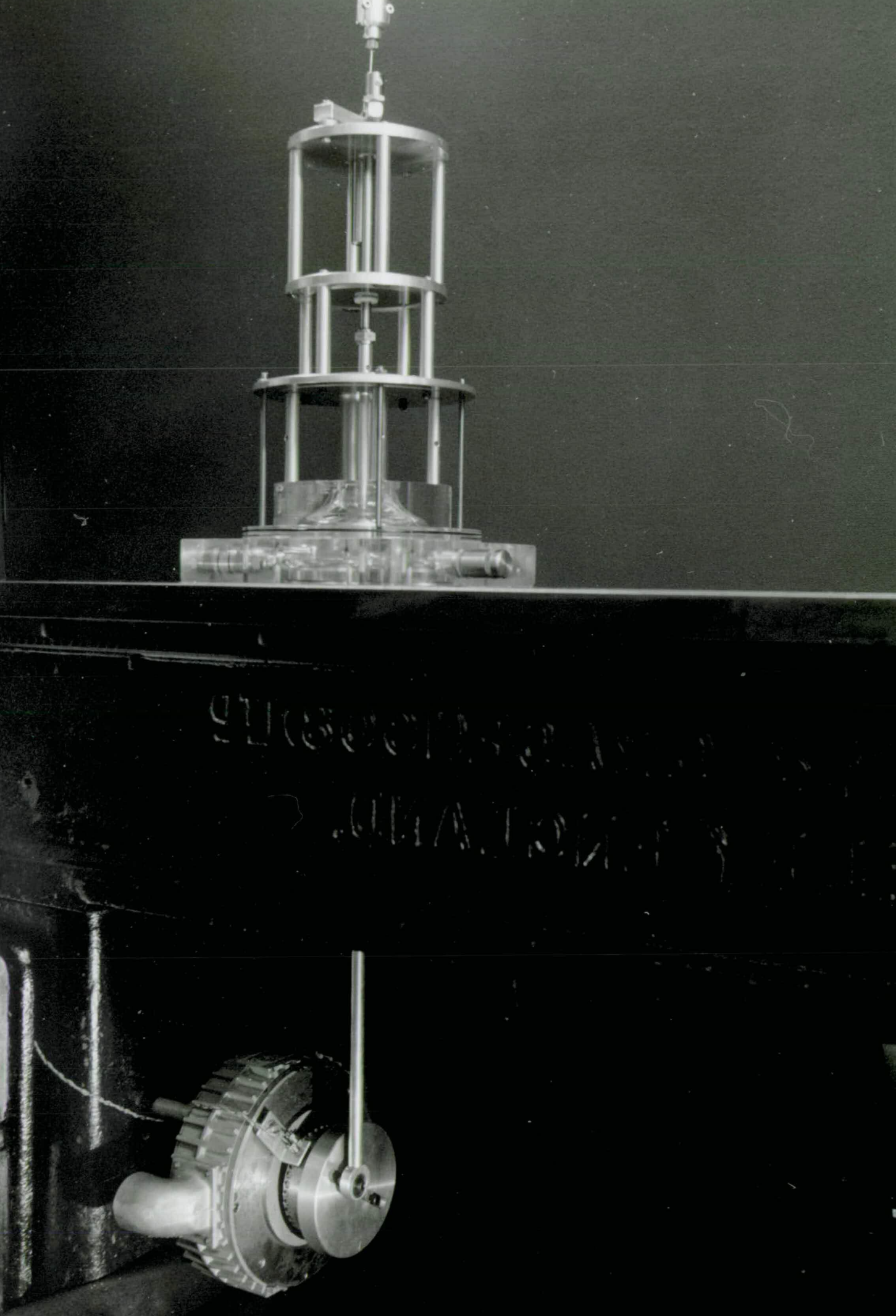

4.5 Speed Control and Sampling Trigger

The important relationship between flow velocity and power loss in the rig meant that the control of the pump speed was exceptionally critical. Additionally, the FFT's requirement of exactly 2^n samples and integral piston cycles for accurate phase results, dictated that the sampling had also to be tied into the piston motion. A quartz clock and programmable dividers were used to produce precise timing pulses for both systems. By changing the division constants on one of these dividers, a range of precisely defined speeds could be set without need for further calibration. Changing the division constant of the second divider allowed the number of samples taken during an integral cycle to be varied in precise steps.

The pump drive-motor was a one KW, direct-current, printed circuit armature machine fitted with both a tacho-generator and a crude position encoder, the latter being made from a row of equally spaced holes on the periphery of the flywheel and a magnetic pickup. Absolute position was detected once per revolution, at top-dead-centre, by a second pickup and a single hole adjacent to the others.

The flywheel speed and position were controlled by a system with both velocity and position error feedback. The speed setting switch was connected to an analogue-to-digital convertor which produced an analogue demand signal. A pulse-train, originating from the master clock, was divided in frequency and compared to the signal from the flywheel encoder using an up/down counter. The output count was, thus, a measure of the position error at any instant. The counters were actually used in cascaded form in order to provide a sufficiently large error signal range. The error count

was then converted to an analogue voltage which could then be summed with both the demand and the velocity signal (fed back from the tacho-generator), and the result output to the motor-drive power amplifier.

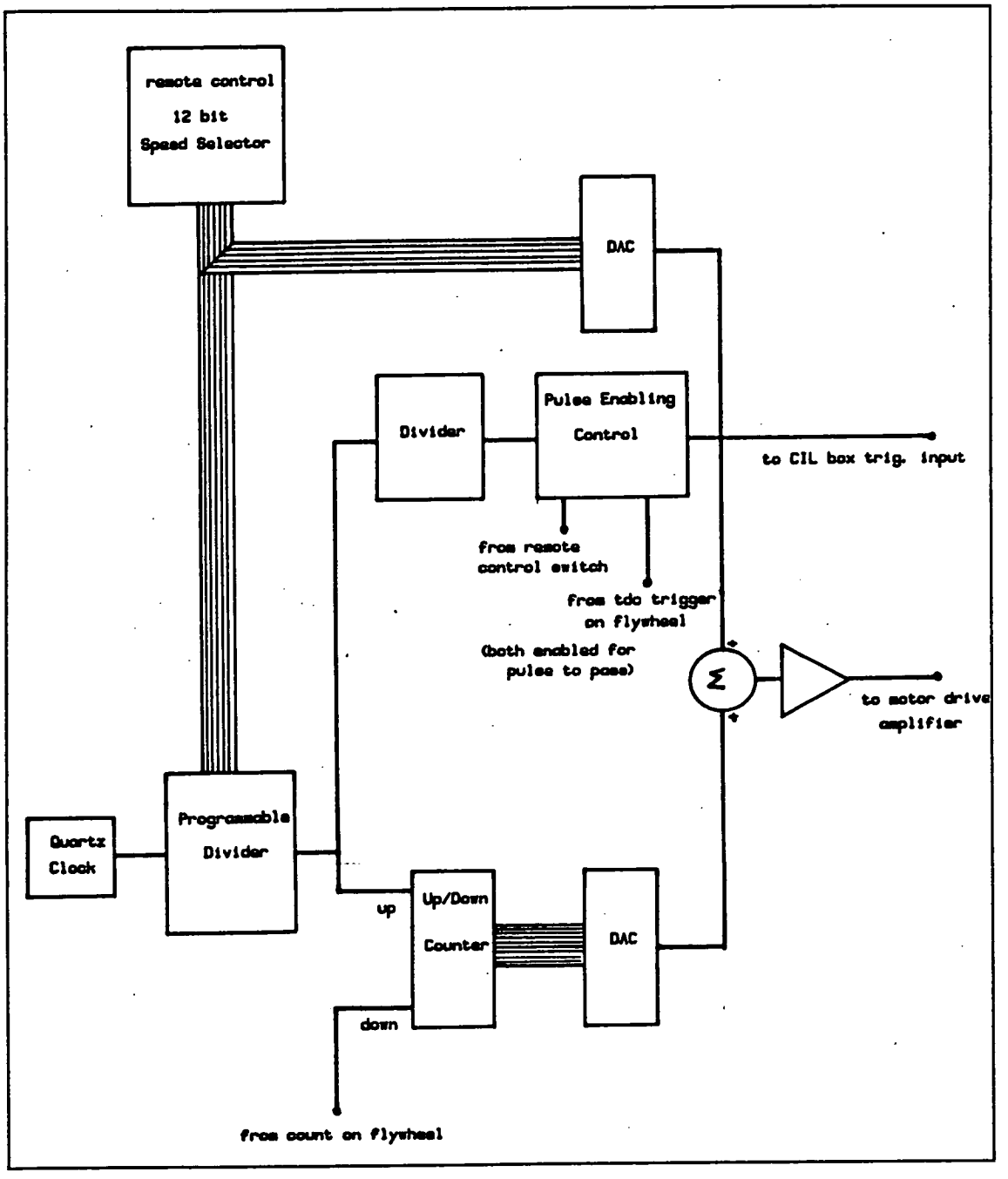

Figure 4.4: Schematic Diagram of Flywheel Speed and Sampling Control System.

The sampling trigger pulse-train was controlled synchronously by the master clock and divider circuit such that 2^n samples were taken per crankshaft revolution in even angular increments. The divider range was sufficient to allow between one and 2,056 samples per revolution. The sampling system was manually armed and then triggered by the next passing of the flywheel notch at the top-dead-centre of the piston. The speed and sampling control system is illustrated schematically in figure 4.4.

4.6 Instrumentation and Sampling System

The force transducer was located in line with the poppet as shown in figure 4.5. It was isolated from misalignment-induced bending moments by the use of flexible wire attachments. The transducer was of the piezo-resistive type (transducer specifications in appendix E) and had the desirable characteristics both of being axially stiff and of providing a flat frequency response down to DC levels. The conditioning board, to which it was attached, contained both a voltage stabilized supply and an output amplification stage.

The two pressure transducers, also of a piezo-resistive type, were connected differentially. One sensed the cylinder pressure whilst the other was connected to the reservoir at the level of the poppet head. The differential signal was used to remove the effects of reservoir head and any externally applied boost pressure. The pressure signal was also conditioned prior to being sampled.

Both the pressure and force signals, in the form of analogue voltages, were fed into a transient signal recorder. This instrument, once armed by the computer, sampled the two channels and stored the analogue levels

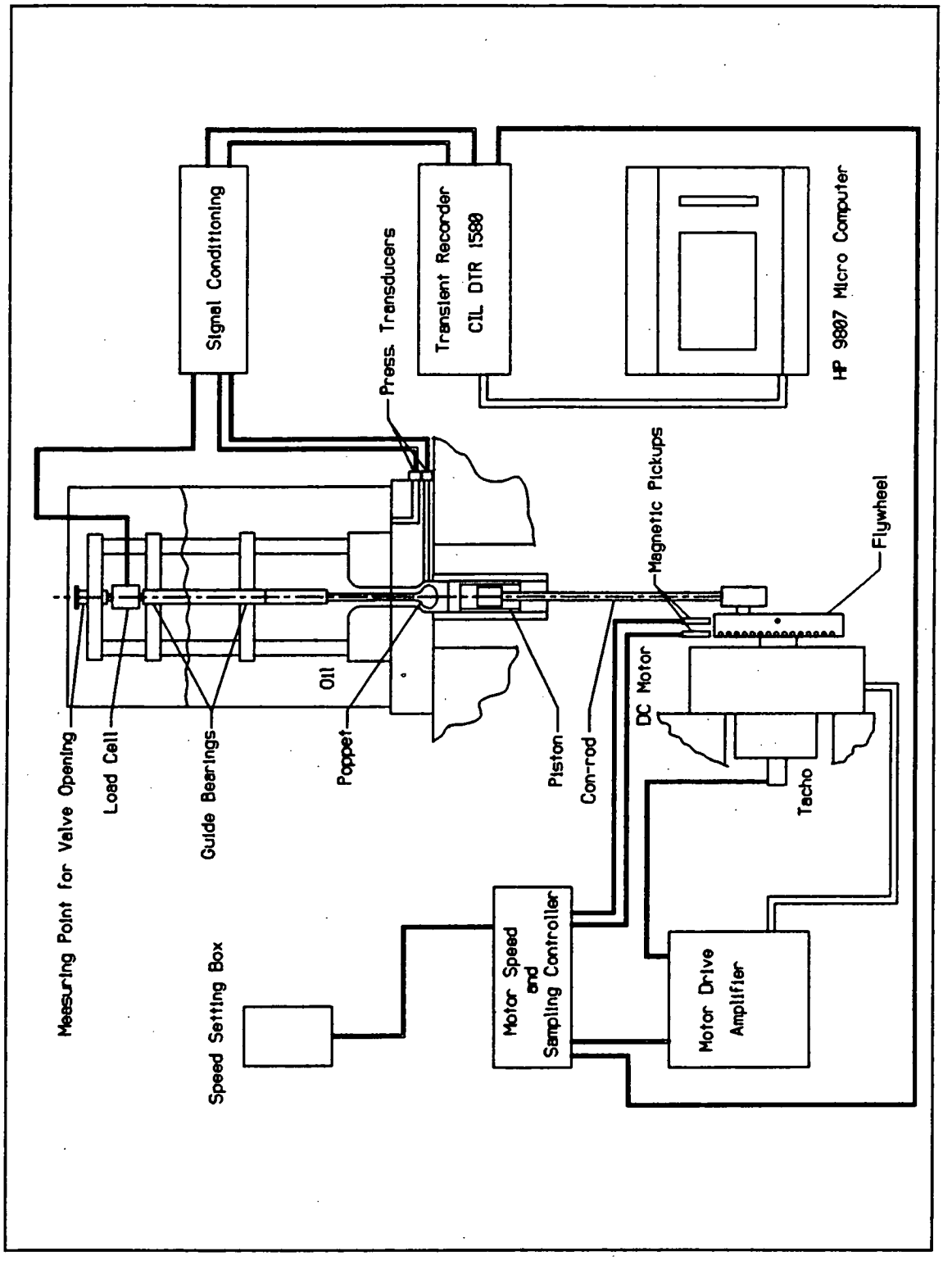

Figure 4.5: Schematic Diagram of Poppet Flow Force Rig Instrumentation.

as 16 bit integers. When the sampling was completed, the waveform data was downloaded to the control computer for analysis and archiving.

4.7 Software

The first program required was one to control the process of collecting data from the disabled valve experiments. The program had six major functions:

1. To create logically derived file names that could, on inspection, yield the experimental parameter settings for that experiment.

2. To control the transient recorder, both arming it and retrieving its data.

3. To manipulate the data into calibrated waveform arrays.

4. To allow graphical inspection of the waveforms in order to ensure the validity of an experiment.

5. To manipulate the data in order to provide values for power, minimum cylinder pressure during intake and maximum force.

6. To store the time series and also the processed data in an accessible way on floppy disc.

The flow chart of the program "popexp" (poppet experiment) written for this purpose, in Hewlett-Packard Technical Basic, is shown in figure 4.6.

A second program was written to condense the force and power information from the 303 experiment result files

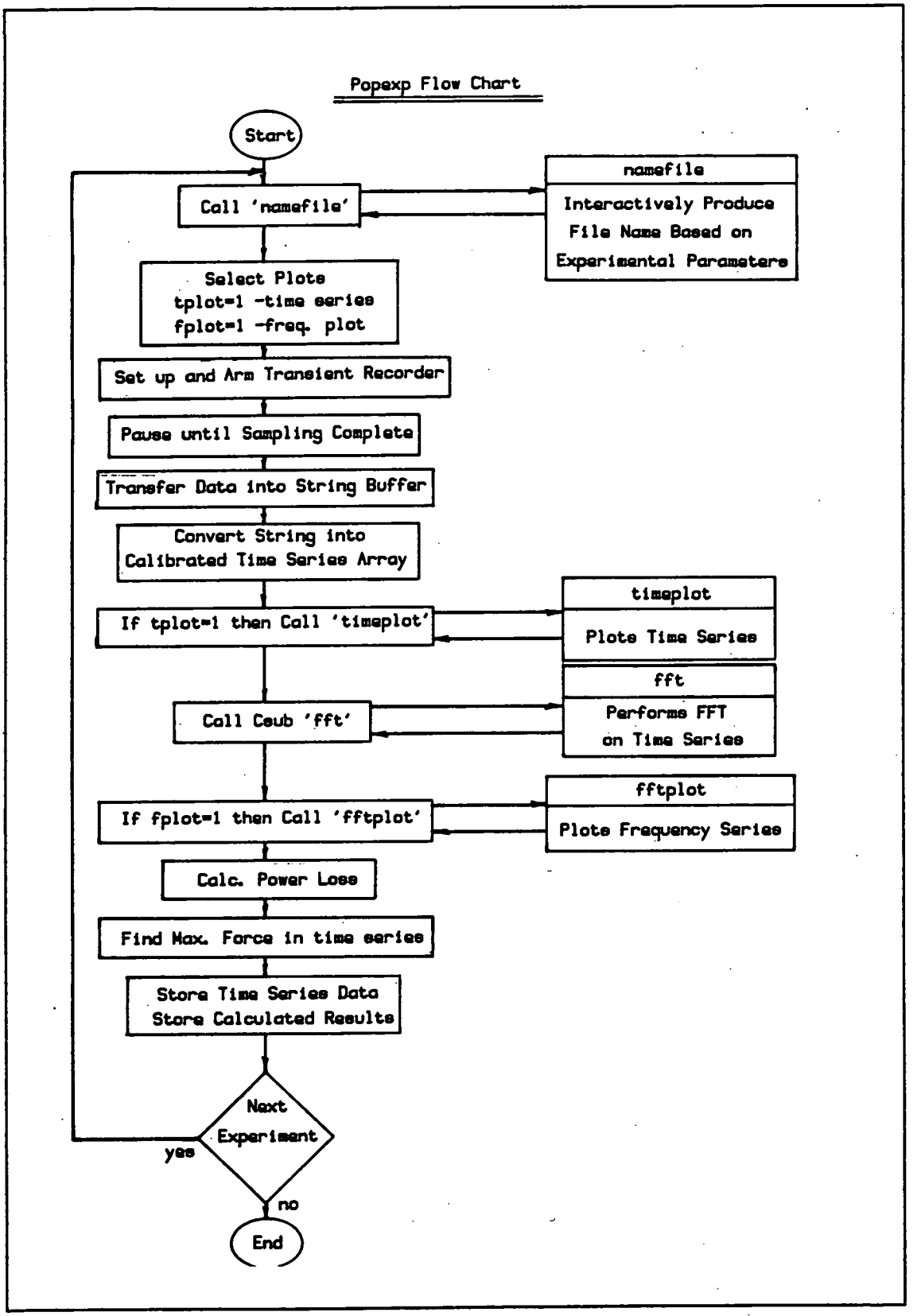

Figure 4.6: Flow Chart for Disabled Poppet Experiment Software.

into a single one. Finally, a third program was created to correlate the data with respect to the experimental parameters using a weighted least squares algorithm. The weighting was based on the larger, inertial term and served to reduce the significance of the higher force/loss experiments with respect to the lower ones. The algorithm also computed the standard deviation of the experimental data from the predicted results.

4.8 Experimental Results

Two series of experiments were performed:

1. Tests with different valve shapes over a limited range of valve openings, strokes and speeds. These were run in order to determine the potential gains of shape optimisation as well as to suggest the most appropriate profile.

2. Tests with the preferred ellipsoidal shape using three different oil viscosities, two valve/bore sizes and a range of strokes, speeds and poppet openings. These were designed to determine the form and coefficients of modelling equations.

4.8.1 Valve Shape Experiments

The valve shapes in the series were chosen for different reasons. The automotive shape represented current practice in several fields of application and was chosen as a reference from which to gauge improvement. The conical valve, while not usually seen with a stem attached to its apex, is commonly used in hydraulic pumps and served as a second reference point. The spherical shape was chosen as being representative of ball valves,

which are frequently used to prevent flow reversal. This shape offered both the attraction of uncomplicated manufacture and the presentation of a smooth profile to the flow. The hemispherical shape was an adaptation of the sphere, tried on the basis that the viscous drag reduction offered by truncation would more than offset the other losses it created. This hypothesis was justified by the observation that the flow velocities near the flat surface of the hemisphere would be relatively low in comparison to those closer to the valve seat region. The ellipsoidal shape arose from smoothing the hemisphere so that it combined the characteristics of hydrodynamic smoothness with a minimum of extra surface area and moving valve mass.

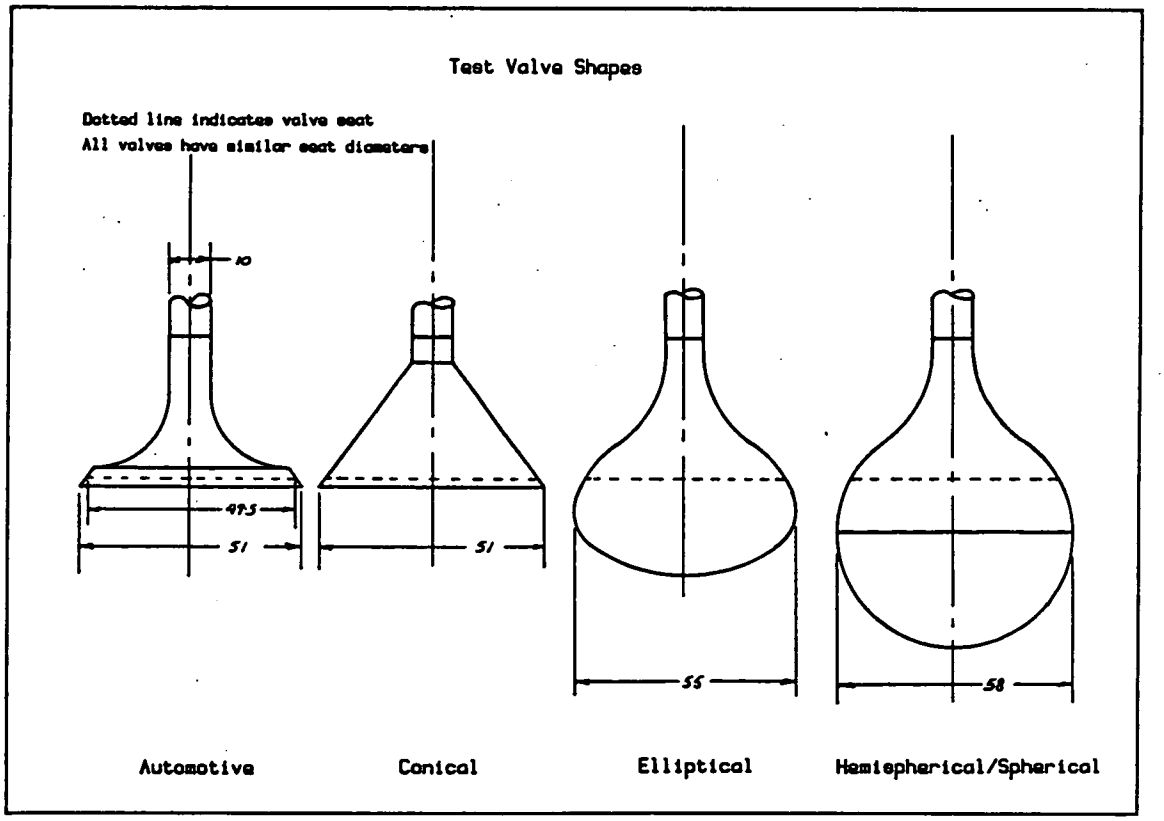

Figure 4.7: Poppet Shapes and Dimensions as Tested in The Poppet Flow Force Rig.

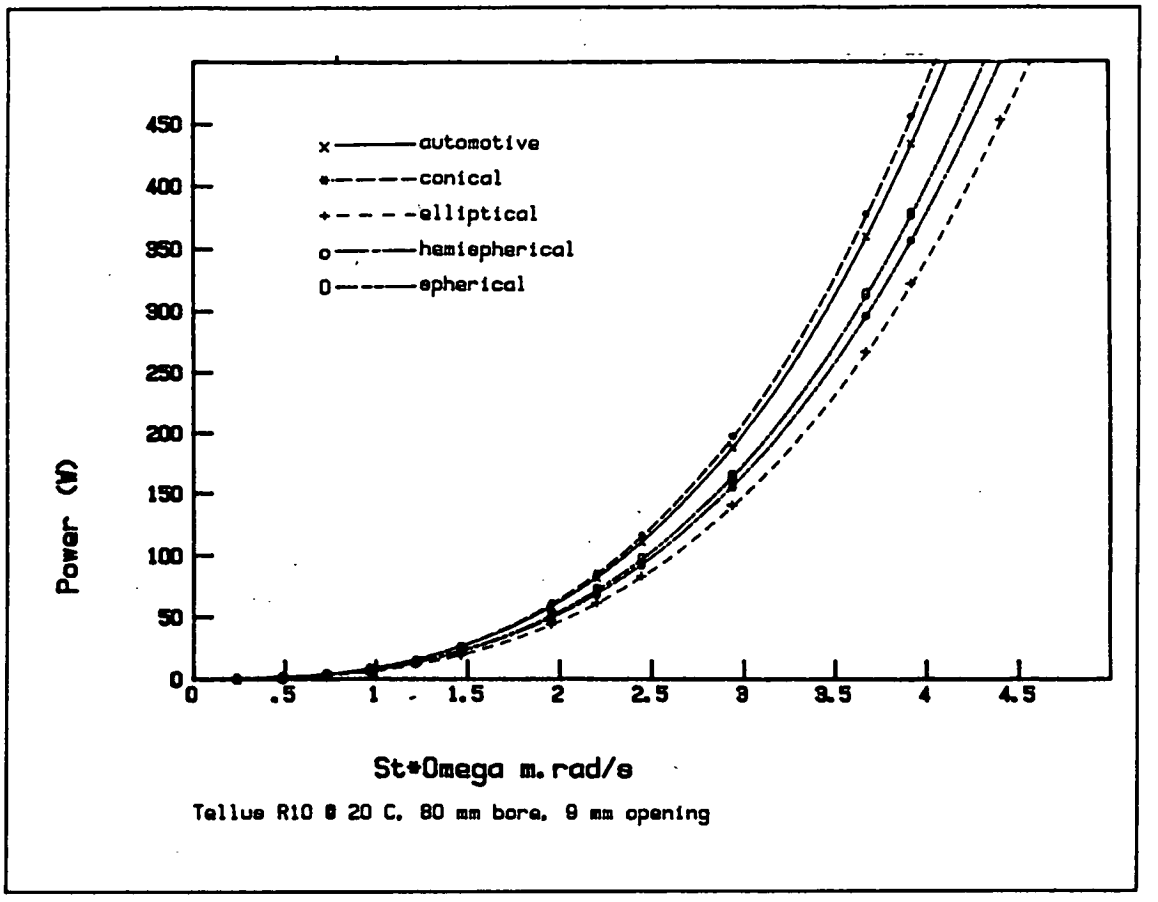

Figure 4.8: Comparison of Disabled Power Loss of Different Poppet Shapes.

The five valve shapes, shown in figure 4.7, used similar dimensions in their respective valve geometries in so far as this was possible. The rounded series of valves were identical from the stem back to the valve seat area while the automotive and conical valves shared all but their neck details. The experimental ranges of the parameters, listed in table 4.1, were determined by a combination of the predicted operating ranges and the observed limits of the apparatus. Figure 4.8 shows the results of the power loss tests with the different valve shapes. The curves are the result of condensing the data into coefficients using the software described in section 4.7 and then plotting the resulting equations. The lower axis, the product of stroke and cycle speed, is proportional to peak flow velocity. Figure 4.9 compares the power loss

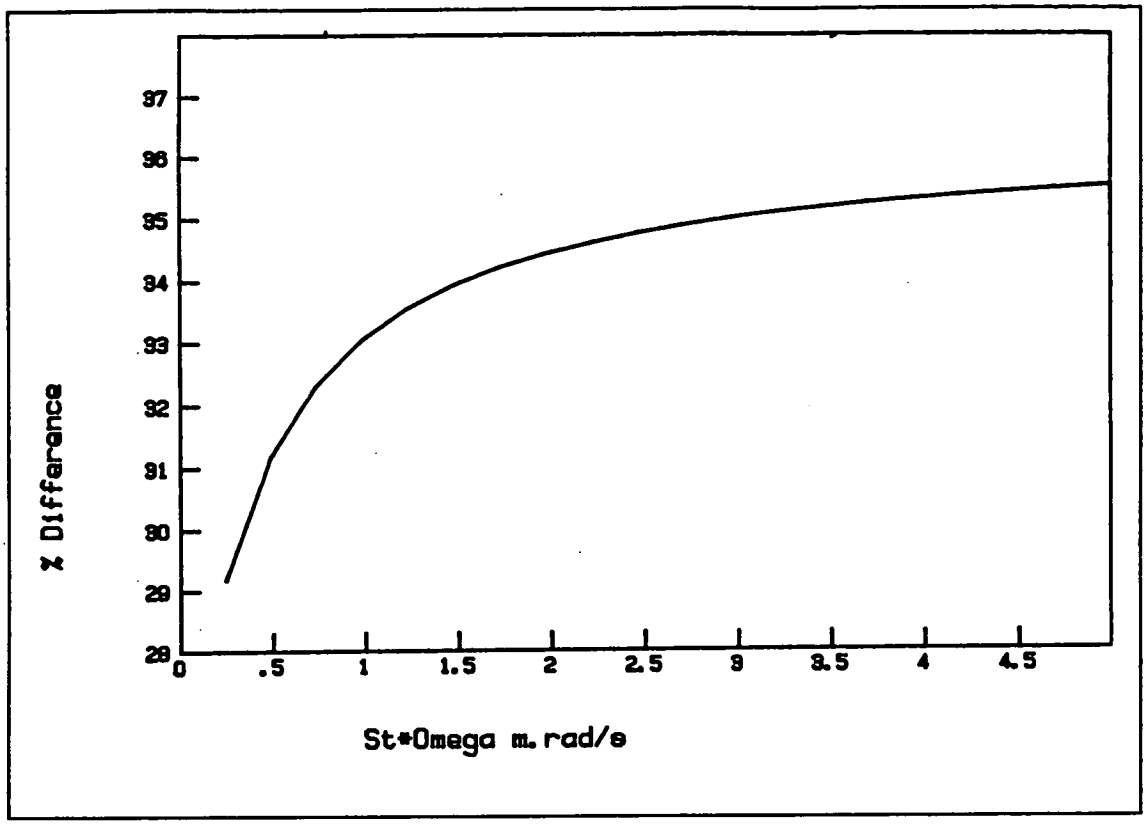

Figure 4.9: Disabled Power Loss Differential Between Automotive and Ellipsoidal Valves as a Function of Flow Rate.

difference between the automotive and the ellipsoidal valves. This graph demonstrates that, at low flow velocities, the difference in loss is small (as skin friction is important) while at higher flow velocities, where inertial effects dominate, it approaches a constant value of approximately 35%. This value is misleading, since it incorporates other flow losses in the duct. In both cases, the kinetic energy of the fluid is effectively lost as the flow emerges from either end of the duct and is decelerated in an uncontrolled way. As such, if the losses attributable only to the flow immediately around the valve heads were to be compared, the difference would be much greater. A minor loss calculation, showing approximate magnitudes of the flow losses in either direction, is presented in appendix F.

Table 4.1 Disabled Valve Experiments: Parameter Ranges

1. Valve Shape Experiments

Bore (D): 80 mm. Strokes: D/2, D

Valve Openings: 0.112D, 0.175D

Cycle Speeds: 1.95, 3.91, 7.81 Hz.

Oil: Shell Tellus R10 @ 20 degrees C,
Density: 869 Kg/m^3, Viscosity: 0.020 N.s/m^2

Valve Shapes: Automotive, Conical, Spherical,
Hemispherical and Ellipsoidal

2. Large Scale Ellpsoidal Valve Experiments

Bore (D): 80 mm. Strokes: D/4, D/2, 5D/8, 3D/4, D

Valve Openings: 0.0038D, 0.0050D, 0.0063D, 0.0075D,
0.0088D, 0.010D, 0.0112D

Cycle Speeds: 1.95, 3.91, 5.86, 7.81, 9.77, 11.71 Hz.

Oils: Shell Tellus R5, Density: 839 Kg/m^3,
Viscosity: 0.007 N.s/m^2
Shell Tellus R10, Density: 869 Kg/m^3,
Viscosity: 0.020 N.s/m^2
Century PWLA, Density: 878 Kg/m^3,
Viscosity: 0.097 N.s/m^2

all oils at 20 degrees C.

3. Small Scale Ellipsoidal Valve Experiments

Bore (D): 24 mm. Stroke: 0.625D

Valve Openings: 0.0042D, 0.0054D, 0.0067D, 0.0079D,
0.0092D, 0.0104D
Cycle Speeds: 3.91, 7.81, 11.71,15.62, 19.54, 23.42 Hz.

Oils: Shell Tellus R5, R10 Century PWLA
(properties as above)

This calculation is not particularly accurate for quantifying the loss of the disabled valve but is helpful in identifying the most important components of power loss in the valve/duct system.

As the initial set of tests used a piezo-electric load cell (prior to the arrival of the piezo-resistive one), the resulting force data lack a reliable DC reference. Nevertheless the difference in peak-to-peak force levels for the different shapes was very large. At the highest flow rates tested, using the automotive shape as a reference, the conical valve required 80% more force to resist the flow while the ellipsoidal valve needed 50% less. The spherical and hemispherical shape results were somewhere between those of the reference automotive shape and the ellipsoidal valve. Because of the limited instrumentation present on the rig at the time and the difficulty in repeating these tests, no attempt has been made to consolidate these values. For the development of the digital pump, these tests were sufficient to demonstrate that hydrodynamically smooth valve shapes provided both flow losses and holding force reductions of sufficient magnitude to justify their development.

The previous observations were reinforced by the use of flow visualisation. A plane of light, produced by a flash tube and collimated by a series of slits, was used to illuminate the flow through the perspex housing. The flash was timed by an electronic circuit which took its trigger from the flywheel and added a controlled amount of delay before firing. By experimentation it was discovered that, by running the rig at high speed, the oil would froth sufficiently to create small air bubbles which could then be used to illustrate the flow streamlines.

The flow visualisation photographs of the automotive and

ellipsoidal valves dramatically demonstrate the difference in flow patterns of the two shapes. Figure 4.10 shows the automotive valve during a disabled discharge stroke at the instant of peak flow. Despite the shape of the traces, the flow is moving out of the cylinder (the bubbles are illuminated more brightly at the start of the flash period). Figure 4.11 shows the ellipsoidal valve at the same instant in time. Comparison of the two photographs demonstrates the differences in flow separation and the resulting vortices. The separation bubble, which begins at the inner edge of the automotive valve seat generates a region of low pressure which acts over the projected area of the bubble. While separation is also present with the ellipsoidal shape, it begins at a smaller radius where the flow velocity is reduced such that the overall area of the bubble and its associated pressure differential are both reduced. Similarly, the comparative photographs of figures 4.12 and 4.13 illustrate the intake flow at the instant of maximum piston velocity.

Overleaf:

Figure 4.10: Automotive Poppet During Disabled Discharge at the Instant of Maximum Flow

Figure 4.11: Disabled Discharge Stroke of Ellipsoidal Valve under Conditions Similar to those of Figure 4.10

Figure 4.12: Intake Stroke through Automotive Valve at Instant of Maximum Flow

Figure 4.13: Intake Stroke through Ellipsoidal Valve under Similar Conditions to those of Figure 4.12

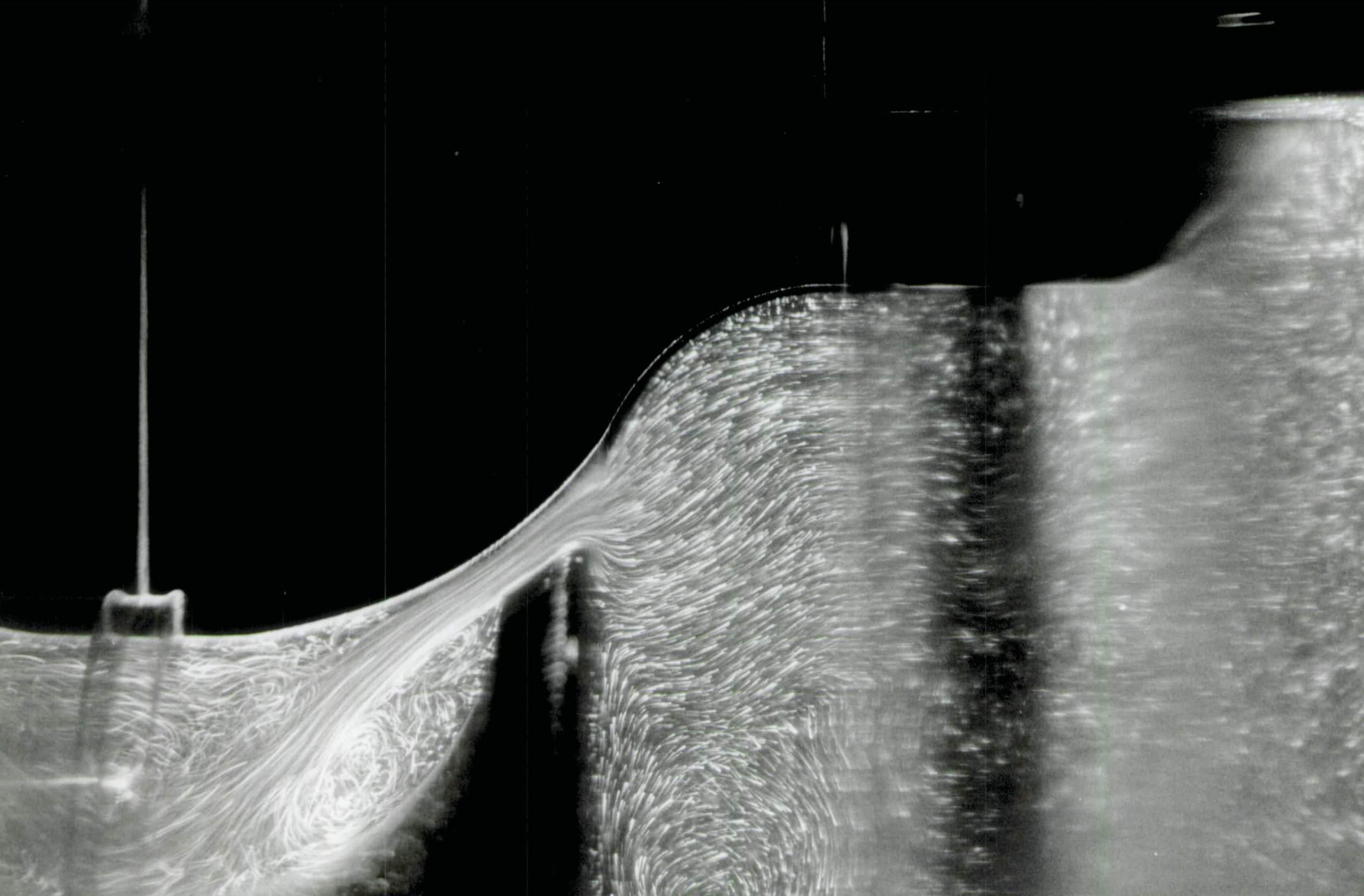

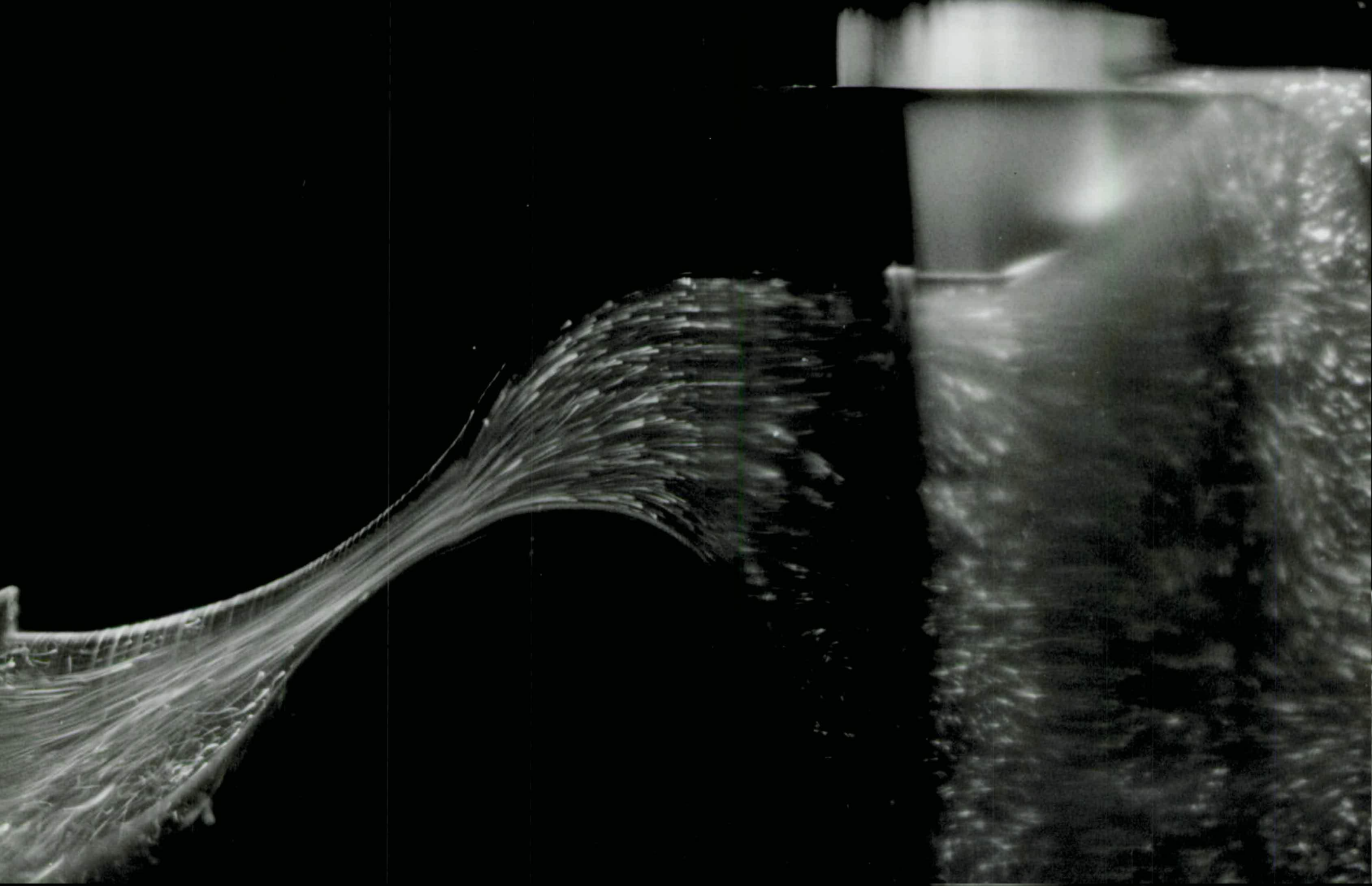

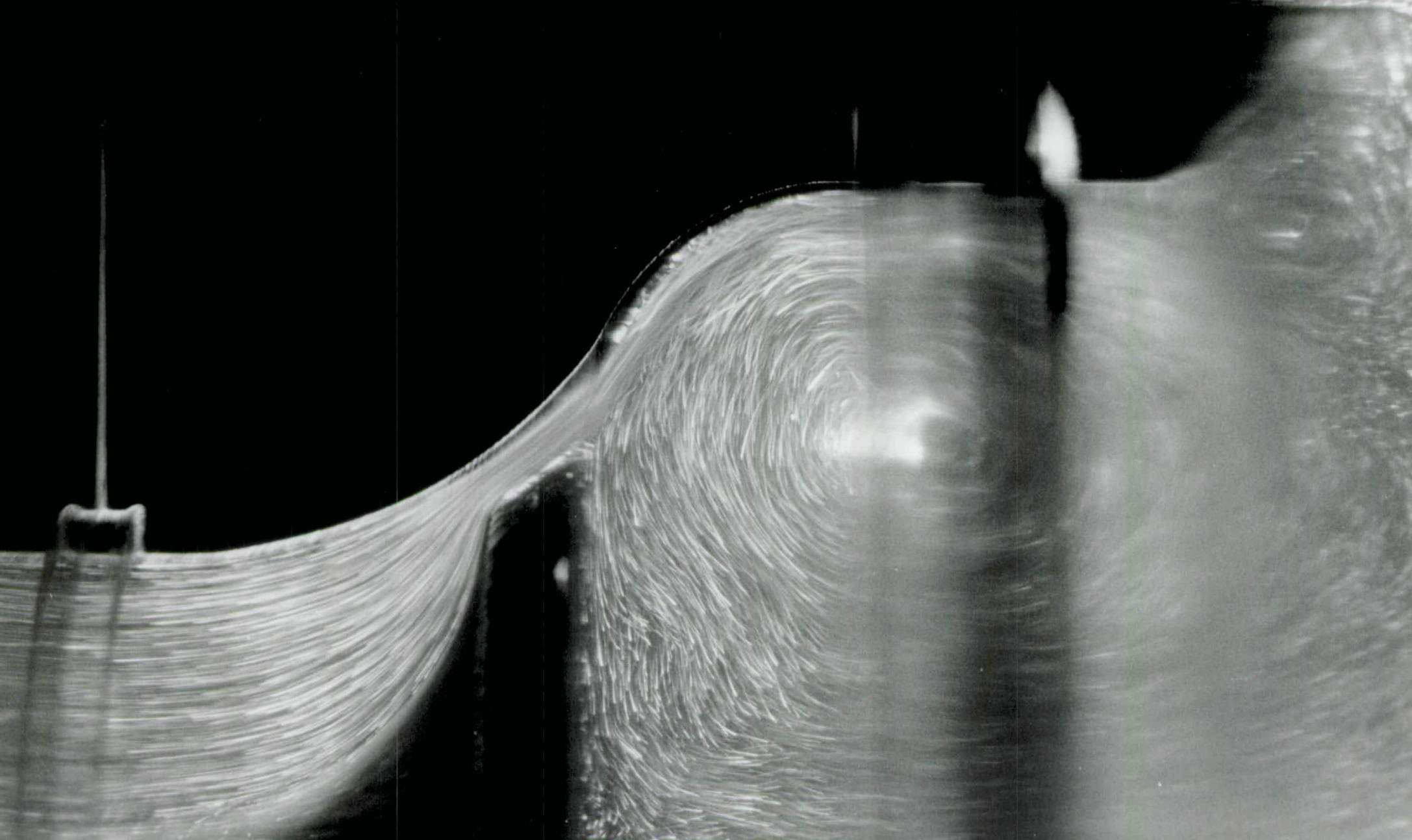

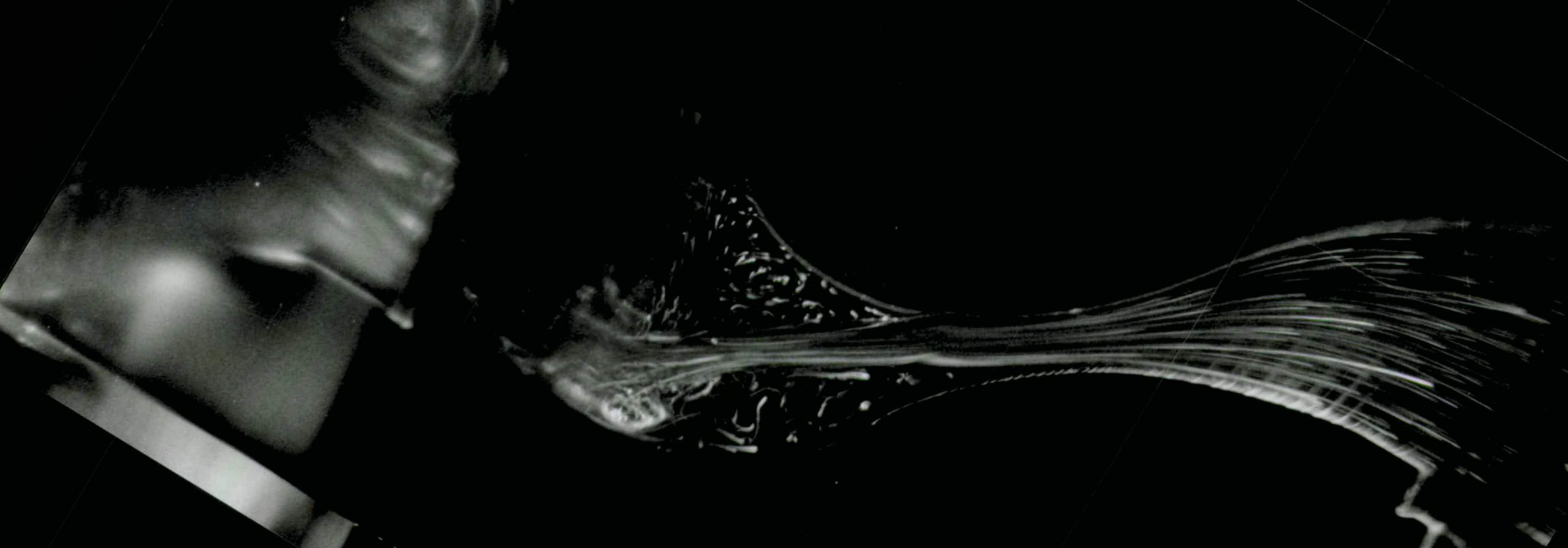

In this case the expansion of flow area around both valve shapes is too severe and the resulting vortices are roughly equivalent. This observation is borne out by the limited force results which show similar levels amongst all of the valve shapes for this direction of flow.

4.8.2 Ellipsoidal Valve Experiments

The first set of experiments confirmed the intuitive selection of the ellipsoidal valve shape on both force and loss grounds. Although there were certainly further improvements to be wrung from development of the ellipsoidal valve shape, the relative differences of the three smoother shapes demonstrated that these were liable to be of diminishing value. The rewards for this work would be further diminished by the practical issues of available space and working fluid which, in each pump design, would force the use of different configurations, seat angles and flow paths. For these reasons the first ellipsoidal shape was adopted and used exclusively for the remaining experiments.

The second series contained 303 individual experiments conducted at different parameter settings, although some of these were later discounted in the analysis process. There were two main causes for rejecting data. The tests involving the highest power losses and forces tended to overload the speed control system, which led to slippage between the flywheel position and the sampling time. The phase error between the pressure waveform and the associated theoretical flow function was sufficient to corrupt the power loss calculation. As the power value from such experiments was generally an order of magnitude out from the expected value, this type of failure was easy to identify. Additionally, the validity of the power results could be verified by checking the spread of the FFT teeth around the fundamental frequency.

The second main cause of data rejection lay with the small forces measured at the lowest speeds and strokes. The reason for inconsistent data was the tendency for the load cell to develop small offsets, during the course of experimentation, which equalled or exceeded the magnitudes of the measured forces of these tests. The condensed results of the 219 valid experiments are presented in appendix G.

The two time traces of figure 4.14 show representative force and pressure drop cycles. While it is immediately obvious that both signals are primarily sinusoidal it should also be evident that there are even and odd harmonics present.

The large DC offset of the force trace can only be due to a combination of the rectified velocity-phase force, which acts in the region of the valve seat, and the differential pressure drop in the duct for the two flow directions. The duct losses should be greatest during the intake stroke because of the uncontrolled expansion into the cylinder from the region of highest velocity near the valve seat. This should generate a larger pressure differential across the valve and thus a higher force than that of the discharge stroke. The magnitude of the DC offset indicates that these two factors must account for a relatively large percentage of the overall poppet force. It can also be noted that the trace has the pointed peaks expected in a signal composed primarily of a sine-squared term. The rectified force need not be the same during both intake and delivery cycles since the duct, as seen by the fluid, is quite different in each direction. Thus the two positive humps in the force trace, created by the inertial velocity- phase term, need not be the same height. The FFT of the force signal, shown in figure 4.15, has a large velocity-phase second-harmonic component as a result of this effect.

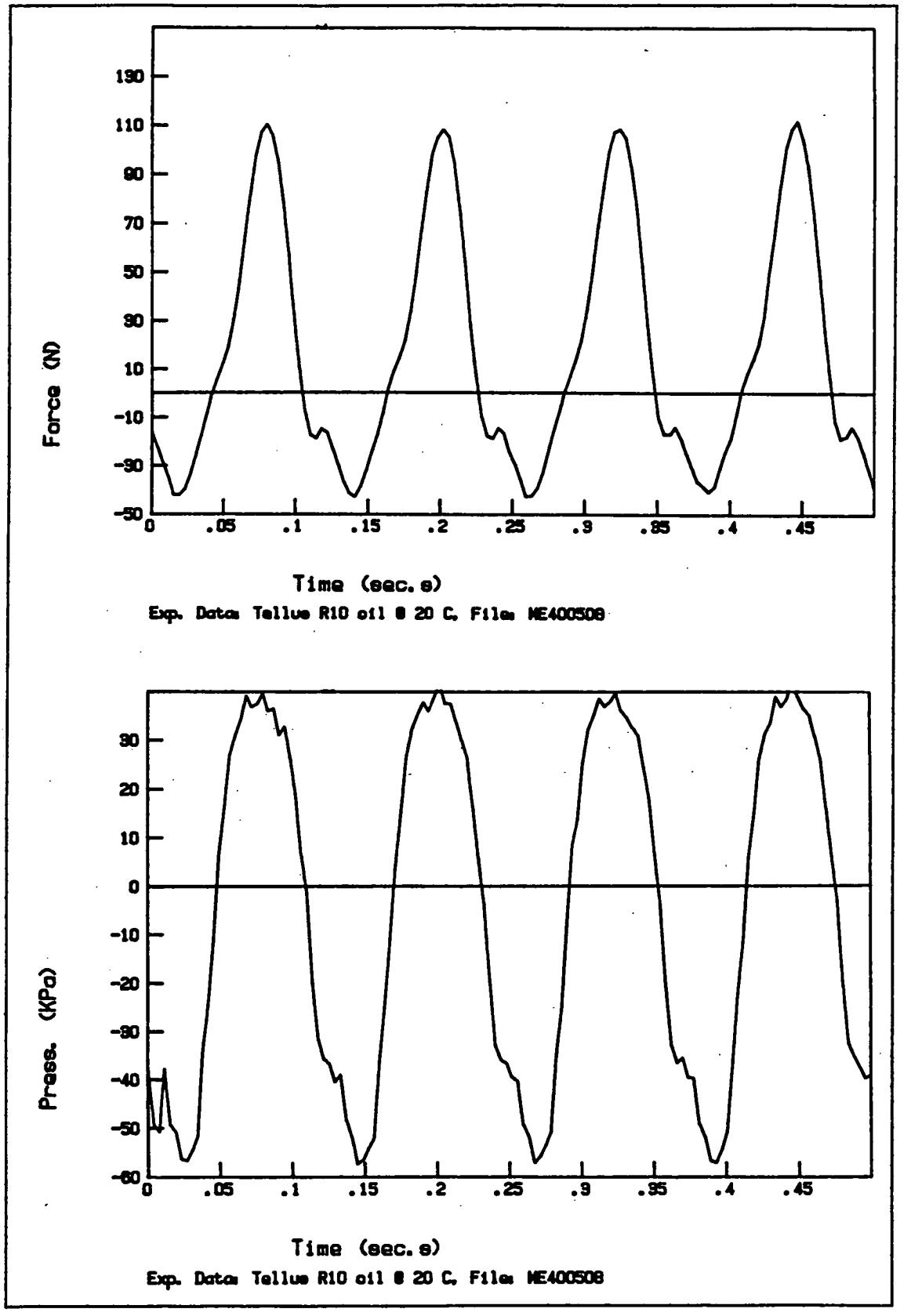

Figure 4.14: Typical Force and Pressure Time Traces for Disabled Ellipsoidal Poppet Valve.

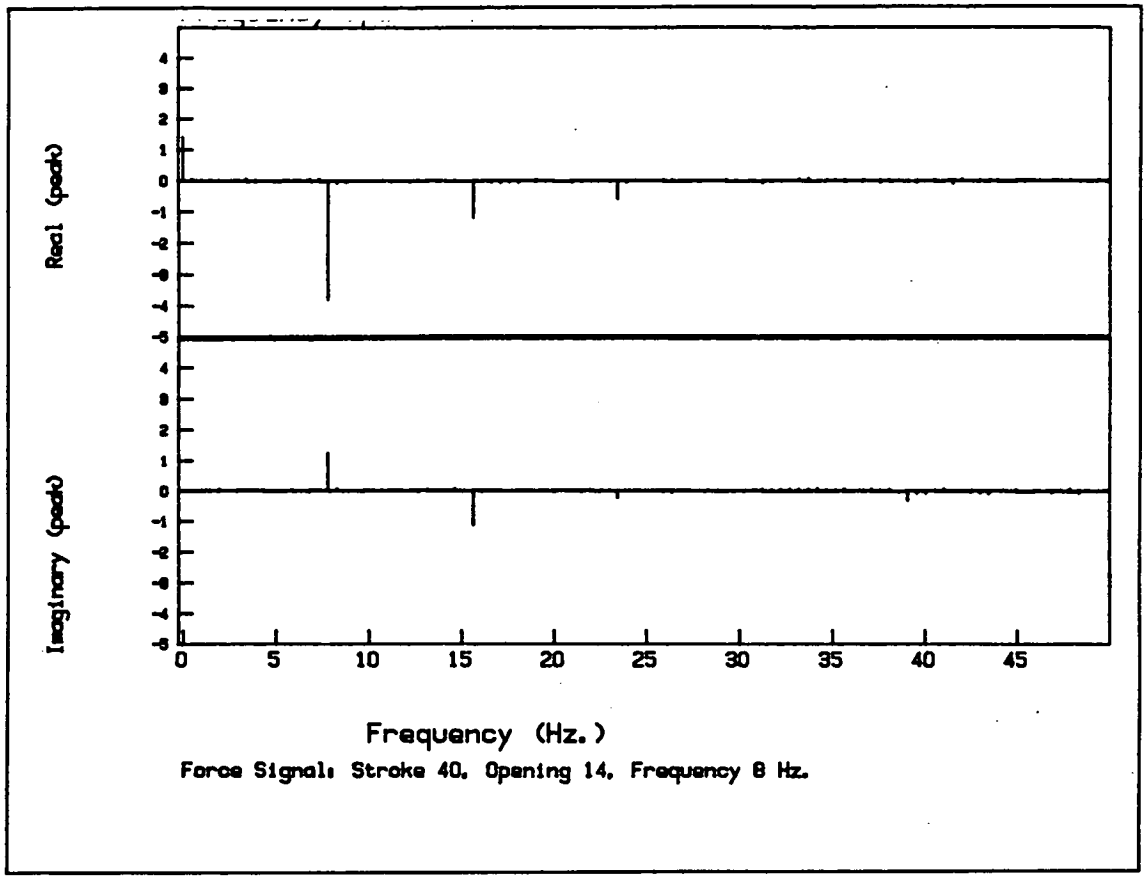

Figure 4.15: Typical Frequency Spectrum of the Force on the Disabled Ellipsoidal Poppet.

This graph requires some interpretation since both the DC force offset and a non-negligible second-harmonic appear in the real array and yet must be associated with velocity-phase effects. The pressure generated by the temporal acceleration of the fluid past the valve is in phase with piston acceleration and could reasonably be expected to be sinusoidal in form. It is within the nature of Fourier transforms that DC levels have meaning only in the real phase and thus cannot appear in the imaginary array. The second-harmonic is a representation of the sine-squared term caused by the rectified flow

force in the region of the poppet seat. The trigonometric equality:

$$Sin^2(\omega t) = \frac{1-\cos(2\omega t)}{2}$$

allows a fuller understanding of the situation since the DC offset in the real array should be entirely offset by the second harmonic term in order that the acceleration-phase force has the expected pure sinusoidal shape. The third harmonic component in the real array could be due to a combination of phase error, due to either imprecision in calibration of the trigger or flywheel velocity variation, and imperfection in the harmonic motion, due to the crank/con-rod geometry.

The important effect of the temporal acceleration is, primarily, that it moves the phase of the force peaks slightly away from the two maximum velocity points in the cycle. The skin friction force component plays an increasingly important role as the oil viscosity increases and the pump size drops. The force trace of figure 4.16, captured under these lower Reynolds number conditions, demonstrates the difference in waveform shape due to the increased significance of the viscous term. As would be expected, the abrupt change in the force during suction, as was visible in figure 4.14, is much reduced in the smaller cylinder. This abrupt change would appear to be caused by the flow separating away from the poppet surface on the duct side of the poppet head. As such, the upstream surface of the poppet is suddenly exposed to a higher pressure and the net upward thrust on the valve increased.

The pressure traces of figures 4.14 and 4.16 can also be seen to be mostly harmonic, though the phases at the

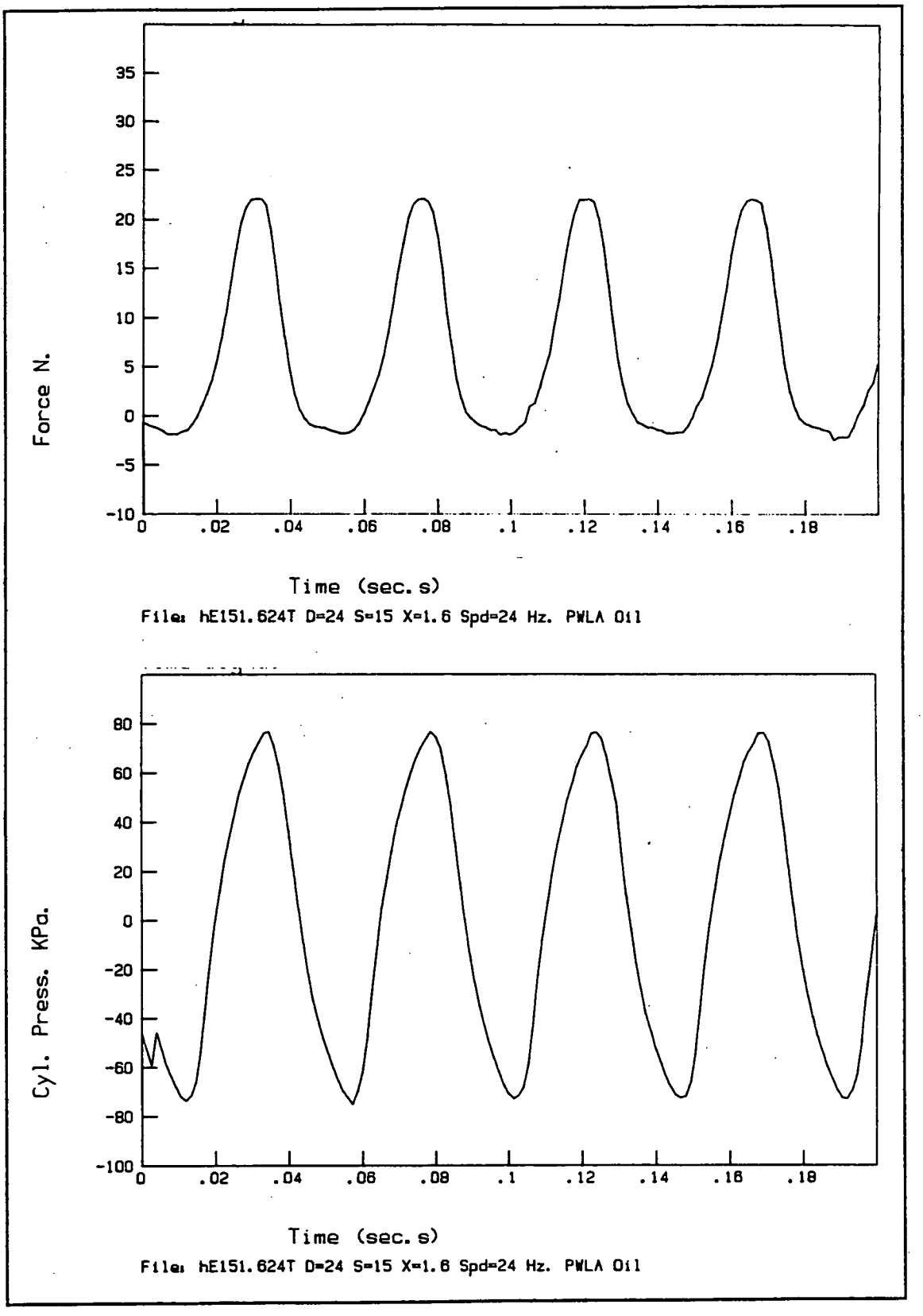

Figure 4.16: Typical Force and Pressure Time Signals for the Disabled Ellipsoidal Poppet at Low Reynold's Number.

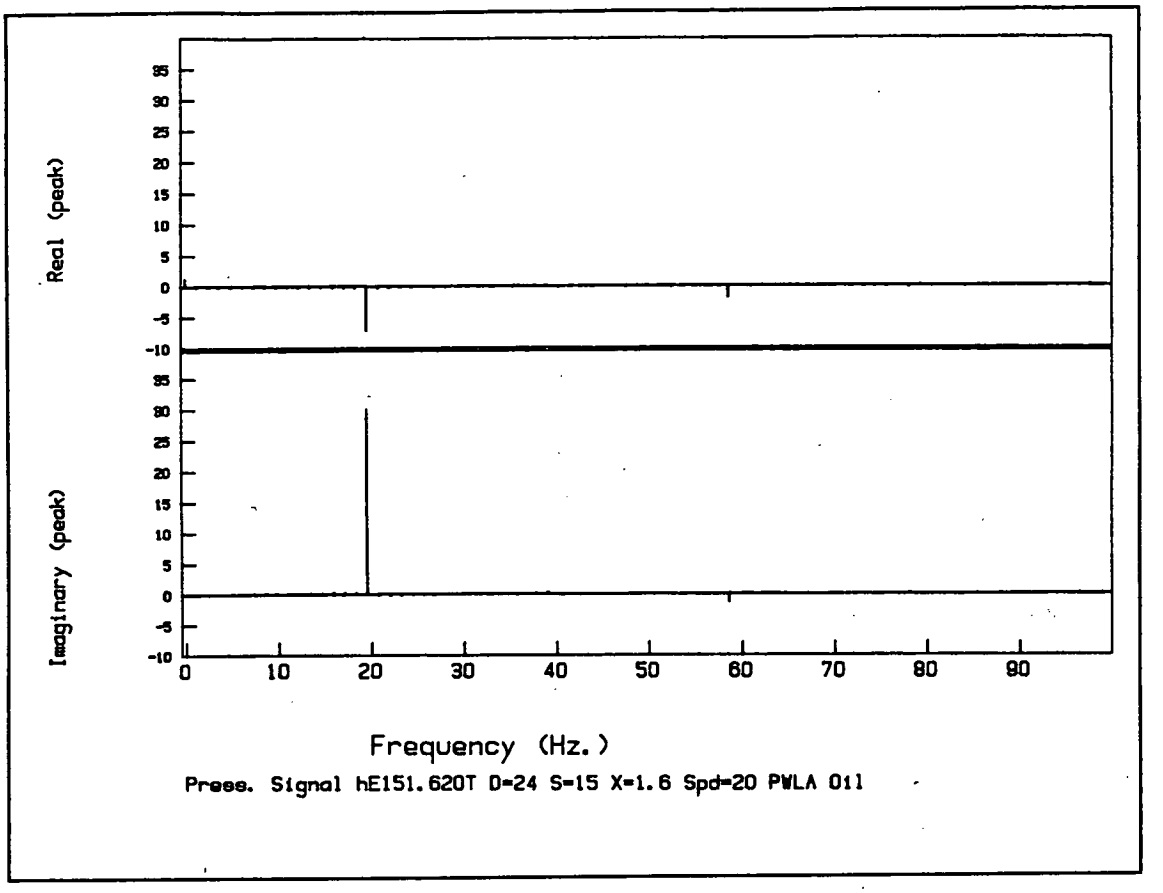

Figure 4.17: Typical Frequency Spectrum of the Pressure Drop Across the Disabled Ellipsoidal Poppet Valve Under Low Reynold's Number Conditions.

fundamental frequency are considerably shifted from those of the piston velocity. The frequency plot of the pressure waveform, shown in figure 4.17, illustrates the ratio of velocity and acceleration phase pressure drops at the fundamental frequency. The high frequency ripple of approximately 70 Hz., seen at the pressure extremes of figure 4.14, may well be due to resonances in the apparatus structure and pump mechanism. This ripple is not apparent in the equivalent plot of figure 4.16 since the rig is not operating at the extreme of its performance envelope, as it was in the first instance.

4.9 Experimental Data Reduction

For maximum design flexibility, the disabled poppet force and loss equations were designed to incorporate the parameters of shaft speed, stroke, valve opening, cylinder bore, fluid viscosity and density. The work of both Tanaka [56] and McGinn [57] allows the prediction that these equations would contain both inertial and viscous terms, in phase with velocity, as shown in equation 4.1.

$$P = C_1 \mu Q + C_2 \rho Q^2 \qquad (4.1)$$

Where: P= *Pressure drop*
Q= *Maximumflowrate*
μ= *viscosity*
ρ= *density*
C_1, C_2= *Duct geometry coefficients*

The general constitution of these two terms can be formulated using elementary fluid mechanics for both equations and verified by comparison with McGinn's equation. As several papers mention the importance of cylinder wall interactions, i.e. Stone [53], the equations have been expanded to incorporate each parameter explicitly so that effects attributable to any one of them are not lost through their combination with others as in equation 4.2. The constants C1 and C2 still contain information about the valve opening which might be usefully included in the equation as parameters.

$$P = \frac{C_1 \mu S \omega \pi D^2}{8} + \frac{C_2 \rho (S \omega \pi D^2)^2}{64} \qquad (4.2)$$

Where: S= *Stroke (m)*
ω= *Pump shaft rot. vel. (rad./sec.)*
D= *Cylinder bore (m)*

A third term, that modelling the inertial component due to temporal acceleration, is useful in the case of both the pressure and force prediction equations (though not employed for power loss calculations since it is out of phase with the flow):

$$P_{a\,max} = \frac{C_3 S \omega^2}{2} \qquad (4.3)$$

Where: $P_{a\,max}$ = *Peak acceleration-phase pressure (Pa)*
C_3 = *Const. approx. of equiv. duct length (m)*

Using dimensional analysis the pressure can be non-dimensionalised and expressed in terms of appropriate non-dimensional parameter terms:

$$P' = \frac{P}{\rho \omega^2 D^2} = fn\left[N_r,\ \frac{S}{D},\ \frac{x}{D} \right] \qquad (4.4)$$

Where: N_r = *Reynolds Number*
x = *Valve opening*

The constants and exponents, appropriate to each of the terms, for a given geometry then need to be assessed experimentally. The technique can also be used to express the valve force and power loss in terms of non-dimensionalised parameters.

The force, power and pressure measurements from the 264 valid experiments were condensed in two stages to produce the three modelling equations.

1. The non-dimensionalised measurements were systematically compared to the dimensionless parameter terms, such as those of equation 4.4, so that the correct exponent of each term could be established.

2. Secondly, constants were determined using a weighted least squares algorithm which was designed to reduce the significance of the larger values. This weighting was based solely on the experimental parameters which formed the inertial term, since it was dominant over the viscous one.

Ultimately this process allowed all of the data to be plotted on three graphs, for each of maximum poppet force, power loss and minimum cylinder pressure, as shown in figures 4.18 and 4.19. The resulting modelling equations, with parameter range restrictions, are set out in table 4.2. The acceleration phase term of the force modelling equation was found, during the least-squares procedure, to be negligible with respect to the velocity-phase terms and so has been dropped from the equation.

The suction pressure results were much less consistent than the force and power ones. The modelling predictions seem to be accurate only to within fifty percent. The variability in the results, which were not easily explained in terms of deviation with respect to any one of the modelling parameters, might stem from the same flow separation phenomena visible in the force trace of figure 4.14. Since the onset of separation is, to some degree, random in its timing, the negative pressure levels seen in the cylinders might also be slightly random with respect to the controlled variables. As might be expected, this effect is demonstrated in figure 4.19 to be of greater significance under conditions where the suction pressure does not fall significantly below atmospheric levels.

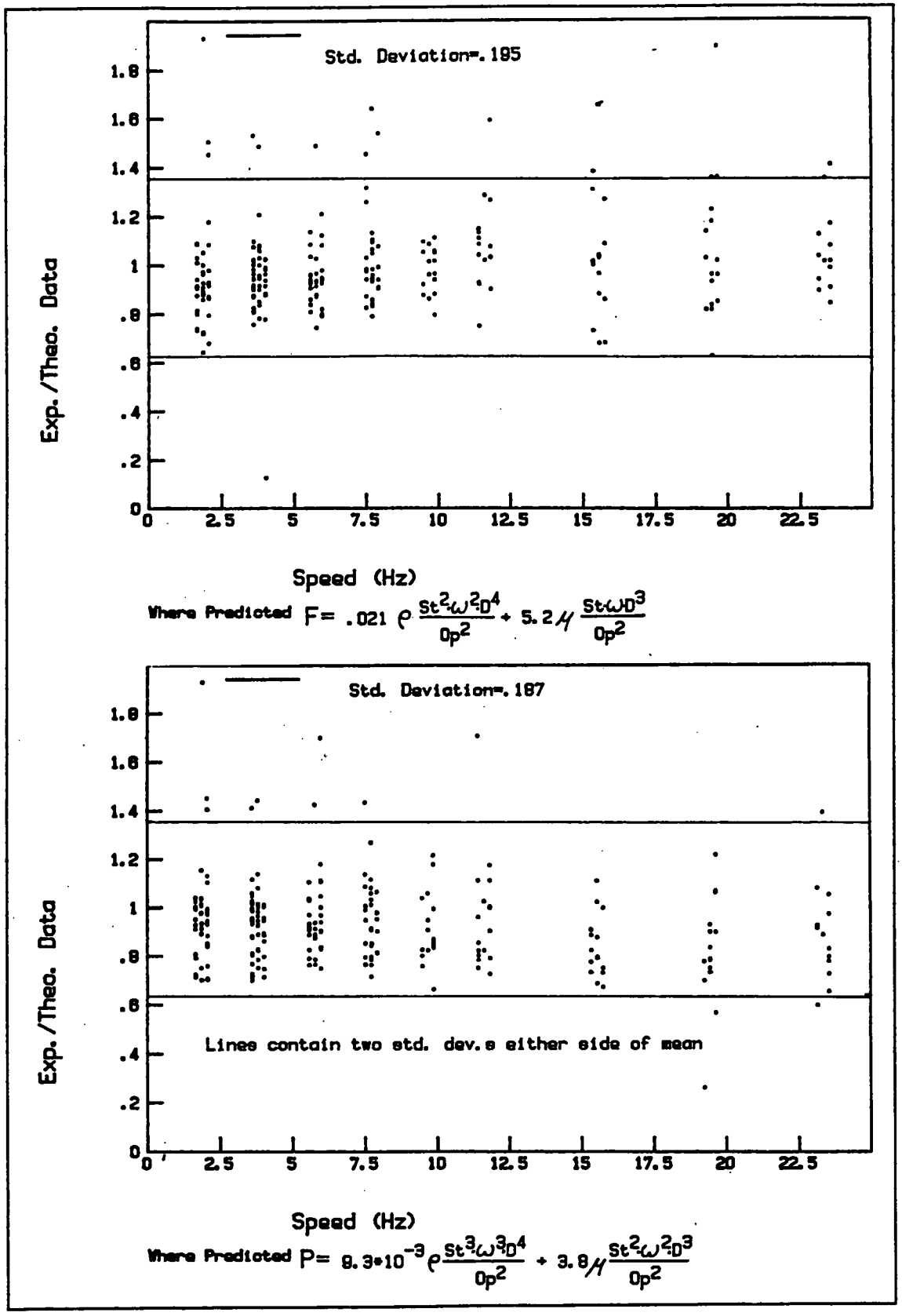

Figure 4.18: Condensed Data From Disabled Ellipsoidal Poppet Experiments: Force and Power Results.

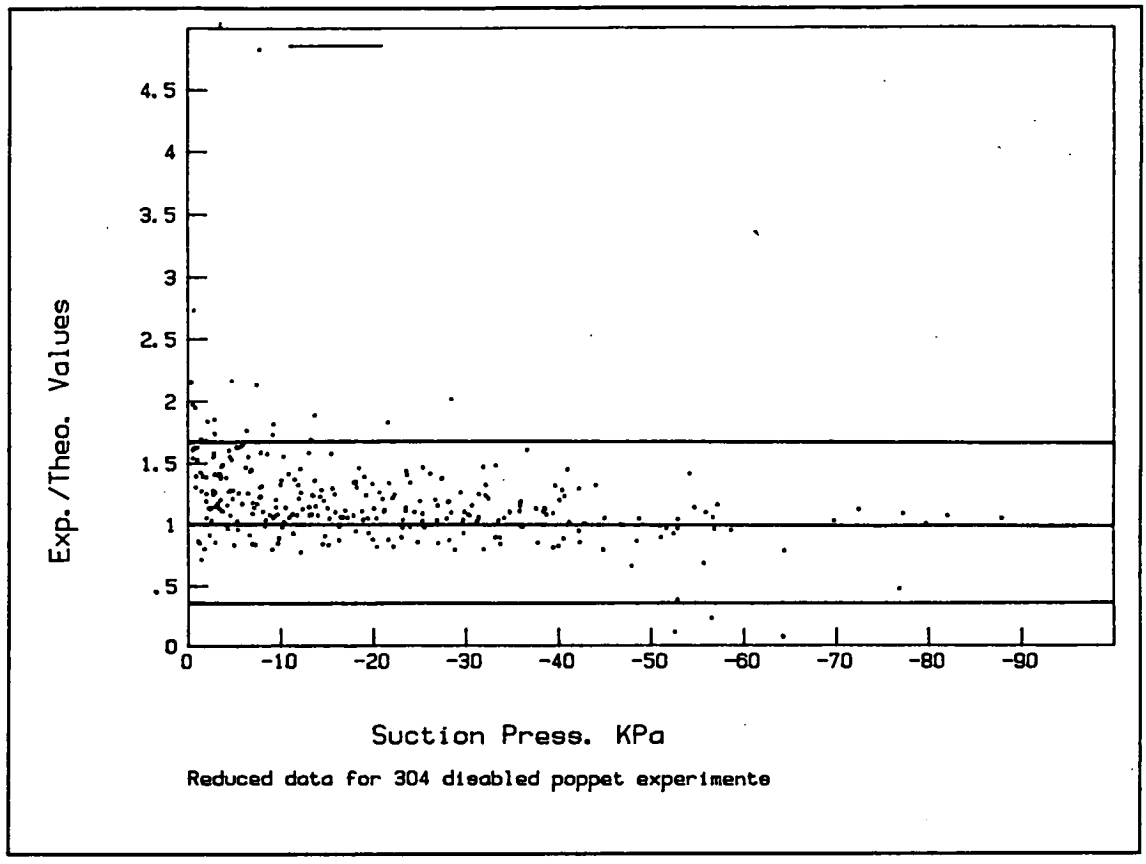

Figure 4.19: Condensed Results from Disabled Ellipsoidal Poppet Experiments; Minimum Cylinder Pressure

4.10 Error Analysis

The validity of the data reduction exercise can be judged by the deviation of the experimental data from the mean. It would appear that two standard deviations, or a band containing 99 percent of the data, equates to approximately 38 percent of the mean value for both the force and power data. This spread is higher than would be desired with, perhaps, a 20 percent error band being the acceptable maximum given the nature of the measurement task and the end use of the data. This error level would be achieved with the discounting of the dozen most errant experiments. Most of these can be seen in figure 4.18 to originate from the lower speed tests where the signals were orders of magnitude down on the high-

speed ones. The deletion of these experiments would not affect the actual coefficient values since the remaining results are symmetrically clustered along the line which represents a perfect fit.

Other sources of experimental error can be identified as well. The effect of valve opening on the force and pressure measurements becomes quite large as the valve opening is, itself, made small. Small inaccuracies in measurement, especially on the small-scale valve, could lead to substantial errors in the equation coefficients. If the combined position error, caused by setting inaccuracy and the flexure of the load cell and valve support column, totalled 0.10 mm, then at a nominal opening of 1.0 mm there would be a ten percent difference in opening and a 23 percent error in the result. The other parameters of stroke and speed were much more precisely controlled and would contribute much smaller error components.

The second large source of error may well arise out of the geometry differences of the large and small scale valves. Although quite similar in shape, the small valve was designed to be supported on three forward-thrusting partially-streamlined stalks. These supports interrupt the flow and generate drag. The flow tube of the small-scale valve is coupled to the load cell while the large one is not. The doubling of area of the moving poppet exposed to skin friction drag will most certainly have an effect on the viscosity-term force coefficient.

Table 4.2 Design Equations Resulting from Ellipsoidal Valve Tests

Maximum Closing Force on Disabled Poppet:

$$F = 0.021\rho\frac{S^2\omega^2D^4}{X^2} + 5.2\mu\frac{S\omega D^3}{X^2} \quad N.$$

Averaged Power Loss Across Disabled Valve:

$$P = 9.3 \times 10^3\rho\frac{S^3\omega^3D^4}{X^2} + 3.8\mu\frac{S^2\omega^2D^3}{X^2} \quad Watts$$

Minimum Cylinder Pressure During Suction Stroke:

$$p_s = -0.022\rho\left[\frac{S\omega D}{X}\right]^2 - 12\mu\frac{S\omega D}{X^2} - 0.31\rho\frac{S\omega^2 D}{X} \quad Pa.$$

These Equations Apply Over the Following Parameter Ranges:

Bore:	$0.024 < D < 0.080$
Stroke:	$0.25D < S < D$
Valve Opening:	$0.041D < X < 0.104D$
Cycle Speed:	$0 < \omega < 150$ *rad/sec.*
Density:	$839 < \rho < 878$ *Kg./m*^{3}
Viscosity:	$0.007 < \mu < 0.096$ *N.s/m*^{2}

While the equations might be useful beyond the experimental operating ranges, care should be exercised when considering valve openings smaller than those tested as cavitation may well invalidate the result.

The accuracy of the force and power prediction equations is +/- 30 % (2 std deviations).

The accuracy of the minimum pressure equations +/- 50 %. The imprecision of the pressure result is due to the variable nature of flow separation during the intake stroke. A factor of safety of 1.5 is recommended when employing the pressure prediction equation.

5.0 Hardware Implementation of the Digital Displacement Concept

5.1 Chapter Overview

In the course of this study a commercial poppet-valved piston pump was converted into a variable output digital displacement pump. In performing this conversion, several pieces of the original pump were modified and many new ones designed and machined. This chapter documents this process with the aim of recording the problems encountered, the design calculations appropriate to their resolution as well as the resulting solutions so that subsequent conversions have an established path to follow. As such the chapter is divided into many diverse sub-headings, all of which share only the common theme of mechanical hardware design.

5.2 Poppet Material and Compressive Stress in the Seat Area

The most highly stressed components requiring redesign were the inlet poppet valve and its mating seat. Traditionally hardened steel valves have been used on softer steel seats for this application. This material combination seems to provide more than adequate life and has not, to the knowledge of the author, been cited as the principal cause of failure for any poppet pump. Piston/cylinder bore wear, valve spring fatigue and rolling element bearing disintegration seem to be the frequently cited causes [64]. With the inclusion of a magnetic latch design around the valve, as discussed in chapter three, it becomes important that the valve be made of non-ferromagnetic material so that ferrous particles are not attracted into the sliding bearing of the poppet shank. Various grades of stainless steel can

be considered as candidate materials, as they combine both the requisite strength and magnetic properties. Titanium or ceramic might also be considered as a possibility but would be hard to justify on both material and machining cost grounds.

Several high-strength reinforced thermo-plastics were, on the advice of the industrial partner, investigated as well. While none of these have the hardness of conventional valve materials, they do have a much lower elastic modulus and are able to conform to the valve seat so that the load is both adequately and evenly spread. There are several major advantages to the use of a thermo-plastic, providing that its service life in pumping conditions is adequate:

1. The mass is approximately one eighth of its metal equivalent, which allows a much faster closing response.

2. The noise produced on valve closure is reduced since the low modulus valve deforms significantly during the sudden pressure rise as pumping begins.

3. The production cost of an injection moulded component will be much less than a machined one, despite the very high cost of the raw materials (£50/Kg, 1990).

The data available for these plastics is of limited use for evaluating their performance in this type of service. The repetitive compressive loading cycle of the poppet seats is not duplicated by any of the standard tests [65,66]. The additional factors of surface abrasion, creep and elevated temperature performance would also

need to be included in any representative test. To complicate matters still further, the non-homogenous composition of the reinforced mouldings will cause the plastic properties to differ in relation to the direction of fibre alignment.

Despite these uncertainties, the advantages of the plastic poppets seemed sufficiently strong to warrant their testing. After the failure of the first phosphor bronze poppets (due primarily to an unforeseen stress raiser), the prototype pump was fitted with equal numbers of poppet valves machined from either PAI or PEEK bar stock (both 30% graphite fiber filled).

Finite element analyses were conducted by Paul Griffiths, of J.H. Fenner Ltd., to gauge the level of contact stresses for the two materials. Figure 5.1 shows the mesh of the axi-symmetric model with gap elements used to join the poppet and its seat. Figure 5.2 shows the compressive stress distribution near the contact line for the PEEK poppet. While there is a high level of compressive stress at the contact, it should also be noted that there is a tensile stress of significant magnitude in the unpressurised valve-throat region. This is due, most probably, to the localised stretching of the poppet surface as it conforms on its seat.

The stresses appeared to be marginally lower in the PAI poppets, but the difference was insufficient to yield a clear choice. In the event, after two years of intermittent use in the laboratory prototype, the PEEK poppets were still fully serviceable while the PAI ones showed signs of brittle delamination at the contact area of the seat (possibly due to the predicted high levels of tensile stress). As the pump was being run as a development machine and demonstrator, there is no

possibility of inferring poppet life data from this observation.

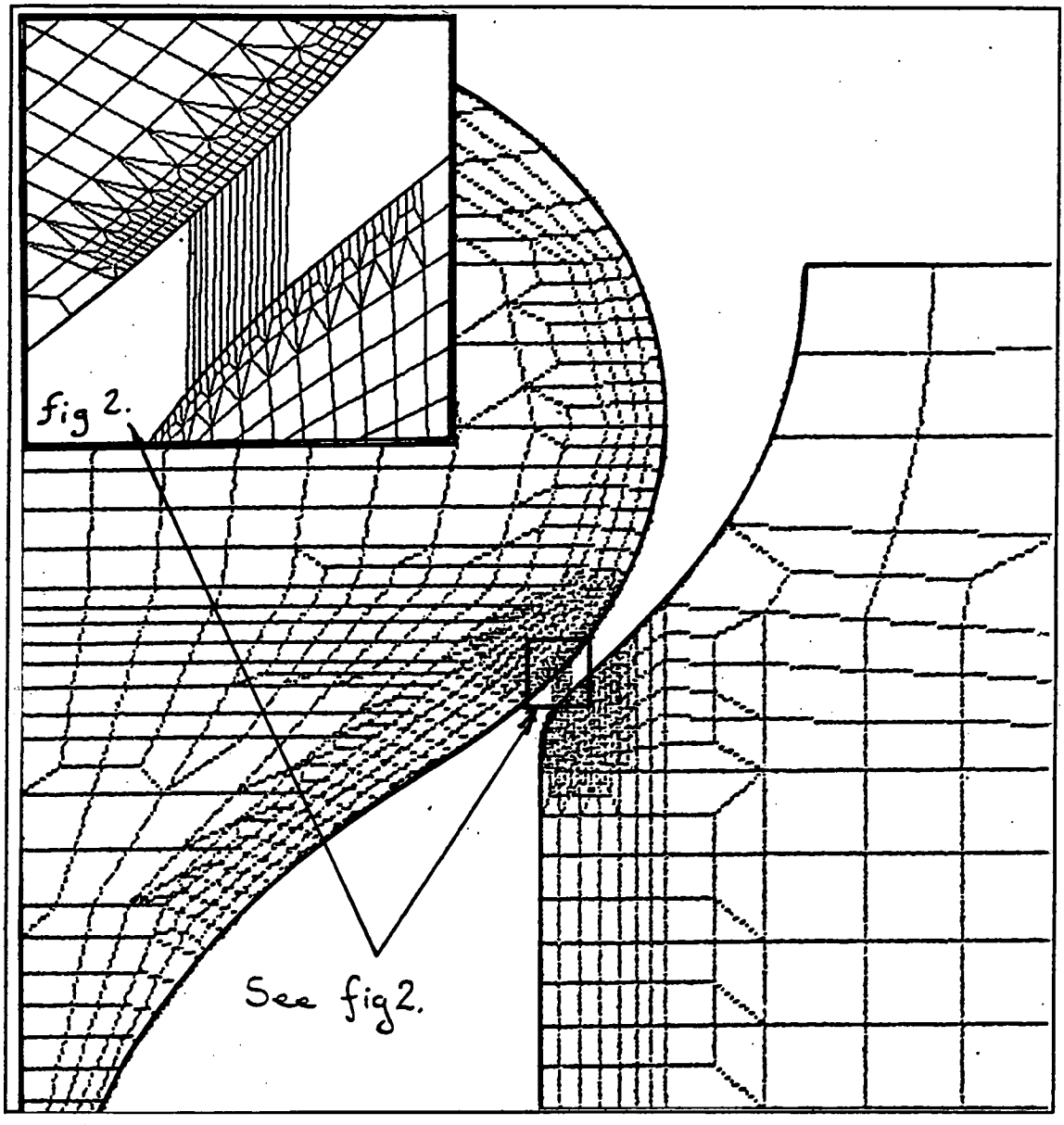

Figure 5.1: Axisymmetric Finite Element Mesh of Poppet Valve and Seat. From an Internal Report by Paul Griffiths of J.H. Fenner Ltd.

The material comparison does show that the documented properties and analytical techniques are not reliable enough in this area to be used in isolation. The PEEK

poppets had receded slightly along the sealing line but, being softer and less brittle than PAI, this did not cause delamination. The recession of the seat seemed to be self-limiting since the seat area grew simultaneously, thus reducing the contact stress to a level where it could not progress further. Exhaustive testing of this and other candidate materials would seem to be the only way to ensure adequate service life. While accelerated cycling of the components is an attractive way of reducing testing time, great care must be exercised to ensure that internal heat generation in the plastic, which would not occur in practice, does not cause non-representative and misleading failures.

5.3 Squeeze Film and Damping Effects in the Latch

The magnetic latch unavoidably involves small gaps between moving surfaces in a flooded chamber. These characteristics give rise to the two effects of squeeze film and viscous damping. The forces on the moving pole due to the latter effect are not of great concern since they affect the valve motion only as a function of velocity. Once the solenoid has forced the moving pole to unlatch itself from the permanent magnet, it works with an increasing advantage as the valve closes. Step response tests of a latch working both in air and oil, with the fluid damping coefficients orders of magnitude apart, demonstrate that the transit time varies only by 10 percent as shown in figure 5.3. Nevertheless, attempts have been made in the design of the latch to minimise the resistance to fluid flow through and around the moving pole. Holes have been drilled through the radial web of this piece for this purpose.

The squeeze film forces are of concern since, when the valve is open and there are contacting magnetic surfaces

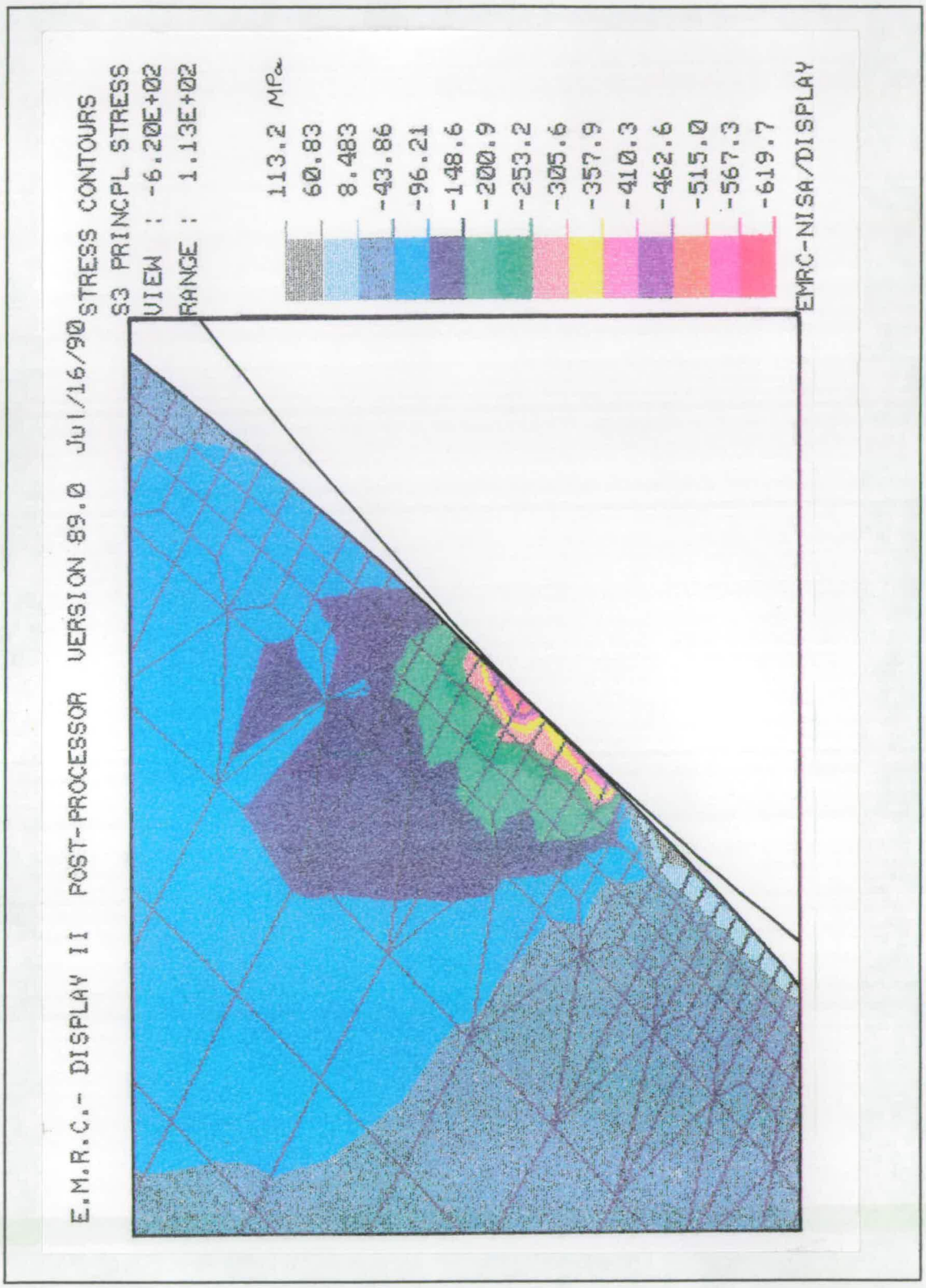

Figure 5.2: Compressive Stress Contour Plot of PEEK Poppet with 200 Bar Fluid Loading. From Internal Report by Paul Griffiths.

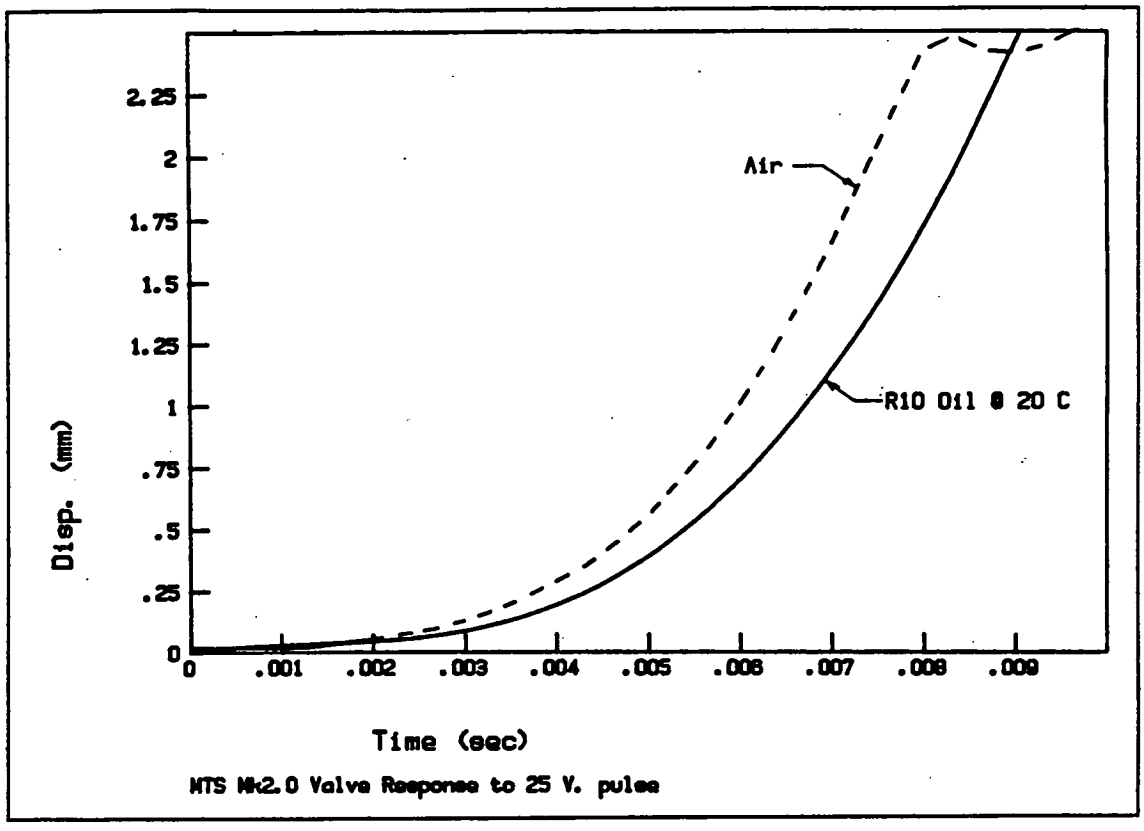

Figure 5.3: Poppet Displacement as a Function of Time. Tests in Both Air and Oil with Zero Flow in Valve Duct.

latching it, the solenoid is working at its greatest disadvantage. The standard equations for evaluating squeeze film forces can be employed to establish minimum clearances for the non-contacting parts of the approaching magnetic poles.

$$F = \mu \frac{dW}{dt} \frac{1}{W^3} fn(r^2)$$

Where: F = *Squeeze film force* (N)
μ = *Viscosity* $(N.s/m^2)$
W = *Squeeze film gap* (m)
$fn(r^2)$ = *Surface geometry function* (m^2)

In order to calculate forces, a knowledge of the velocity function of the pole as it detaches is required. This is

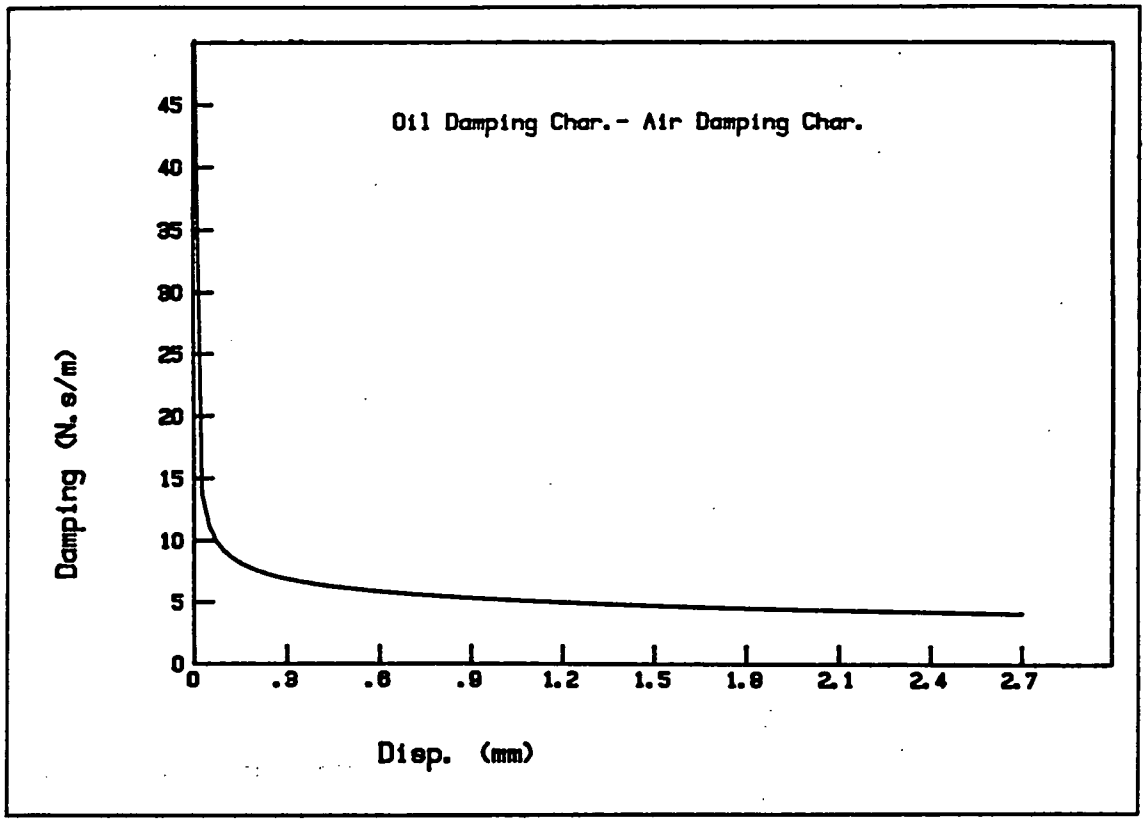

Figure 5.4: Damping Coefficient of Fluid Within the Magnetic Latch as a Function of Poppet Displacement.

difficult to estimate theoretically, since so many other time variant forces are acting on the valve. A valve from an early prototype was instrumented with an inductive proximity sensor in order to produce a time trace of valve position (as previously shown in figure 5.3). In order to resolve the noise created by digital differentiation, the signal was fitted with a polynomial approximation using a least-squares technique. The polynomial was then differentiated to produce an approximate velocity function. This produced a damping coefficient curve of a convincingly asymptotic shape, as shown in figure 5.4. The very nature of this curve, with its sharp knee, demonstrates that it is not actually necessary to quantify the squeeze film effects but merely to design the pole gaps to be large enough to render

these forces insignificant with respect to the other elements of the system.

5.4 Compliant Element, Accumulator or Spring

As was discussed in chapter two, the cylinder selection technique creates a quantisation error where a partial cylinder of fluid must be stored near the pump in order to avoid rapid changes of output flow and pressure. In chapter two it was assumed that a gas spring of conventional design would be employed for this function. This type of device has three major limitations:

1. If the device is to be designed for compactness and is sized to restrict the quantisation error to a few percent of the mean pressure level then its volume will be on the order of ten times that of a pumping cylinder. High pressure gas in such a small volume will tend to diffuse through both the steel and the rubber membranes of the accumulator at such a rate that recharging will need to be frequent (experience with the prototype would suggest every two months).

2. A gas accumulator, which is working over a large pressure range, will need to double its gas volume to halve the charge pressure, according to Boyle's law of isothermal compression of gases. The non-linear nature of this relationship reduces the precision of the volumetric error measurement at low pressure. Since the resolution of volume change is effectively reduced at low pressure, the pressure control algorithm may lose its ability

to smoothly control the enabling pattern of cylinders over this end of the pressure range.

3. The response time required to change system pressure is high since the pump must supply a substantial volume of fluid to the accumulator in order to compress the gas from one mean pressure level to another.

A solution to all of the foregoing problems is to employ a compliant element with a linear or near-linear characteristic, such as a metal spring. Unfortunately metal springs are subject to fatigue, have end-stops and, in most potential accumulator configurations, require some form of fluid seal which is itself subject to either fatigue or sliding wear. Another approach is to use a trapped volume of fluid of higher compressibility than the working fluid. Low bulk modulus fluids have served as springs in such applications as aircraft undercarriages [67] where high levels of shock are experienced.

The primary advantages of a fluid spring lie in its infinite fatigue life, the absence of end-stops and, also, in the low maintenance associated with such a design. In its reduced form it is simply a trapped volume of liquid contained within a flexible bladder. For the purposes of the test pump, a conventional 1.2 litre accumulator was converted into such a spring by discharging the bladder and refilling it with a low bulk modulus liquid.

There is a danger of unintentionally designing a resonance into the hydraulic system through the inclusion of any compliance and this is especially so with a liquid

spring, since it has both spring and mass which may interact with other components in the system. The inertial effects of the accumulator are small, since the fluid accelerations in the large volume of the accumulator and the large bore manifold connecting it to the discharge valves are low relative to those usually seen in the longer and smaller bore delivery lines typical of most hydraulic systems.

The spring of any compliant element will substantially reduce the natural frequency of the load system. The broad-band low-frequency excitation will limit the use of digital displacement machines to installations either where adequate damping can be applied between the pump and the load, or where the resonance occurs within the frequency response range of the pump.

While this may at first seem a major limitation, in practice most loads in conventional circuits are isolated from the supply by control valves which, for fine motion control, provide very high levels of damping. In applications where these valves are not present and where the power levels, and therefore inertias and damping terms, are liable to be substantial, the resonances will almost certainly occur at very low frequencies where they can be controlled by the pump itself.

The second concern about the dynamic behaviour is that of the high-frequency cut off point of the accumulator. The liquid spring and its supply galleries can be modelled as a mass-spring-damper system. The first resonant frequency of the device employed in the prototype pump can be calculated as being approximately 160 Hz., using a lumped parameter model after Lallement [68], which is just above the excitation frequency of the cylinder pulsing rate at induction motor speeds. The highest

pulsation frequency which can be created by the digital displacement pump is one half the fully enabled cylinder pulsing rate, or the first sub-harmonic. At this frequency (75 Hz. for a 1500 rpm induction motor and six cylinder pump) the phase margin of the compliant system seems to be adequate to prevent the inertial effects of the oil from disturbing the pump's behaviour. The galleries to the spring could be made to offer sufficient resistance to flow such that any excitation near the resonant frequency is critically damped, though this may have a significant effect on the overall energy efficiency of the compliant element since a significant fraction of the damping might be present at lower frequencies.

There are practical difficulties associated with liquid springs. The most important one is that of space efficiency since, from a survey of most listed liquids [69,70], there seems to be a lower limit of approximately 200 MPa on the bulk modulus (roughly one eighth that of mineral oil). For the purposes of an accumulator, it would be useful if this value could be lowered, perhaps by as much as an order of magnitude. The availability of fluids with this characteristic would greatly reduce the volume of fluid required and, more importantly, the size and weight of the accompanying high-pressure containment vessel. One way of simulating a lower bulk modulus, and thus of reducing the volume of the compliant element, is through the use of a pressure intensifying piston.

This possibility reveals a second problem, that of containing fluids, at high pressure and across moving

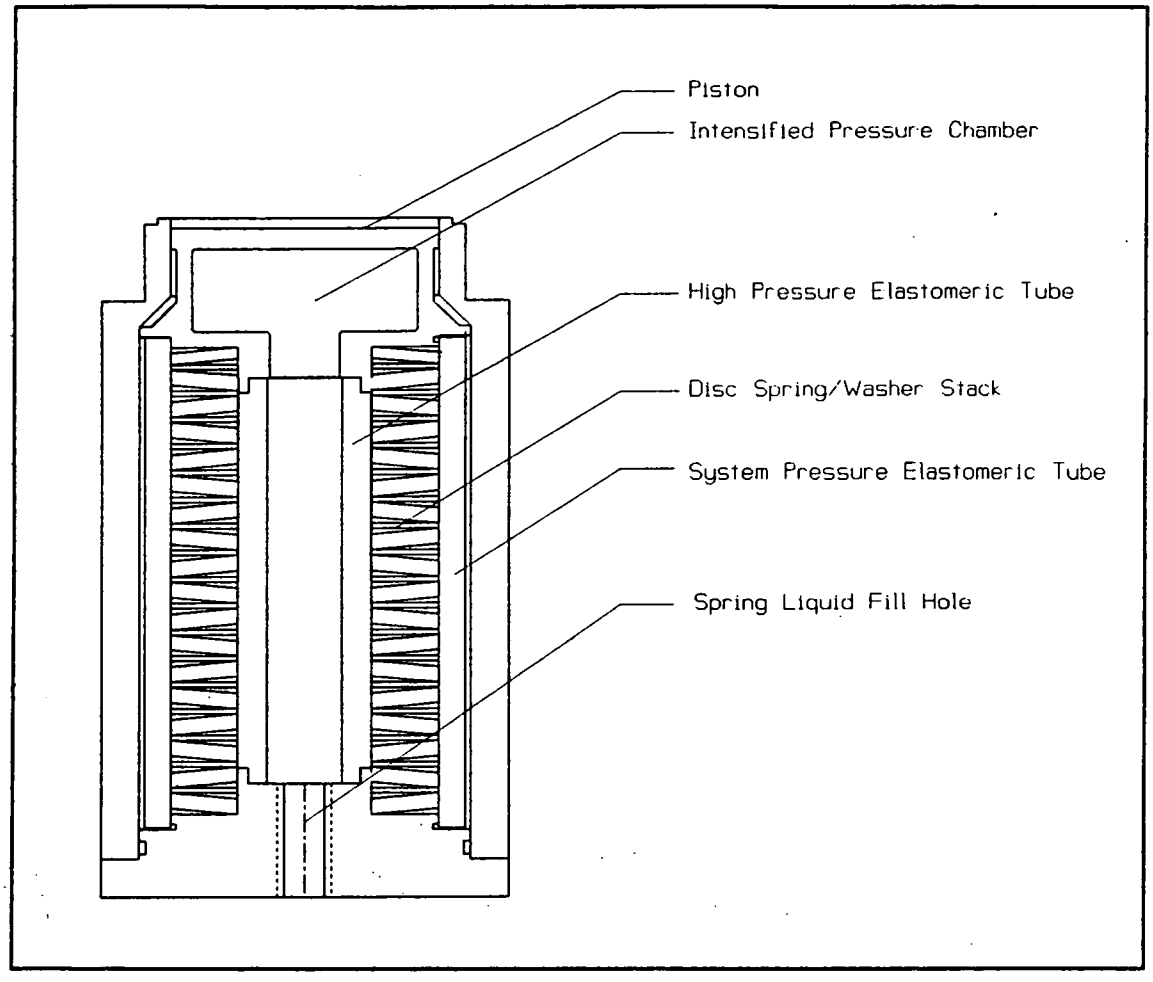

Figure 5.5: Compliant Element Incorporating both Pressure Intensification and a Liquid Spring.

seals, without leakage. As sliding seals, such as o-rings and packings, will not be capable of enduring the rapid cyclical loading experienced in the accumulator, another solution will be required. A provisional design of pressure intensifed accumulator is illustrated in figure 5.5. The principle behind its construction is the use of elastomeric tubes to contain the two fluids with closely spaced stacks of steel washers to control the radial deflection of the rubber tubes under pressure. It is estimated that this form of accumulator might have one third the overall volume of a non-intensified design.

A search of candidate fluids revealed three main groups of interest: light fraction hydrocarbons, per-fluorocarbons and related refrigerants, and, cyclic silicones. Surprisingly, the most practical candidates from each group had roughly equivalent compressibility curves (see appendix H). These were on the order of four to five times the compressibility of mineral oil. As each of the liquids had positive and negative attributes, the choice would be largely dependent on the application of the equipment in which the pump was to be used.

The hydrocarbons, i.e. propane and pentane, are inexpensive and widely available but also flammable and therefore unsuited to hazardous environments. The cyclic silicones are less flammable, relatively inexpensive but have a rather high freezing point (10 °C) and so would be unsuited to cold environments and would also be excluded from applications where mineral oils were considered too dangerous.

The per-fluorocarbons and the refrigerants currently being developed to replace chloro-fluorocarbons (such as R134) are inert and thus acceptable for hazardous environments. The refrigerants are gaseous at room temperature and would require charging equipment (as commonly used for air conditioning and refrigeration plant). Per-fluorohexane is liquid at room temperature and would be suitable in every respect aside from its limited availability (only as laboratory reagent) and high cost.

5.5 Piston Loading Consequences of the Cylinder Selection Technique

Concern has arisen from several sources during the development of the pump, i.e. [71], about the

mechanical consequences of off-loading cylinders and the load imbalances that might arise. Generally there is a very positive effect which results from disabling cylinders, when the pump is at part output, since no leakage occurs across the disabled pistons and, since their associated bearings remain unloaded. This property allows the part-load efficiency of the digital displacement pump to be significantly higher than an equivalent variable-swash machine, where the losses are are almost constant irrespective of swash position.

Nevertheless the off-loading of cylinders will have a consequence on the dynamics of the machine and so the effects must be considered. There are mechanical features common to all forms of piston pumps as well as those which are present only in specific configurations. The common ones are:

1. The need for a sliding interface between the piston end and the eccentric (as well as any supporting surface), and;

2. The need for main shaft bearings.

In the radial configuration, the pistons generally push against a central rotating eccentric and the sliding interface is provided by either hydrodynamic, rolling element, pressure-ballasted or fully hydro-static bearings. Often two bearing surfaces are used in combination where a second degree of freedom is required, as with fixed cylinders [72]. Hydrostatic and pressure ballasted bearings should, in principle, remain almost unaffected in their clearance by changes in cylinder pressure while hydrodynamic ones will run at a lower eccentricity when the radial load is reduced. The great concern with rolling element bearings is the fatigue

induced by rapid load fluctuations. In a conventional radial pump, the load borne by each rolling-element changes during each revolution when it crosses over from free-running -on the intake side of the pump, to load-bearing -under the pumping pistons. With cylinder disabling, the cyclical load function experienced by each rolling element will have the same general form but different amplitudes dependent on the fraction of cylinders active in a given revolution. On this basis, since the load cycle frequency remains unchanged, and, since the average of the loading peaks will be lower than those of the pump at full output, rolling element bearings should have a considerably longer life in such service [73].

The main shaft bearings in a radial configuration will be subject to the same effects. These bearings tend to be of the rolling-element type since these are most tolerant of the uncontrolled shaft loads imposed by the connection to the prime-mover. Significant reductions in main bearing loads can be achieved by using closely spaced banks of radial cylinders with the eccentrics 180 degrees out of phase [74]. If the cylinder selection technique were to be employed on such a machine, it would be necessary to link the control of cylinders in the two banks such that active cylinders always worked in opposition. The single disadvantage of this strategy is that it effectively doubles the pulse size and thus the quantisation error which must be dealt with by the accumulator.

Most axial machines start with the handicap that their rotating wedge must be isolated by bearings on both sides, which effectively doubles the bearing losses in this single component over that of a radial machine. Thrust bearings of all of the previously cited types

could be used in this application so the comments relating to radial machines apply equally here. Double ended machines, i.e. [75], can be likened to the multi-banked radial, in that provision would have to be made to enable opposing cylinders such that force imbalances across the cam-plate were avoided. The main shaft bearings, which resist the radial load resulting from the tangential force needed to drive the pistons up the incline, are exposed to essentially the same type of load function as those of the radial machine. As such the same observations regarding extended life should apply.

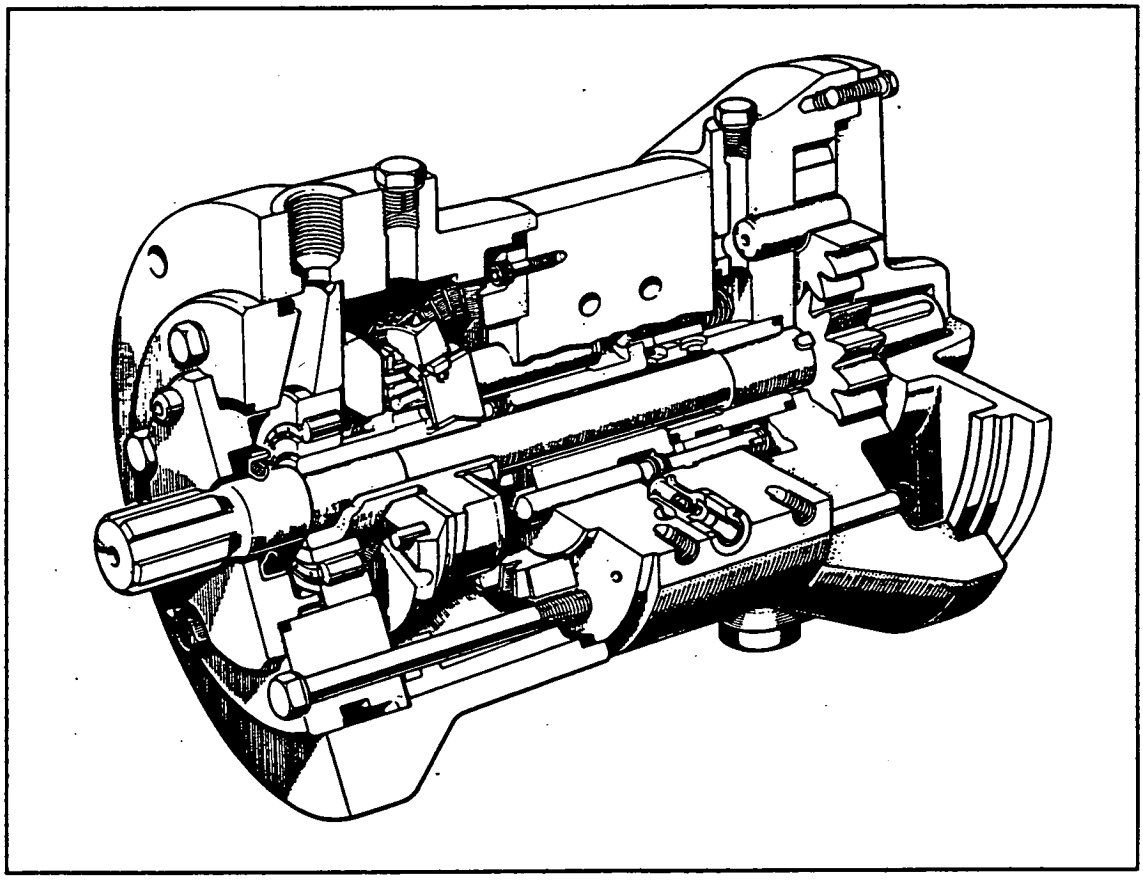

Figure 5.6: Cut-away Drawing of Towler A-Series Poppet Valve Pump Prior to Modification. From Oilgear-Towler Ltd.

5.6 Design of the Prototype Pump

A Towler A-series six cylinder pump, shown in figure 5.6, was stripped, measured and modified to form the basis of the first digital displacement pump. The pistons and the mechanism for driving them were left unchanged as were the high-pressure delivery valves. The inlet valves were removed along with their seats such that a large cavity was opened up in the end of the cylinder block. This was filled by the actively controlled valves and their associated magnetic latches, as shown in the sectional drawing of figure 5.7. The latch cavity is separated from the intake side of the pump in order to prevent ferro-magnetic particles from settling onto the permanent magnets and their associated poles. A flow of cooling and lubricating oil passes through this chamber after it is filtered by a porous bronze plug.

The parts of the latch are identifiable from diagrams in the earlier chapters (in which their shapes and sizes were decided). Figure 5.7 also shows the method of attachment used secure the moving pole to the poppet. The current design is the result of several iterations which followed an equal number of failures, each attributable to a different cause. As the poppet suffers severe shock and vibration, it is very important to have a reliable interface between these two components. Most conventional techniques, such as screw threads or circlips, are incompatible with either the loads, materials or service requirements. The design shown here uses a moving pole ring which has six radial slits originating at the inside diameter, five of which end at the outer rim while one cuts completely through. The slits render the pole radially compliant so that it can be slipped over the poppet shank and squeezed into a recess. A nylon ring is then pushed onto the inner pole

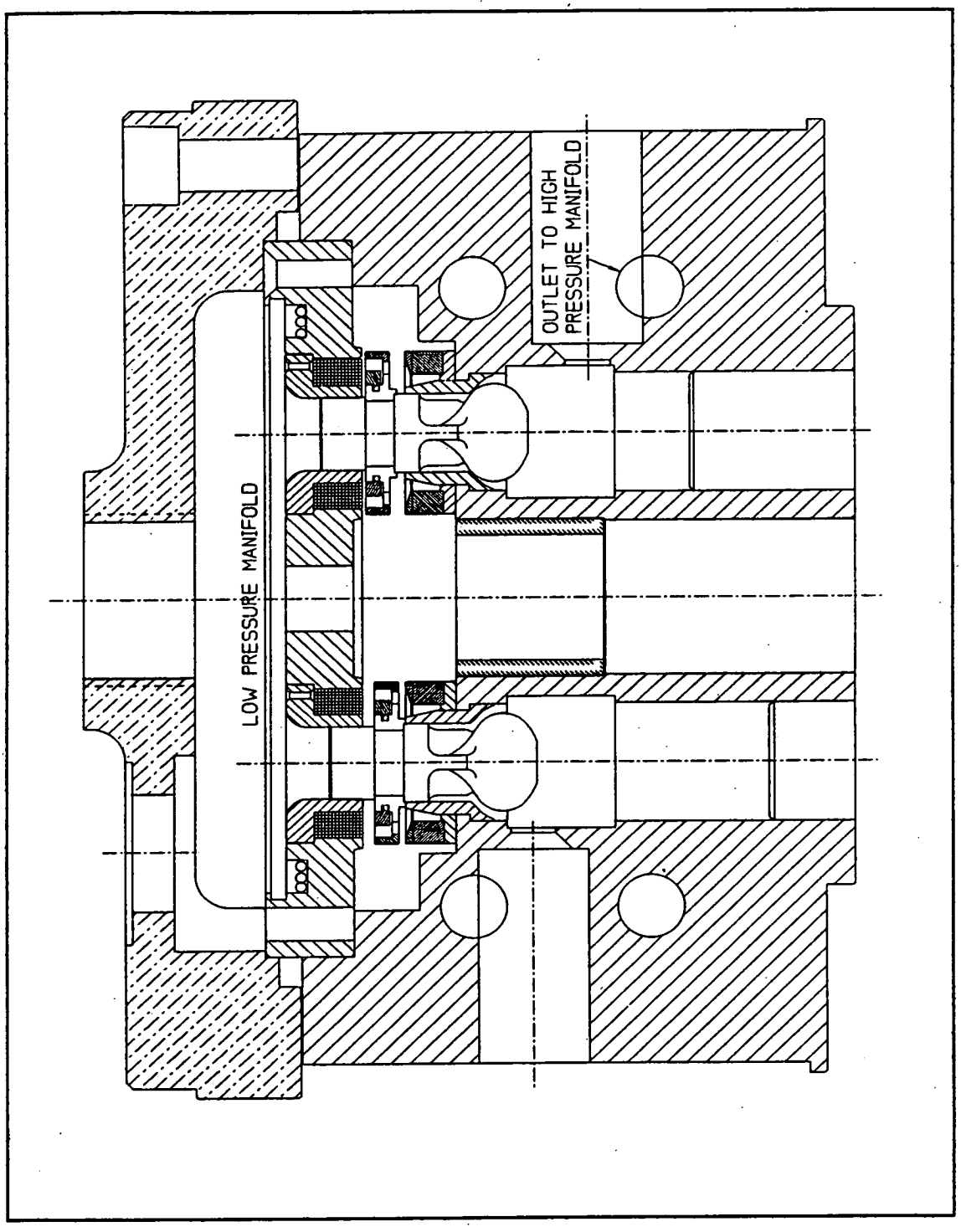

Figure 5.7: General Arrangement of Modified Towler Pump Head with Active Inlet Poppet Valves.

from above in order to lock the pole into the groove. The ring has a small lip which engages a groove in the pole in order to prevent it becoming dislodged. This attachment has proved problem free, since its adoption, throughout the testing of the prototypes. The discontinuity at the full slit breaks the electrically conductive path around the pole, thus preventing shorted-turn effects in the latch while also reducing eddy currents (as discussed in chapter 3).

The second major area of modification of the pump was made to the high pressure galleries. These were extended around the periphery of the pump in order to reduce flow losses and to shorten the effective length between the delivery valves and the compliant element. The original pump has the compact gas accumulator was built into the body of the cylinder block as shown in the photograph of figure 5.8, while the later, liquid spring equipped, variant has the compliant element as an external appendage.

The final modification was the insertion of a magnetic pickup into the crankcase which could sense the passing of a notch in the wobble plate. The pulse generated by its passage was used by the controller to locate the crankshaft position and indicate the rotational period.

Overleaf:
Figure 5.8: Modified Towler Pump Prior to Reassembly

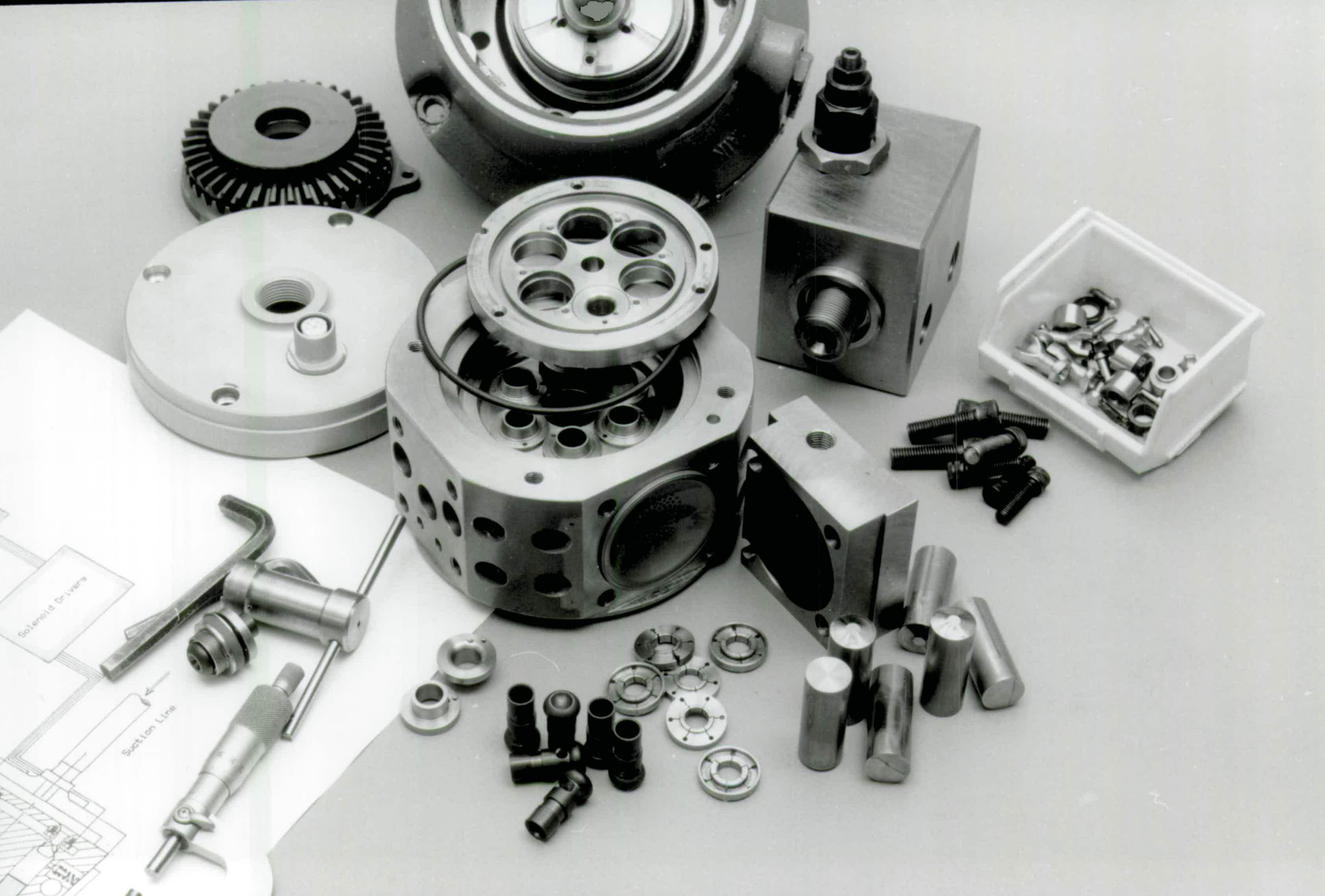
Solenoid Drivers
Suction Line

6.0 Controller Design and Implementation

6.1 Introduction

While it is possible to imagine that the tasks of controlling the digital displacement pump and of making the cylinder enabling decisions could be achieved with a combination of hard wired analogue and digital circuits, it would not appear to be the easiest nor the most adaptable approach. Certainly the power and flexibility afforded by a microprocessor and its controlling software make it the obvious choice for pump control. Having embarked on the micro-processor route many more decisions arise, since several compatible components must be selected from a large, and rapidly changing, list of possibilities.

In the case of the digital pump these decisions were effectively taken by the collaborating industrial partner. As they employed a specialist, trained in writing real-time C language code, and were testing an Intel based 16 bit micro-controller for another application, at the time that these were needed for the pump, this combination was favoured. Once it was evident that the operating speed and functionality of the controller were adequate, the choice was confirmed.

Because Fenner had a great deal of in-house expertise in this area, the work was largely carried out there by Alan Fussey under the direction of the author. As such this chapter should be seen primarily as one of documentation rather than one of original work.

6.2 Controller Hardware

The 12 MHz. Intel 196 controller was chosen for the following reasons:

1. It was offered with a choice of at least two C compilers, which meant that code could be written in a high level language. This made the code accessible to non-specialist programmers for subsequent modification and expansion. This would not have been the case if assembly language had been used (as has been the practice).

2. It contained sufficient interfacing ports, including a 10 bit A/D convertor, eight analogue inputs and configurable digital I/O, to fulfill the immediate needs of the pump and its external interfacing while leaving some spare for future requirements.

3. It had a development card version which allowed programs to be downloaded from an IBM PC for testing and calibrating purposes.

4. Versions were available with sufficient on board RAM and ROM memory such that variants could function as single chip embedded controllers in commercial pumps.

5. It was fast enough to allow the various analogue reads, integer calculations, and digital outputs required between cylinder decisions to occur without overlap at both pump speeds and cylinder numbers well above those currently foreseen.

6. It was widely supported, inexpensive and readily available.

While other more sophisticated controllers have since become available and, while the 196 has itself been increased in speed to 20 MHz., the current needs of pumps (and most probably poppet-motors) are more than adequately provided for by the current device. The inevitable obsolescence of the 196 processor has the short-to-middle term advantage of making it less expensive.

The entire control circuit, in functional block form, is shown in figure 6.1. Its principal features are:

1. Analogue filtering and conditioning circuitry on the inputs from the pressure transducer and the analogue demand.

2. Digital conditioning circuitry, to improve noise rejection and false triggering, for the shaft trigger signal.

3. Optical isolation on the digital output ports between the controller and the power semiconductors which drive the solenoids.

4. A transistor stage with a pulse time limiting circuit designed to interface the low-power isolators with the high power solenoid drivers. This is incorporated to ensure that the solenoids will not burn out as a result of either controller or software malfunction.

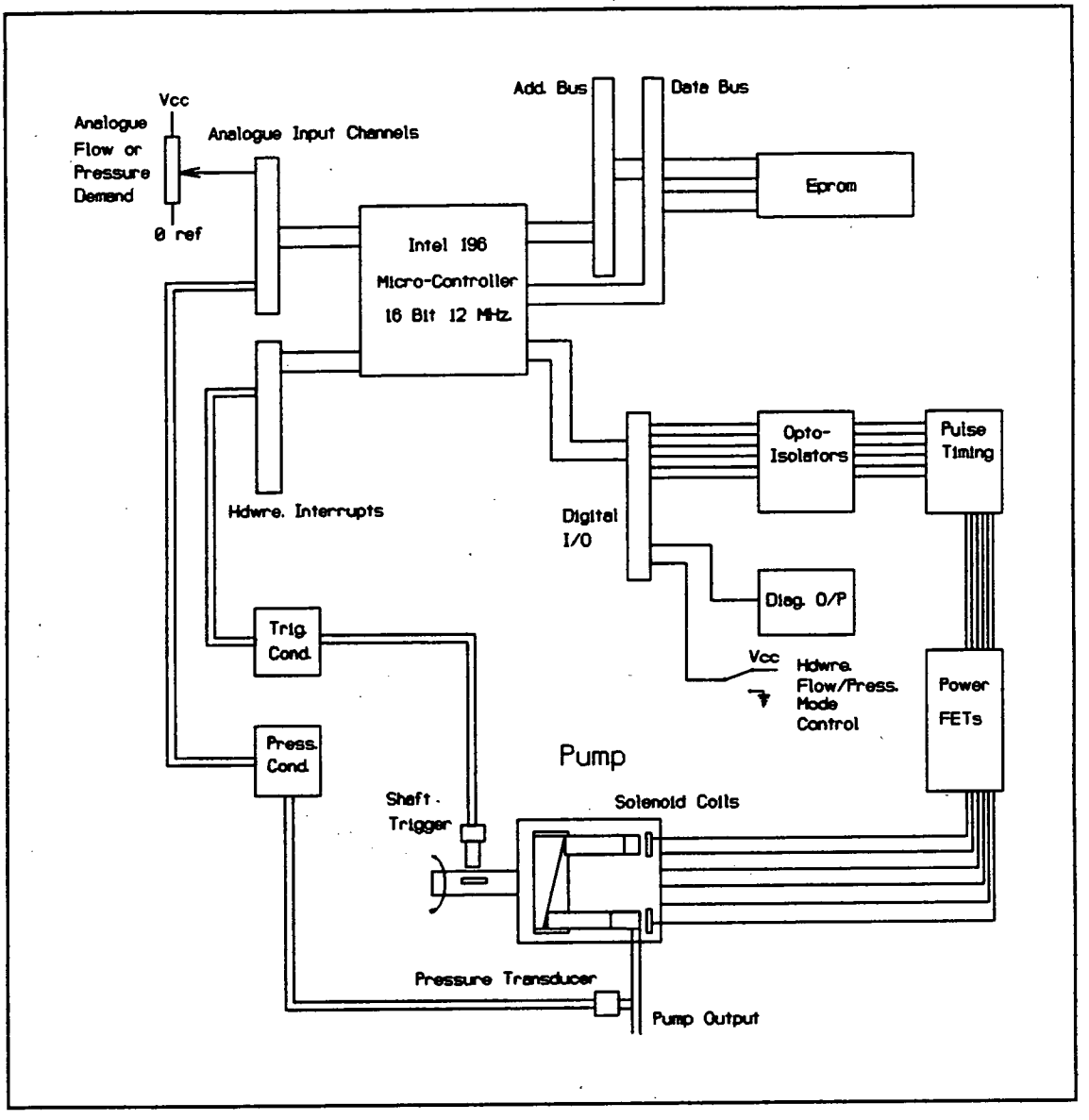

Figure 6.1: Schematic Diagram of Electronic Pump Controller Circuit

5. A power semiconductor stage, initially using Darlington transistors (for their hardiness) but at a later stage incorporating power FETs (for their reduced power dissipation and fast switching).

The electronics were incorporated into three purpose designed printed circuit boards which were installed in an eurocard format rack case. Two proprietary power supplies were also fitted into the case, one provided for the logic level circuitry while the second, a 24 volt 20 amp. unit, drove the solenoids.

6.3 Controller Function

The controller has to manage two quite different tasks. It must perform all of the time keeping routines required to ensure that the proper signals are travelling to and from the pump at their appropriate times. It must also manage the accounting algorithms needed to calculate the decisions for the cylinder selection process.

6.3.1 Time Keeping Functions

The time keeping activity is initiated by the shaft trigger interrupt which gives the controller both an instantaneous shaft position once per revolution and, through timing successive pulses, a value for the rotational period. This interrupt resets one of the on-board timers while also copying its elapsed value to a memory register. The count from the previous revolution is then divided by six to provide the count between cylinders over the next revolution. This value is halved again and the result used to measure the count between the shaft trigger and the first cylinder's bottom-dead-centre position. An advance from the bottom-dead-centre timing is established from an empirically derived equation, which models the valve closing time as a function of shaft speed, so that the valve can be turned on at the correct timer count. A second offset is calculated from the bottom-dead-centre position in order to turn the pulse off again, while a third offset is used

to time a series of analogue reads of the pressure transducer for the pressure control algorithm.

At each interrupt the comparison register is loaded with the appropriate count value, in order to signal the next task, and a timer comparison loop put into operation such that, when the two values become equal, other interrupt routines begin and a new value is put in the comparison register.

The time keeping routine is complicated somewhat by the necessity of completing the timing of the final cylinder while the trigger interrupt is occuring. This is dealt with by starting a second timer when the first is reset by the trigger. The second timer then manages the final events of the shaft rotation.

The timing sequence actually runs an entire cylinder past the receipt of the trigger in order to allow sufficient computing time for the controller to service the trigger interrupt and calculate the timings for the next revolution.

The final feature of the timing part of the code is a loop which counts through the cylinder order such that it selects the bit of the digital output port which corresponds to the cylinder approaching bottom-dead-centre so that, in the event of an enabling decision, it can be turned on.

6.3.2 Enabling Decision Calculations

Each interrupt task begins with an activity which requires precise timing, i.e. valve operation. Once this has been completed the interrupt routine goes on to perform other necessary, if not time critical, operations. For example, the interrupt which turns off the valves is used to trigger an analogue read of the system pressure which, in turn, is followed by a cylinder enabling calculation. The interrupt which turns the valves on is followed by a routine which allows other analogue channels to be read so that designated parameters, such as delays and pulse lengths, can be adjusted while the pump is operational. A digital port can also be read in order to signal a change between pressure and flow control modes.

In performing the enabling decision calculations, it is very important to ensure that the time required to complete the sequence of arithmetic operations does not exceed that which is available. If this happens, the following interrupts will queue up, waiting for earlier ones to finish, and the interrupt stack will overflow. For this reason the calculations were performed wherever possible with 16 bit integers. Where multiplication created potential overflow problems unsigned or long integers were used. The algorithm was written by expressing all values in terms of one cylinder's displacement with one cylinder given the integer value of 1024 in order to provide sufficient resolution for partial cylinder calculations and, in particular, integer division operations. The equations used in the code are versions of those presented in chapter two, though modified for integer use.

6.3.3 Starting Functions

When the pump is first switched on, the controller is forced to execute an initialisation routine. At the time of writing, this part of the code is used primarily for the setting of constants. It could be used to allow the controller to quantify various parameters through the performance of a set pattern of enablings followed by the interpretation of the resulting pressure trace. In this way, things such as accumulator compliance or optimum valve timing could be established.

Experience with the pump has demonstrated that it is extremely difficult to characterise the local compliance by any other means than dynamic measurement. An algorithm was developed which, on start-up, would pump one cylinder and then continuously sample the pressure signal until it returned to its original level. During the pumping stroke a known amount of fluid is introduced into the system, though by the time the pressure reaches a maximum, some of the fluid may have escaped through a leak downstream of the pump, i.e. through a partially open control valve. As long as this leak performs as a constant, and purely resistive, impedance it can be characterised through the use of numerical integration of the square roots of the pressure time trace samples as shown in figure 6.2. Since, over the time the pressure rises and falls back to the same level, one cylinder will have been dissipated through this resistance, the known displacement can be equated to the sum of the square roots of pressure in order to calculate an orifice impedence value. Once this is known, the displacement lost through the orifice by the time at which maximum pressure occurs can be calculated by doing a similar integration for the duration of the pumping stroke. The actual displacement stored in the accumulator at this

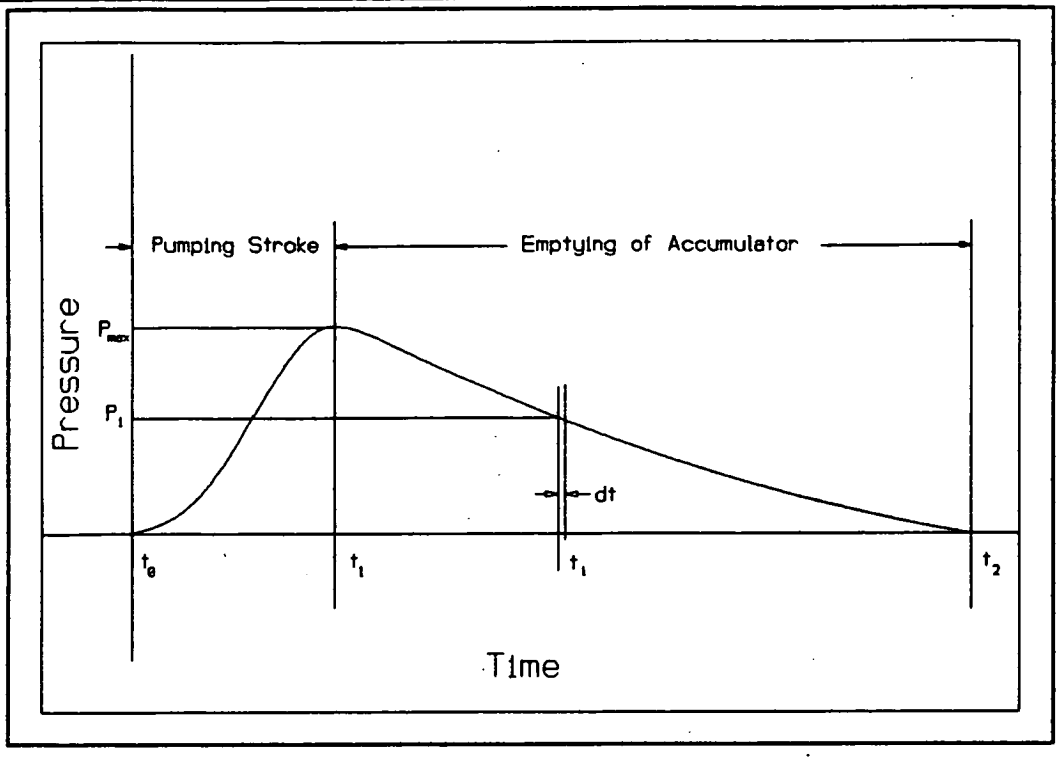

The orifice constant of the system downstream of the pump is characterised:

$$Q = C_1 P^{\frac{1}{2}}$$

$$1\ cyl = \int_{t_0}^{t_2} q\ dt = C_1 \int_{t_0}^{t_2} P^{\frac{1}{2}}\ dt$$

$$C_1 = \frac{1\ cyl}{\int_{t_0}^{t_2} P^{\frac{1}{2}}\ dt}$$

Then the orifice displacement during the pumping stroke is calculated and deducted from the total displacement to determine the maximum accumulator fill:

$$V_a = 1\ cyl - C_1 \int_{t_0}^{t_1} P^{\frac{1}{2}}\ dt$$

The accumulator constant C_2 can now be calculated:

$$C_2 = \frac{V_a}{P_{max} - P_0}$$

Figure 6.2: Operating Principle of Compliance Sensing Starting Procedure.

instant can then be divided by the maximum pressure rise in order to produce a linearised spring constant for the accumulator.

If the orifice at start up is too big to allow a single pumped cylinder to raise the pressure sufficiently, such that adequate resolution in the measurement is achieved, then a second attempt can follow with two cylinders pumped in succession. If this strategy fails, due to system loading conditions preventing sufficient pressure rise, then a warning would sound and the default accumulator constant value used.

Other compliance sensing strategies which continuously and adaptively modify the controller's parameter settings may be possible. Techniques, which analyse the previous pumping history and compare them to patterns of maximal smoothness for the same averaged load flow, may provide a solution to the problem. An algorithm which varied the compliance parameter in response to the pressure deviation from the set level might also be effective, though such a simple approach might be encumbered by a lengthy set of rules. These would be required in order to prevent tuning during events such as high frequency transients where the inherent delay of the pressure control algorithm causes mis-enabling of cylinders.

The actual C code used to control the pump is listed in appendix I. It compiles to an executable program two kilobytes in length, which is small enough to reside in the processor's on-board ROM.

7.0 Digital Displacement Pump Performance

7.1 Introduction

This chapter brings together the rather diverse subjects of chapters two to six. It marks the point at which the cylinder disabling principle, modelled in chapter two, could finally be physically tested with the latches, valves and controllers developed in the chapters which followed.

The chapter begins with a description of the test rig and its instrumentation, it then continues with an exploration of the behavioural anomalies found when the pressure control algorithm was first implemented. The chapter concludes with two separate series of experiments, both of which were conducted in parallel with simulations, in such a way that the simulation technique and the implementation of the control algorithm could be validated. The first tests deal with the step and ramp responses of the pump, as were previously examined in chapter two, while the second concludes with a range of experiments designed to determine the frequency reponse of the pressure control algorithm.

7.2 Test Rig

The test rig used to test the pump was built previously for use with a much larger machine [76] and required only slight modification to be adapted for the prototype digital displacement pump. The rig consisted of two large tanks; the first, of 800 litres, at atmospheric pressure and a second, of 350 litres which acted as a supply to the machine on test, and could be maintained at a set boost pressure. Positive boost was required for

the prototype pump to hold its pistons against the actuating wobble plate during suction and was held constant at 5 Bar throughout the various tests. The low pressure tank had facilities for both heating and cooling the oil such that its temperature could be controlled. The oil was filtered to 10 microns absolute on exiting the boost pump and passing into the boost tank.

The pump drive was provided by an invertor system driving a three phase induction motor. This allowed speed variation, which was useful for determining the values of the speed sensitive parameters used in the control algorithms. The pump itself was mated to a large steel disc, supported on rolling element bearings, which allowed the resistive torque of the pump to be mechanically measured. The photograph of figure 7.1 shows the pump and part of the test rig at the time of the first installation.

7.3 Initial Testing and Algorithm Correction

Once the pump was running on test it became apparent that the actual monitoring of the algorithm decision behaviour would pose a significant problem. This was not only due to the difficulty of interfacing with the real-time controller without significantly influencing its timings (interfering with its normal running), but also because, for each interesting transient event, there was a large quantity of data which had to be rejected.

The diagnostic software tools, which were built up during the initial phases of testing, allowed defects in the algorithm implementation to be found. What may not be immediately obvious is that, unlike in a conventional

Overleaf:
Figure 7.1: Digital Displacement Pump on the Test Rig

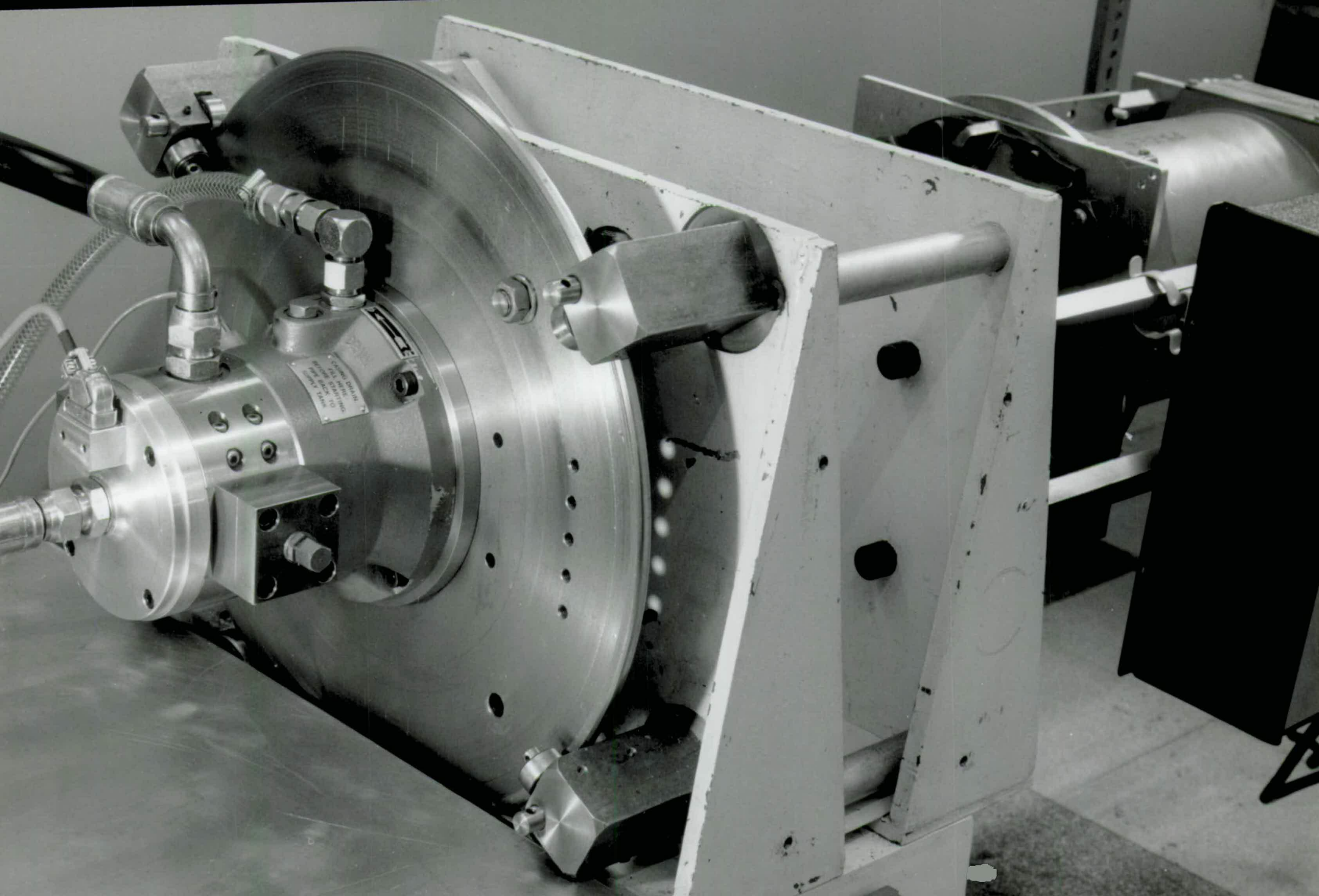

control system where problems occur at the edges of the operating envelope, with the cylinder selection technique aberrant behaviour could appear in different conditions and for varying reasons and was inevitably, due to the periodic nature of cylinder selection, transient.

Due to the interfacing restrictions mentioned earlier and the problems associated with capturing transients, the diagnostic software was designed to work using a batch capture technique. The control algorithm functioned normally until a special interrupt was triggered from the keyboard of a secondary computer, which was connected via a serial link to the real-time controller. This interrupt instructed the controller to store all of the parameters for the following 100 decisions in unused on-board memory. Following the conclusion of these decisions, the controller shut down the pump and relayed the stored parameter values back to the secondary computer for analysis and permanent storage.

The software was used in conjunction with a digital storage oscilloscope so that the occurrence of the sought transient event within the stored data could be quickly verified. If the capture process had failed on the first attempt, then it was repeated until the required event was logged.

The recurring fault in the pressure control algorithm was its tendency to cause group enabling and disabling. Rather than producing decisions in a maximally smooth sequence while under constant load, the pump would enable a series of cylinders which would raise the pressure well above the set level. The controller, belatedly recognising the error of its ways would then desist, leaving subsequent cylinders disabled, until the pressure had fallen somewhat below the set level. Several

hypotheses were put forward at this time and subsequently investigated:

1. That the controller's predictive model of the system was offset in time from the actual response. This was explored by writing software which allowed the timing to be varied by a potentiometer while the pump was running. It did not, in the first instance, cure the problem.

2. That there was insufficient sensitivity in the chain of components which fed the pressure signal back to the controller, or, that amplification of the measuring error (caused by projecting the load flow ahead over three decision intervals) would compromise the precision of the decision calculation. After a noise problem in the conditioning circuitry had been rectified and the signal noise level had been reduced to 1 mV. RMS (which would allow a pressure resolution of 30 millibar), it was observed that the computer A/D convertor injected noise onto the pressure signal which was an order of magnitude greater than its own. Subsequent investigation revealed that this noise was synchronous with the analogue sampling and so was not, in effect, actually measured by the controller. The conditioning circuit was also increased in gain to make best use of the 5 V., 1024 bit, input range of the A/D convertor. All of these attempts produced no discernable effect on pump performance. Little could be done about the error amplification problem so it remains uninvestigated.

3. That there was a mismatch between the controller's model of the compliance and the accumulator constant. A program was written where the accumulator constant value could be set while the pump was running. The pump behaviour proved to be very sensitive to this parameter. Experimental determination of the compliance solved the bulk of the group enabling problems.

Once the fundamental difficulty had been resolved, it was possible to return to the matter of the first hypothesis and to examine the effects of timing mismatches more carefully. This investigation revealed that there was a significant delay between the physical bottom-dead-centre of a cylinder and the start of the pressure rise associated with its pumping. This mismatch (speed sensitive and ranging from 1 to 2 milliseconds in magnitude), was compensated by using an empirically determined delay in the control program. The delay in pressure rise was undoubtedly caused by a combination of fluid compressibility, imperfect valve timing and by some phase delay in the pressure pulse as it travelled from the cylinder through the manifold to the accumulator (since the pressure transducer was on the gas side). The inclusion of this delay parameter produced a smaller, but still significant, improvement in pump behaviour.

The final difficulty with the pressure algorithm was a kind of ringing mis-firing which occurred just either side of the 50 percent output point as shown in figure 7.2. This loading condition is much harder to manage than would be at first apparent. As the cylinder decisions are alternately reversing, they are often taken near the threshold point. At either end of the load range the decision which breaks the pattern can happen

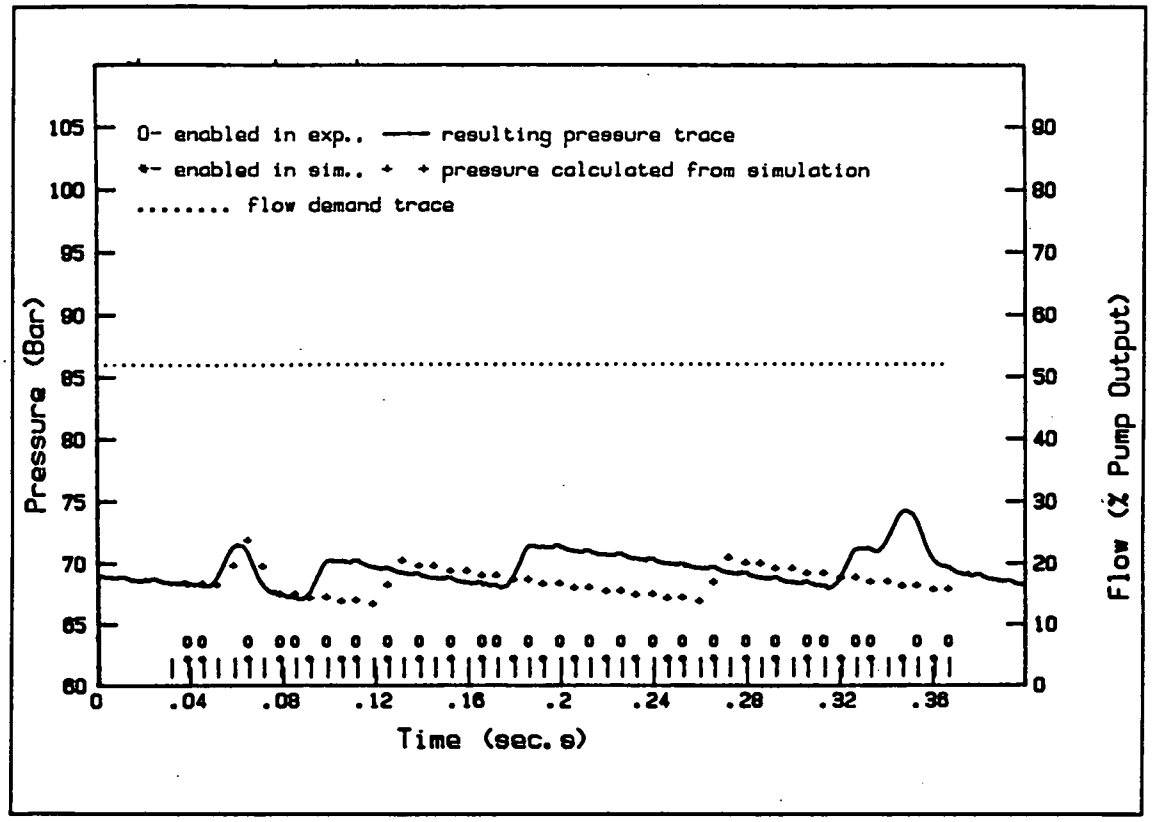

Figure 7.2: Ringing Mis-fire of Constant-Pressure Control Algorithm when Delivering 51% of Pump Output.

ahead or behind of its optimal position without causing much error, whereas at the fifty percent load case its position is crucial. The problems of measurement error and the amplification of the load flow over the look-ahead period, both described earlier, as well as the uncertainty of the decision governing the following cylinder (which will be contributing something prior to the look-ahead point) sum to create ringing after the pattern transitions occur. Two techniques were used to resolve this problem.

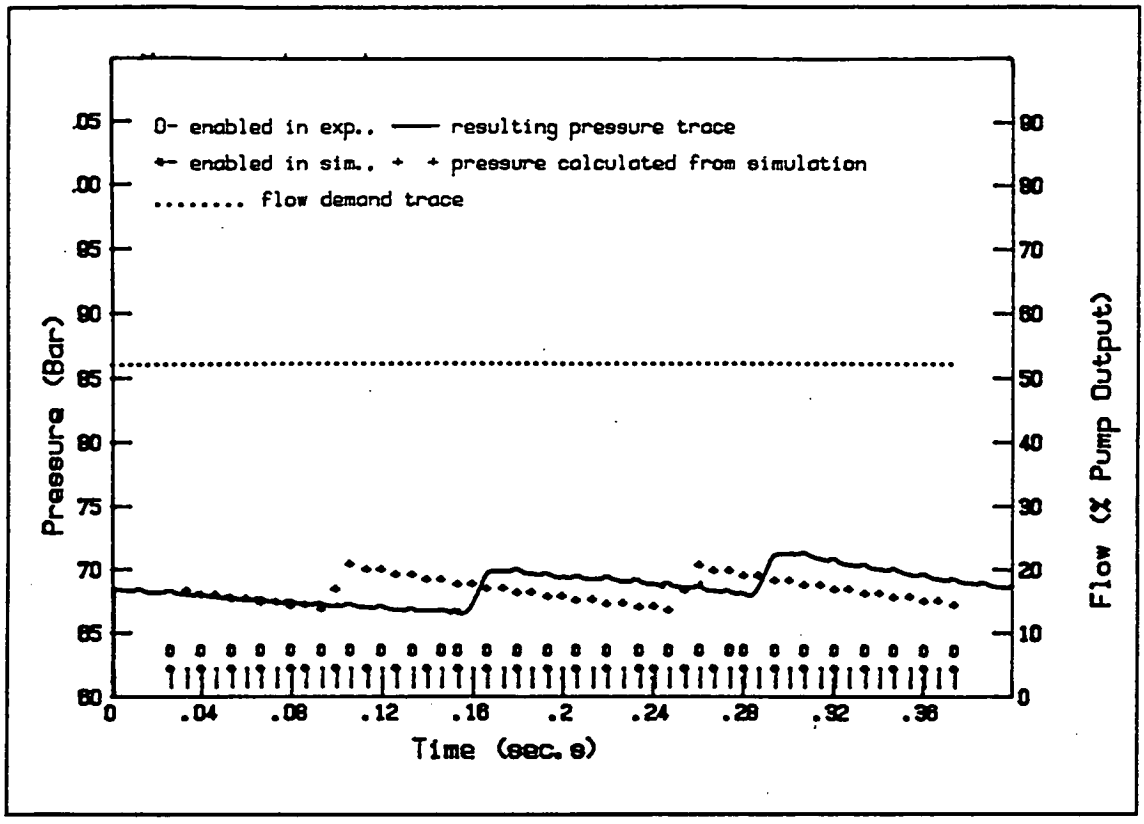

Figure 7.3: Ringing Mis-fire Cured using Reduced Gain. Note Greater Pressure Amplitude.

The first is borrowed from conventional feedback theory. The error signal, which in this case is the corrective displacement required to bring the accumulator back to the set-pressure level by the look-ahead time, can be reduced by a gain factor. This has the effect, equally analagous to conventional control systems, of reducing the control stiffness and thus allowing the pressure to deviate more than theoretically necessary from the set level. The result of the reduced gain modification, under the same conditions, is shown in figure 7.3.

The second oscillation-curing technique involved the implementation of a probability model which forecast the next cylinder decision. The operating range was broken into three bands: zero to forty percent where the

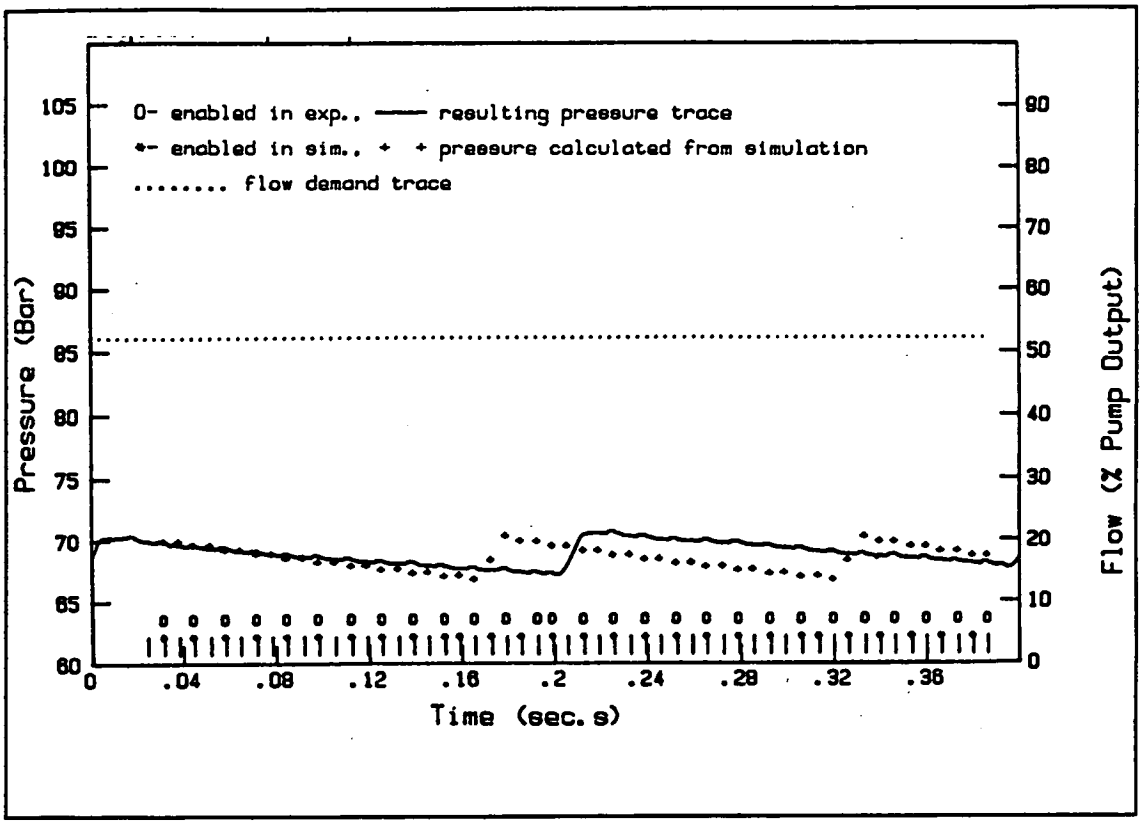

Figure 7.4: Ringing Mis-fire Cured by Application of Probability Rules.

following cylinder was unlikely to be enabled and was discounted; forty to sixty percent output where, if the previous cylinder was enabled, there was a high probability of the one following the decision cylinder and; sixty to one hundred where the next cylinder was likely. These probabilities were implemented in the real-time code as "rules" and their effect on the enabling pattern is shown in figure 7.4. Not only has the oscillation been cured, but the system also retains the control stiffness of the original algorithm, giving a pressure amplitude variation approximately 25 percent lower than that of the reduced gain technique.

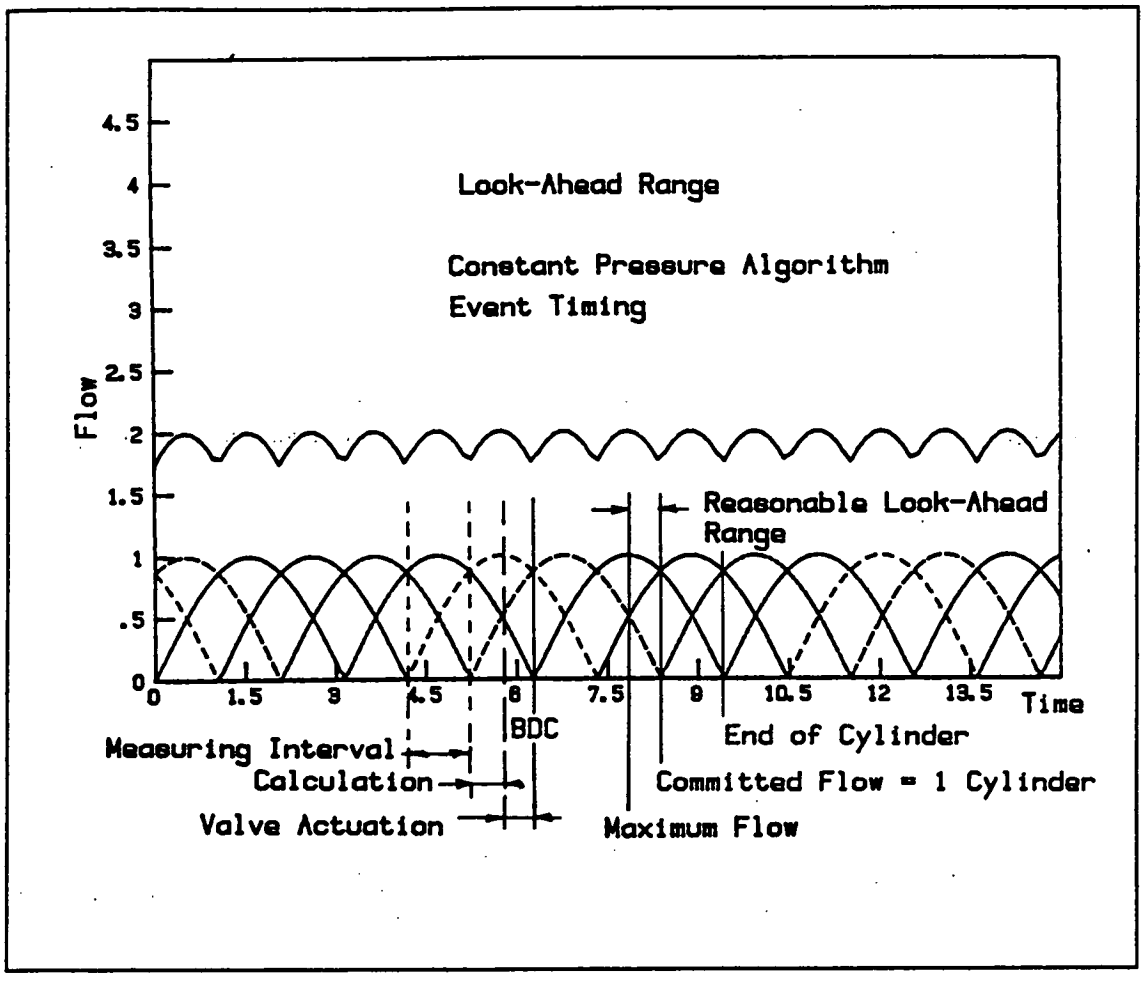

Figure 7.5: Event Timing of the Constant-Pressure Algorithm.

The effect of the look-ahead time was also investigated experimentally during the exhaustive search for a cure to the final ringing mis-fire problem. Closer examination of the theoretical error introduced with various look-ahead points on the test pump configuration suggested that the error was both a function of pump output and past enabling history and that there was no simple expression which would provide a best point. A series of tests were conducted on the pump where the look-ahead

shaft angle was varied from 90 (the point of maximum flow) to 120 degrees after bottom-dead-centre (75 % spent, uncommitted displacement = 1 cylinder) as shown in figure 7.5. The pump behaviour seemed to change very little over this range, indicating a relative lack of sensitivity to this parameter.

7.4 Step and Ramp Response Experiments

7.4.1 Experimental Control Apparatus and Instrumentation

The experiment was conducted with a host computer controlling a series of instruments on the IEEE 488 bus in an arrangement shown schematically in figure 7.6. The pump delivers into a manifold connected directly to a proportional valve. This is used as a variable load and is controlled independently by an arbitrary function generator. This is in turn programmed by the control computer such that it produces a ramping function between two calibrated flow levels.

The valve was calibrated in terms of pump output i.e. cylinders/sec. rather than in absolute units. This was done both for ease of calibration, since it could be effected on the rig at any time that it was found to be necessary, and, since it produced a calibration in the units most useful for the purposes of the subsequent analysis. To calibrate the valve at constant pressure conditions, the pump was run with the flow control algorithm such that it was pumping a stable short pattern, i.e. 1:2, 2:3 etc., the valve was then adjusted until the pressure reached the set level and the output voltage of the LVDT read. The process was repeated for a range of flows such that a calibration curve could be fitted to the data.

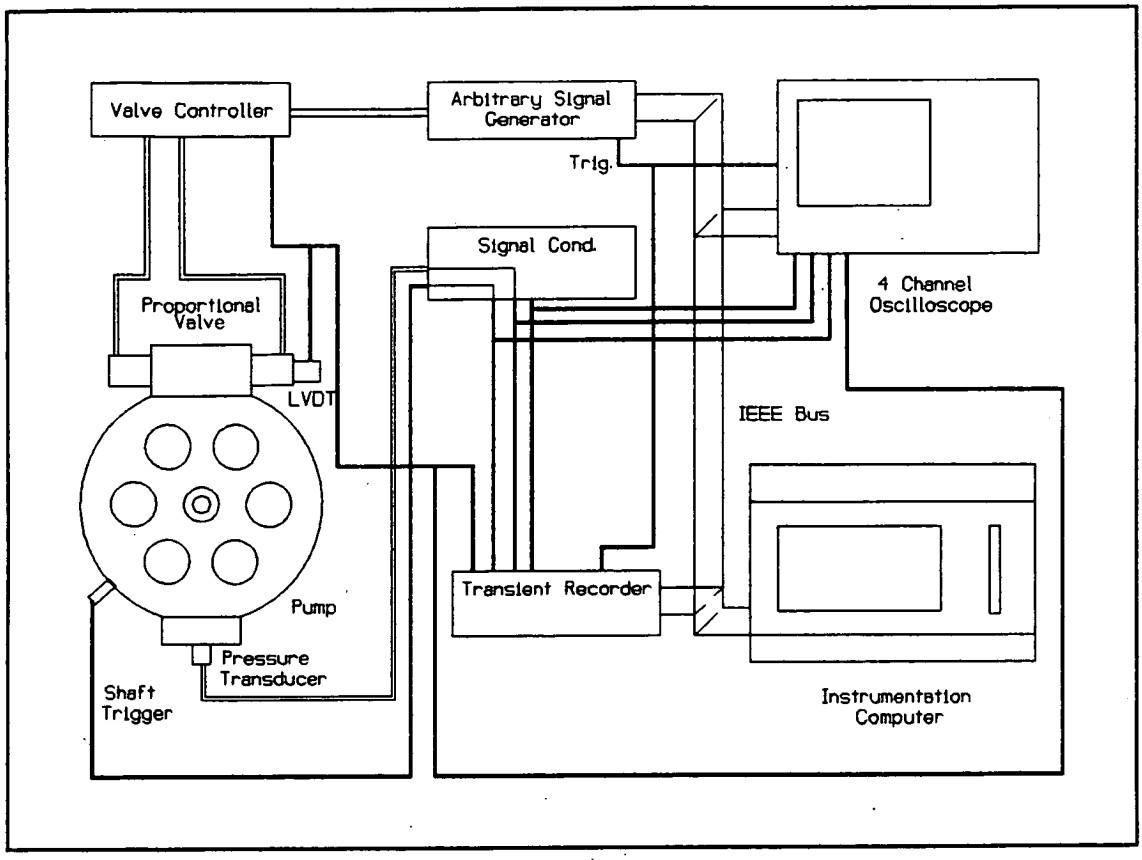

Figure 7.6: Schematic Arrangement of Digital Displacement Pump Instrumentation.

The instrument control computer was equipped with a simplified system model written as a compiled sub-program in C language. Once given a record of the initial system pressure and the first few decisions from the experiment, it re-enacted the experiment in simulation, producing both a pressure trace and series of decisions over the time of the experiment. The simulation used the Newton method to iteratively solve for the delivery pressure, given the flow demand and the displacement provided by the pump and its accumulator. The simple model seems well justified by the experimental results, since the high-frequency pressure transients (observed and modelled

by Edge et. al [12]), while present, are effectively removed from the control system by both the accumulator and low-pass second-order filter.

7.4.2 Step-Response and Output Ramping Results

The graph of figure 7.7. illustrates a typical experiment. Here the pump is supplying the load at fifty percent of its full output. It is then ramped up to sixty percent over 50 milliseconds. The pattern which develops at the sixty percent level illustrates the periodicity of output, though the ripple can be seen to have a peak amplitude of less than 5% of the set level.

There is a limit to what can be achieved in terms of the agreement of both experiment and simulation. The proportional valve is on the limit of reliable calibration at higher flow rates and can create a flow demand error of several percent, which is particularly visible in the longer periodic patterns. The noise in both the hydraulics and electronics, as well as the resolution of the A/D converter, generate some uncertainty in the pressure reading which can effectively change the threshold for a given cylinder-enabling decision. Changes in the accumulator temperature also affect its calibration and are not included in the simulation. Thus the graphs of figures 7.7 through 7.9 all show some differences between the pattern-altering threshold levels of the experiment and simulation. The LVDT readings which provide a record of valve position also show some oscillation; a result of intentional dither originating from the valve controller.

Figures 7.8 and 7.9 show extreme variations from 10 to 90 percent of full output and back again. The ramp slope

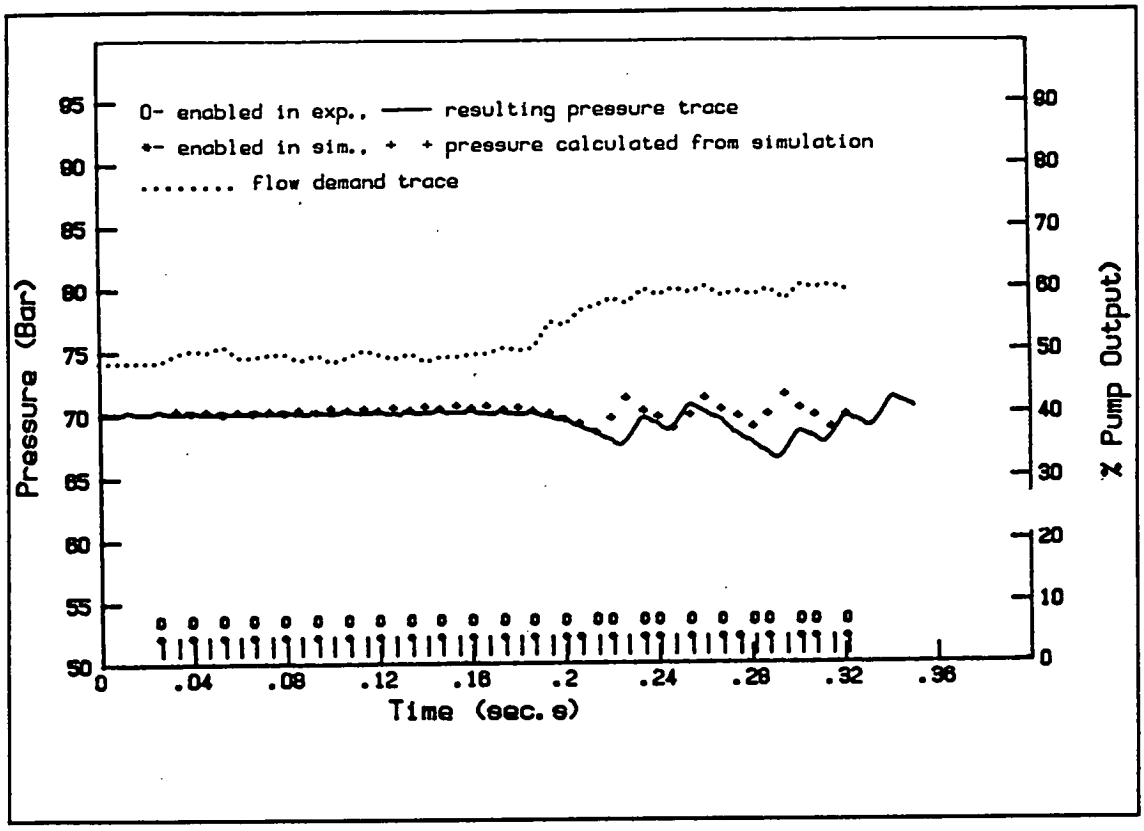

Figure 7.7: Pump Response to Ramping Flow Demand from 50% to 60% of Maximum Output over 50 milliseconds.

was limited by the 30 millisecond full excursion response of the proportional valve. In the first case the pump takes some time to recover to the set pressure, due both to the delay between sensing the load change and in implementing a compensatory increase, and the inability of the pump to work above its full capacity to catch up. In ramping downward, the load sensing delay causes the most recently enabled cylinders to be pumped into an almost closed system, raising the pressure well above the set level. In both cases the system has recovered after approximately 50 milliseconds.

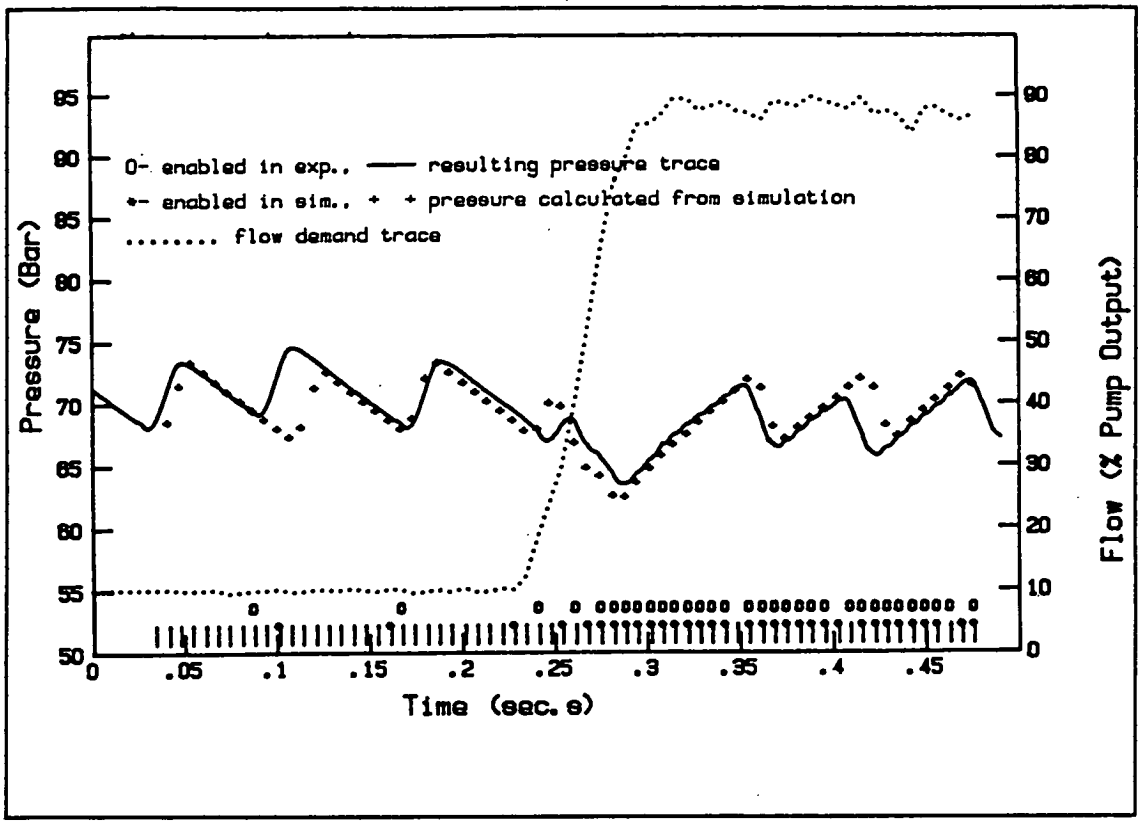

Figure 7.8: Constant-Pressure Control Algorithm Response to Flow Demand Increase from 10 to 90% of Maximum Pump Output over 30 msec.

Because the pump and valve controllers are operating entirely independently, the onset of a demand change can happen at any point in an established pumping pattern. If the experiment of figure 7.8 was rerun so that the proportional valve began to open when the system was at the highest point in its pattern, then the droop would be considerably smaller. For the purposes of a simulation to model a system response, the worst case would always have to be assumed. While the pump being modelled in chapter two is of different dimensions and cylinder count, comparison of the step-response graphs of both chapters demonstrates that the behaviours are largely similar.

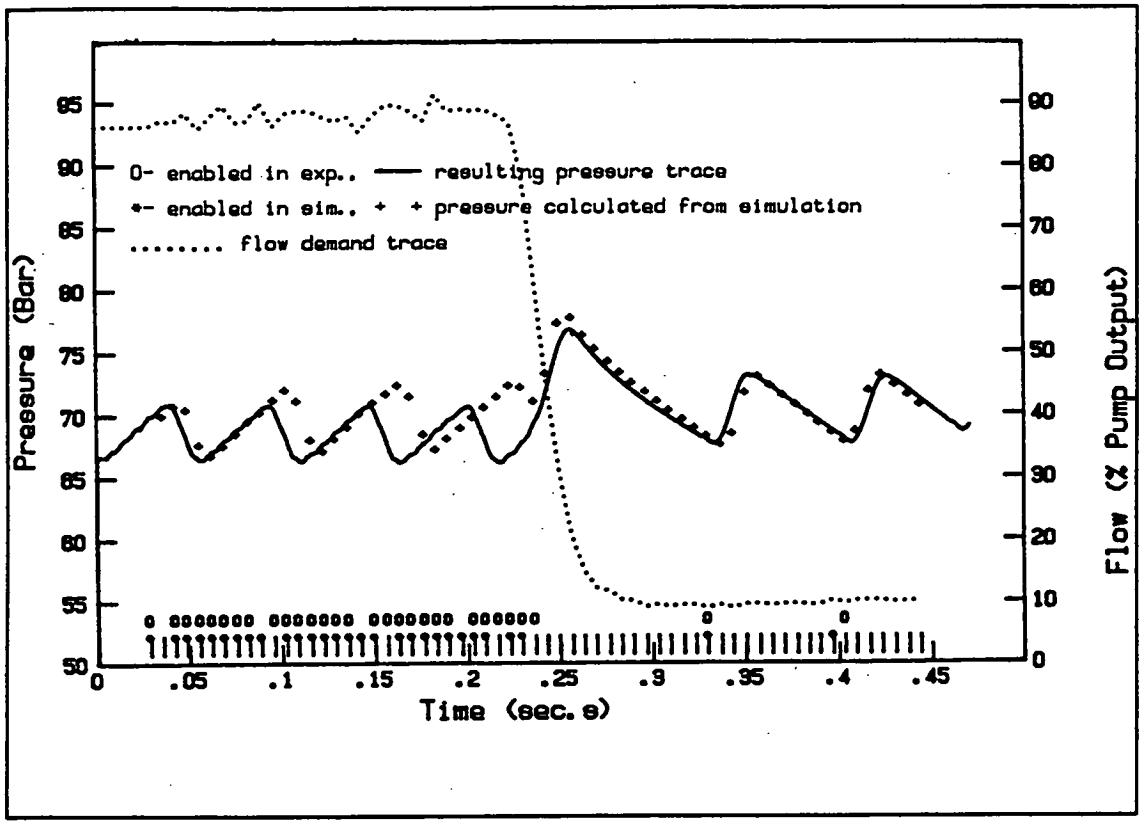

Figure 7.9: Constant-Pressure Algorithm Response to Flow Demand Ramping Down from 90 to 10% of Maximum Pump Output over 30 msec.

7.5 Frequency Response Experiments

These experiments were designed to evaluate the load-following capabilities of the pump, when subjected to a sinusoidal flow demand, while it attempted to maintain a constant pressure at the pump outlet.

7.5.1 Technique for Frequency Response Measurement

When the frequency response of a swash-plate pump is measured, the common practice is to record the angle of swash-plate tilt and equate that to ouput flow [16]. Indeed it is possible to monitor the physical position of

several components in the chain of command from the servo-valve through to the actuator. This, unfortunately, is not possible with the digital pump since the control is direct to each individual cylinder. The output must somehow be sensed within the fluid rather than through a component of the machine. As measuring instantaneous flows is problematic, this is best done by measuring pressure. Given that the pump is driving an orifice and that such devices can be approximated as a pure resistance at the frequencies considered here [77], the pressure measurements should allow flows to be inferred with reasonable accuracy, should these be required.

The second difficulty in measuring the output of the digital pump lies in its inherent output ripple. As this is a by-product of cylinder enabling, and therefore with components at any or all of the sub-harmonic frequencies below that of the fundamental cylinder pulsation, its pressure ripple will overlay the pressure variations caused by the load at its fundamental frequency. Spectral information extracted from the pressure output waveform is therefore of limited use.

A less orthodox approach to quantifying the frequency response of the digital displacement pump was suggested by Kevin Edge [78]: With the digital pump attempting to maintain a constant pressure behind the orifice, despite the harmonic disturbance of the load, the peak pressure variation at each operating point could be measured. If sampling was continued over a sufficient number of load cycles then the probability of the cylinder selection ripple being maximally superposed on the load flow ripple would be high enough to assume that the worst case at each operating point had been captured in the data.

While there may be a way of analytically calculating this value from the pump and load parameters, it has not occurred to the author. For this reason the simulation was run as before (as per the step-response tests) and the worst case data selected for comparison to that of the experiments. Phase data could not be captured using this technique as there was more than one likely point of greatest pressure deviation in loading cycle, i.e. where the actual and expected loads were maximally different.

7.5.2 Instrumentation and Experiment Control

The instrumentation was arranged identically to that of the step-response tests though, in this case, the function generator and sampling system were programmed differently. The computer created a distorted sine wave of the correct amplitude and wavelength and then downloaded it to a waveform generator which replayed it continuously to the proportional valve. The distortion was used to compensate for the non-linear characteristic of the proportional valve such that a close approximation to a sinusoidal flow function was generated within the pipe. The pressure waveform was then sampled at 1.25 KHz. with a 16 bit transient recorder and the data uploaded to the controller. The maximum and minimum values in the time trace were stored and the process repeated for the next experimental point.

7.5.3 Frequency Response Results

The two surface contour plots of figures 7.10 and 7.11 represent the results of 90 experiments and simulations respectively. The spike plot of figure 7.12 shows the error between the two plots in the same units. While the error has some trends which follow both load frequency

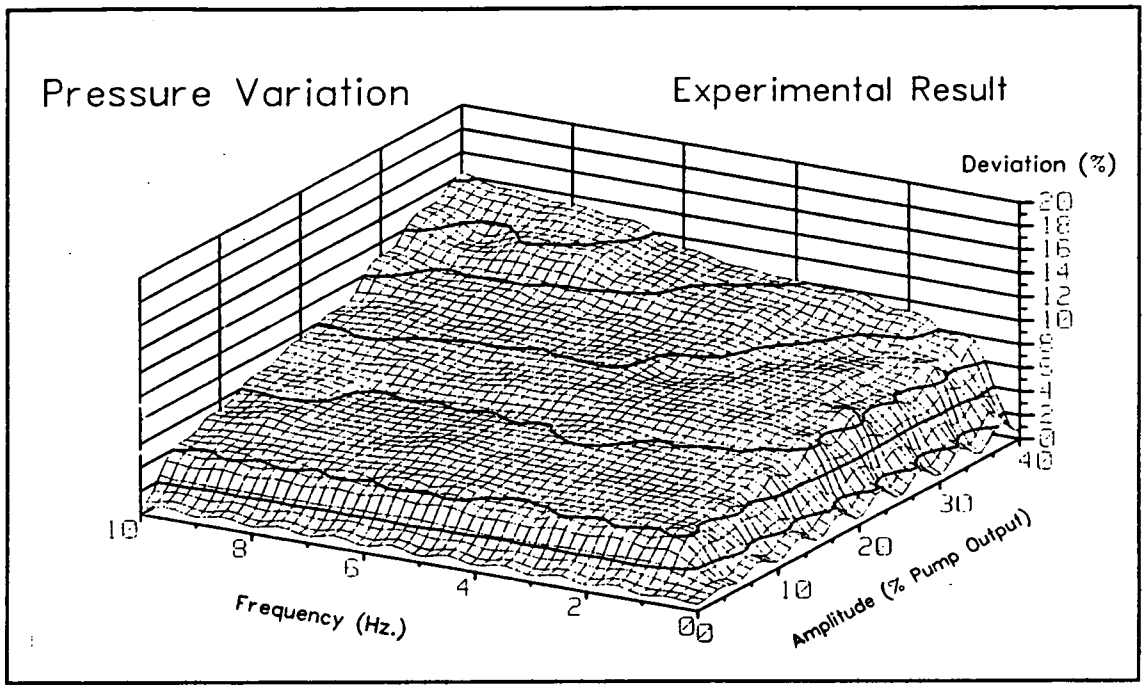

Figure 7.10: Deviation of Control Pressure as a Function of both Load Frequency and Amplitude; Experimental Result.

and amplitude, it is for the most part within two percent of the control pressure. For this reason it would seem reasonable to accept that the simulation provides a useful model of the pump.

The two plots of figures 7.10 and 7.11 illustrate some useful, but hardly surprising, results. The first point of interest is the plateau which occurs just inside the zero ordinates of the x-y plane. The pump is operating at fifty percent output along these axes, and is pumping alternate cylinders and therefore producing a relatively smooth output. Once the frequency and amplitude of the load excitation are non-zero, the quantisation error appears and the pressure error makes a discrete step (this is rounded somewhat by the surface interpolation used to produce the plots).

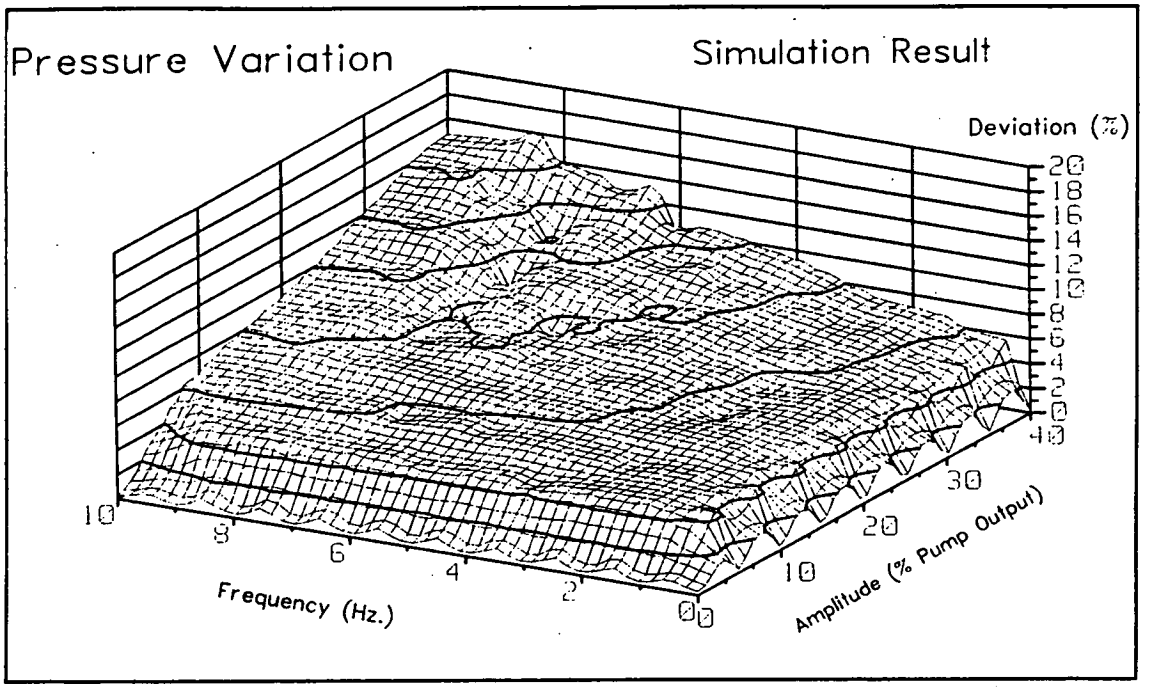

Figure 7.11: Deviation of Control Pressure as a Function of both Load Frequency and Amplitude; By Simulation.

The plateau region describes an operating range below an almost constant product of frequency and amplitude. This would seem sensible as both factors will upset the constant pressure algorithm by changing the instantaneous flow demanded by the orifice from that projected by the previous load flow calculation. Following this same line of thought, it is not surprising to see that the greatest pressure variations occur at the highest frequencies and amplitudes.

While the frequency range of the experimental results was limited by the bandwidth of the proportional valve, the simulation could be used to extend this range in order to explore possible resonances within the algorithm. Figure 7.13 shows a superset of the simulations, previously plotted in figure 7.11, covering a much larger frequency

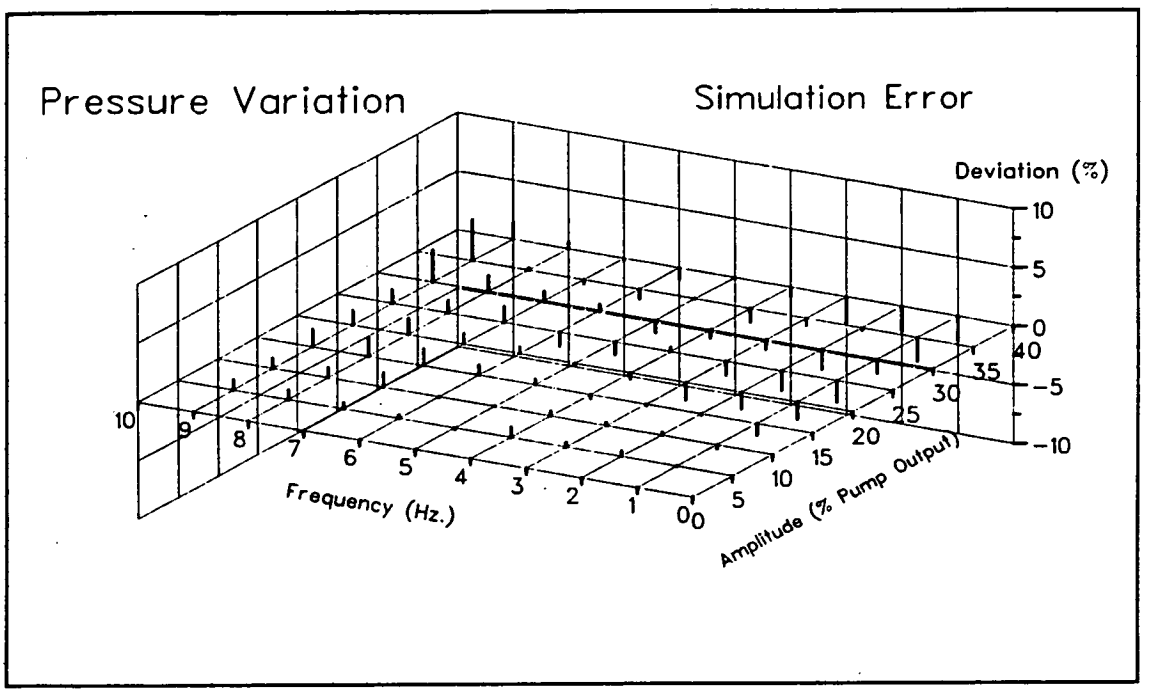

Figure 7.12: Difference Between Simulation and Experimental Values as a Function of Load Frequency and Amplitude.

range. The two frequency peaks at the highest amplitudes on the surface plot illustrate a less obvious effect. The first peak corresponds to the 180 degree phase shift point of the pressure control algorithm. The peak, at approximately 17 Hz., has a half period of 29 milliseconds which can be compared to the total load calculating and accounting time of the algorithm of 27 milliseconds, as can be seen in figure 7.5. In equating these values there is some uncertainty with regard to the fraction of the algorithm time that should be considered, since the load calculation is essentially an averaging process and, since the accounting period finishes prior to the end of the decision cylinder's pumping.

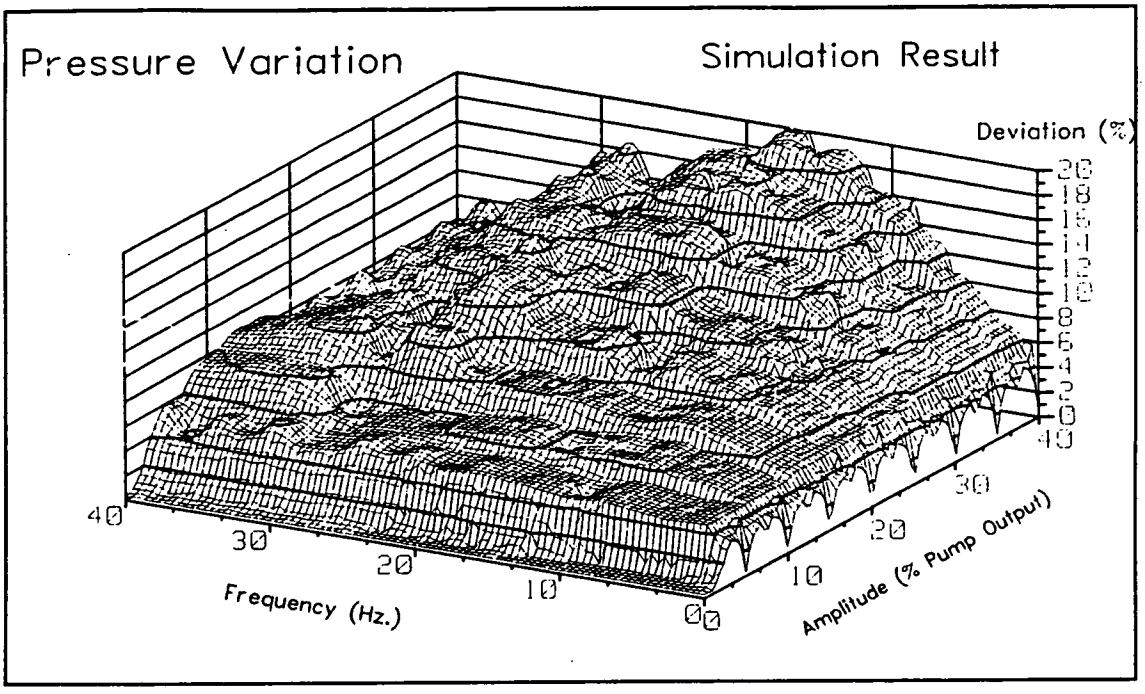

Figure 7.13: Deviation of Control Pressure as a Function of Both Load Frequency and Amplitude; By Simulation over an Extended Frequency Range

The second peak is more difficult to explain since it does not, at 27 Hz., correspond to the expected frequency of the second harmonic. The algorithm's use of low frequency digital sampling of the pressure may well account for the shifting of the second harmonic since successive sampling points will cover a larger amplitude change in the load function at higher frequencies. This sampling effect will, at increasingly higher frequencies, tend to average the demand until the algorithm is neither sensing nor responding to the high frequency load flow demands. The fact that the region beyond the second peak on the plot of figure 7.13 descends to what would appear to be a constant level would confirm this.

The explanations for the second harmonic shift and the region beyond are all somewhat academic in any case since it is unlikely that the pump would be placed in a circuit

where the large signal bandwidth was required to extend beyond the first plateau region.

The peak amplitude pressure error at the 90 degree phase point of the algorithm (8.5 Hz.) and 40 percent flow amplitude is 13% of the set pressure. This corresponds to slightly more than a full cylinder of displacement error.

7.6 Summary of Pump Performance Experimental Results

The important results from the two sets of experiments and their corresponding simulations can be summarised as follows:

1. The low frequency simulation model provides a reasonable approximation of pump behaviour.

2. The pressure algorithm generates a primary resonance related in frequency to the length of time between inferring load flow and pumping the majority of the decision cylinder.

3. The pressure control algorithm is stable under all but the most extreme load flow conditions, whether transient or harmonic. At these extremes, i.e. algorithm-induced resonance and large-signal disturbances, pressure error limits in the real-time code curtail uncontrolled pressure excursions.

8.0 Concluding Observations and Recommendations for Further Work

As was stated in the introduction of chapter one, this is essentially an introductory study to assess the feasibility of using the digital displacement principle as a means of controlling the output of a hydraulic piston pump. The extent to which this objective was achieved can be gauged from the results described in the previous chapter. While there may always be doubts about the perceptual acceptability of a technique which uses discrete pulses of fluid (coupled with an accumulator), as compared to one which is closer to the ideal of a ripple-free variable output, the other characteristics of the machine make it an attractive option in several types of application:

1. Transmission and control of large powers; where part-load efficiency is of prime concern and where dissipative control devices are not desirable due to both energy loss and the consequent fluid heating.

2. Variable flow control for high-pressure water and emulsion pumps; where low fluid lubricity and poor filtration tend to eliminate other alternatives.

3. Pressure control of water ring-mains. These are used increasingly in the food industry and have the potential to replace halon CFCs in the fire control market. Such installations might ultimately employ ultrasonic telemetry within the fluid to allow ring users to alter the mains pressure level.

The established oil fluid-power pump market is not likely to be affected by the digital displacement pump in its most basic form, as has been described thus far, since it provides only a subtle increase in functionality. If, however, the pump can be made to motor such that it can accept high-pressure flow in the reverse direction, then such machines could be directly coupled to conventional actuators. Further, if such machines could be banked to provide multiple services (and poppet-valve pumps are usually supplied as such), then actuator control could be effected directly from the digital displacement pump/motor without the need for control valves and their associated plumbing. There are rather too many applications, which could be beneficially served by this device, to list here.

8.1 Recommendations for Further Work

Many of the subjects described in the previous chapters have been dealt with in a cursory manner and, as a result, many elements of the digital pump have still to achieve their optimum forms. In some cases this is due to both insufficient analysis and understanding of the most significant parameters while in other cases it is because some aspect of the design needs to be imaginatively re-examined such that new solutions can replace existing ones. The following list gives a specific summary:

1. Fluid flow around poppet valves: Chapter four illustrates that a large improvement in poppet restraining forces can be achieved in one or two generations of poppet/duct shape development. Since this aspect of the work was completed, computational fluid mechanic techniques have gained a maturity, in terms of model geometry

and transient flow capability, that may well now allow them to be used as a shape development tool. Particle image velocimetry (PIV) has developed during the same time, with the use of scanning lasers for flow illumination and with computational image analysis, and may prove a useful technique for validating the computer flow predictions.

2. The magnetic latch, as described in chapter three, has, at the time of writing, been superseded by a latch which employs a flat-faced plunger configuration. This was not thought to be a realisable option at the time of writing, due to the problem of attracting debris into the sliding bearings between the poppet and its guides. Subsequently it was realised that the solenoid could be turned inside out such that the attractive poles were at the centre of the annulus and the debris sensitive surfaces around the periphery of the latch in filtered fluid. The debris immunity could thus be achieved without compromising the magnetic configuration.

The digital displacement technique is effectively limited, in terms of flow/cylinder, by the strength of the magnetic actuator. While there is much scope for increasing the passive latching force (by substituting more powerful permanent magnet types), there is less in prospect for the active side since the solenoid coils currently in use are driving the ferro-magnetic parts of the latch well into saturation. A new approach may be required to gain useful improvement.

3. The PEEK poppets have served remarkably well during the operational life of the demonstration digital displacement pump but, prior to any commercial use, these components will have to be thoroughly life tested. Ceramics might be usefully investigated as an alternative material for high-pressure use.

4. The search in chapter five for a mechanism which could both provide sufficient compliance, such that the quantisation error was kept to acceptable limits, and pressure range, such that the response time of the pump was not unduly impaired, led to the use of a liquid spring. The most frequent use of such flow controlled systems is in mobile equipment hydraulics where space and weight are often at a premium. For this reason the pursuit of a compliant device, which is more compact than a steel shell full of low bulk modulus fluid, would seem desirable. The pressure intensifying liquid spring described in chapter five might prove one possibility, as might mechanical devices such as stacked Belleville washers in elastomeric tubes. In both cases the design becomes a materials exercise since success depends on the fatigue life of the combination of components. Devices like these need to be built and life tested.

5. Compliance sensing; the pressure control algorithm needs an accurate model of the local compliance in order to predict the load flow and the extent of the displacement error such that it can return the system to the set pressure level by the end of the decision cylinder and so that its decisions follow a maximally smooth

pattern. Adaptive techniques, which can infer compliance from a record of past cylinder enablings and the corresponding pressure trace or which can tune the compliance parameter by relating it to an averaged record of pressure excursions, might prove useful in implementing this feature.

6. Fluid-Borne Noise Consequences: Preliminary work done to assess the fluid-borne noise of cylinder selection indicates that the noise can be roughly separated into two types:

   Low frequency noise, due to cylinder selection, which is not perceptually unpleasant and which can be controlled within specified limits through compliance sizing, and;

   High-frequency noise, due to valve closing and transient oscillations in the cylinders and manifolds.

   In addition, with the compliance closely coupled to the pump, there is the attenuation response of the accumulator superposed on the pump ripple. With the prototype pump the maximum attenuation lay just above the cylinder pulsation frequency and provided a useful reduction of the fundamental ripple. At higher frequencies, however, the tendency of small accumulators to intensify the underlying ripple may prove an unfortunate characteristic. The extent of this effect needs to be measured and, if found to be significant, solutions sought.

The preliminary results also showed some variation of valve actuation noise which was not attributable to cylinder position in the manifold, valve actuation timing or different poppet materials. From this result it is likely that some small difference in poppet-valve or latch geometry is able to significantly affect the fluid-borne noise amplitude.

As noise is of increasing significance in fluid-power installations, a serious examination of the high-frequency noise generated by actively timed poppet-valve closure needs to be carried out such that the resulting noise can be reduced to a minimum level.

7. Digital displacement pump/motor: Large scale commercial success is only likely to take place if the digital machines can supplant other components currently in use with oil hydraulic systems. Realistically, this will only occur when the advantages of the challenging technology are sufficient to overcome the combination of resistance to change, the lost investment in current production lines and the fears of the end user in relying on something new and untried. The poppet pump/motor comes much closer to providing this quantum leap in performance than does the pump, since it allows a reduction in components and plumbing over current installations while also offering a substantial improvement in operator control. The development of the pump/motor can thus be seen to be of greatest importance to the success of the digital displacement technique.

List of References

1. Edinburgh-Scopa-Laing, Wave Energy Group, 5th Year Report to ETSU, Dept. of Energy, UK, 1979, Vols 1-3.

2. Edinburgh-Scopa-Laing, op. cit., Vol. 2, pp. 36-37.

3. Moller, C.B., Force Pump for Slurries (with solenoid valves), US. Patent 2,785,638, 1957.

4. MacTaggart-Scott MSBV Dual Displacement Radial RHP pump, 1969, Tom Craig, Technical Director MTS ltd., Personal Communication, 1992.

5. Miller, J.E., The Reciprocating Pump; Theory, Design and Use, Wiley-Interscience, 1987, pp. 261-262.

6. Whitson, R.J., The Measured Transmission Loss Characterisitics of Some Hydraulic Attenuators, Proc. of Instn. Mech. Engrs., Vol?, 1980, pp. 105-116

7. Whitson, R.J., Henderson, A.R., The Measurement of Pump Noise Properties and Their Use in Predicting the Insertion Loss of Hydraulic Silencers, Internoise 86 Conference, Cambridge, USA, 1986, pp. 211-216.

8. Henderson, R.A., Silencing Fluid-Borne Noise, Quieter Fluid Power Handbook, BHRA, 1980, pp. 33-44.

9. Edge, K.A., Positive-Displacement Pumps as Generators of Fluid-Borne Noise, Quieter Fluid Power Handbook, pp. 77-85.

10. Tilley, D.G., Fluid-Borne Noise in Hydraulic Systems, Quieter Fluid Power Handbook, pp. 67-75.

11. Horowitz, P., Hill, W., The Art of Electronics, Cambridge University Press, 2nd Ed., 1989, pp. 360-368.

12. Edge K.A., Brett, P.N, and Leahy, J.C., Digital Computer Simulation as an aid in Improving the Performance of Positive Displacement Pumps with Self-Acting Valves, Proc. Instn. Mech. Engrs., Vol. 198, No. 14, 1984, pp. 267-274.

13. Dynex-Rivett Model PV-4000 variable displacement poppet valve pump.

14. Johnston, D.N., Numerical Modelling of Reciprocating Pumps with Self-Acting Valves, Proc. Instn. Mech. Engrs., Vol. 205, pp. 94.

15. Rogers, D.J., Dept. of Computer Science, University of Edinburgh, Personal Communication, 1988.

16. Akers, A. & Lin, S.J., Dynamic Analysis of an Axial Piston Pump with a Two-Stage Controller and Swashplate Position Feedback, Proc. of the 8th Intl. Sym. on Fluid Power, BHRA, Birmingham, 1987, pp. 547-564.

17. Taylor, R., Pump Noise and Its Treatment, Quieter Fluid Power Handbook, pp. 53-65.

18. Steiger, A., Solenoid Poppet Valve, German Patent: DE 33 12 054 A1, 1984.

19. Moller, C.B., op. cit.

20. Lungu, C., Magnetic Poppet Valve, European Patent: EP 0312527, 1987.

21. Slemon, G.R., Straughen, A., Electric Machines, Addison-Wesley, 1982.

22. Roters, H.C, Electromagnetic Devices, Wiley, 1941.

23. McCaig, M., Permanent Magnets in Theory and Practice, Pentech Press, London, 1977.

24. Yonnet, J.P., Chercher, Laboratoire d'Electrotechnique, C.N.R.S., Grenoble, France, Personal Communication, 1987.

25. Sauer, H., Modern Relay Technology, SDS Relais 0908.56, 1987.

26. Neubert, H.K., Instrument Transducers, Oxford, 1974, pp. 96-104.

27. ibid., pp. 89.

28. Tk!solver, Universal Technical Systems Inc., Rockford Ill., USA.

29. PE2D 2D Magnetic Finite-Element Solver, Vector Fields Ltd, Oxford.

30. ANSYS PC Magnetic, Swanson Analysis Systems, Houston, PA, USA.

31. Edge K.A., Brett, P.N. & Leahy, J.C., op. cit., pp. 273.

32. Johnston, D.N., op. cit., pp. 92-93.

33. Salter, S.H., Edinburgh-Scopa-Laing Fifth Year Report to Dept. of Energy, Vol. 2, Appendix 8: Recent Progress on Ducks, 1979, pp. 14,15.

34. Roters, op. cit., pp. 242

35. Diver, B., Magnetic Material Consultant (formerly of Swift-Levick Supermagloy Ltd.), Personal Communication, 1991.

36. Roters, op. cit., pp. 228.

37. McCaig, M., op. cit., pp. 83-154.

38. Swift Levick Supermagloy Ltd., Technical Data Sheet for Neodymium-Iron-Boron material properties, 1989.

39. Roters, op. cit., pp. 242.

40. Neubert, op. cit., pp. 98.

41. Martin Blake, Ansys Magnetic Consultant, Strucom Ltd, London, Personal Communication, 1992.

42. PE2D User Manual, Vector Fields Ltd., Oxford, 1988.

43. ANSYS PC Magnetic User Manual Version 4.4A, Swanson Analysis Systems, Houston, PA. USA., Vol. 1 pp. 4.47.

44. ANSYS PC Magnetic User Manual,op. cit., Vol 1 pp. 4-14.

45. Diver, B., Personal Communication, 1992.

46. Green, W.L., The Stability of Poppet Relief Valves -A Summary, Hydraulic Pneumatic Power, Sept. 1972.

47. Green, W.L., The Poppet Valve -Force Compensation, Proc. of 1970 Fluid Power Intnl. Conf., BHRA, 1970.

48. Maeda, T., Studies on the Dynamic Characteristic of a Poppet Valve, Bull. JSME, Vol. 13, No. 56, 1970, pp. 281-289.

49. Urata, E., Thrust of a Poppet Valve, Bull. JSME., Vol. 12., No. 53., 1969, pp. 1099-1109.

50. Johnston, D.N., Edge, K.A., Vaughan, N.D., Experimental Investigation of Flow and Force Characteristics of Hydraulic Poppet and Disc Valves, Proc. Instn. Mech. Engrs., Vol. 205, 1991, pp. 168.

51. Oshima, S. and Ichikawa, T., Cavitation Phenomena and the performance of Oil Hydraulic Valve, Reports 1,2,3,5, Bul. JSME, Vol. 28, No. 244, 1985, pp. 2264-2271, 2272-2279, Vol. 29, No. 249, 1986, pp. 743-750, No. 251, pp. 1427-1433 respectively, Report 4 not published in english.

52. Shrenk, E., Disc Valves; Flow Patterns, Resistance and Loading, Transl. from German Original of 1927, BHRA, Pub. T. 547, 1957.

53. Stone, J.A., Discharge Coefficients and Steady-State Flow Forces for Hydraulic Poppet Valves, Trans. ASME, Jrnl. Basic Eng., March 1960, pp. 144-154.

54. Ward-Smith, A.J., Internal Fluid Flow, Oxford, 1980, pp. 341-348

55. Vaughan, N.D., Johnston, D.N., Edge, K.A., Numerical Simulation of Fluid Flow in Poppet Valves, Proc. of Instn. Mech. Engrs., No. C413/079, 1991, pp. 119-127.

56. Takenaka, T., Yamane, R., Iwamizu, T., Thrust of Disc Valves, Bull. JSME., Vol. 7, No. 27, 1964, pp. 558-566.

57. McGinn, J.H., Observations on the Radial Flow of Water Between Fixed Parallel Plates, Applied Scientific Research (Section A), Vol. 5, 1955, pp. 255-264.

58. Schlitting, H., Boundary-Layer Theory, McGraw-Hill, 7th ed., 1979, pp. 436-438.

59. Craig, T., Technical Director of MacTaggart-Scott, Pump/Motor Parametric Design Method (developed for use within MTS), Personal Communication, 1987.

60. Bergemann, M., Noise Problems of Hydraulic Piston Pumps with Odd and Even Numbers of Cylinders, Fluid Power Proc. 9th Int. Sym., Cambridge, 1990, pp. 235-248.

61. Towler six cylinder A-series poppet-valve pumps, Oilgear-Towler Ltd., Rodley, Leeds.

62. Dynex-Rivett PV 4000 and 8000 series, 8 cylinder pumps.

63. Daugherty, R.L., Franzini, J.B., Fluid Mechanics with Engineering Applications 7th Ed., McGraw-Hill, 1977. pp. 222.

64. Tom Craig, MacTaggart-Scott Ltd., Personal Communication, 1987.

65. ICI Victrex PEEK, Technical Data Sheet no. VK2/0586, ICI PLC, 1986.

66. Brian Lightfoot, ICI Polymer Research Laboratory, Personal Communication, 1990.

67. Dowty Aerospace, internal sprung wheel, suspension for Gloucestor Gladiator employing silicone fluid springs, 1937, Personal Communication, Roger Hatton, Chief Design Engineer, Landing Gear Division, 1992.

68. Lallement, J., Hydropneumatic Accumulators, Fluid Power Components and Systems, 2nd Bath Intl. Fluid Power Workshop, RSP, 1989, pp. 43-57.

69. Kaye and Laby, Tables of Physical and Chemical Constants, Longman, 1986, pp. 35.

70. Handbook of Chemistry and Physics 67th ed., CRC Press, 1986, pp. F12-15.

71. Rampen, W.H.S., Salter, S.H., Fussey, A., "Constant Pressure Control of the Digital Displacement Hydraulic Piston Pump", proc. of 4th Bath Intl. Fluid Power Workshop, RSP Wiley, 1991, pp. 62 (questions).

72. Racine radial piston pump range, technical data sheet no. RE2-006, VFP Ltd., 1981.

73. Faires, V.M., Design of Machine Elements 4th Ed., Macmillan, 1965, pp. 345.

74. Poclain PS series modular pumps, technical data sheet no. CR677 777 797, Poclain Hydraulics SA., Verberie, France.

75. Towler FCM and FCS series double ended axial machines, technical data sheet no. 2P139/140, Oilgear-Towler Ltd., Rodley, Leeds.

76. Salter, S.H., Clerk, R.C., Rea, M., "Evolution of the Clerk Tri-link Machines", proc. 8th Intl. Sym. on Fluid Power, Birmingham, Elsevier, 1988, pp. 611-632.

77. McCandlish, D., Edge, K.A., Tilley, D.G., "Fluid Borne Noise Generated by Positive Displacement Pumps", Proc. Instn. of Mech. Engrs. Conf.: Quieter Oil Hydraulic Systems, 1977, pp. 108.

78. Edge, K.A., Professor, Bath University Fluid Power Centre, Personal Communication, 1992.

Acknowledgements

While all of those joining the general melee that is, or has been, the Wavepower Project over the years have contributed to a greater or lesser extent to the work presented here, some are due special mention:

Stephen Salter, without whom the fundamental idea and motivation for the thesis would not have occurred.

Carn Gibson and Tully Peacocke, who worked on the project and created some finely crafted pieces of metal and the photographs to exhibit them. Matthew Rea and Robert Clerk, who worked alongside me on their Tri-link machine and who brought to light many of the difficulties inherent in working with high-pressure oil. Peter Woodhead, who patiently assisted with mysterious computer ills. David Jeffrey, who helped with the original real-time controller. Doug Rogers, who came up with some of the ideas on real-time cylinder enabling. Colin Anderson, whose fine thesis set an aesthetic example for all to follow.

David Skyner and Jean-Baptiste Richon, who have not only provided advice but who have kindly aided in proof-reading the manuscript.

George Alder, for his sound and practical help as second supervisor.

The people at J.H. Fenner, with whom I have been collaborating over the past four years. In particular: John McCullough and Colin Seabrook for their vision, Alan Fussey, Ashley Derrick and John Almond for their practical assistance.

Finally, and most importantly, to my wife Rosie, who encouraged and selflessly supported me despite the tremendous workload imposed by our three very young children.

To all, I offer my sincerest gratitude.

Win Rampen

December 1992

Appendix A: Toggling Latch

Poles in attraction were specified on the basis that repellant poles would require a circuit composed entirely of hard magnetic material (i.e. permanent magnet) and would, therefore, cost more. The decision to use magnet poles in shear, rather than as approaching surfaces, was forced by the required combination of an over-centre characteristic and a low rate spring in the "able" region. This is less magnet efficient than an approaching surface configuration.

The magnetic system contains a moving assembly, composed of two mild steel rings with an annular magnet sandwiched in between, surrounded by a static arrangement of three equally spaced steel rings, separated by two steel spacers as shown in figure A-1. The magnetic circuit is bistable, preferring to align itself so that one of the moving magnetic poles is opposite the central ring of the static assembly and the other pole facing either of the two outer rings. The steepness of the characteristic curve can be altered by changing the pole shape and gap between the moving and static assemblies.

A rig which allowed the measurement of axial force/displacement data for the various latch configurations was built. Trial and error was used to produce pole faces of the sizes and shapes which would produce the desired force characteristic, an example of which is presented in figure A-2.

In the first region the curve has a low spring rate, for its "able" or operating condition, which tends to pull the valve lightly onto its seat. The second region is a rapid rise in rate which serves as a soft end-stop to the "able" valve, arresting its motion as it opens with the intake stroke. In the third region the mechanism goes over-

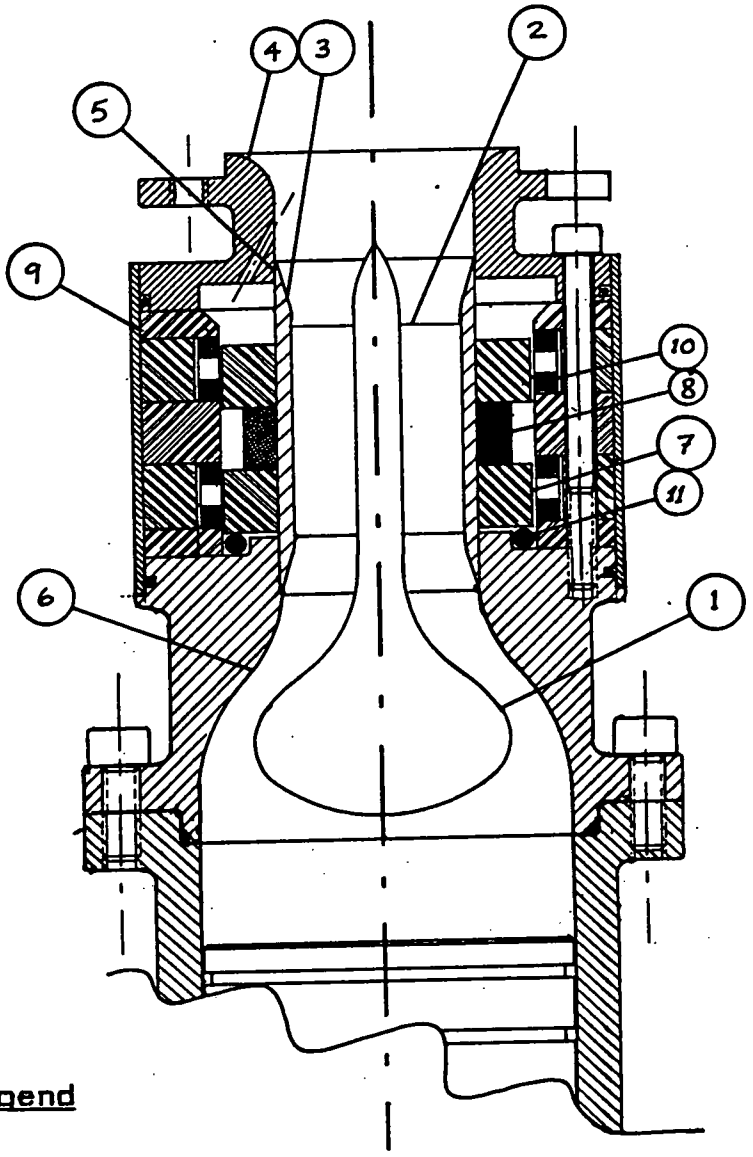

Legend

1. Low Drag Poppet Valve Element
2. Septum
3. Valve Support Tube
4. Bell-Mouthed Manifold Entrance
5. Valve Guide Journal
6. Low Drag Valve Seat
7. Moving Polepiece Ring (steel)
8. Moving Rare-Earth Magnet Ring
9. Profiled Static External Polepiece
10. Static Coils for Toggling Position
11. Resilient End-Stop

Figure A-1: Configuration of Magnetic Toggling Latch

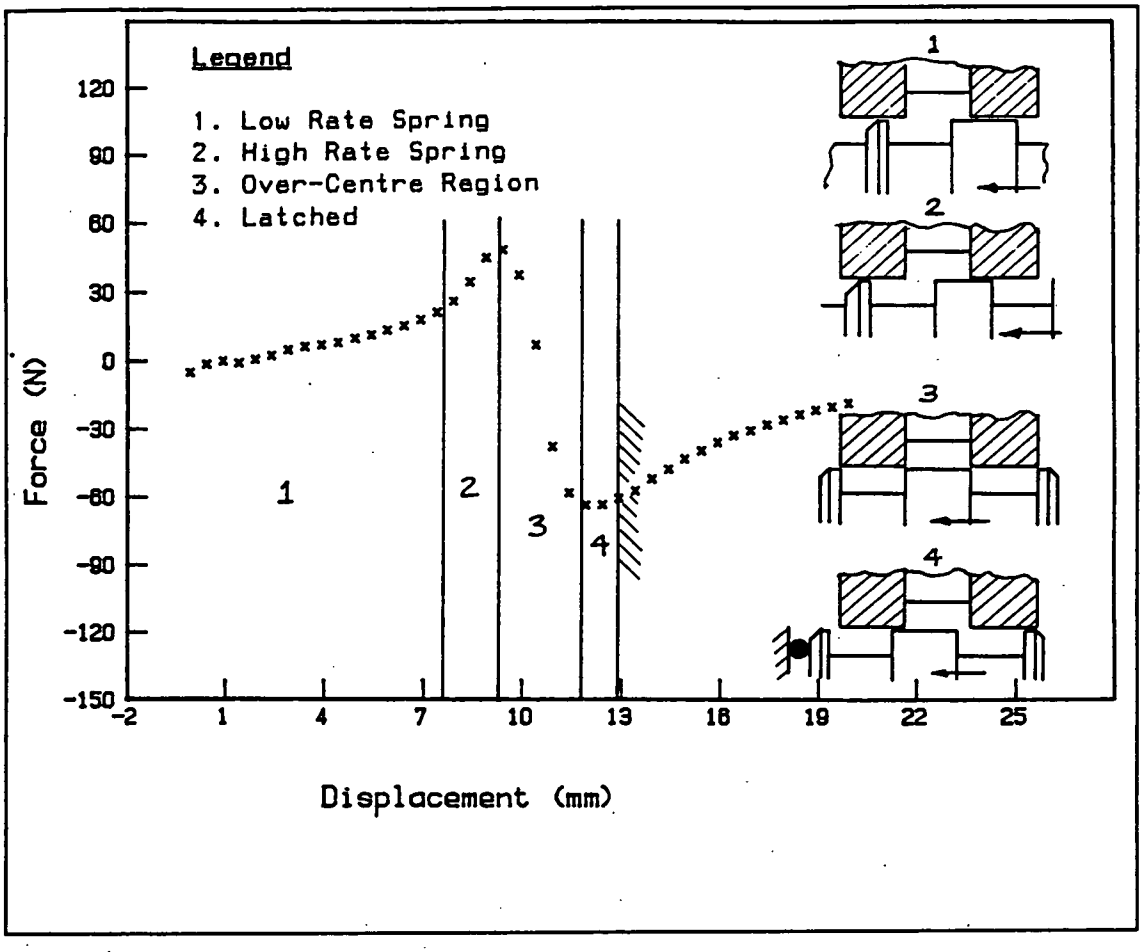

Figure A-2: Magnetic Spring Force/Deflection Characteristic.

centre. Here the rate rapidly reverses, first pulling hard to close the valve then pushing hard to open it. The fourth region is that of latching and the location of the resilient mechanical end-stop. The axial position of this stop is chosen so that the valve is held open with the maximum force that the latch can develop. The required height of the two peaks (regions 2 and 4) is determined by the fluid forces on the valve under the worst operating conditions. In turn, the peaks of the characteristic curve determine the amount of permanent magnet required in the latch.

This magnetic stator has been fitted with coils wound in the grooves between the pole faces. These link with enough

fringing flux in all positions of the travel that they can cause the latch to toggle from one state to the other. In the valve design of figure A-1 the coils are in the static external part of the system which eliminates flying leads that might otherwise fail in fatigue. The other advantage of this rather unconventional voice coil motor is that it makes use of the existing magnetic circuit.

Appendix B: Moving-Magnet Latch Analysis

The moving-magnet latch is shown in figure B-1. In the latched open position, shown on the left of the figure, the flux can be seen to be circulating through the magnet and into the static pole-piece in the lower valve body. The latching force developed in this position must exceed that expected of the fluid forces during flow reversal.

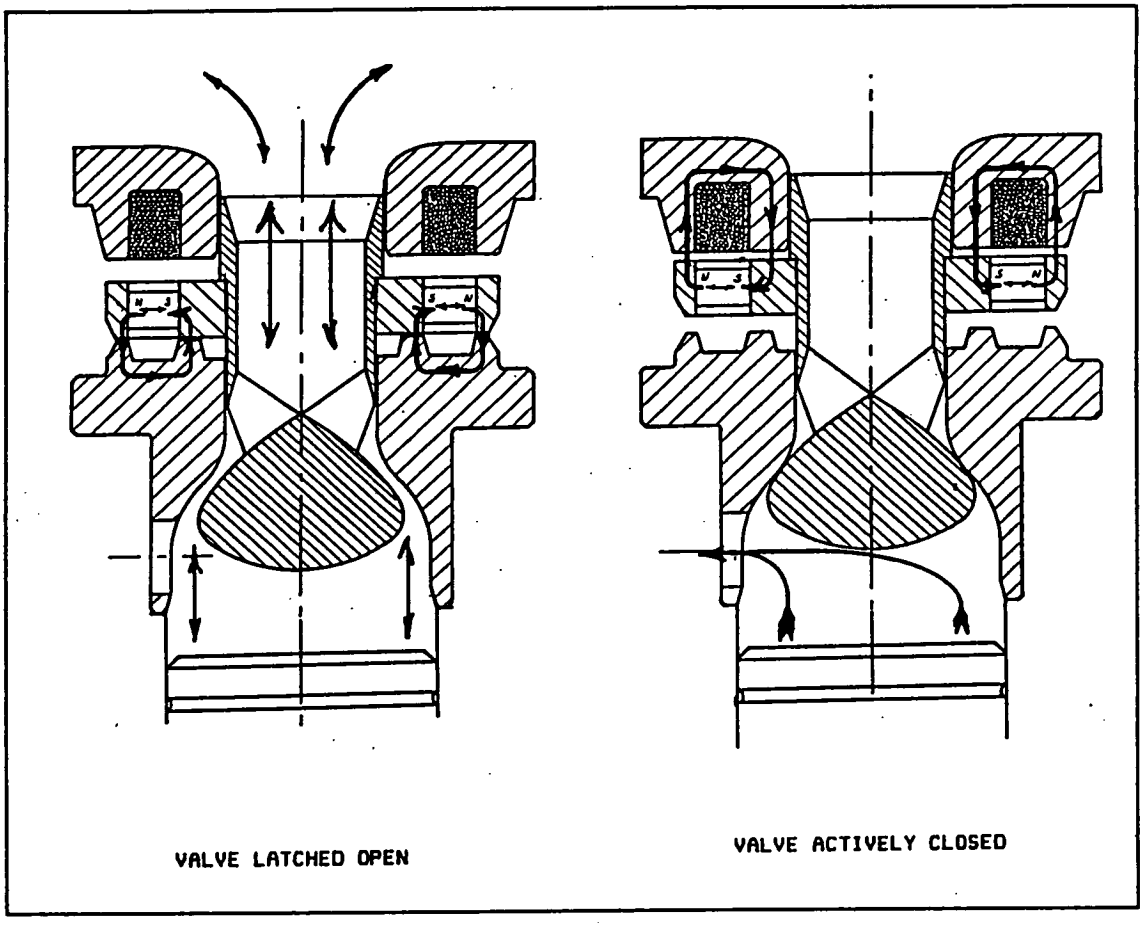

Figure B-1: Moving-Magnet Latch

When a pulse is sent to the coil the flux pattern changes dramatically, as can be seen in the drawing on the right. The coil generates a toroid of flux around itself, circulating inside the top pole-piece, which then passes across the air gaps to the moving poles and magnet ring.

The magnet reinforces this flux path, since it is increased in its own magnetisation, and the net force between the poles also raised. The flux that had been passing into the lower pole-piece is almost entirely diverted into the top circuit, thereby negating the latching force.

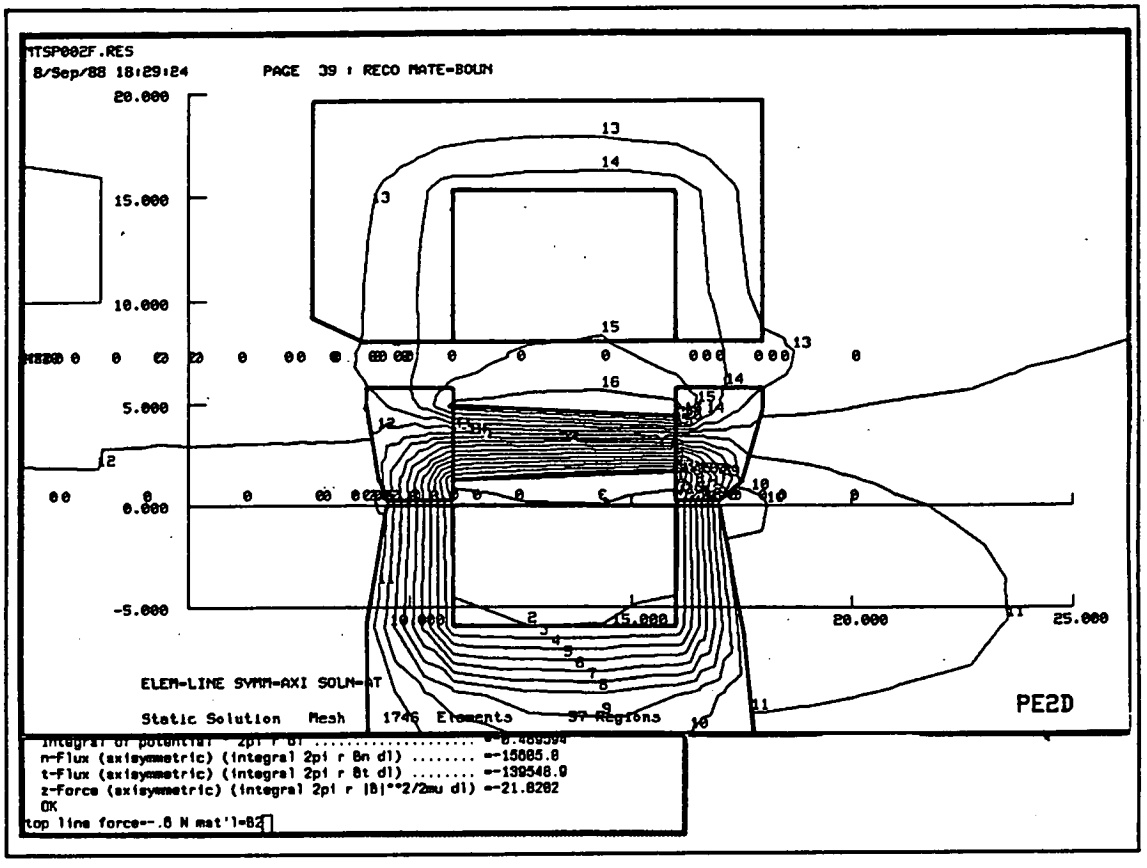

Figure B-2: Finite Element Model of Moving-Magnet System in the Passively Latched State

After the experiments on the toggling latch, it was felt that some way of looking at the flux inside the circuit was needed. The SERC developed magnetic finite element software package, PE2D, was acquired in order to model the flux pattern generated within the circuit. The post-processor allowed forces along a line to be calculated. By creating two measuring lines, one above the moving pole and the other below, it was possible to calculate the net force applied to the poppet. The screen-dump of figure B-2 shows

a typical post-processor display with the measuring lines and the forces in an overlapping window. This technique was used to refine the geometry and improve the permanent magnet latching force. Typical modifications included reducing pole area in order to concentrate the flux and increasing the pole-piece section thickness in regions nearing saturation.

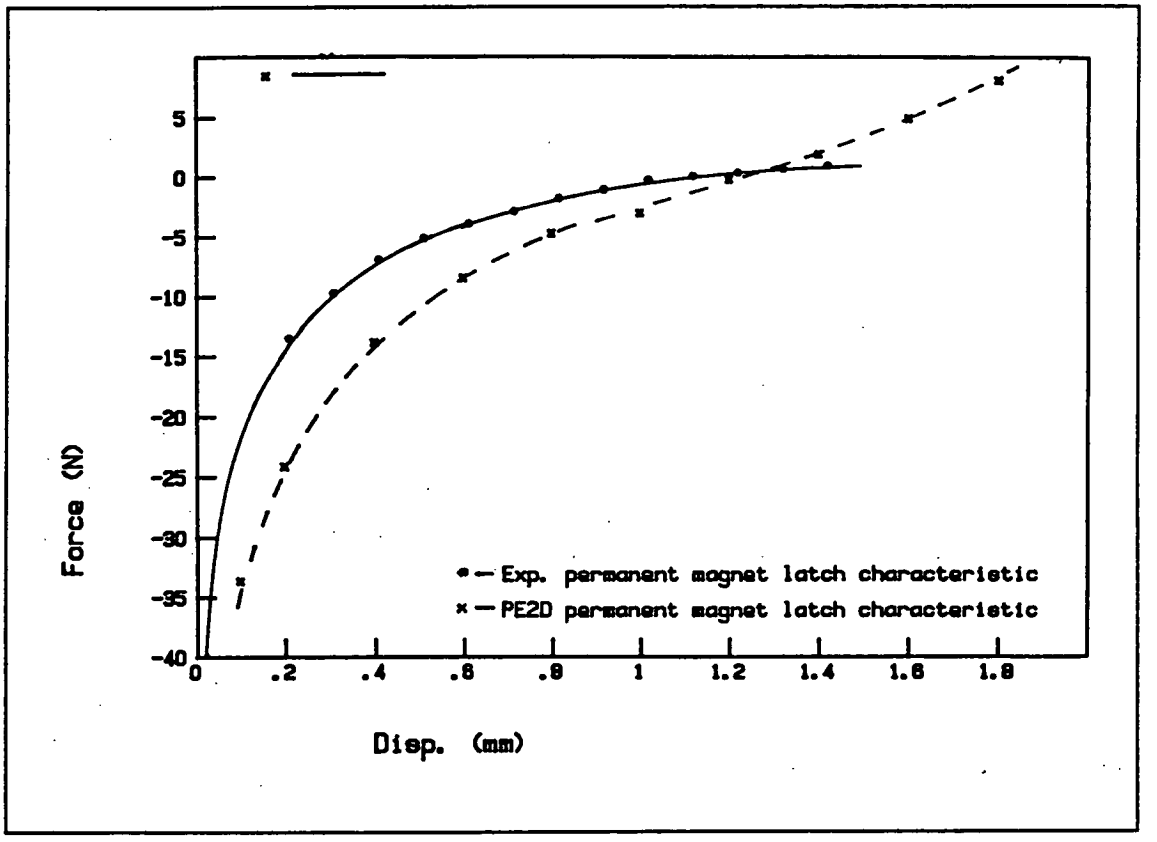

Figure B-3: Force/Deflection Characteristic for Passive Latch

The PE2D program was also used to produce the results for the characteristic curve shown at the top of figure B-3. To generate these, the moving pole was incrementally shifted in the model geometry and in each case sent to the solver. The resulting force is shown here plotted against the displacement.

The second curve on this graph is one found by experimentation on an actual valve latch. The measurement rig consisted of a load cell in series with the poppet head. A series of force and displacement measurements were then taken as the poppet was moved between its end-stops.

In comparing the experimental results with those from PE2D, the two curves can be seen to be of similar shape though of different magnitude. The PE2D curve is based on a slightly simplified model since the radial magnet could not be made as it was represented. The actual latch contained somewhat less magnetic material as a result. It is not surprising, then, that the forces associated with the model are somewhat higher than those in the actual latch.

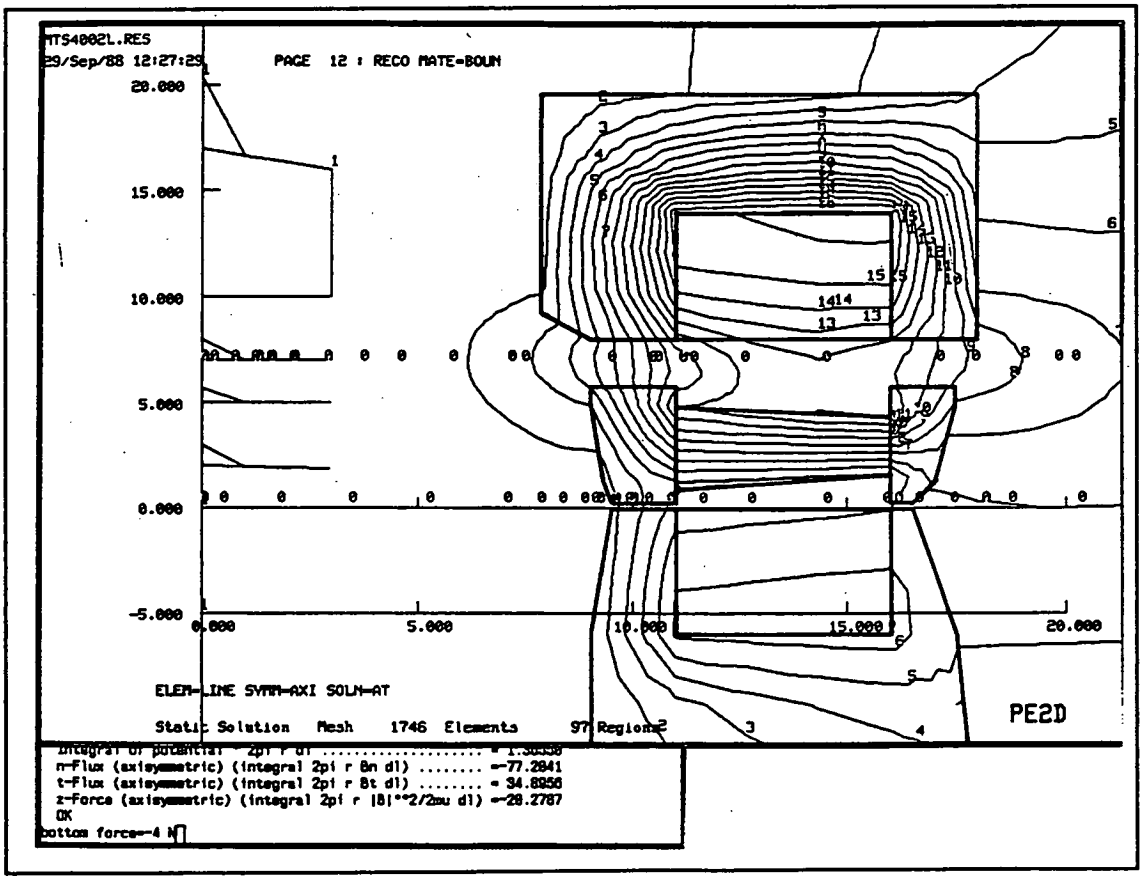

Figure B-4: Finite Element Model of Moving-Magnet Latch with Solenoid Enabled

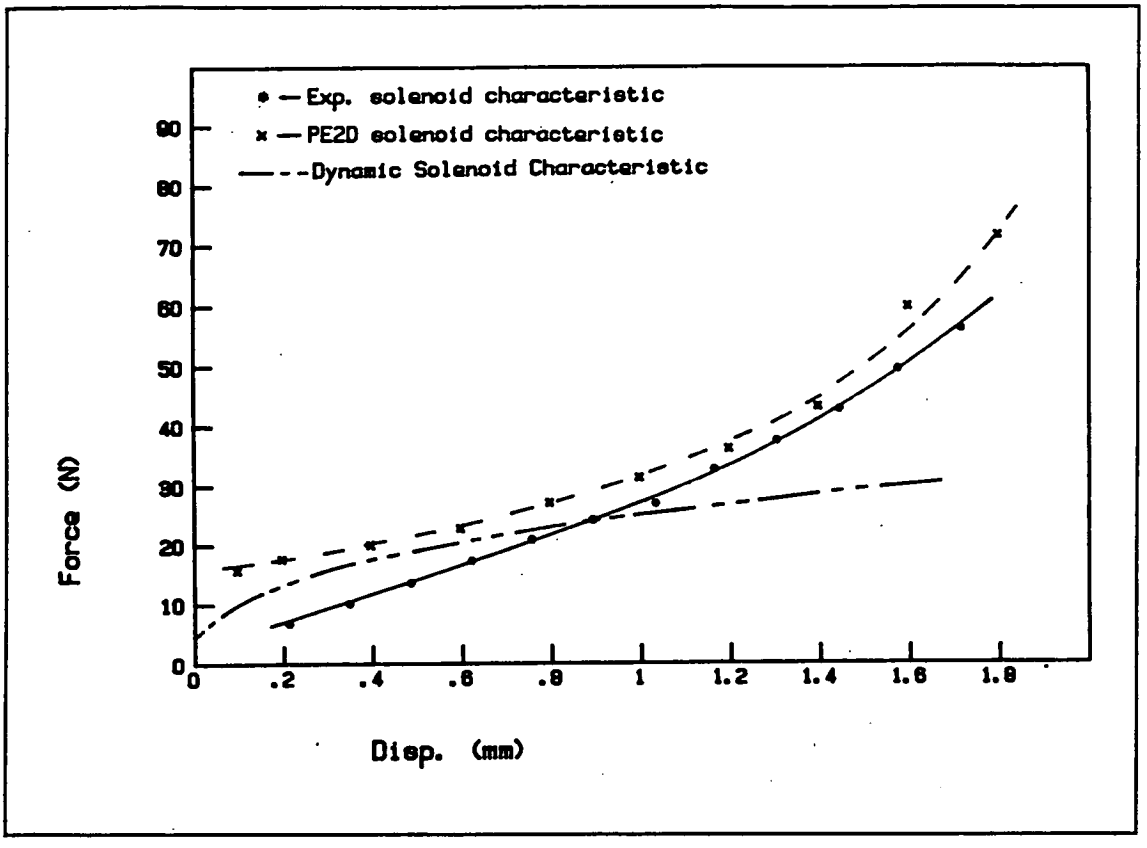

Figure B-5: Force/Deflection Characteristic of Latch with Solenoid Enabled

The PE2D model was also used with the coils energized as shown in the screen-dump of figure B-4. It is interesting to compare the flux distribution of this with the previous permanent magnet model of figure B-2. The two figures can also be related to the valve schematic shown in figure B-1. Using the same technique of incrementing the moving pole position, the solenoid characteristic force curve of figure B-5 was produced with PE2D.

The previously described apparatus was also employed to measure the force/deflection characteristic with the coils energized. The results are plotted alongside those of the PE2D model. As in the permanent magnet case the two curves share a similar shape but are different in magnitude. All of the comments used to reconcile the inaccuracies in the permanent magnet case should also apply.

During the course of dynamic valve testing an interesting effect was noticed in the solenoid response. At the onset of a pulse the poppet would start to move toward its seat but then would hesitate and return to the latched position. This effect was caused by the changing inductance in the circuit as the poles moved. The movement of the magnet and its pole pieces itself generated a current in one of the coils which opposed the current of the pulse. This indicated that the solenoid force was largely dominated by dynamic effects and that attempts to model it statically were bound to be inaccurate.

As a result of this discovery a third approach was used to create a solenoid force curve. If the poppet and moving magnet assembly are considered as mass and, if the damping forces can be ignored (with the volume around the magnet filled with air rather than oil), then the displacement of the valve with respect to time will allow the solenoid force characteristic to be determined. An experiment was conducted using a proximity measuring device to record displacement. The apparatus is essentially the one shown in figure B-6 and the resulting displacement curve that of figure B-7. This curve was fitted with a fourth order polynomial and then differentiated twice to give acceleration. The time/displacement relationship was inverted, using an iterative method, to generate a time for a given displacement. The solenoid force was then calculated by multiplying the acceleration at each displacement interval by the moving mass. The resulting characteristic curve is plotted on top of the other two on the lower graph of figure B-5. It is immediately apparent that it bears very little similarity in shape with those derived from static analysis. It is equally apparent that static methods of solenoid analysis are invalid in the dynamic case.

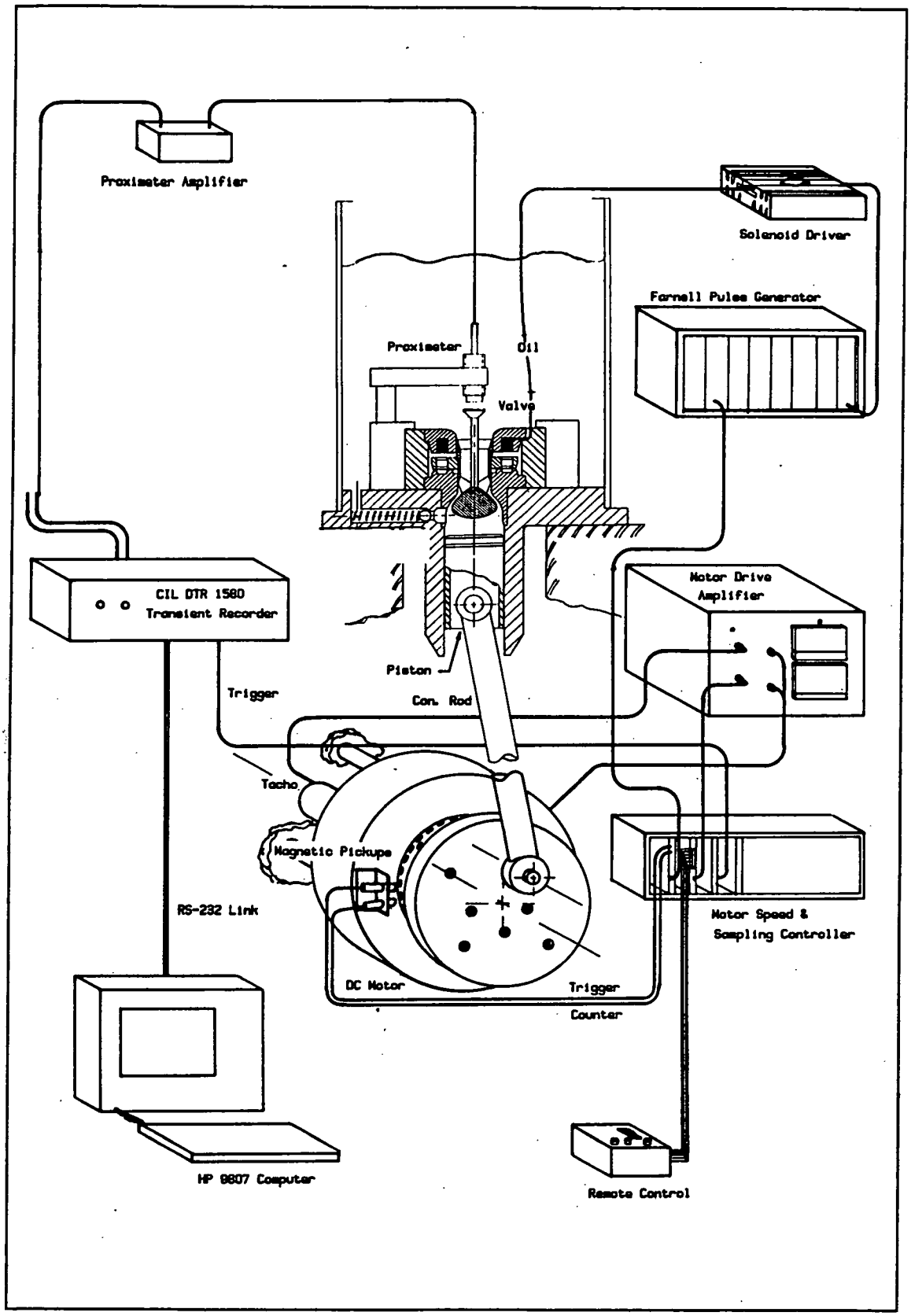

Figure B-6: Step-Response Test Rig

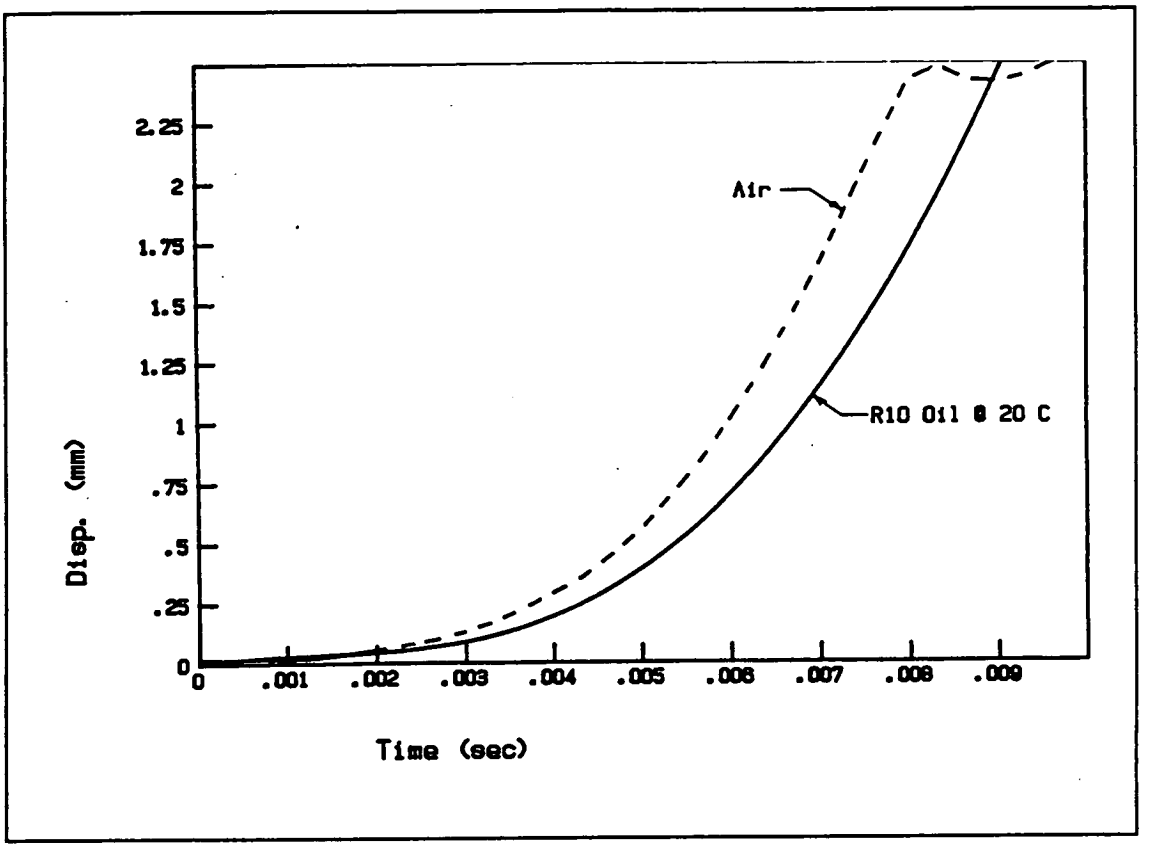

Figure B-7: Step-Response of Closing Poppet Valve

Appendix C: Simple Numerical Modelling of Moving-Iron Latch Using TK!solver

The schematic diagram of the latch, figure C-1, identifies all of the various dimensions used in the following series of equations.

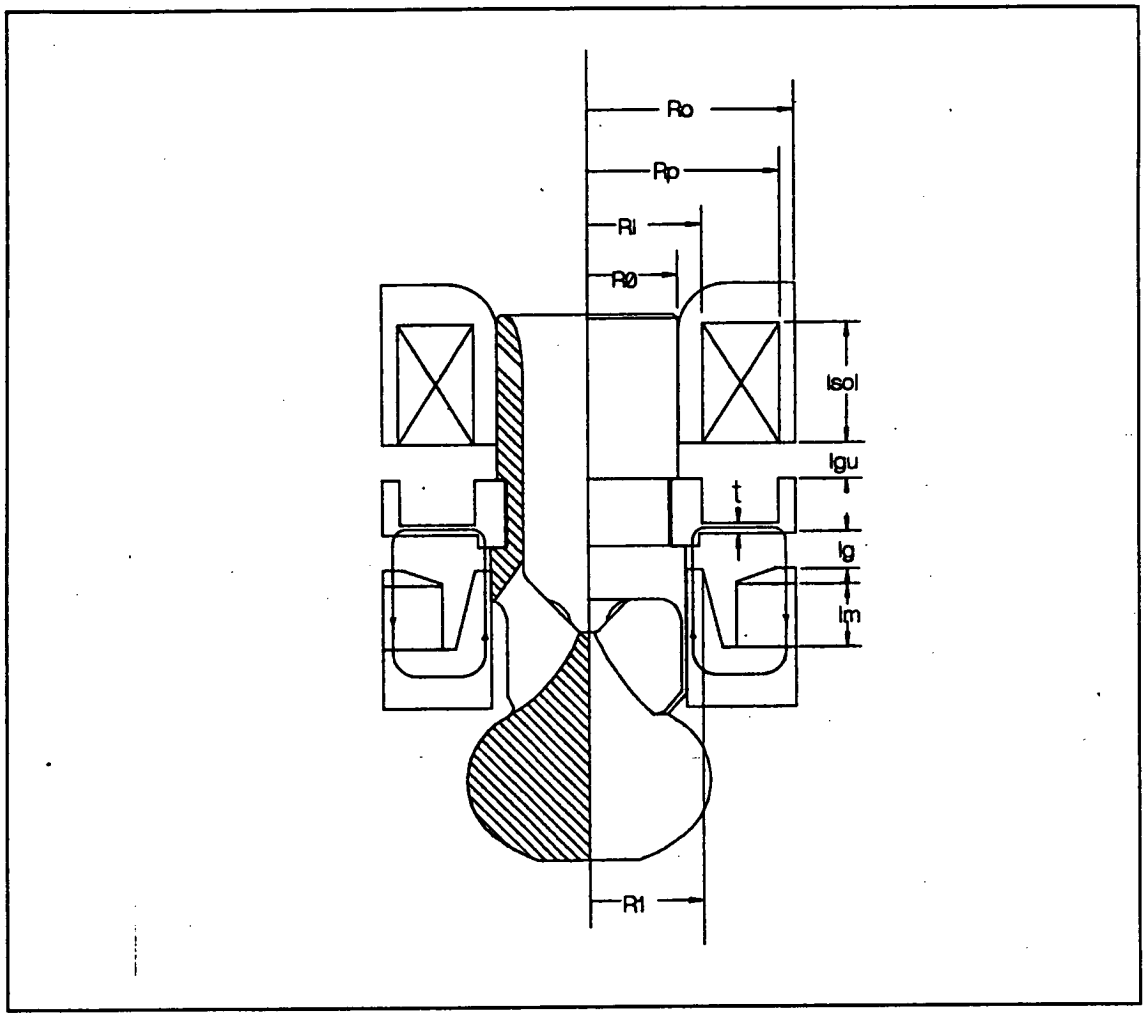

Figure C-1: Schematic Diagram of Moving-Iron Latch with Associated Dimensions

The variable sheet of figure C-2 lists the values of the parameters used in the equations. The identifying label "L" on the left identifies a one dimensional variable array, otherwise variables are single value. The rule sheet of figure C-3 lists the equations which describe the

```
S Rule
* Lstl=Ro-R0 "                          Radial Length of saturated pole web
* Agi=pi()*(R1^2-R0^2) "                Area of inner pole
* Astl=pi()*R1*t "                  Cross-sectional area of radial web (average)
* Ag=(Ro^2-Rp^2)*pi() "                 Area of outer pole
* Am=(Ro^2-Ri^2)*pi() "                 Area of magnet

* Bm=Br*(1-Hm/Hsc) "                    BH relationship for permanent magnet
* Bg=Bm*Am/Ag "    Flux density in gap related to that of magnet by resp. areas
* Astl*Bstl=(Bg+Bgu)*Ag "               Flux summation through radial web
* Bgi=Bg*Ag/Agi "                       Flux density of inner pole
* u0=4*pi()*10^-7 "                     Permeability of free space

* NIperm=-lm*Hm "                       Magnetising force of permanent magnet
* NIsol=lsol*(Rp-R1)*CURD "             Magnetising force of solenoid
* NIsol=k1*lgu*Bgu/u0+NIstl "        Magnetising equation for closing circuit
* NIperm=k1*lg*Bg/u0+NIstl "         Magnetising equation for latching circuit
* NIstl=Lstl*hb(Bstl)                    " Demagnetising force of radial web

* Fu=Bgu^2*Ag/u0 "          Closing force exerted by solenoid across upper gap
* Fo=Bg^2*Ag/(2*u0) "                   Opening force from outer pole
* Fi=Bgi^2*Agi/(2*u0) "                 Opening force on inner pole
* F=Fo+Fi "                        Opening force sum of inner and outer poles
* Ft=Fu-F "                             Summation of moving pole forces
```

Figure C-3: TK Solver Rule Sheet for Moving-Iron Latch Analysis

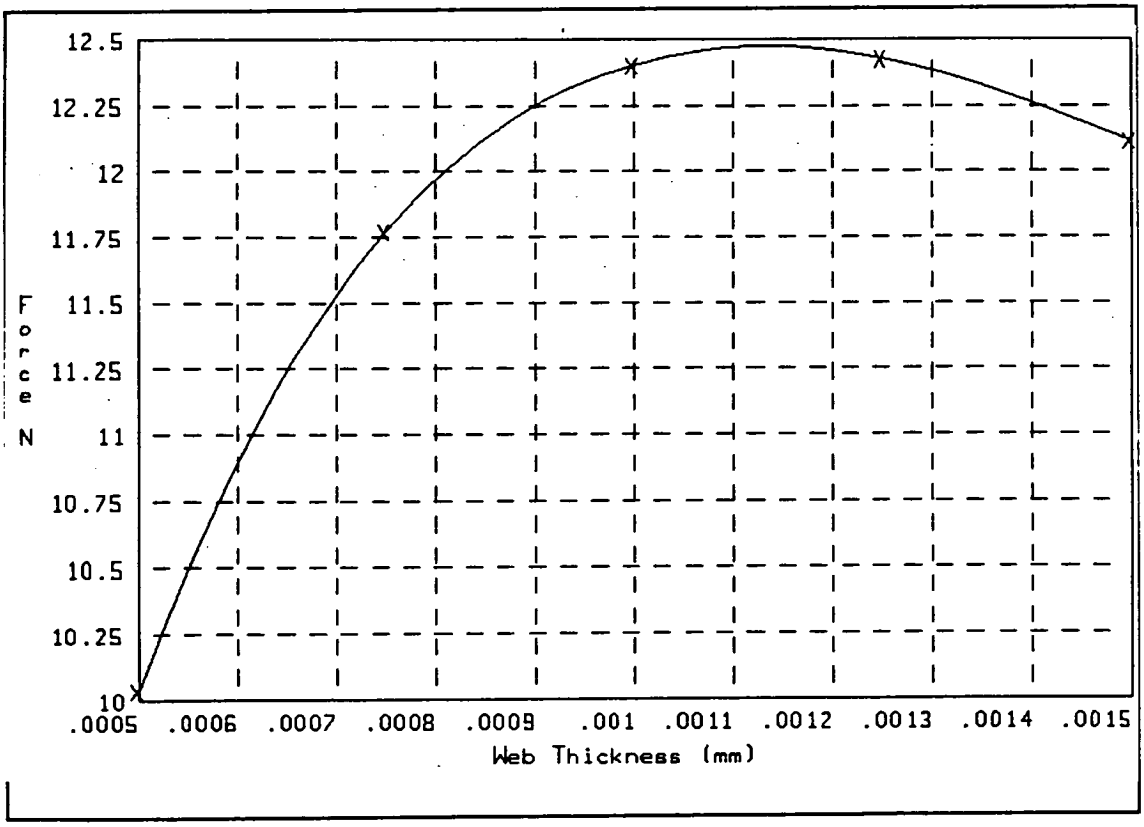

Figure C-4: Optimisation of Moving Pole Thickness for Maximum Detaching Force

Appendix D: Derivation Equating Power to FFT Fundamental of Pressure Trace

$F = p \cdot A \quad u = q/A$

where: F= instantaneous force on piston

p= instantaneous pressure drop across valve manifold

A= cylinder area

q= instantaneous flow rate

u= instantaneous velocity of piston

Then average power loss can be found with the summation:

$$P = \frac{1}{T}\int_0^T \underline{F}(t).\underline{u}(t)\,dt$$

$$= \frac{1}{T}\int_0^T \frac{1}{2}\sum_{n=-\infty}^{\infty}\underline{F}(\omega_n)e^{i\omega_n t}\cdot\frac{1}{2}\sum_{m=-\infty}^{\infty}\underline{u}(\omega_m)e^{i\omega_m t}\,dt$$

$$= \frac{1}{4}\sum_{n=1}^{\infty}\sum_{m=1}^{\infty}\frac{1}{T}\int_0^T (\underline{F}(\omega_n)e^{i\omega_n t} + \underline{F}^*(\omega_n)e^{-i\omega_n t}).(\underline{u}(\omega_m)e^{i\omega_m t} + \underline{u}^*(\omega_m)e^{-i\omega_m t})\,dt$$

$$= \frac{1}{4}\sum_{n=1}^{\infty}\sum_{m=1}^{\infty}\frac{1}{T}\int_0^T \underline{F}(\omega_n).\underline{u}(\omega_m)e^{i(\omega_n+\omega_m)t} + \underline{F}^*(\omega_n).\underline{u}^*(\omega_m)e^{-i(\omega_n+\omega_m)t} + \underline{F}(\omega_n).\underline{u}^*(\omega_m)e^{i(\omega_n-\omega_m)t} + \underline{F}^*(\omega_n).\underline{u}(\omega_m)e^{-i(\omega_n-\omega_m)t}\,dt$$

$$= \frac{1}{4}\sum_{n=1}^{\infty}\sum_{m=1}^{\infty}\ (\ 0 + 0 + \underline{F}(\omega_n).\underline{u}^*(\omega_n) + \underline{F}^*(\omega_n).\underline{u}(\omega_n)\ )\ \delta_{nm}$$

$$= \frac{1}{4}\sum_{n=1}^{\infty}\underline{F}(\omega_n).\underline{u}^*(\omega_n) + \underline{F}^*(\omega_n).\underline{u}(\omega_n)$$

$$= \frac{1}{2}\sum_{n=1}^{\infty}\mathrm{Re}\{\underline{F}(\omega n)\}\cdot\mathrm{Re}\{\underline{u}(\omega n) + \mathrm{Im}\{\underline{F}(\omega n)\}\cdot\mathrm{Im}\{\underline{u}(\omega n)\}$$

Since the velocity is simple harmonic motion $u(\omega n)=0$, $n \neq m$ and $\mathrm{Re}\{u(\omega_m)\}=0$

so: $$P = \frac{1}{2}\,\mathrm{Im}\{\underline{F}(\omega_m)\}\cdot\mathrm{Im}\{\underline{u}(\omega_m)\}$$

for the purposes of the experiments: $\mathrm{Im}\{\underline{F}(\omega_m)\} = A\cdot\mathrm{Im}\{p(\omega_m)\}$

and $$\mathrm{Im}\{u(\omega_m)\} = \frac{St\times\omega}{2}$$

and, finally: $$P = \frac{A\cdot St\cdot\omega}{4}\cdot\mathrm{Im}\{p(\omega_m)\}$$

where: P= Power (Watts)
A= Cylinder Area (m^2)
St= Stroke (m)
$\mathrm{Im}\{p(\omega_m)\}$= imaginary component of pressure fundamental FFT component

Appendix E: Flow Rig Instrumentation Specification

1. Force Transducer: Piezo-resistive strain gauge type

Type: Entran MLGL

Range: +/- 90 N. Over-range: 150 % of full scale
Sensitivity: 29.64 mV/V., Excitation: 5 V. d.c.
Input Impedence: 128 Ohms, Output Impedence: 91 Ohms
Linearity: 0.1% full scale, Hysteresis: 0.05% full scale
Repeatability: 0.05% full scale
Compensated temperature range: 0 - 55 C
Thermal Zero Shift: 0.5% full scale
Axial deflection at maximum rated load: 0.018 mm.

2. Pressure Transducers: Piezo-resistive diaphragm type

Type: RS 303-337

Range: 0 - 2 Bar, Over-range: 200% of full scale
Full Scale Output: 79 mV.
Null Offset: +/- 1 mV.
Sensitivity: 38.1 mV/Bar.
Response Time: 1 ms.
Linearity: 0.5% full scale
Temperature Error: Sensitivity Shift: +\- 1.5% full scale
Null Shift: +\- 2% full scale
Hysteresis and Repeatability: 0.15% full scale

3. Transient Data Recorder

Type: CIL DTR 1580 16 Channel 16 Bit

Input Resolution: +\- 15 bits
Input Range: 100 mV - 10 V.
Input impedence: > 1 Mohm.
Initial accuracy: +/- 0.05% full scale
Sampling and storage time: 20 us /channel.
Trigger delay resolution: 100 us.

Appendix F: Disabled Ellipsoidal Poppet Valve Flow Loss Calculated using a Minor Losses Approach

If the power loss attributable to the skin friction is considered to be negligible when compared to that generated by velocity squared losses, as is the case when the Reynolds Number is high, then a simple calculation based on pipe flow could be used to find power loss.

at any instant: $P=q*p$ where $q=v*A$ and $p=K\rho\frac{v^2}{2}$

$$P=\frac{K\rho Av^3}{2}$$

for Simple Harmonic Motion:

$$\text{average } v=\frac{1}{\pi}\int_0^{\frac{\pi}{\omega}}\left(\frac{St\omega}{2}\sin\omega t\right)dt=\frac{St\omega}{\pi}$$

then average power loss:

$$P=\frac{(Ki+Kd)}{16\pi^2}\rho D^2 St^3\omega^3$$

Where Ki, Kd are intake and delivery duct loss coefficients.

The loss coefficients can be calculated by dividing the valve and duct into separate components, each of which has a documented loss coefficient. The losses are each multiplied by a correction for velocity, so that they are all referred back to the piston velocity. Hence:

$$Ki=(K_{entrance}+K_{duct})*\left(\frac{A_{cyl.}}{A_{duct}}\right)^2+K_{expansion}*\left(\frac{A_{cyl.}}{A_{duct}}-1\right)^2+K_{cyl.}$$

$$Kd=(K_{exit}+K_{duct})*\left(\frac{A_{cyl.}}{A_{duct}}\right)^2+K_{contraction}*\left(\frac{A_{cyl.}}{A_{duct}}\right)^2+K_{cyl.}$$

The ratio of duct to cylinder area is 1:4 in the chosen valve geometry.

From a general text on fluid mechanics [1] the values of the minor loss constants are as follows:

$K_{entrance}$ = 0.04 for bell mouthed entrance

$K_{duct} = f\frac{L}{D} = .16$ where f comes from Moody as 0.08 and $\frac{L}{D} = 2$

$K_{expansion}$ = 1 for expansions exceeding 50 degrees

$K_{cyl} = f\frac{L}{D} = .04$ where f comes from Moody as .08 and $\frac{L}{D} = 0.5$

K_{exit} =1 for sudden expansion

$K_{contraction} = .33$ for $\frac{D_{duct}}{D_{cyl.}} = 0.5$

Putting numbers in the equations produces:

Ki= 12.2 (where 75% of the loss comes from the expansion)

Kd= 23.6 (where 2/3rds of the loss comes from the exit)

and returning to the power equation:

$$P = 0.23 \rho D^2 St^3 \omega^3$$

If we compare this equation from that derived through experimentation, we find that it corresponds to the first term. The experiment produced a relationship for valve opening which is not accounted for in the minor loss equation. If we were to replace this term with a value corresponding to the least constricting opening tested, we could compare the two constants. Taking a bore/opening ratio of 5.7 the first term of the power equation becomes:

$$P = 0.30 \rho D^2 St^3 \omega^3$$

This is approximately 30 % greater than that predicted by the minor loss equation.

The sensitivity of the power loss to the valve opening is such that the minor loss estimation would have to be carried out using an accurate model of the contractions and expansions in the valve seat area if the valve opening restricted the flow in any way.

[1] Fluid Mechanics with Engineering Applications, Daucherty and Franzini, 1977, pp. 219-226.

Appendix G: Disabled Ellipsoidal Poppet Experiment Data

Exp.	Bore	Str	Spd	Open	Dens	Vis	Nr	Fmax	Fmin	Pmin	Power
1	24	15	4	1.0	839	.007	1074	.4	-.2	-16.5	.2
2	24	15	8	1.0	839	.007	2149	3.7	1.2	-21.3	1.1
3	24	15	12	1.0	839	.007	3223	6.2	-.8	-34.6	3.4
4	24	15	16	1.0	839	.007	4297	12.4	-4.4	-57.5	6.4
5	24	15	20	1.0	839	.007	5372	23.2	-9.4	-96.9	14.3
6	24	15	24	1.0	839	.007	6446	39.3	-15.9	-91.9	22.4
7	24	15	4	1.3	839	.007	1074	.3	-.1	-11.0	.1
8	24	15	8	1.3	839	.007	2149	1.5	.2	-17.0	.7
9	24	15	12	1.3	839	.007	3223	4.4	.9	-25.7	2.0
10	24	15	16	1.3	839	.007	4297	8.3	.6	-35.5	4.4
11	24	15	20	1.3	839	.007	5372	14.1	-1.4	-54.3	7.5
12	24	15	24	1.3	839	.007	6446	20.5	-4.2	-78.0	15.1
13	24	15	4	1.6	839	.007	1074	.2	-.1	-14.1	.1
14	24	15	8	1.6	839	.007	2149	.2	-.2	-11.4	.5
15	24	15	12	1.6	839	.007	3223	1.3	-.2	-18.7	1.2
16	24	15	16	1.6	839	.007	4297	3.6	.1	-25.3	2.9
17	24	15	20	1.6	839	.007	5372	6.7	.4	-39.1	4.0
18	24	15	24	1.6	839	.007	6446	11.9	-1.0	-53.1	11.1
19	24	15	4	1.9	839	.007	1074	.2	-.1	-10.9	.1
20	24	15	8	1.9	839	.007	2149	0.0	-.3	-9.2	.3
21	24	15	12	1.9	839	.007	3223	.2	-.5	-11.9	1.0
22	24	15	16	1.9	839	.007	4297	1.0	-.7	-18.3	1.8
23	24	15	20	1.9	839	.007	5372	3.2	-.4	-32.9	1.4
24	24	15	24	1.9	839	.007	6446	5.9	-.6	-47.0	6.8
25	24	15	4	2.2	839	.007	1074	.2	-.1	-12.3	0.0
26	24	15	8	2.2	839	.007	2149	-.3	-.7	-9.8	.2
27	24	15	12	2.2	839	.007	3223	-.3	-.8	-17.7	.8
28	24	15	16	2.2	839	.007	4297	.8	-.1	-16.3	2.3
29	24	15	20	2.2	839	.007	5372	2.3	.2	-23.2	3.1
30	24	15	24	2.2	839	.007	6446	4.8	.3	-40.8	6.2
31	24	15	4	2.5	839	.007	1074	.2	-.1	-5.6	0.0
32	24	15	8	2.5	839	.007	2149	-.1	-.3	-14.1	.2
33	24	15	12	2.5	839	.007	3223	-.2	-.7	-9.1	.9
34	24	15	16	2.5	839	.007	4297	.6	-.1	-22.7	.8
35	24	15	20	2.5	839	.007	5372	1.7	-.1	-23.5	.9
36	24	15	24	2.5	839	.007	6446	3.9	-.1	-32.6	2.9
37	80	20	2	3.0	839	.007	2387	4.0	-2.1	-13.7	.6
38	80	20	4	3.0	839	.007	4775	16.6	-8.3	-17.2	4.4
39	80	20	6	3.0	839	.007	7162	36.9	-18.0	-24.7	13.0
40	80	20	8	3.0	839	.007	9550	65.7	-30.4	-43.5	28.4
41	80	50	2	3.0	839	.007	5969	33.9	-17.5	-17.9	10.0
42	80	50	4	3.0	839	.007	11937	131.8	-67.4	-62.0	73.1
43	80	20	2	4.0	839	.007	2387	2.8	-1.3	-9.7	.3
44	80	20	4	4.0	839	.007	4775	10.4	-4.7	-12.8	2.6
45	80	20	6	4.0	839	.007	7162	23.8	-10.6	-24.6	9.7
46	80	20	8	4.0	839	.007	9550	42.0	-18.3	-26.2	18.5
47	80	20	10	4.0	839	.007	11937	66.7	-28.5	-40.0	34.1
48	80	50	2	4.0	839	.007	5969	18.8	-8.7	-10.7	5.3
49	80	50	4	4.0	839	.007	11937	73.5	-33.1	-36.4	39.8

Exp. Bore Str Spd Open Dens Vis Nr Fmax Fmin Pmin Power

Exp.	Bore	Str	Spd	Open	Dens	Vis	Nr	Fmax	Fmin	Pmin	Power
50	80	20	2	5.0	839	.007	2387	1.6	-.7	-12.8	.2
51	80	20	4	5.0	839	.007	4775	4.6	-2.3	-11.5	1.4
52	80	20	6	5.0	839	.007	7162	12.0	-5.2	-13.5	4.6
53	80	20	8	5.0	839	.007	9550	21.5	-9.2	-28.8	9.3
54	80	20	10	5.0	839	.007	11937	34.2	-14.3	-28.8	16.7
55	80	50	2	5.0	839	.007	5969	8.9	-3.8	-8.6	3.0
56	80	50	4	5.0	839	.007	11937	38.2	-14.6	-21.9	20.7
57	80	50	6	5.0	839	.007	17906	83.2	-33.5	-45.5	69.0
58	80	20	2	6.0	839	.007	2387	1.3	-.5	-7.4	.1
59	80	20	4	6.0	839	.007	4775	4.1	-1.6	-7.8	1.0
60	80	20	6	6.0	839	.007	7162	9.5	-4.2	-11.9	3.4
61	80	20	8	6.0	839	.007	9550	17.4	-8.2	-24.9	7.3
62	80	20	10	6.0	839	.007	11937	27.8	-13.1	-29.3	13.2
63	80	50	2	6.0	839	.007	5969	5.9	-2.4	-17.6	2.0
64	80	50	4	6.0	839	.007	11937	25.5	-9.8	-22.9	15.3
65	80	50	6	6.0	839	.007	17906	54.4	-21.5	-33.4	48.0
66	80	50	8	6.0	839	.007	23875	104.4	-39.4	-63.6	115.3
67	80	20	2	7.0	839	.007	2387	1.2	-.5	-13.3	.2
68	80	20	4	7.0	839	.007	4775	2.7	-1.7	-6.9	.7
69	80	20	6	7.0	839	.007	7162	6.3	-3.9	-21.1	2.7
70	80	20	8	7.0	839	.007	9550	11.8	-7.4	-27.6	5.3
71	80	20	10	7.0	839	.007	11937	19.1	-11.9	-26.8	10.6
72	80	20	12	7.0	839	.007	14325	27.7	-17.3	-39.8	8.3
73	80	50	2	7.0	839	.007	5969	4.1	-1.5	-11.5	1.5
74	80	50	4	7.0	839	.007	11937	17.8	-6.5	-14.1	11.9
75	80	50	6	7.0	839	.007	17906	40.2	-15.5	-27.3	38.3
76	80	50	8	7.0	839	.007	23875	77.9	-27.1	-53.1	99.1
77	80	20	2	8.0	839	.007	2387	1.1	-.4	-10.7	.1
78	80	20	4	8.0	839	.007	4775	2.3	-1.4	-16.0	.6
79	80	20	6	8.0	839	.007	7162	5.0	-3.4	-17.2	2.0
80	80	20	8	8.0	839	.007	9550	9.5	-6.9	-18.5	4.0
81	80	20	10	8.0	839	.007	11937	15.5	-11.1	-27.7	11.9
82	80	20	12	8.0	839	.007	14325	23.0	-16.5	-39.7	10.8
83	80	50	2	8.0	839	.007	5969	2.9	-1.1	-9.4	1.2
84	80	50	4	8.0	839	.007	11937	13.5	-4.5	-15.4	9.8
85	80	50	6	8.0	839	.007	17906	31.2	-10.8	-24.9	31.6
86	80	50	8	8.0	839	.007	23875	57.5	-19.5	-43.9	77.6
87	24	15	4	1.0	869	.020	1074	.8	-.4	-11.5	.4
88	24	15	8	1.0	869	.020	2149	5.4	.2	-33.5	1.9
89	24	15	12	1.0	869	.020	3223	14.1	-1.4	-48.8	6.0
90	24	15	16	1.0	869	.020	4297	25.0	-6.4	-83.1	13.1
91	24	15	20	1.0	869	.020	5372	43.3	-19.0	-91.0	23.3
92	24	15	4	1.3	869	.020	1074	.6	-.3	-9.1	.2
93	24	15	8	1.3	869	.020	2149	1.8	-.7	-15.5	1.0
94	24	15	12	1.3	869	.020	3223	5.2	-.4	-31.0	2.6
95	24	15	16	1.3	869	.020	4297	10.2	-1.3	-43.8	6.4
96	24	15	20	1.3	869	.020	5372	16.9	-3.8	-73.4	11.6
97	24	15	24	1.3	869	.020	6446	24.5	-11.6	-89.1	19.1
98	24	15	4	1.6	869	.020	1074	.2	-.1	-8.5	.1
99	24	15	8	1.6	869	.020	2149	.6	-.1	-9.8	.7
100	24	15	12	1.6	869	.020	3223	2.0	-.1	-19.5	1.8

Exp. Bore Str Spd Open Dens Vis Nr Fmax Fmin Pmin Power

Exp.	Bore	Str	Spd	Open	Dens	Vis	Nr	Fmax	Fmin	Pmin	Power
101	24	15	16	1.6	869	.020	4297	4.2	-.5	-34.9	4.0
102	24	15	20	1.6	869	.020	5372	7.3	-.7	-41.5	6.7
103	24	15	24	1.6	869	.020	6446	11.7	-2.2	-58.0	11.1
104	24	15	4	1.9	869	.020	1074	.3	-.1	-11.5	.1
105	24	15	8	1.9	869	.020	2149	1.0	.5	-9.1	.5
106	24	15	12	1.9	869	.020	3223	2.2	.9	-17.3	1.3
107	24	15	16	1.9	869	.020	4297	4.3	1.2	-24.9	3.3
108	24	15	20	1.9	869	.020	5372	6.8	1.4	-34.0	6.4
109	24	15	24	1.9	869	.020	6446	10.1	.9	-48.1	6.9
110	24	15	4	2.2	869	.020	1074	.2	-.1	-3.0	.1
111	24	15	8	2.2	869	.020	2149	-.1	-.5	-6.5	.4
112	24	15	12	2.2	869	.020	3223	.7	-.0	-19.4	1.3
113	24	15	16	2.2	869	.020	4297	1.5	-.4	-25.9	2.2
114	24	15	20	2.2	869	.020	5372	3.0	-.8	-27.8	4.2
115	24	15	24	2.2	869	.020	6446	5.4	-.9	-41.3	8.1
116	24	15	4	2.5	869	.020	1074	.2	-.1	-4.5	.1
117	24	15	8	2.5	869	.020	2149	.3	-.1	-8.2	.3
118	24	15	12	2.5	869	.020	3223	.7	0.0	-18.8	.9
119	24	15	16	2.5	869	.020	4297	1.5	0.0	-21.4	1.7
120	24	15	20	2.5	869	.020	5372	2.8	.1	-25.2	4.3
121	24	15	24	2.5	869	.020	6446	5.0	.1	-37.8	8.1
122	80	20	2	3.0	869	.020	853	9.3	-4.8	-10.3	1.3
123	80	20	4	3.0	869	.020	1706	34.5	-17.2	-17.5	8.2
124	80	20	6	3.0	869	.020	2559	72.6	-36.6	-34.3	25.8
125	80	20	8	3.0	869	.020	3413	123.5	-60.6	-57.2	58.7
126	80	40	2	3.0	869	.020	1706	33.4	-17.3	-17.4	8.5
127	80	40	4	3.0	869	.020	3413	127.0	-64.4	-60.1	59.1
128	80	50	2	3.0	869	.020	2133	31.9	-16.5	-17.7	10.3
129	80	50	4	3.0	869	.020	4266	131.9	-60.1	-59.8	60.1
130	80	60	2	3.0	869	.020	2559	52.8	-27.3	-27.5	20.9
131	80	60	4	3.0	869	.020	5119	115.9	-51.1	-50.0	3.0
132	80	80	2	3.0	869	.020	3413	80.8	-41.8	-41.6	42.1
133	80	20	2	4.0	869	.020	853	2.8	-1.3	-11.6	.4
134	80	20	4	4.0	869	.020	1706	12.3	-5.0	-13.8	3.1
135	80	20	6	4.0	869	.020	2559	26.4	-10.7	-24.9	9.6
136	80	20	8	4.0	869	.020	3413	46.2	-18.3	-30.9	25.1
137	80	20	10	4.0	869	.020	4266	70.5	-27.5	-38.4	41.5
138	80	20	12	4.0	869	.020	5119	97.5	-38.9	-55.0	82.5
139	80	40	2	4.0	869	.020	1706	14.9	-6.9	-8.4	3.7
140	80	40	4	4.0	869	.020	3413	57.8	-25.7	-34.4	26.3
141	80	40	6	4.0	869	.020	5119	127.5	-55.7	-61.6	82.2
142	80	50	2	4.0	869	.020	2133	19.5	-9.1	-14.0	5.8
143	80	50	4	4.0	869	.020	4266	76.1	-32.6	-44.9	43.1
144	80	50	6	4.0	869	.020	6399	128.5	-53.8	-63.8	10.8
145	80	60	2	4.0	869	.020	2559	25.2	-11.7	-21.0	9.7
146	80	60	4	4.0	869	.020	5119	108.0	-44.5	-51.2	71.2
147	80	80	2	4.0	869	.020	3413	47.4	-22.0	-25.2	22.6
148	80	20	2	5.0	869	.020	853	1.6	-.7	-2.9	.3
149	80	20	4	5.0	869	.020	1706	6.8	-2.5	-12.8	1.9
150	80	20	6	5.0	869	.020	2559	15.8	-5.8	-10.7	5.9
151	80	20	8	5.0	869	.020	3413	32.9	-11.6	-31.8	16.0

Exp. Bore Str Spd Open Dens Vis Nr Fmax Fmin Pmin Power

Exp.	Bore	Str	Spd	Open	Dens	Vis	Nr	Fmax	Fmin	Pmin	Power
152	80	20	10	5.0	869	.020	4266	51.2	-18.1	-38.5	29.1
153	80	20	12	5.0	869	.020	5119	72.1	-25.0	-56.5	42.9
154	80	40	2	5.0	869	.020	1706	6.9	-3.0	-12.9	1.9
155	80	40	4	5.0	869	.020	3413	29.7	-11.6	-26.6	14.0
156	80	40	6	5.0	869	.020	5119	64.2	-24.4	-46.4	43.3
157	80	40	8	5.0	869	.020	6825	111.2	-43.4	-58.1	99.9
158	80	50	2	5.0	869	.020	2133	11.0	-4.7	-13.3	3.6
159	80	50	4	5.0	869	.020	4266	45.3	-17.4	-35.4	26.6
160	80	50	6	5.0	869	.020	6399	97.6	-39.3	-53.3	80.9
161	80	60	2	5.0	869	.020	2559	17.2	-7.4	-21.0	6.5
162	80	60	4	5.0	869	.020	5119	68.2	-26.5	-36.6	48.4
163	80	60	6	5.0	869	.020	7678	138.2	-60.7	-78.9	8.2
164	80	80	2	5.0	869	.020	3413	30.3	-13.0	-20.4	14.9
165	80	20	2	6.0	869	.020	853	1.4	-.6	-10.2	.2
166	80	20	4	6.0	869	.020	1706	5.1	-2.0	-13.0	1.5
167	80	20	6	6.0	869	.020	2559	12.5	-5.4	-15.2	4.4
168	80	20	8	6.0	869	.020	3413	22.0	-9.4	-21.6	10.6
169	80	20	10	6.0	869	.020	4266	33.8	-14.4	-38.0	16.5
170	80	20	12	6.0	869	.020	5119	48.2	-21.5	-45.4	31.7
171	80	40	2	6.0	869	.020	1706	4.4	-1.8	-4.1	1.5
172	80	40	4	6.0	869	.020	3413	20.0	-7.3	-20.7	9.7
173	80	40	6	6.0	869	.020	5119	43.7	-15.7	-32.5	29.9
174	80	40	8	6.0	869	.020	6825	76.3	-26.6	-46.7	69.5
175	80	40	10	6.0	869	.020	8531	98.7	-37.1	-57.6	33.4
176	80	50	2	6.0	869	.020	2133	6.1	-2.5	-11.2	2.3
177	80	50	4	6.0	869	.020	4266	28.1	-10.1	-18.2	17.2
178	80	50	6	6.0	869	.020	6399	62.6	-21.9	-35.8	56.2
179	80	50	8	6.0	869	.020	8531	104.1	-39.9	-57.4	4.6
180	80	60	2	6.0	869	.020	2559	12.4	-5.0	-10.7	4.6
181	80	60	4	6.0	869	.020	5119	45.2	-16.7	-38.6	33.2
182	80	60	6	6.0	869	.020	7678	99.5	-44.4	-55.3	101.1
183	80	80	2	6.0	869	.020	3413	18.6	-7.5	-12.3	10.
184	80	80	4	6.0	869	.020	6825	74.0	-25.7	-40.2	73.1
185	80	20	2	7.0	869	.020	853	1.1	-.4	-13.5	.2
186	80	20	4	7.0	869	.020	1706	3.7	-1.8	-6.8	1.2
187	80	20	6	7.0	869	.020	2559	9.1	-4.8	-22.6	3.4
188	80	20	8	7.0	869	.020	3413	16.2	-8.7	-22.9	8.0
189	80	20	10	7.0	869	.020	4266	25.5	-13.5	-35.4	13.0
190	80	20	12	7.0	869	.020	5119	36.4	-19.6	-43.5	28.5
191	80	40	2	7.0	869	.020	1706	3.0	-1.1	-3.6	1.0
192	80	40	4	7.0	869	.020	3413	14.4	-4.2	-14.0	7.2
193	80	40	6	7.0	869	.020	5119	31.3	-9.6	-25.4	22.3
194	80	40	8	7.0	869	.020	6825	54.5	-16.7	-39.1	54.9
195	80	40	10	7.0	869	.020	8531	80.3	-25.6	-62.8	114.2
196	80	50	2	7.0	869	.020	2133	4.8	-1.8	-16.6	1.9
197	80	50	4	7.0	869	.020	4266	21.5	-7.4	-14.2	13.6
198	80	50	6	7.0	869	.020	6399	48.1	-15.9	-30.4	43.6
199	80	50	8	7.0	869	.020	8531	87.9	-34.0	-51.2	122.6
200	80	60	2	7.0	869	.020	2559	7.9	-3.0	-16.5	3.3
201	80	60	4	7.0	869	.020	5119	32.3	-10.7	-32.6	24.3
202	80	60	6	7.0	869	.020	7678	70.7	-26.7	-42.3	79.3

Exp. Bore Str Spd Open Dens Vis Nr Fmax Fmin Pmin Power

Exp.	Bore	Str	Spd	Open	Dens	Vis	Nr	Fmax	Fmin	Pmin	Power
203	80	80	2	7.0	869	.020	3413	13.6	-5.2	-14.0	7.5
204	80	80	4	7.0	869	.020	6825	57.2	-18.7	-31.1	57.0
205	80	20	2	8.0	869	.020	853	1.0	-.4	-13.4	.1
206	80	20	4	8.0	869	.020	1706	2.5	-2.1	-18.8	.9
207	80	20	6	8.0	869	.020	2559	6.8	-4.4	-10.7	4.3
208	80	20	8	8.0	869	.020	3413	12.6	-8.4	-26.3	6.4
209	80	20	10	8.0	869	.020	4266	19.6	-12.9	-28.5	10.9
210	80	20	12	8.0	869	.020	5119	28.4	-18.0	-41.6	31.6
211	80	40	2	8.0	869	.020	1706	2.5	-.9	-5.0	.8
212	80	40	4	8.0	869	.020	3413	11.1	-3.7	-10.4	6.1
213	80	40	6	8.0	869	.020	5119	24.3	-8.6	-21.7	19.5
214	80	40	8	8.0	869	.020	6825	43.2	-15.2	-37.7	45.5
215	80	40	10	8.0	869	.020	8531	67.0	-23.6	-61.5	97.2
216	80	50	2	8.0	869	.020	2133	3.3	-1.2	-7.0	1.2
217	80	50	4	8.0	869	.020	4266	16.0	-4.6	-13.4	10.6
218	80	50	6	8.0	869	.020	6399	34.5	-10.4	-25.9	32.8
219	80	50	8	8.0	869	.020	8531	67.0	-18.9	-46.4	78.7
220	80	60	2	8.0	869	.020	2559	6.0	-2.2	-13.4	2.6
221	80	60	4	8.0	869	.020	5119	24.1	-7.8	-18.4	18.8
222	80	60	6	8.0	869	.020	7678	52.3	-20.1	-43.9	62.9
223	80	60	8	8.0	869	.020	10238	98.3	-39.6	-58.4	14.5
224	80	80	2	8.0	869	.020	3413	10.1	-3.7	-17.7	6.0
225	80	80	4	8.0	869	.020	6825	39.7	-12.5	-26.2	42.9
226	80	80	6	8.0	869	.020	10238	96.5	-34.2	-53.3	166.5
227	24	15	4	1.0	878	.097	80	3.0	-1.5	-22.6	.9
228	24	15	8	1.0	878	.097	161	9.9	-4.0	-48.9	3.7
229	24	15	12	1.0	878	.097	241	19.8	-7.7	-69.8	8.9
230	24	15	16	1.0	878	.097	321	33.0	-24.5	-95.5	17.6
231	24	15	4	1.3	878	.097	80	1.7	-.8	-14.7	.5
232	24	15	8	1.3	878	.097	161	5.0	-1.8	-29.1	2.3
233	24	15	12	1.3	878	.097	241	10.4	-3.4	-44.2	5.5
234	24	15	16	1.3	878	.097	321	17.8	-5.4	-63.9	10.4
235	24	15	20	1.3	878	.097	402	27.0	-8.8	-82.9	17.8
236	24	15	24	1.3	878	.097	482	62.3	-67.1	-92.5	3.4
237	24	15	4	1.6	878	.097	80	.7	-.3	-9.6	.4
238	24	15	8	1.6	878	.097	161	2.7	-.4	-29.3	1.5
239	24	15	12	1.6	878	.097	241	5.9	-.6	-33.2	3.8
240	24	15	16	1.6	878	.097	321	9.9	-1.2	-47.4	7.3
241	24	15	20	1.6	878	.097	402	15.9	-2.7	-72.4	12.5
242	24	15	24	1.6	878	.097	482	20.3	-4.6	-84.0	2.5
243	24	15	4	1.9	878	.097	80	.4	-.2	-14.7	.2
244	24	15	8	1.9	878	.097	161	1.1	-.2	-26.0	1.1
245	24	15	12	1.9	878	.097	241	2.9	-.5	-22.3	2.7
246	24	15	16	1.9	878	.097	321	5.3	-.8	-32.4	5.0
247	24	15	20	1.9	878	.097	402	8.4	-1.4	-45.3	8.5
248	24	15	24	1.9	878	.097	482	12.4	-3.0	-60.0	11.6
249	24	15	4	2.2	878	.097	80	.3	-.1	-11.5	.2
250	24	15	8	2.2	878	.097	161	.7	-.3	-11.4	.8
251	24	15	12	2.2	878	.097	241	1.7	-.4	-19.1	2.1
252	24	15	16	2.2	878	.097	321	3.2	-.9	-28.7	4.1
253	24	15	20	2.2	878	.097	402	5.3	-1.3	-45.1	7.6

Exp. Bore Str Spd Open Dens Vis Nr Fmax Fmin Pmin Power

Exp.	Bore	Str	Spd	Open	Dens	Vis	Nr	Fmax	Fmin	Pmin	Power
254	24	15	24	2.2	878	.097	482	8.4	-2.2	-60.2	12.0
255	24	15	4	2.5	878	.097	80	.3	-.1	-6.0	.2
256	24	15	8	2.5	878	.097	161	.7	-.1	-10.3	.8
257	24	15	12	2.5	878	.097	241	.9	-.6	-25.7	1.9
258	24	15	16	2.5	878	.097	321	2.2	-.9	-34.2	3.8
259	24	15	20	2.5	878	.097	402	4.1	-1.3	-35.1	5.9
260	24	15	24	2.5	878	.097	482	6.8	-1.9	-47.4	10.7
261	80	20	2	3.0	878	.097	178	12.8	-6.6	-12.6	1.8
262	80	20	4	3.0	878	.097	357	37.4	-18.2	-18.8	9.5
263	80	20	6	3.0	878	.097	535	75.7	-35.2	-43.4	27.2
264	80	20	8	3.0	878	.097	714	4.1	3.1	-11.4	.8
265	80	50	2	3.0	878	.097	446	45.6	-23.6	-22.0	14.9
266	80	20	2	4.0	878	.097	178	5.8	-2.7	-6.4	.9
267	80	20	4	4.0	878	.097	357	18.9	-8.1	-10.7	4.6
268	80	20	6	4.0	878	.097	535	38.6	-15.9	-24.2	13.2
269	80	20	8	4.0	878	.097	714	63.9	-26.2	-40.2	30.1
270	80	20	10	4.0	878	.097	892	95.2	-38.7	-50.2	51.1
271	80	50	2	4.0	878	.097	446	24.7	-11.5	-23.8	7.8
272	80	50	4	4.0	878	.097	892	84.9	-36.6	-41.6	50.1
273	80	20	2	5.0	878	.097	178	3.4	-1.5	-14.9	.6
274	80	20	4	5.0	878	.097	357	11.3	-4.4	-16.2	3.0
275	80	20	6	5.0	878	.097	535	24.1	-9.2	-14.3	8.5
276	80	20	8	5.0	878	.097	714	39.9	-15.0	-23.2	19.5
277	80	20	10	5.0	878	.097	892	60.9	-22.3	-34.5	34.9
278	80	50	2	5.0	878	.097	446	16.3	-7.0	-10.	5.3
279	80	50	4	5.0	878	.097	892	59.3	-23.0	-29.7	35.1
280	80	20	2	6.0	878	.097	178	2.0	-.8	-14.8	.4
281	80	20	4	6.0	878	.097	357	6.7	-2.3	-13.9	2.0
282	80	20	6	6.0	878	.097	535	15.2	-5.8	-17.5	6.1
283	80	20	8	6.0	878	.097	714	26.4	-10.2	-21.1	12.2
284	80	20	10	6.0	878	.097	892	40.6	-15.3	-31.3	23.6
285	80	20	12	6.0	878	.097	1071	56.6	-22.2	-42.9	46.9
286	80	50	2	6.0	878	.097	446	9.9	-4.0	-17.8	3.5
287	80	50	4	6.0	878	.097	892	37.2	-13.2	-19.7	23.0
288	80	20	2	7.0	878	.097	178	1.5	-.6	-13.7	.3
289	80	20	4	7.0	878	.097	357	5.4	-1.3	-9.4	1.6
290	80	20	6	7.0	878	.097	535	11.9	-4.6	-22.1	4.5
291	80	20	8	7.0	878	.097	714	19.9	-8.7	-19.4	9.5
292	80	20	10	7.0	878	.097	892	30.1	-13.5	-30.7	17.1
293	80	20	12	7.0	878	.097	1071	42.4	-19.9	-41.8	33.7
294	80	50	2	7.0	878	.097	446	6.5	-2.5	-7.7	2.6
295	80	50	6	7.0	878	.097	1338	56.7	-18.4	-36.9	53.7
296	80	20	2	8.0	878	.097	178	1.3	-.5	-12.0	.2
297	80	20	4	8.0	878	.097	357	3.9	-1.4	-16.6	1.2
298	80	20	6	8.0	878	.097	535	8.6	-4.2	-12.5	3.2
299	80	20	8	8.0	878	.097	714	15.0	-7.9	-18.3	11.3
300	80	20	10	8.0	878	.097	892	22.6	-12.5	-28.5	12.3
301	80	20	12	8.0	878	.097	1071	32.4	-18.4	-40.4	25.7
302	80	50	2	8.0	878	.097	446	4.5	-1.6	-5.8	2.0
303	80	50	4	8.0	878	.097	892	20.2	-6.0	-14.3	14.2
304	80	50	6	8.0	878	.097	1338	43.9	-12.8	-28.9	51.7

Exp. Bore Str Spd Open Dens Vis Nr Fmax Fmin Pmin Power

Appendix H: Compressibility Testing of Liquids

The search for the optimum working fluid for use in the liquid spring revealed several likely candidates for which compressibility data could not be found. Therefore, in order to quantify the bulk modulus of these liquids, a compressibility testing apparatus was built.

There are several problems inherent in testing compressibility, the first being that, in straining the liquid, the containment vessel is itself strained. The test container was machined from a thick walled steel cylinder for this reason. The inaccuracy attributable to vessel strain was calculated as being equivalent to 0.16 percent volume change at the maximum test pressure of 700 bar. While not negligible, this change is less than five percent of that experienced by the test liquids.

The second problem is that of containing the liquid within a shell which is both rigid yet which possesses a direction of controlled compliance in order that the fluid can be strained. Conventional seals, i.e. O-rings, might be used against a piston but might cause inaccuracies through weeping and would also make air entrapment difficult to avoid. The solution adopted used a polyurethane rubber liner with integral sealing lip as shown in figure H-1. Once the liner was filled with liquid, the piston was brought into contact with the rubber and any extra liquid in the vessel was forced out as the seal was established. During the compression process the liner contracted in length in opposition to the piston motion.

The testing rig was then calibrated by measuring the piston deflection against a range of piston loads for two well documented liquids (water and mineral oil) with the vessel installed in the jaws of a compression testing machine.

This calibration procedure allowed the compressibility of the liner to be both established and then confirmed.

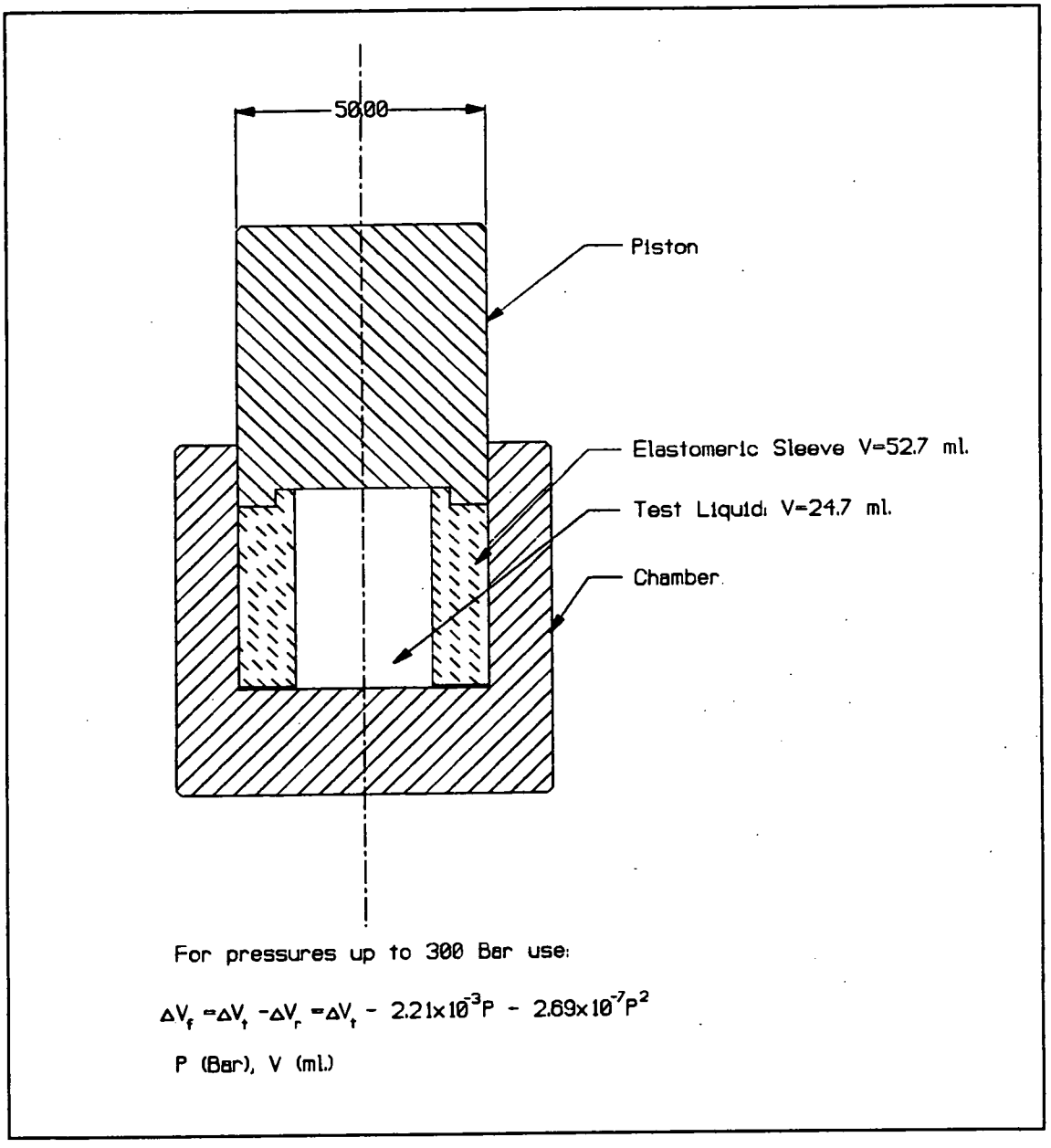

Figure H-1: Compressibility Testing Apparatus

Tests were then run on Pentane and the Cyclic Silicone Fluids. The Dow Corning 244 fluid and the Pentane produced almost identical results, giving a bulk modulus of 0.38 GPa at 100 Bar and 20 C. which can be compared to 1.6 GPa for mineral oil and 2 GPa for water.

Other potentially useful materials can be summarised as follows:

1. Dow Corning 245, 210:	0.9 GPa	[1]
2. C6-F14 Perfluorohexane:	0.347 GPa	[2]
3. C6-H14 Hexane:	0.67 GPa	[3]
4. HFC 142 (Freon Replacement):	0.21 GPa	[4]
5. ICI HFC 134 (Freon Replacement):	0.225 GPa	[5]
6. 2 Methylbutane (tested):	0.443 GPa	
7. Propane (not found but approx.):	0.2-0.25 GPa	
8. Buckminster Fullerene C60 (Solid):	18 GPa	[6]

1. Technical Data Sheet no. 22-069L-01, Dow Corning Ltd., 1991.

2. Serratrice, G., Delpuech, J.-J., Compressibilites des Fluorocarbures: Relation avec la Solubilite des Gas, Nouveau Journal de Chimie, Vol. 6, No. 10, 1982, pp.489-493.

3. Eduljee, H.E., Newitt, D.M., Weale, K.E., Pressure-Volume-Temperature Relations in Liquids and Liquid Mixtures. Part I. The Compression of n-Hexane, n-Heptane, n-Octane, and of their Binary and Ternary Mixtures, up to 5000 Atmospheres, J. Chem. Soc., 1951, pp. 3086-3091.

4. Maezawa, Y., Sato, H., Watanabe, K., Liquid Densities and Vapour Pressures of 1-Chloro-1,1-difluoroethane (HCFC 142b), J. Chem. Eng. Data., Vol. 36, 1991, pp. 148-150.

5. Maezawa, Y., Sato, H., Watanabe, K., Liquid Densities and Vapour Pressures of 1,1,2,2-Tetrafluoroethane (HFC 134) and 1,1-Dichloro-1-fluoroethane (HCFC 141b), J. Chem. Data. Vol. 36, 1991, pp. 151-155.

6. Regueiro, M.N., Monceau, P., Hodeau, J.L., "Crushing C60 to Diamond at Room Temperature", Nature, vol. 355, no. 6358, 1992, pp. 237-239.

Appendix I: Digital Displacement Pump Control Software Listing

```
/*
   POPMIRA.C            Alan Fussey            21-October-1991

   Poppet Valve Flow / Pressure Controller.

   The system consists of a hydraulic six cylinder axial piston pump
   and an electronic control unit.  Each cylinder of the pump has an
   electro-magnetic  valve  which enables the displacement of that
   cylinder. Each of the valves may be closed once per revolution of
   the  pump,  therefore  giving  zero  or  maximum  flow  for  that
   cylinder.  A magnetic inductive pickup is used to produce a pulse
   for  each  revolution  of  the  pump.  For  Flow  control,  a  flow
   demand pot. is used to provide an analogue signal  which is used
   for  closed loop control of flow. For Pressure control, a pressure
   transducer is used along with a flow prediction equation for closed
   loop control of pressure. A proportional control  valve is also
   fitted to the output  of the pump  to allow the  flow to  be
   restricted. A switch is used to select the flow or pressure mode of
   operation at any time.

   Computer Control System.

   The  above system is controlled by a stand-alone  INTEL  80C196KB
   16-bit embedded microcontroller board. This board has Analogue and
   digital I/O and an internal timer. The board is programmed in the
   'C' Language using the INTEL IC96 compiler.

   Control Sequence.

   The  computer  controls  the flow / pressure of the system in the
   following manner.

   A reading of the internal timer is taken once every revolution of
   the  pump.  This time is then used to determine when each of  the
   six  poppet  valves  should be closed.  The  poppet  valves  take
   approximately  2.5 milliseconds to close after the request by the
   computer,  so this delay time is accounted for in each of the six
   timings. These timings are then placed into software timers which
   will  cause an internal interrupt when each of the poppets should
   be closed. When a software interrupt occurs, a calculation is done
   using  the  current flow demand / Pressure reading taken and  the
   expected flow / pressure produced by this and the last two valves.
   The poppet  valve is then closed if  the expected flow / pressure
   is expected to go below a  set  level.
   When  all six poppets valves have been accounted  for,  the  next
   revolution pulse will be timed and the sequence will start again.

   ------------------------------------------------------------------

   Program to time External Interrupt HSI.0 using Timer1 which
   runs at 750,000 Hz at 12Mhz cpu speed. This time is then split into
```

```
   6 equal units ( 1 for each valve ) and a 12th of the time.
   The activation length is where the first valve is activated, this
   time is placed into a software timer (t1 for poppets 2 to 6 and t2
   for poppet 1)  which will cause an interrupt when the time has
   elapsed, the software  interrupt will then be set again for the
   second 6th of the time later and so on. A third software interrupt
   will be set to turn off the poppet valve, this will normally be 3
   milliseconds in length (t3). A new time reading is then taken at the
   next pulse ( approx 12th after valve 6).

   An analogue input is used to detect the demand flow and a formula is
   used to determine whether or not to open each value when the
   software interrupt occurs.

   The Flow or Pressure mode of operation is selected at any time by a
   switch which will be connected between 5v and Digital Input pin 6 on
   JP1 ( channel 1 ). Flow Control is selected by pulling this pin High
   5v, Pressure Control is selected by pulling this pin to Ground.
*/
#include<stdio.h>
#include<80c196.h>
#include<user96.h>

#define FALSE     0
#define TRUE      1
#define PRESSURE_MODE   0x80
#define FLOW_MODE 0x00
#define PULSE_WIDTH     2252u       /* 3 milliseconds */

#pragma CCB(0xFA)
#pragma interrupt (timer1_overflow = 0)
#pragma interrupt (reset_timer = 4)
#pragma interrupt (fire_poppet = 5)

register int st2_flag, st3_flag, operation_mode, overflow_count;
register int err, dec_cyl, d[4], pop_number;
register int sp, sc, s0, k;
register long ss, old_ss;
register int ad_value, ad_offset, ad_set, ad_min, set_press_vol;
register int vf, old_vf, set_pt_rat;
register unsigned long cycle_time;
register unsigned short t1, old_time, new_time, time_passed, freq;
register unsigned short delay, ad_delay, is1, st2_time, st3_time;
register unsigned char bdc;
register unsigned char poppet[6];

void timer1_overflow(void)
{
   overflow_count++;
}

void fire_poppet(void)
{
   t1 = timer1;
   is1 = ios1;
```

```
   if( (isl & 0x004) == 0x004 )          /* t3, turn off poppet */
   {
     ioportl = 0x80;
      st3_flag = FALSE;
      if( operation_mode == PRESSURE_MODE )
      {
/*
      Delay reading of pressure depending on speed in Hz.
      2.05 Milliseconds - 0.0226 Milliseconds for every Hz above 10.
*/

      freq = 7500001 / cycle_time;
      if( freq >= 101 )  /* 0.61 mSec to 1.98 mSec - 0.0226 above 10
*/
         ad_delay = 4601 +(long)ad(4) - ((freq-10)*171);
      else
         ad_delay = 4601 +(long)ad(4);
      do
         time_passed = timerl-tl;
      while( time_passed < ad_delay );
        ad_value =0;
      for (k=0; k<=4 ; k++)
         ad_value += ad(1);  /* Initiate Analogue read for pressure */

      ad_value = ad_value/5; /* averages 3 press readings 40 microsecs
ea.                                */
      ad_value -= ad_set;           /* offset of trans. to set press*/
      set_pt_rat = 198;
      if (vf > 512) set_pt_rat -= 15;
      vf = set_press_vol + (long)set_pt_rat * ad_value/10;
      /* approximates adiabatic compression by adding second rate */
      }
   }
   else
   {
      if( (isl & 0x001) == 0x001 )        /* Poppet 1-5 */
      {
       if( pop_number < 5 )
          hso_command = 0x18;
       else
       {
          st2_time = tl + delay;
          st2_flag = TRUE;
          hso_command = 0x19;
       }
       hso_time = tl + delay;
      }
      else
      {
       st2_flag = FALSE;
       pop_number = 0;
      }

      if( operation_mode == PRESSURE_MODE )
      {
```

```
 /*  Calculate demand. */

        sp = d[0]/4 +  d[1]/2 + 2*d[2]/9;
        sc = d[1]/4 + 3*d[2]/4 + d[3];
        ss = (sp + old_vf - vf) * 3;
              /* set up for 0 degrees before i-1 cyl. */
        s0 = vf - set_press_vol ;

/* reduced gain suppresses
        instabilities and group firing in operating range */

        dec_cyl = 10*( ss - s0 - sc )/7;
        old_vf = vf;
        if (ss < 1300 && d[3] == 1024) dec_cyl = 0;
        if (ss > 1700 && d[3] == 0) dec_cyl = 1024;
/* the prev. rules prevent burst firing or disabling */
        if (ss >= 1800) dec_cyl -= 293;
/* this rule assumes that above 50% load high prob. of next
          cylinder being enabled, below 50% load there is a high prob.
          of next cylinder not being enabled - thus no correction */
        if (1200 < ss < 1800 && d[3] == 1024) dec_cyl -= 293;
/* probability of i+1 cyl enabling at half load */
        if (vf > 1600)   dec_cyl = 0;
        d[0] = d[1];
        d[1] = d[2];
        d[2] = d[3];
       }
       else  /* Flow Control Mode */
       {
        ad_value = ad(0);  /* Initiate Analogue read for flow demand */
/*
       Calculate demand.
*/
        err += ( ad_value - ( (d[3]/4) + (d[2]/2) + (d[1]/4) ) );
        dec_cyl = 4*( err - (3*d[3]/4) - (d[2]/4) + (2*ad_value) )/3;
        d[1] = d[2];
        d[2] = d[3];
       }

       st3_flag = TRUE;
       st3_time = timer1 + 1252 + ad(2); /* Between 1.67 mSec and 3.03
mSec */
       hso_command = 0x1A;              /* Software interrupt timer 3 */
       hso_time = st3_time;

       if( dec_cyl > 512 )     /* Open poppet */
       {
        ioport1 |= poppet[pop_number] | 0x040;
           d[3] = 1024;
       }
       else                /* Dont open poppet */
       {
           d[3] = 0;
       }
       pop_number++;
```

```
      if( pop_number >= 6 )
       pop_number = 0;

   }
}

void reset_timer(void)
{

   new_time = timer1;
   cycle_time = ((overflow_count * 65536) + new_time - old_time);
   old_time = new_time;
   overflow_count = 0;
   ioc2 = 0x80;                /* Clear any software timers */
   if( cycle_time > 250000 )   /* Slower than 3 Hz so ignore */
      return;
   if( st2_flag == TRUE )      /* Restore software timer 2 for poppet 1
*/
   {
      if( st2_time < timer1 && (st2_time+100 > timer1) )
       st2_time += 100u;
      hso_command = 0x19;
      hso_time = st2_time;
   }
   else if( st3_flag == TRUE )      /* Restore software timer 3 for
poppet 1 */
   {
      if( st3_time < timer1 && (st3_time+100 > timer1) )
       st3_time += 100u;
      hso_command = 0x1A;
      hso_time = st3_time;
   }

   hso_command = 0x18;         /* Setup poppet 2 */
   hso_time = (new_time + ((cycle_time/4u) - 375u-(ad(3)*2)));    / *
0.5 mSec to 3.2 mSec */
   delay = cycle_time/6;

   pop_number = 1;
}

unsigned short ad(channel)
int channel;
{

   ad_command = 0x008+channel;
   while( (ad_result_lo & 0x008) != 0x008 )
   ;
   while( (ad_result_lo & 0x008) == 0x008 )
   ;
   return((ad_result_hi&0xFF)*0x004)+((ad_result_lo/0x040)&0x003);

}

main()
```

```
{

   poppet[0] = 0x010;
   poppet[1] = 0x008;
   poppet[2] = 0x004;
   poppet[3] = 0x002;
   poppet[4] = 0x001;
   poppet[5] = 0x020;
   ioport1 = 0x80;       /* Set bit 1.7 High for Input */
   bdc = 0x002;
   ioc1 = 0x004;  /* Timer1 overflow */
   int_mask = 0x31;      /* External HSI.0 & Software timer  &
                        Timer overflow interrupts */

/*
   Calculate Set pressure from accumulator pressure.
*/
   set_press_vol = 512;
   ad_set = 9*ad(1)/8; /* set pressure a/d reading */
   set_pt_rat = 198;

   do
   {
      set_pt_rat = 170+(ad(5)/17);  /* 170 to 230 */
      dec_cyl = 1024;
      st2_flag = FALSE;
      st3_flag = FALSE;
      err = 0;
      d[0] = 0;
      d[1] = 0;
      d[2] = 0;
      d[3] = 0;
      pop_number = 1;
      overflow_count = 0;
      operation_mode = ioport1 & 0x80;    /* Pressure or Flow control
*/

/*
   take first reading of bottom dead centre.
*/
      while( (hsi_status & bdc) != bdc ) /* Wait for bottom dead centre
HSI.0 */
      ;     /* Loop */

      old_time = timer1;
      while( (hsi_status & bdc) == bdc )
      ;     /* Wait for pulse to go off */
      int_pending = 0;
      enable();

      while( operation_mode == (ioport1 & 0x80) )
      ;
   }
   while(1);
}
```